DISS. ETH NO. 29149

Development and Evaluation of Sampling and Electrochemical Detection Techniques for Airborne Soluble Metals

A thesis submitted to attain the degree of
DOCTOR OF SCIENCES of ETH ZURICH
(Dr. sc. ETH Zurich)

presented by
Yibo ZHAO
MSc, Peking University

born on *04.07.1993*
citizen of China

accepted on the recommendation of
Prof. Dr. Jing Wang, examiner
Prof. Dr. Eric Bakker, co-examiner
Dr. Modini Robin Lewis, co-examiner
Prof. Dr. Sheng-Chieh Chen, co-examiner

2023

Acknowledgements

First of all, I would like to express my deepest gratitude to my supervisor Prof. Jing Wang for giving me the opportunity to achieve my Ph.D. degree. With constant support and guidance from Prof. Jing Wang, I had a lot of freedom in my research life, in which I grew up as an independent researcher, and gained invaluable experience in research and life, which also sharpened my critical thinking and personality.

I am grateful for the suggestions and guidance from Prof. Christian Ludwig, Prof. Sheng-Chieh Chen and Prof. Eric Bakker, which improved the papers in many ways, such as discussions and paper revision. I would also like to extend my sincere thanks to Dr. Modini Robin Lewis, Prof. Sheng-Chieh Chen and Prof. Eric Bakker, who were willing to be co-examiners in my committee.

I would like to thank China Scholarship Council for the financial support that allowed me to pursue my Ph.D. studies.

I have the pleasure of collaborating with Tianyu Cen and Prof. Christian Ludwig at EFPL, who supported me as good friends and colleagues. I would like to acknowledge Weidong and Wenbo who taught me a lot about aerosol and electrochemical experiments from scratch, which are the fundamental and valuable knowledge during my studies. This thesis would not have been finished without the support from them.

Thanks should also go to the group members and alumni in Prof. Jing Wang's group, where I have pleasurable discussions, corporations, and friendships. I would also like to express my gratitude to other colleagues in Empa, especially Adrian, Kevin, Daniel, Robin, and Beat. They are always helpful and tolerant to me.

I would be remiss in not mentioning my friend Laibao, who have been my schoolmate and friend for a decade. I cannot forget the time we gathered, shared and celebrated each accomplishment.

Lastly, I would like to express my appreciation to my parents, and my wife Xueying, who are always by my side and make my day. They have always been trying to understand me best and accompany me through any tough and joyful time.

Abstract

Transition metals in the atmosphere are raising a significant threat to human health and the environment, which are now considered a poorly-understood global problem requiring time-consuming efforts of sampling and analysis. More importantly, the soluble fraction of particle-bound transition metals enhances the persistent toxicity and health effects, which is particularly harmful to humans due to its toxicity and bioaccessibility, accounting for 0 – 80 % of total metals in airborne particulate matter (PM). Therefore, the detection of the soluble fraction in particle-bound transition metals is of great significance for public health, ideally in a cost-effective and mobile way. Nonetheless, the monitoring techniques of atmospheric soluble metals is constrained due to their low concentrations and technique limitations. For example, the extraction of airborne soluble metals usually requires time-consuming efforts, such as submicron filter filtration after sonication. After the development of sampling and detection platforms for airborne soluble metals, it becomes hard to estimate the sampling performance using the conventional upstream and downstream particle counting under high pressure drops out of working ranges. Higher pressures drops indicate higher flow rates and larger amount of collected particle mass in environmental applications, which requires alternative ways to evaluate the sampling performance under various pressure drops. This thesis aims to develop new strategies and concepts of capture and detection of airborne soluble metals by introducing dual-functional interfaces for both sampling and detection, unlike the conventional coupling of sampling and detection units in sequence, and explore the method for measuring collection efficiencies of samplers under high pressure drop, which can cause the malfunction of aerosol measure instruments.

In Chapter 2, an inertial-impaction-based fluidic chip integrated with electrochemical detection was developed to achieve high collection efficiency and measurements of the bioaccessible metal fraction at the nanogram level. The average collection efficiency for ultrafine and fine particles larger than 50 nm, obtained at a flow rate of 2.5 L/min, was above 70 %. The detection ranges of aerosol soluble copper depended on the collection duration and airflow rate. At a working flow rate of 3.1 L/min and collection efficiency of 70 %, the microsystem was capable of detecting Cu concentrations above 53 ng/m^3, 32 ng/m^3 and 8 ng/m^3 with 3h, 5 h and 20 h collection periods, respectively, which were in the range of reported atmospheric concentrations. The detection ratio of real-world samples (i.e. PM_{10}-like aerosol) was 100 ± 14 %, indicating excellent aerodynamic collection and reliable electrochemical detection. The collection and sensing performance of the microsystem demonstrates a new step towards an online, mobile, low-cost, and miniaturized routine monitoring system for bioaccessible metals and possibly other soluble components in the aerosols.

In Chapter 3, the concept of aerosol-into-liquid capture and detection is proposed, which allowed one-step particle capture and detection via the Janus-membrane electrode at the gas-liquid interface, enabling active enrichment and enhanced mass transport of metal ions. The integrated aerodynamic/electrochemical (IAE) system was capable of capturing airborne particles with a cutoff size down to 50 nm and detecting Pb(II) with a limit of detection of 95.7 ng. The proposed concept can pave the way for cost-effective and miniaturized systems, for the capture and detection of airborne soluble metals in air quality monitoring, especially for abrupt air pollution events with high airborne metal concentrations (e.g. wildfires and fireworks).

In Chapter 4, an elution-based method using NaCl aerosol was proposed to estimate the size-resolved collection efficiency which was not affected by the pressure drop. More specifically, a Condensation Particle Counter (CPC) was used to count the upstream particle number, and the collected NaCl particles were eluted and determined by Inductively Coupled Plasma Mass Spectrometry (ICP-MS) for estimating the collected particle number. The relationship between number-based concentration and mass-based concentration of NaCl particles was established. A stainless steel impactor for Differential Mobility Analyzer (DMA), polydimethylsiloxane (PDMS)-based microchannel, and a homemade impactor containing 151 nozzles with a diameter of 0.1 mm were employed to investigate the feasibility of the elution method. DMA-selected particles with a nominal size are considered to be the monodisperse aerosol, which was commonly used for estimating the collection efficiencies of samplers, but size redistribution of downstream monodisperse aerosol with the particle size smaller than 100 nm and larger than the cutoff size (D_{50}) was revealed through the elution method, which affected the collection efficiency measured by either conventional CPC- or elution-based method. It was found that the elution method was dependent on the D_{50} value of the sampler, and the applicable size range was from 100 nm to D_{50} (D_{50} < 500 nm) or from 100 nm to 500 nm (D_{50} > 500 nm). This study provided insights into the size-dependent particle transport through aerosol samplers, and the development of an elution-based method to estimate pressure drop-independent collection efficiencies.

In summary, The proposed concepts and systems for the capture and collection of atmospheric metals enable the capture of nanoparticles and detection of metals at the nanogram level, which will pave a new way towards cost-effective and mobile monitoring of air quality with a high spatial and temporal resolution. Given the fact that electrochemical detection is a liquid-based method, these concepts and systems enable the evaluation of metal toxicity with proper electrolytes as leaching agents. In addition, these concepts can also provide new insights into sampling and detection of other airborne components. For the estimation of collec-

tion efficiency, the elution-based method could contribute to evaluation of sampling performance of samplers and investigations of particle behaviors during particle capture within samplers.

Zusammenfassung

Übergangsmetalle in der Atmosphäre stellen eine erhebliche Bedrohung für die menschliche Gesundheit und die Umwelt dar, die heute als kaum verstandenes globales Problem angesehen werden, das zeitaufwändige Probennahmen und Analysen erfordert. Noch wichtiger ist, dass die lösliche Fraktion der partikelgebundenen Übergangsmetalle die anhaltende Toxizität und die gesundheitlichen Auswirkungen verstärkt, die aufgrund ihrer Toxizität und Biozugänglichkeit für den Menschen besonders schädlich sind und 0 – 80 % der gesamten Metalle in luftgetragenen Feinstaubpartikeln (PM) ausmachen. Daher ist der Nachweis des löslichen Anteils in partikelgebundenen Übergangsmetallen von großer Bedeutung für die öffentliche Gesundheit, idealerweise auf kostengünstige und mobile Weise. Dennoch sind die Überwachungstechniken für atmosphärisch lösliche Metalle aufgrund ihrer geringen Konzentrationen und technischen Einschränkungen eingeschränkt. Beispielsweise erfordert die Extraktion von luftgetragenen löslichen Metallen normalerweise zeitaufwändige Anstrengungen, wie z. B. eine Submikron-Filterfiltration nach der Beschallung. Nach der Entwicklung von Probenahme- und Nachweisplattformen für luftgetragene lösliche Metalle wird es schwierig, die Probenahmeleistung unter Verwendung der herkömmlichen vor- und nachgeschalteten Partikelzählung unter hohen Druckabfällen außerhalb der Arbeitsbereiche abzuschätzen. Höhere Druckabfälle weisen auf höhere Durchflussraten und eine größere Menge an gesammelter Partikelmasse in Umweltanwendungen hin, was alternative Methoden zur Bewertung der Probenahmeleistung bei verschiedenen Druckabfällen erfordert. Hier zielt diese Arbeit darauf ab, neue Strategien und Konzepte zur Erfassung und Detektion von luftgetragenen löslichen Metallen zu entwickeln, indem dual-funktionale Schnittstellen sowohl für die Probenahme als auch für die Detektion eingeführt werden, im Gegensatz zur herkömmlichen Kopplung von Probenahme- und Detektionseinheiten in Folge, und die Methode für untersucht Messung der Sammeleffizienz von Probenehmern unter hohem Druckabfall, der zu Fehlfunktionen von Aerosolmessgeräten führen kann.

In Kapitel 2 wurde ein auf Trägheitswirkung basierender Fluidchip mit integrierter elektrochemischer Detektion entwickelt, um eine hohe Sammeleffizienz und Messungen der biozugänglichen Metallfraktion auf Nanogrammebene zu erreichen. Die durchschnittliche Sammeleffizienz für ultrafeine und feine Partikel mit einer Größe von mehr als 50 nm, die bei einer Durchflussrate von 2,5 l/min erzielt wurde, lag bei über 70 %. Die Nachweisbereiche von aerosollöslichem Kupfer waren abhängig von der Sammeldauer und der Luftströmungsgeschwindigkeit. Bei einer Arbeitsflussrate von 3,1 l/min und einer Sammeleffizienz von 70 % war das Mikrosystem in der Lage, Cu-Konzentrationen über 53 ng/m^3, 32 ng/m^3 und 8 ng/m^3 mit 3 h, 5 h und 20 h Sammelperioden zu erkennen , die im Bereich der gemeldeten atmosphärischen Konzentrationen lagen. Das Erkennungsverhältnis von Proben aus der realen Welt (d. h. PM_{10}-ähnliches Aerosol) betrug 100 ± 14 %, was auf eine hervorragende aerodynamische Sammlung

und einen zuverlässigen elektrochemischen Nachweis hinweist. Die Erfassungs- und Erfassungsleistung des Mikrosystems zeigt einen neuen Schritt in Richtung eines mobilen, kostengünstigen und miniaturisierten Online-Routineüberwachungssystems für biozugängliche Metalle und möglicherweise andere lösliche Komponenten in den Aerosolen.

In Kapitel 3 wird das Konzept der Aerosol-in-Flüssigkeit-Abscheidung und -Detektion vorgeschlagen, das die Partikelabscheidung und -detektion in einem Schritt über die Janus-Membran-Elektrode an der Gas-Flüssigkeits-Grenzfläche ermöglichte, was eine aktive Anreicherung und einen verbesserten Massentransport von Metallionen ermöglichte . Das integrierte aerodynamische/elektrochemische (IAE)-System war in der Lage, luftgetragene Partikel mit einer Grenzgröße von bis zu 50 nm einzufangen und Pb(II) mit einer Nachweisgrenze von 95,7 ng nachzuweisen. Das vorgeschlagene Konzept kann den Weg für kostengünstige und miniaturisierte Systeme zur Erfassung und Detektion von luftgetragenen löslichen Metallen bei der Überwachung der Luftqualität ebnen, insbesondere bei plötzlichen Luftverschmutzungsereignissen mit hohen Metallkonzentrationen in der Luft (z. B. Waldbrände und Feuerwerk).

In Kapitel 4 wurde ein elutionsbasiertes Verfahren unter Verwendung von NaCl-Aerosol vorgeschlagen, um die größenaufgelöste Sammeleffizienz abzuschätzen, die nicht durch den Druckabfall beeinflusst wird. Genauer gesagt wurde ein Kondensationspartikelzähler (CPC) verwendet, um die stromaufwärts gelegene Partikelzahl zu zählen, und die gesammelten NaCl-Partikel wurden eluiert und durch Massenspektrometrie mit induktiv gekoppeltem Plasma (ICP-MS) bestimmt, um die gesammelte Partikelzahl abzuschätzen. Die Beziehung zwischen zahlenbasierter Konzentration und massenbasierter Konzentration von NaCl-Partikeln wurde hergestellt. Ein Impaktor aus rostfreiem Stahl für den Differential Mobility Analyzer (DMA), ein auf Polydimethylsiloxan (PDMS) basierender Mikrokanal und ein selbstgebauter Impaktor mit 151 Düsen mit einem Durchmesser von 0,1 mm wurden eingesetzt, um die Machbarkeit des Elutionsverfahrens zu untersuchen. DMA-selektierte Partikel mit einer Nenngröße gelten als das monodisperse Aerosol, das üblicherweise zur Schätzung der Sammeleffizienz von Probenehmern verwendet wurde, aber Größenumverteilung des nachgeschalteten monodispersen Aerosols mit einer Partikelgröße kleiner als 100 nm und größer als die Cutoff-Größe (D_{50}) wurde durch das Elutionsverfahren aufgedeckt, was die Sammeleffizienz beeinflusste, die entweder durch herkömmliche CPC- oder elutionsbasierte Verfahren gemessen wurde. Es wurde festgestellt, dass die Elutionsmethode vom D_{50}-Wert des Probenehmers abhängig war und der anwendbare Größenbereich von 100 nm bis D_{50} (D_{50} < 500 nm) oder von 100 nm bis 500 nm (D_{50} > 500 nm) reichte. Diese Studie lieferte Einblicke in den größenabhängigen Partikeltransport durch Aerosolsammler und die Entwicklung einer elutionsbasierten Methode zur Abschätzung der druckabfallunabhängigen Sammeleffizienz.

Zusammenfassend lässt sich sagen, dass die vorgeschlagenen Konzepte und Systeme zur Erfassung und Sammlung atmosphärischer Metalle die Erfassung von Nanopartikeln und den Nachweis von Metallen auf Nanogrammebene ermöglichen, was einen neuen Weg zu einer kostengünstigen und mobilen Überwachung der Luftqualität mit hoher räumlicher Reichweite ebnen wird und zeitliche Auflösung. Angesichts der Tatsache, dass die elektrochemische Detektion eine flüssigkeitsbasierte Methode ist, ermöglichen diese Konzepte und Systeme die Bewertung der Metalltoxizität mit geeigneten Elektrolyten als Auslaugmittel. Darüber hinaus können diese Konzepte auch neue Einblicke in die Probenahme und den Nachweis anderer luftgetragener Komponenten liefern. Zur Abschätzung der Sammeleffizienz könnte die elutionsbasierte Methode zur Bewertung der Probenahmeleistung von Probenehmern und Untersuchungen des Partikelverhaltens während des Partikeleinfangs in Probenehmern beitragen.

Table of Contents

List of Abbreviations and Symbols

Abbreviations

PM	particulate matter
ROS	reactive oxygen species
UV/VIS	ultraviolet-visible
ICP-MS	inductively coupled plasma mass
SMPS	scanning mobility particle sizer
HPLC	high-performance liquid chromatography
GC	gas chromatography
CPC	condensation particle counter
XRF	X-ray fluorescence
DEHS	Di-Ethyl-Hexyl-Sebacat
PDMS	polydimethylsiloxane
RE	reference electrode
WE	working electrode
CE	counter electrode
IPA	Isopropyl alcohol
FTIR	Fourier transform infrared
DMA	Differential Mobility Analyzer
OCP	open circuit potential
CV	cyclic voltammetry
SWASV	square wave anodic stripping voltammetry
SW	square wave
FWHM	full width at half-maximum
IAE	integrated aerodynamic/electrochemical
PAN	polyacrylonitrile
AILE	aerosol-into-liquid electrode
DMF	N, N-dimethylformamide

RHE	reversible hydrogen electrode
SEM	scanning electron microscopy
RDE	rotating disk electrode
ASV	anodic stripping voltammetry
PTFE	polytetrafluoroethylene
MOUDI	Microorifice Uniform Deposit Impactor
ABS	acetate buffer solution
UPD	underpotential deposition
OPD	overpotential depositions
SWV	square wave voltammetry
LOD	limit of detection
PILS	particle-into-liquid sampler
ALF	artificial lysosomal fluid
APS	aerodynamic particle sizer
DMPS	Differential Mobility Particle Sizer
PSL	Polystyrene Latex

Symbols

C_{up}	upstream particle number
C_{down}	downstream particle number
η	collection efficiency
ø	diameter
R^2	the coefficient of determination
St	Stokes numbers
ρ_p	particle density
D_p	particle diameter
U_0	air velocity
C_C	Cunningham slip correction

ρ_g	air density
v_g	air viscosity
D_H	hydraulic diameter
Re	Reynolds number
W	mass flowrate of the air
μ	dynamic viscosity of the fluid
A	cross-sectional area
De	Dean number
R_c	radius of curvature of the path of the channel
d_p	50% cutoff diameter of particles
U	average jet velocity
D_j	diameter of the nozzle
Q	flow rate
V_0	velocity
S/W	ratio of the jet-to-plate distance to the jet diameter
N_P	total NaCl particle number
C_P	NaCl mass concentration in water
V_{sample}	volume of the liquid sample
V_P	volume of a single NaCl particle
η_{cal}	calculated collection efficiency
η_{CPC}	CPC-counted collection efficiency
C_{ICP}	Na concentration derived from ICP-MS measurements
C_{up}	mass concentration of Na in upstream particles
p_0	pressure at the reference state
λ_0	mean free path at the reference state
p	pressure

Table of Figures and Tables

Figures

Tables

References

[1] C.L.S. Wiseman, F. Zereini, Characterizing metal(loid) solubility in airborne PM10, PM2.5 and PM1 in Frankfurt, Germany using simulated lung fluids, *Atmospheric Environment*, **2014**, 89, 282-9, https://doi.org/10.1016/j.atmosenv.2014.02.055.

[2] V. Mugica-Álvarez, J. Figueroa-Lara, M. Romero-Romo, J. Sepúlveda-Sánchez, T. López-Moreno, Concentrations and properties of airborne particles in the Mexico City subway system, *Atmospheric Environment*, **2012**, 49, 284-93, https://doi.org/10.1016/j.atmosenv.2011.11.038.

[3] G. Zhang, H. Li, X. Wei, Z. Fu, Preliminary assessment of size distribution of airborne metals and metalloids in the urban aerosols of Guiyang, southwest China, *Atmospheric Pollution Research*, **2015**, 6, 635-43, https://doi.org/10.5094/APR.2015.072.

[4] V. Mohr, M. Miró, A. Limbeck, On-line dynamic extraction system hyphenated to inductively coupled plasma optical emission spectrometry for automatic determination of oral bioaccessible trace metal fractions in airborne particulate matter, *Analytical and Bioanalytical Chemistry*, **2017**, 409, 2747-56, 10.1007/s00216-017-0219-8.

[5] A. Limbeck, C. Wagner, B. Lendl, A. Mukhtar, Determination of water soluble trace metals in airborne particulate matter using a dynamic extraction procedure with on-line inductively coupled plasma optical emission spectrometric detection, *Analytica Chimica Acta*, **2012**, 750, 111-9, https://doi.org/10.1016/j.aca.2012.05.005.

[6] A. Mukhtar, V. Mohr, A. Limbeck, The suitability of extraction solutions to assess bioaccessible trace metal fractions in airborne particulate matter: a comparison of common leaching agents, *Environmental Science and Pollution Research*, **2015**, 22, 16620-30, 10.1007/s11356-015-4789-8.

[7] J.J. Figueroa-Lara, J.M. Murcia-González, R. García-Martínez, M. Romero-Romo, M. Torres Rodríguez, V. Mugica-Álvarez, Effect of platform subway depth on the presence of Airborne PM2.5, metals, and toxic organic species, *Journal of Hazardous Materials*, **2019**, 377, 427-36, https://doi.org/10.1016/j.jhazmat.2019.05.091.

[8] Q. Wang, Y. Ma, J. Tan, N. Zheng, J. Duan, Y. Sun, et al., Characteristics of size-fractionated atmospheric metals and water-soluble metals in two typical episodes in Beijing, *Atmospheric Environment*, **2015**, 119, 294-303, https://doi.org/10.1016/j.atmosenv.2015.08.061.

[9] A. Mukhtar, A. Limbeck, Recent developments in assessment of bio-accessible trace metal fractions in airborne particulate matter: A review, *Analytica Chimica Acta*, **2013**, 774, 11-25, https://doi.org/10.1016/j.aca.2013.02.008.

[10] E. von Schneidemesser, E.A. Stone, T.A. Quraishi, M.M. Shafer, J.J. Schauer, Toxic metals in the atmosphere in Lahore, Pakistan, *Science of The Total Environment*, **2010**, 408, 1640-8, https://doi.org/10.1016/j.scitotenv.2009.12.022.

[11] S.-P. Wu, X. Li, S.-H. Xiao, J. Zhang, J.J. Schwab, Solubility of aerosol minor and trace elements in Xiamen Island, Southeast China: Size distribution, health risk and dry deposition,

Science of The Total Environment, **2022**, 844, 157100, https://doi.org/10.1016/j.scitotenv.2022.157100.

[12] X. Luo, Z. Zhao, J. Xie, J. Luo, Y. Chen, H. Li, et al., Pulmonary bioaccessibility of trace metals in PM2.5 from different megacities simulated by lung fluid extraction and DGT method, *Chemosphere*, **2019**, 218, 915-21, https://doi.org/10.1016/j.chemosphere.2018.11.079.

[13] B. Leclercq, L.Y. Alleman, E. Perdrix, V. Riffault, M. Happillon, A. Strecker, et al., Particulate metal bioaccessibility in physiological fluids and cell culture media: Toxicological perspectives, *Environmental Research*, **2017**, 156, 148-57, https://doi.org/10.1016/j.envres.2017.03.029.

[14] X. Huang, J. Cheng, D. Bo, R. Betha, R. Balasubramanian, Bioaccessibility of Airborne Particulate-Bound Trace Elements in Shanghai and Health Risk Assessment, *Frontiers in Environmental Science*, **2016**, 4,

[15] B.T. Cartledge, B.J. Majestic, Metal concentrations and soluble iron speciation in fine particulate matter from light rail activity in the Denver-Metropolitan area, *Atmospheric Pollution Research*, **2015**, 6, 495-502, https://doi.org/10.5094/APR.2015.055.

[16] N.K. Gali, S.Y. Jiang, F. Yang, L. Sun, Z. Ning, Redox characteristics of size-segregated PM from different public transport microenvironments in Hong Kong, *Air Quality, Atmosphere & Health*, **2017**, 10, 833-44, 10.1007/s11869-017-0473-0.

[17] S.Y.N. Jiang, F. Yang, K.L. Chan, Z. Ning, Water solubility of metals in coarse PM and PM2.5 in typical urban environment in Hong Kong, *Atmospheric Pollution Research*, **2014**, 5, 236-44, https://doi.org/10.5094/APR.2014.029.

[18] S. Mbengue, L.Y. Alleman, P. Flament, Bioaccessibility of trace elements in fine and ultrafine atmospheric particles in an industrial environment, *Environmental Geochemistry and Health*, **2015**, 37, 875-89, 10.1007/s10653-015-9756-2.

[19] D. Voutsa, A. Anthemidis, G. Giakisikli, K. Mitani, A. Besis, A. Tsolakidou, et al., Size distribution of total and water-soluble fractions of particle-bound elements—assessment of possible risks via inhalation, *Environmental Science and Pollution Research*, **2015**, 22, 13412-26, 10.1007/s11356-015-4559-7.

[20] X. Huang, R. Betha, L.Y. Tan, R. Balasubramanian, Risk assessment of bioaccessible trace elements in smoke haze aerosols versus urban aerosols using simulated lung fluids, *Atmospheric Environment*, **2016**, 125, 505-11, https://doi.org/10.1016/j.atmosenv.2015.06.034.

[21] G. Polezer, A. Oliveira, S. Potgieter-Vermaak, A.F.L. Godoi, R.A.F. de Souza, C.I. Yamamoto, et al., The influence that different urban development models has on PM2.5 elemental and bioaccessible profiles, *Scientific Reports*, **2019**, 9, 14846, 10.1038/s41598-019-51340-4.

[22] Y. Sun, X. Hu, J. Wu, H. Lian, Y. Chen, Fractionation and health risks of atmospheric particle-bound As and heavy metals in summer and winter, *Science of The Total Environment*, **2014**, 493, 487-94, https://doi.org/10.1016/j.scitotenv.2014.06.017.

[23] N.J. Schleicher, S. Norra, F. Chai, Y. Chen, S. Wang, K. Cen, et al., Temporal variability of trace metal mobility of urban particulate matter from Beijing – A contribution to health impact assessments of aerosols, *Atmospheric Environment*, **2011**, 45, 7248-65, https://doi.org/10.1016/j.atmosenv.2011.08.067.

[24] N.M. Mahowald, D.S. Hamilton, K.R.M. Mackey, J.K. Moore, A.R. Baker, R.A. Scanza, et al., Aerosol trace metal leaching and impacts on marine microorganisms, *Nature Communications*, **2018**, 9, 2614, 10.1038/s41467-018-04970-7.

[25] B. Fang, H. Zeng, L. Zhang, H. Wang, J. Liu, K. Hao, et al., Toxic metals in outdoor/indoor airborne PM2.5 in port city of Northern, China: Characteristics, sources, and personal exposure risk assessment, *Environmental Pollution*, **2021**, 279, 116937, https://doi.org/10.1016/j.envpol.2021.116937.

[26] J. Malloy, A. Quintana, C.J. Jensen, K. Liu, Efficient and Robust Metallic Nanowire Foams for Deep Submicrometer Particulate Filtration, *Nano Letters*, **2021**, 21, 2968-74, 10.1021/acs.nanolett.1c00050.

[27] C.W. Haig, W.G. Mackay, J.T. Walker, C. Williams, Bioaerosol sampling: sampling mechanisms, bioefficiency and field studies, *Journal of Hospital Infection*, **2016**, 93, 242-55, https://doi.org/10.1016/j.jhin.2016.03.017.

[28] G.J. Parker, C.H. Ong, R.B. Manges, E.M. Stapleton, A.P. Comellas, T.M. Peters, et al., A Novel Method of Collecting and Chemically Characterizing Milligram Quantities of Indoor Airborne Particulate Matter, *Aerosol and Air Quality Research*, **2019**, 19, 2387-95, 10.4209/aaqr.2019.04.0182.

[29] E.O. Gaga, T. Harner, E. Dabek-Zlotorzynska, V. Celo, G. Evans, C.-H. Jeong, et al., Polyurethane Foam (PUF) Disk Samplers for Measuring Trace Metals in Ambient Air, *Environmental Science & Technology Letters*, **2019**, 6, 545-50, 10.1021/acs.estlett.9b00420.

[30] M. Pan, A. Eiguren-Fernandez, H. Hsieh, N. Afshar-Mohajer, S.V. Hering, J. Lednicky, et al., Efficient collection of viable virus aerosol through laminar-flow, water-based condensational particle growth, *Journal of Applied Microbiology*, **2016**, 120, 805-15, https://doi.org/10.1111/jam.13051.

[31] K.J. Heo, H.S. Ko, S.B. Jeong, S.B. Kim, J.H. Jung, Enriched Aerosol-to-Hydrosol Transfer for Rapid and Continuous Monitoring of Bioaerosols, *Nano Letters*, **2021**, 21, 1017-24, 10.1021/acs.nanolett.0c04096.

[32] Y. Guo, Y. Guo, W. He, Y. Zhao, R. Shen, J. Liu, et al., PET/TPU nanofiber composite filters with high interfacial adhesion strength based on one-step co-electrospinning, *Powder Technology*, **2021**, 387, 136-45, https://doi.org/10.1016/j.powtec.2021.04.020.

[33] Y.-B. Zhao, T. Cen, J. Tang, W. He, C. Ludwig, S.-C. Chen, et al., An elution-based method for estimating efficiencies of aerosol collection devices not affected by their pressure drops, *Separation and Purification Technology*, **2022**, 287, 120590, https://doi.org/10.1016/j.seppur.2022.120590.

[34] M. Pirhadi, A. Mousavi, S. Taghvaee, M.H. Sowlat, C. Sioutas, An aerosol concentrator/diffusion battery tandem to concentrate and separate ambient accumulation mode particles for evaluating their toxicological properties, *Atmospheric Environment*, **2019**, 213, 81-9, https://doi.org/10.1016/j.atmosenv.2019.05.058.

[35] J.H. Byeon, J. Hwang, J. Hong Park, K. Young Yoon, B. Ju Ko, S. Hoon Kang, et al., Collection of submicron particles by an electrostatic precipitator using a dielectric barrier discharge, *Journal of Aerosol Science*, **2006**, 37, 1618-28, https://doi.org/10.1016/j.jaerosci.2006.05.003.

[36] D.S. Kim, S.B. Hong, J.-T. Kwon, K. Park, Evaluation of particle growth systems for sampling and analysis of atmospheric fine particles, *Particuology*, **2011**, 9, 606-10, https://doi.org/10.1016/j.partic.2011.04.007.

[37] G. Qiu, M. Spillmann, J. Tang, Y.-B. Zhao, Y. Tao, X. Zhang, et al., On-Site Quantification and Infection Risk Assessment of Airborne SARS-CoV-2 Virus Via a Nanoplasmonic Bioaerosol Sensing System in Healthcare Settings, *Advanced Science*, **2022**, 9, 2204774, https://doi.org/10.1002/advs.202204774.

[38] D. Wang, M.H. Sowlat, M.M. Shafer, J.J. Schauer, C. Sioutas, Development and evaluation of a novel monitor for online measurement of iron, manganese, and chromium in

ambient particulate matter (PM), *Science of The Total Environment*, **2016**, 565, 123-31, https://doi.org/10.1016/j.scitotenv.2016.04.164.

[39] J. Mettakoonpitak, J. Volckens, C.S. Henry, Janus Electrochemical Paper-Based Analytical Devices for Metals Detection in Aerosol Samples, *Analytical Chemistry*, **2020**, 92, 1439-46, 10.1021/acs.analchem.9b04632.

[40] H. Sun, Y. Jia, H. Dong, L. Fan, Graphene oxide nanosheets coupled with paper microfluidics for enhanced on-site airborne trace metal detection, *Microsystems & Nanoengineering*, **2019**, 5, 4, 10.1038/s41378-018-0044-z.

[41] M.H. Sowlat, D. Wang, G. Simonetti, M.M. Shafer, J.J. Schauer, C. Sioutas, Development and field evaluation of an online monitor for near-continuous measurement of iron, manganese, and chromium in coarse airborne particulate matter (PM), *Aerosol Science and Technology*, **2016**, 50, 1306-19, 10.1080/02786826.2016.1221051.

[42] J. Mettakoonpitak, J. Mehaffy, J. Volckens, C.S. Henry, AgNP/Bi/Nafion-modified Disposable Electrodes for Sensitive Zn(II), Cd(II), and Pb(II) Detection in Aerosol Samples, *Electroanalysis*, **2017**, 29, 880-9, https://doi.org/10.1002/elan.201600591.

[43] J. Mettakoonpitak, D. Miller-Lionberg, T. Reilly, J. Volckens, C.S. Henry, Low-cost reusable sensor for cobalt and nickel detection in aerosols using adsorptive cathodic square-wave stripping voltammetry, *Journal of Electroanalytical Chemistry*, **2017**, 805, 75-82, https://doi.org/10.1016/j.jelechem.2017.10.026.

[44] M.R. Palomo-Marín, F. Rueda-Holgado, J. Marín-Expósito, E. Pinilla-Gil, Disposable sputtered-bismuth screen-printed sensors for voltammetric monitoring of cadmium and lead in atmospheric particulate matter samples, *Talanta*, **2017**, 175, 313-7, https://doi.org/10.1016/j.talanta.2017.07.060.

[45] F. Rueda-Holgado, E. Bernalte, M.R. Palomo-Marín, L. Calvo-Blázquez, F. Cereceda-Balic, E. Pinilla-Gil, Miniaturized voltammetric stripping on screen printed gold electrodes for field determination of copper in atmospheric deposition, *Talanta*, **2012**, 101, 435-9, https://doi.org/10.1016/j.talanta.2012.09.054.

[46] H.d.A. Silva-Neto, T.M.G. Cardoso, W.K.T. Coltro, R.C. Urban, Determination of bioavailable lead in atmospheric aerosols using unmodified screen-printed carbon electrodes, *Analytical Methods*, **2019**, 11, 4875-81, 10.1039/C9AY01301F.

[47] F. Rueda-Holgado, L. Calvo-Blázquez, F. Cereceda-Balic, E. Pinilla-Gil, A semiautomatic system for soluble lead and copper monitoring in atmospheric deposition by coupling of passive elemental fractionation sampling and voltammetric measurement on screen-printed gold electrodes, *Microchemical Journal*, **2016**, 124, 20-5, https://doi.org/10.1016/j.microc.2015.07.012.

[48] D. Wang, M.M. Shafer, J.J. Schauer, C. Sioutas, A new technique for online measurement of total and water-soluble copper (Cu) in coarse particulate matter (PM), *Environmental Pollution*, **2015**, 199, 227-34, https://doi.org/10.1016/j.envpol.2015.02.006.

[49] D. Wang, M.M. Shafer, J.J. Schauer, C. Sioutas, Development of a Technology for Online Measurement of Total and Water-Soluble Copper (Cu) in PM2.5, *Aerosol Science and Technology*, **2014**, 48, 864-74, 10.1080/02786826.2014.937478.

[50] Y.-B. Zhao, J. Tang, T. Cen, G. Qiu, W. He, F. Jiang, et al., Integrated aerodynamic/electrochemical microsystem for collection and detection of nanogram-level airborne bioaccessible metals, *Sensors and Actuators B: Chemical*, **2022**, 351, 130903, https://doi.org/10.1016/j.snb.2021.130903.

Chapter 1

Introduction

1.1 Airborne soluble metals

Airborne metals are commonly divided into earth crustal elements (Al, Ti, Fe, Mn, and Ca) and anthropogenic elements (As, Se, V, Ni, Cu, Zn, Pb, and Cd) [1]. The solubility and mobility of metals are linked to metal speciation, which largely depends on sources of atmospheric particles [2]. Besides that, the metal speciation in the atmosphere could be different from that in liquid media likely due to atmospheric transport, deposition, and inhalation processes related to particle sizes [3]. In particular, metal speciation will be modified during atmospheric transport by cloud evapocondensation cycles, photochemistry, and organic complexation [2]. Eventually, aerosol particles will reach the oceans and their effects on the marine biogeochemistry cycles depends on the solubilities [4]. Aerosol metals and their solubility are important to understand aerosol-cloud interactions [5], global biogeochemical cycle [4, 6, 7], indoor environment [8, 9], and aerosol toxicity [10-12].

In general, metal speciation states in the particulate matter consist of loosely bound, oxide/carbonate phases, crustal fraction [3]. The loosely bound fraction (e.g. adsorbed metals and salts) is the most exchangeable and environmentally mobile, and soluble [2]. The soluble fraction of metals has been defined such as water solubility, acid solubility, and bioaccessibility, depending on their extractability using different leaching agents, which could be achieved using sequential extraction procedures (e.g. Tessier scheme) and *in vitro* tests. The common leaching agents include water [13], buffer solutions, diluted acids. Following metal fractions with different mobilities can be distinguished using sequential extraction methods (e.g. Tessier sequential extractions scheme): soluble and exchangeable, carbonates, oxides and reducible, bound to organic matter, oxidizable and sulphidic, and residual fraction [14-17]. It is noted that the extraction from solid samples could lose or alter original metal compounds [18]. The *in vitro* tests with high efficiency and operability are the alternatives to *in vivo* tests, which have good correlations with *in vivo* tests [19]. The *in vitro* tests employ serum-based solutions, simulated gastric juices, simulated intestinal juices, surrogate lung fluids, simulated lung fluids (artificial lysosomal fluids and Gamble's solutions) [20, 21].

Airborne metals, in particular soluble fractions, have significant effects on aerosol-cloud interactions since they act as catalysts in aqueous-phase reactions [5]. Soluble metals have potential to catalyze reactions of sulfates and organic compounds in atmospheric water, and therefore affect redox cycles of these compounds [22, 23]. The oxidation of SO_2 catalyzed by transition metal ions on particle surface is a dominate pathway in global sulfate production, influencing the sulfate budget and cloud formation [24]. The photochemical dissociation of metals exerts their effects on budgets of hydrogen peroxide and OH radicals [2, 25]. The soluble concentration of metals is one of the most important factors in these reactions [26]. Airborne metals are also involved in global biogeochemical cycles through atmospheric transport, reaching soil-plant system [27] and ocean [28]. Extensive anthropogenic activities such as combustion and transportation alter global biogeochemical cycles of airborne metals and their solubility [29]. To assess and understand the effects of airborne metals on environment, it is of importance to understand their solubility in airborne aerosols.

Airborne metals in outdoor environments strongly affect the indoor air quality in the order of $PM_1 > PM_{2.5} > PM_{10}$ [30]. The size shift from accumulation mode to quasi-ultrafine or coarse particles was observed when particles penetrated indoors [31]. Seasonal variation of indoor airborne metals also indicated changes in size distribution patterns, and the mass peak of Pb, Mg, and K tends to shift towards larger particle sizes with a lower ventilation condition [32]. Indoor airborne metals are also strongly affected by human activities, ventilation, and outdoor emissions [33]. Ubiquitous airborne metals could significantly influence human health in indoor environments such as oxidative potential [9, 34] and DNA damage [35, 36], where people stay for most of their lives.

Metal elements in atmospheric particulate matter play crucial roles in health effects by enhancing toxicity and health risk [37]. In this regard, soluble metals are more closely correlated with human health exposure and diseases with inflammation [38], cardiotoxicity [39], whole-blood coagulation [40], enhanced pulmonary toxicity [20], and higher lung cancer rates [36], by causing DNA damages. In particular, As, Ni, and V are closely associated with cytokine induction/inhibition responses [38], while Zn and Cu could induce lung injury and inflammation [41]. Particle-bound Ni and V are potentially linked to cardiopulmonary diseases [42]. Nonetheless, metal solubility might vary under different conditions *in vivo*. For example, changes in Pb speciation could be observed post exposure of dust particles, and Pb ions possibly react with phosphates and organic ligands in lung fluid, and are adsorbed onto

metal oxides at neutral pH [43]. The fraction of soluble metals can be higher after particles are inhaled into alveolar regions (pH = 4.5) where the pH is much lower than that of interstitial fluids in the lung (pH = 7.4) [21].

1.2 Emission sources and their solubility

Global metal concentrations exhibit profound spatial variation mainly caused by anthropogenic activities, and Pb, As, Cr, and Zn in $PM_{2.5}$ at some places are higher by factors of 100 – 3000 than crustal concentrations [44]. The evidence showed that mineral aerosols are the major emission source of Al, Ti, Mn, and Fe, while combustion activities contribute to other metal elements, such as Cu, Zn, and Pb [28]. In particular, the main emission sources consist of vehicle emissions (Fe, Zn, Cu, Pb, Cr, and Cd), industrial activities (Mn, Zn, As, Hg, and Cd), coal combustion (Cr, As, Hg, and Co), particle resuspension (Ca, Mg, Fe, Al, Si, and Mn), and break wear (Fe, Zn, Mn, Ni, Cu, and Cr) [45]. Metal solubility varies with different aerosol sources [46]. The dissolution of metal from different emission sources varies [47], and changes in solubility are subject to different types of metals [48]. Metal solubilities depend on different metals, which also vary by folds for each metal (Figure 1). Smaller particles (PM_1 and $PM_{2.5}$) have a higher solubility compared to large particles (PM_{10}) (Figure 1.1a). In addition, the solubility in simulated body fluids is possibly higher than that in water and acetate buffer, suggesting an increasing toxicity after particle entering human body (Figure 1.1b).

The solubility of metals largely depends on different emission sources, and urban aerosols contained a higher fraction of soluble metals (e.g. Cd, Cu, Ni, and Zn) compared to industrial aerosols [49]. In another study, it was also found that the inhalation bioaccessibility of metals (e.g. Pb and Cd) in the urban area than that in the industrial area affected by lead smelting [50]. Despite that metal concentration in subway aerosols is higher, the solubility in subway aerosols is much lower compared to outdoor aerosols [51]. Secondary processes can also be a major source of soluble form of metals originated from primary emission sources due to the dissolution of metals during airborne particle aging [52].

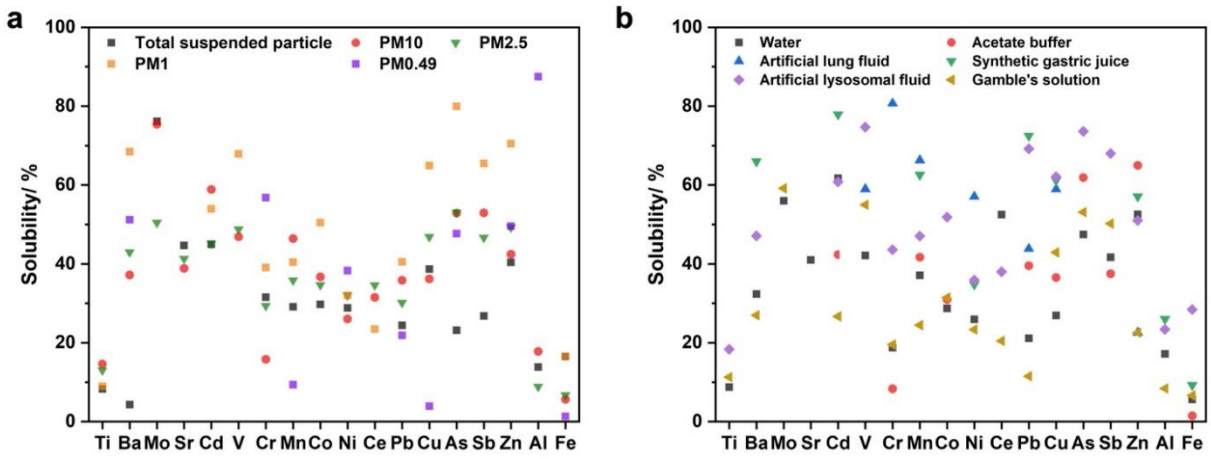

Figure 1.1. Soluble fractions of different airborne metals. The data was summarized based on references [20, 51, 53-73].

After being released into atmosphere from emission sources, aerosol particles experience through atmospheric transport, processes, and deposition (Figure 1.2a). Cloud droplets, raindrops, and ice particles during cloud processes favor the interactions among gas, particles, water, liquid, and ice, which play important roles in cloud radiative properties and atmospheric chemistry [2]. The solubility decreases when metals are transferred from clouds (e.g., pH 2) to rainwater (e.g. pH 5.5) [74]. It is noted that a fraction of mercury is released as gaseous elemental Hg and $HgCl_2$ with oxidation and photoreduction reactions in the atmosphere [75]. Gaseous elemental Hg has a long atmospheric residence time of about 1 year [76], which is much longer than that of particle-bound metals.

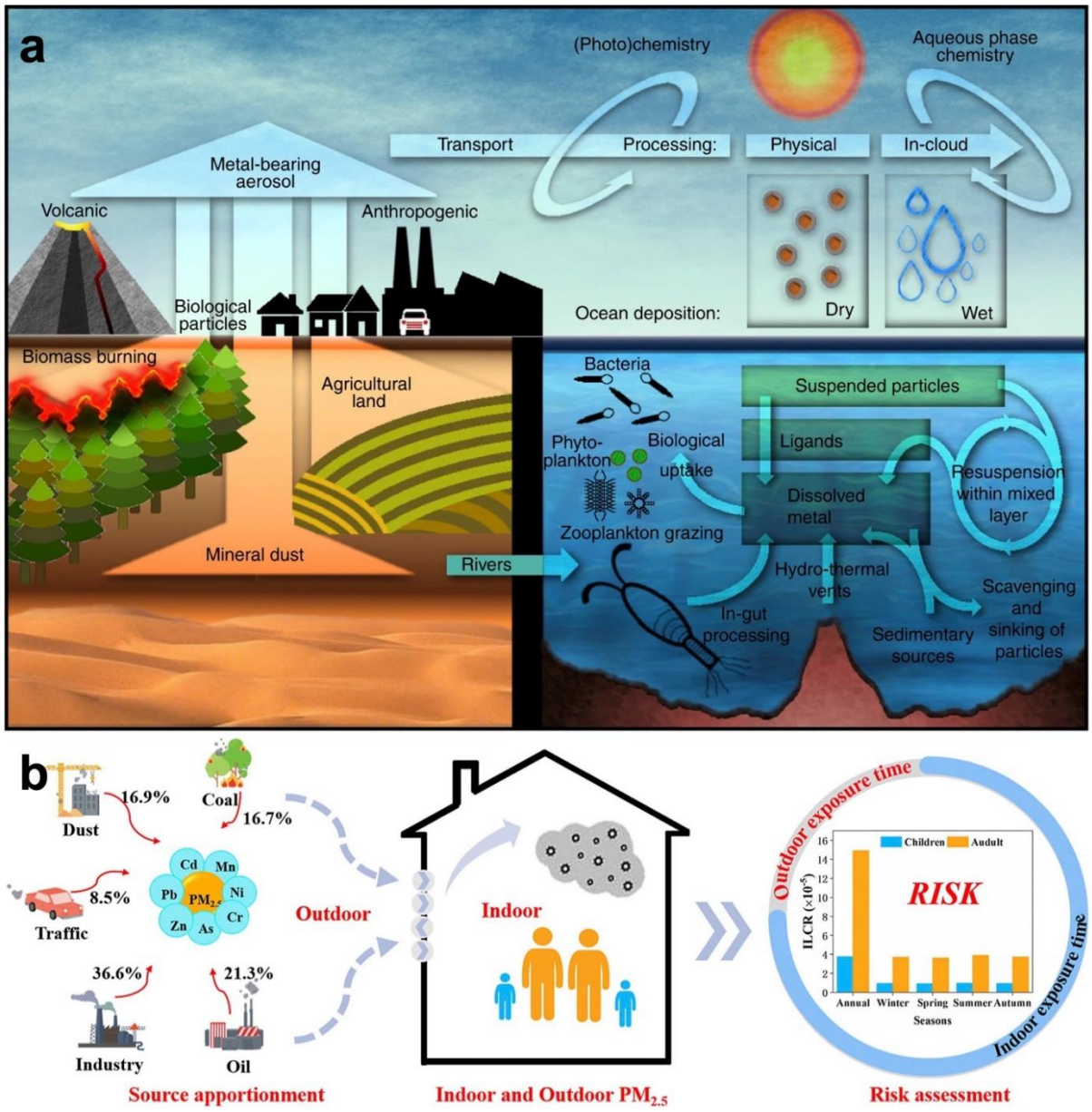

Figure 1.2 (a) Schematic of airborne metal processes [28], (b) outdoor-to-indoor transport from various emission sources [77].

Airborne metals also participate the aerosol exchange between outdoor and indoor environments, resulting in exposure risks (Figure 1.2b). In general, the concentration level of metals reduces in the order of urban aerosol > outdoor aerosol > indoor aerosol [78]. Nonetheless, the trend of dominated metal concentrations was in the similar order for both outdoors and indoors [79]. The ratio of indoor/outdoor concentration suggested that most of indoor metals originated from outdoor emission sources [77]. The indoor aerosol is mainly affected by human activities, indoor emission sources, and outdoor atmospheric particles [33]. In particular,

a comparison of $PM_{2.5}$ metal concentration in indoor environment showed that resident activates led to a higher concentration of soluble fraction [80]. Several emission sources of toxic metals are identified in indoor office environment, such as printing and environmental tobacco smoking [81]. The oxidative potential induced by water-soluble metals were different in indoor environment settings including office, laboratory, and home [9].

The Metal exchange between the pedosphere-atmosphere interface is a significant component affecting the airborne metal solubility. Metals in resuspended particles significantly affect the metal components in both indoor and outdoor particulate matter [82]. Lead in London airborne particles released during the 20th century is persistently an important source in urban environments [83]. Resuspended dust accounts for 38.1 ± 9.7 % of coarse particle mass with an aerodynamic size of 0.9 – 11.5 μm in the traffic environment [84]. In indoor environment, resuspension plays an important role in indoor particulate matter (PM) compared to other indoor emission sources, which increases the particle in the size range of 0.7 – 10 μm [85]. Volatile metals such as Hg have the potential to reenter the atmosphere from soil due to many factors such as their species (Hg^0 and dimethyl-Hg), and concentration in soil and air [86].

1.3 Environmental and Health Effects Related to the Particle Size-Dependent Solubility

Generally, crustal metals such as Fe and Mg were concentrated in coarse particles, whereas toxic metals such as Pb and Cd, were distributed in fine fractions [87]. Many studies found that urban aerosols tend to have a higher metal solubility than crustal aerosols, which is likely due to different emission sources and processes contributing to these two types of aerosols [3]. In this regard, urban aerosols are largely attributed to anthropogenic processes related to the loosely bound metals likely due to high temperature processes, while crustal aerosols are associated with weathering of crustal materials with the aluminosilicate lattice [3]. Metal solubility in fine mode can be higher than that in coarse mode, indicating size-dependent chemical states [88, 89], which renders a longer transport range of bioavailable metals. It is also the case that soluble metals such as Zn and Cu concentrate on particles smaller than 2.1 μm in indoor environments, implying a higher health risk of small particles [35].

Health issues are particle size-dependent, and smaller particles will penetrate deeper in the respiratory system [90] and increase the reactive oxygen species (ROS) activities [91]. In general, particles with an aerodynamic diameter larger than 3.2 μm deposit in the extrathoracic

region, whereas ultrafine particles smaller than 0.18 μm can penetrate into the pulmonary alveoli [9]. Metals concentrated in small particles (e.g., $PM_{2.5}$) exhibit a stronger solubility and toxicity, compared to those in large particles. Soluble fractions in certain size ranges on toxicity agents, such as ROS [10]. In coal-burning indoor environments, water-soluble Zn, Cu, Cd, Rb, Cs, and Sb primarily exit in smaller particles, which positively correlate with DNA damage [35]. Particulate Cu, Mn, and Fe in fine particles ($PM_{3.2}$) were strongly correlated with water-soluble oxidative potential in indoor environments (office, home, and lab) [9]. Metals such as Pb, Cr, Cd, and Zn were also found enriched in outdoor particles smaller than 2 μm, which predominately cause DNA damage by relaxing and linearizing the supercoiled DNA [92]. Size also matters when we consider the deposition efficiency of particles in our respiratory system. It found that metal-rich particle size (0.18 – 0.55 μm) overlaps with the hygroscopic mode (0.10 – 0.32 μm), which can lead to a higher deposition efficiency of metals in the respiratory system [93]. The small particles with high surface area might facilitate the Pb dissolution and adsorption in the lung to rapidly increase tissue Pb concentration during the Pb exposure in the first 0.25 h [43].

1.4 Dry Sampling Techniques for Airborne Metals

Airborne metal solubility and their toxicity might exhibit variations in terms of particle size. Therefore, it is important to select proper sampling devices and their couplings based on targeted particle sizes and metal phases as sampling devices have various collection efficiencies of 0 – 100 % and applicable size ranges of nanoparticles and microparticles. There are two main sampling techniques including dry and wet sampling techniques. Proper sample preparation after sampling is needed to satisfy the determination of airborne metals and their soluble fractions.

Dry sampling techniques tend to collect dry particles without involving the step of particle dissolution, the extraction of collected aerosol particles using solutions (e.g., acetate buffer and deionized water) is therefore employed to obtain samples for determining different solubility of metals and mimic the adsorption in body fluids [56, 59, 94-96]. Dry sampling techniques including active and passive sampling have been widely developed in aerosol sampling studies, and several mechanisms are employed in the design and development of the dry sampling techniques, such as filtration, impaction, electrostatic precipitation, or a combination [97]. In order to achieve the size-resolved sampling of airborne particles, cascade impactors or

sampling units with different sampling size ranges in sequence are utilized. The advantages and disadvantages of sampling techniques are summarized in previous reviews [98, 99].

Filters are one of the most commonly used tools to collect large mass of aerosols with high collection efficiency and sampling volume [97, 100]. Particles larger than 0.5 μm can be captured by interception or inertial impaction on filter fibers, while particles with a size smaller than 0.3 μm are captured via Brownian motion due to a particle concentration gradient, and bonded to filter fibers by van der Waals forces (Figure 1.3a) [101]. Diffusion battery is specifically used to capture particles smaller than 0.2 μm [102], which might be suitable for evaluating toxicological properties of ultrafine particles. Inertial force is widely used to develop aerosol samplers and collect aerosol particles [103], and the commonly used devices are impaction-based samplers in which particles with sufficient stokes number going through nozzles deviate from streamlines and hit the impaction surface [97]. Filters applied on impaction-based samplers should be carefully selected, and it is noted that aluminum foils are used for collection and determination of soluble metals with proper sample preparation to avoid contaminations from aluminum foils. Several sampling methods such as impactors, cyclones, virtual impactors, and slit impactors employ the centrifugal force and inertia to separate particles from streamlines depending on particle sizes (Figure 1.3b) [27, 104]. For electrostatic collection, particles are imparted electrostatic charges and deposited by electrostatic attraction or repulsion in electrostatic precipitators or collectors with a lower deposition velocity than inertia-based techniques (Figure 1.3c) [97, 100].

Conventional sampling devices are metal-based and glass-based, while microfluidics is an emerging technique employed in the development of miniaturized and low-cost samplers [103]. Novel efforts have been made to improve the collection performance of samplers in different settings. For example, an aerosol size separator was developed using inertial microfluidics to separate particles (> 3 μm, 1 – 2 μm, < 0.5 μm) according to inertial differences and Dean vortices, which contains two curved channels and three outlets [105]. Some other different shapes of microfluidic air samplers have also been developed such as 3-loop double-spiral microchannel [103].

Besides active sampling techniques, passive samplers employ gravity or electrostatic forces to collect aerosol particles without power supplies [97]. It is noted that active sampling enables

the quantitative determination of aerosol components, whereas passive sampling is treated as a qualitative way to collect aerosol particles due to the unknown sampling volume [97]. Although the sampling air volume can be estimated by using an active sampling with a 100 % collection efficiency, the passive samplers might deliver different information of aerosol components due to different collection sizes and other parameters [106]. Polyurethane foam disk samplers are proposed to passively collect ambient metals weekly or monthly for measurement of 25 trace metals (Figure 1.3d) [107]. For mercury, sampling strategies can be developed to differentiate elemental Hg and Hg(II) according to its volatile properties. Passive air samplers using sulfur-impregnated activated carbon as the sorbent are used to capture gaseous mercury, which is primarily elemental Hg [76], while quartz filters and quartz chips can be used to sample particle-bound Hg [108]. Biomonitoring by mosses and lichens as samplers is also a satisfied way to investigate environments and air pollutants, with strong relationships between metal levels in mosses or lichens and atmospheric depositions [109, 110].

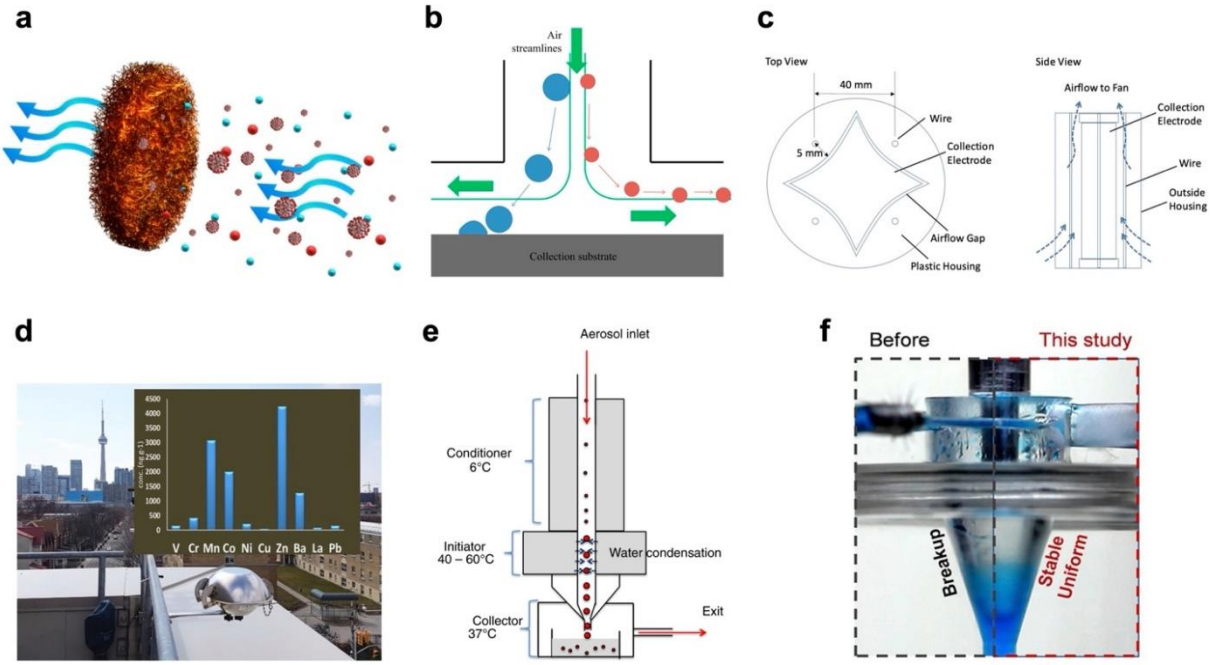

Figure 1.3 Dry and wet sampling techniques. (a) filtration [101], (b) impaction [99], (c) electrostatic precipitation [100], (d) passive samplers [107], (e) particle condensation growth [111], (f) wet surface sampling [112].

1.5 Wet Sampling Techniques for Airborne Metals

Wet sampling techniques capture particles with the assistance of liquid contents (such as water vapor and liquid film), which introduce the step of particle dissolution and sample extraction during the sampling stage [113]. In general, there are two approaches to perform wet sampling, including particle condensation growth (Figure 1.3e) [111, 114-117] and wet surface sampling (Figure 1.3f) [112, 118], which can be used in the capture and dissolution of aerosol particles, sample preparation, and instrumental coupling. Particle condensation growth is achieved by setting two (hot/cool or cool/hot) or three (hot/cool/hot) temperature zones to make particles grow up to micrometer levels by condensing liquid on particle surface, which are readily captured due to higher inertial forces. The sampled growing particles are collected in a slurry form as the prepared analytes, for offline chemical analysis or directly delivered to coupled sensing platforms in a continuous manner [119]. The limit of detection for the coupled detection instruments could be limited by the wet sampling volume of condensed particles [120].

For wet surface sampling methods, aerosol particles are collected on liquid surfaces rather than solid surfaces. In principle, an overlying thin liquid film above solid surfaces [121] or completely liquid medium achieves the purpose of wet sampling. Then the liquid is aliquoted and determined by coupling detection units (e.g. spectrometry and spectroscopic techniques). Inertial force is the main mechanism to separate particles from the streamlines into liquid mediums. For example, a cyclone assisted by a layer of liquid medium was designed to capture aerosol larger than 0.5 μm into liquid continuously with 95 % collection efficiency [112, 121]. Liquid mediums are also used to achieve impingement such as AGI impingers, and a recent impinger with three nozzles called BioSampler combines centrifugal impaction and impingement. The coupling of the BioSampler with ICPMS enables the determination of coarse particles with a time resolution of 17 min [119]. The microfluidic technique is also used to design wet sampling using two-phase fluid to transfer particles into the liquid phase driven by particle inertial differences, which can achieve a collection efficiency of 98 % for 1 μm particles [122]. This technique can also realize the miniaturization of conventional wet air samplers such as impinger [123]. Besides inertial microfluidics, some functional units such as unipolar charging chamber and electrostatic precipitation electrode can also be integrated into the microfluidic sampler to achieve particle sampling [124].

Figure 1.4 listed examples of sampling performance of different dry and wet samplers. Different samplers exhibit various sampling performance in terms of particle size, indicating a careful selection of aerosol samplers that fit in specific purposes. In comparison to other sampling techniques, particle condensation growth could achieve a high collection efficiency (about 100 %). However, the combination of other techniques also improves the sampling performance in studies.

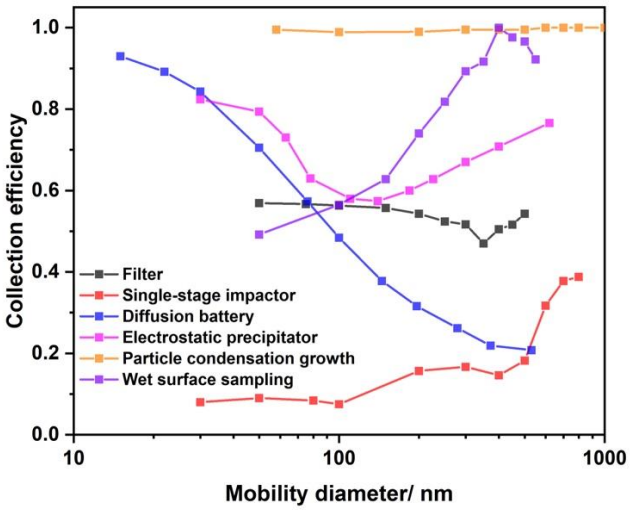

Figure 1.4 Examples of collection efficiencies of dry and wet sampling techniques in the submicron particle size range [102, 104, 125-128].

1.6 Spectroscopic and Mass Spectrometry Techniques

After particle collection with or without sample preparation, coupling strategies of sampling techniques with selected detection platforms are required for further metal determination. The main detection techniques for metals consist of spectroscopic and mass spectrometry, and electrochemical techniques.

Spectroscopic techniques are the powerful tools to determine total metals, which are often employed as the sensing platform coupling with aerosol sampling units (Figure 1.5a) [129-131]. In the available studies, ultraviolet-visible (UV/VIS) spectrophotometry [129, 130] and colorimetric methods [131] are coupled with particle collection modules to measure airborne metal concentrations rapidly and accurately. Colorimetric methods are alternative ways to measure specific metals using a liquid spectrophotometer according to the assumption that the

ligands specifically react with the target metals resulting in a light-absorbing complex [52]. In comparison with mass spectrometer methods, only a specific metal can be measured per analysis in colorimetric methods such as Fe, Cu, Pb, Ni, As, Sr, Hg, and Cr [132], which are however, portable, low-cost, and able to be connected to a sampling unit for offline or online measurements with possible identification of soluble metal speciation [52]. For example, an integrated system consisting of unmanned aerial sampling, graphene oxide-coated paper devices, and cellphone-based colorimetric detection enabled the measurement of Fe, Cu, and Ni within 30 min with a detection limit at the nanogram level [131].

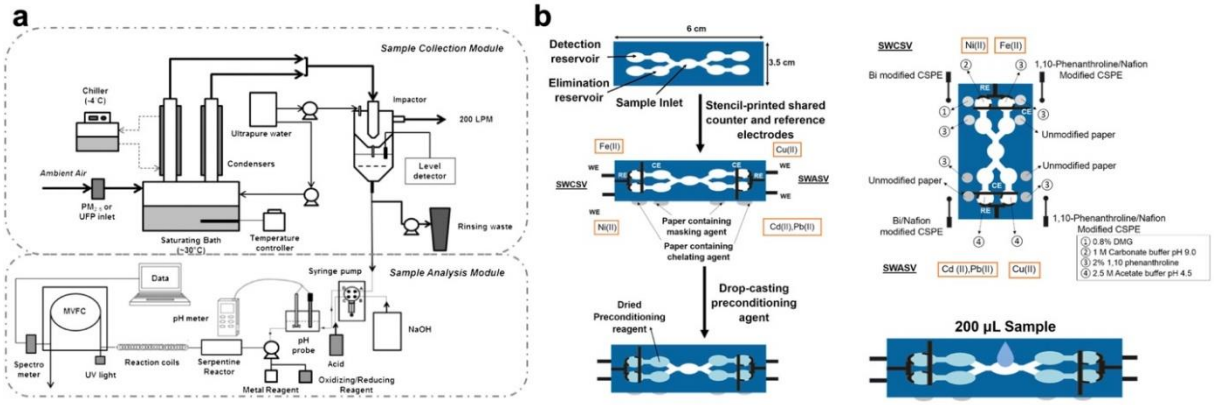

Figure 1.5 Detection techniques of airborne metals. (a) spectroscopic [129] and (b) electrochemical techniques [133].

Inductively coupled plasma mass (ICP-MS) is the commonly used mass spectrometry as a standard method for quantifying metals. There are also several studies achieving real-time measurement of aerosol metals, such as Extractive Electrospray Ionization Mass Spectrometry and Scanning Mobility Particle Sizer (SMPS)-ICP-MS coupling [134, 135]. An extractive electrospray ionization source was coupled with a time-of-flight mass spectrometer to achieve the detection of aerosol metals with a limit of detection of low ng/m^3 and a fast response time of 1 s [134]. ICP-MS was coupled with SMPS to obtain the particle size and chemical information simultaneously [135]. Single-particle ICP-MS is able to rapidly determine size, mass, concentration, and composition of metal nanoparticles at a level of individual particles [136].

The combination of spectroscopic and mass spectrometric techniques can maintain the efficient separation of complex species and sensitive measurements simultaneously [137]. High-performance liquid chromatography (HPLC)-ICP-MS [138, 139] and Gas chromatography

(GC)-ICP-MS [137, 140] has been developed to measure speciation of metals in different chemical forms, such as As, Se, Sb, Hg, Sn, and Pb.

1.7 Electrochemical Techniques

Voltammetry and potentiometry are the main methods to detect aerosol metals in the aqueous phase in a low-cost and portable way, using paper-based and screen-printed electrodes [133, 141-146] and ion selective electrodes [147, 148] respectively. Paper-based electrochemical electrodes achieve simultaneous detection of multiple metals such as Cu, Pb, Ni, and Fe by integrating several working electrodes in the same platform (Figure 1.5b). Screen-printed electrodes employ oxidation current peaks of accumulated metal ions on the electrode surface, while ion selective electrodes utilize highly selective ionophores to obtain zero-current membrane potential linked to the free ion activity of the target [149]. Both methods determine the concentration of metal ions rather than total metals, which can be used to differentiate the metal speciation. Screen-printed electrodes consist of three electrodes including the working electrode, counter electrode, and reference electrode. Several commonly used electrodes such as glass carbon, dropping mercury, noble metal, and nanomaterial-modified electrodes widely serves as working electrodes to detect metal ions [150]. Ion selective electrodes employ designed ionophores to complex, interact, and hold the target metals in molecular cavities [151]. However, their sensing performance are limited by interferences from other metal ions with similar responses, which can be addressed using multivariate calibration methods such as mathematical regression and artificial intelligent methods [151] or screening highly selective ionophores [152].

To realize the on-site, low-cost, and mobile detection of airborne metals, spectroscopic (colorimetric and UV/VIS methods) and electrochemical (voltammetry and potentiometry) methods are mainly used to couple with aerosol sampling techniques. As shown in Figure 1.6, electrochemical techniques especially voltammetry are more widely used in the determination of multiple metals with a possible detection limit lower than 1 µg/L, which is comparable to those using UV/VIS. In contrast, colorimetric methods and potentiometry exhibit a poorer limit of detection of around 10 µg/L. Nonetheless, novel coupling strategies and design with

aerosol sampling might be made to achieve a lower detection limit of airborne concentration (ng/m^3) when using these two techniques.

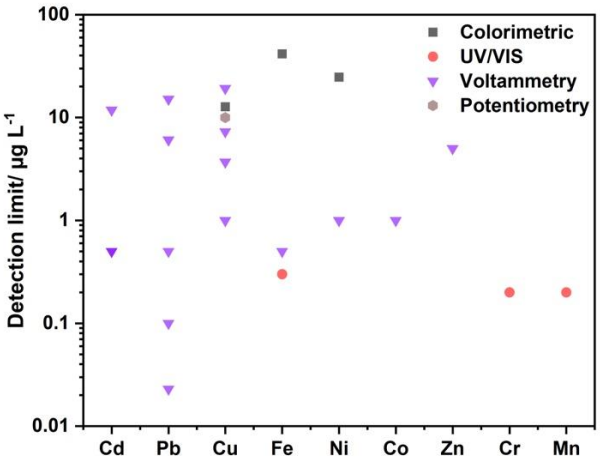

Figure 1.6 Limit of detection of airborne metals using spectroscopic (colorimetric and UV/VIS methods) and electrochemical (voltammetry and potentiometry) techniques in terms of aqueous metal concentration [129-131, 133, 141-148, 153].

1.8 Research Objectives and Outline of the Thesis

Transition metals in the atmosphere are raising a significant threat to human health and the environment, which are now considered a poorly-understood global problem requiring time-consuming efforts of sampling and analysis. More importantly, the soluble fraction of particle-bound transition metals enhances the persistent toxicity and health effects, which is particularly harmful to humans due to its toxicity and bioaccessibility, accounting for 0 – 80 % of total metals in airborne particulate matter (PM). Therefore, the detection of the soluble fraction in particle-bound transition metals is of great significance for public health, ideally in a cost-effective and mobile way. Nonetheless, the monitoring techniques of atmospheric soluble metals is constrained due to their low concentrations and technique limitations. For example, the extraction of airborne soluble metals usually requires time-consuming efforts, such as submicron filter filtration after sonication. After the development of sampling and detection platforms for airborne soluble metals, it becomes hard to estimate the sampling performance using the conventional upstream and downstream particle counting under high pressure drops out of working ranges. Higher pressures drops indicate higher flow rates and larger amount of

collected particle mass in environmental applications, which requires alternative ways to evaluate the sampling performance under various pressure drops.

This thesis intends to develop new strategies and concepts of capture and detection of airborne soluble metals, unlike the conventional coupling of sampling and detection units in sequence, and explore the possibilities of measuring collection efficiencies of samplers under high pressure drop, which can cause the malfunction of aerosol measure instruments. The main goals of this thesis are: (1) to develop an microfluidic-based microsystem to allow user-defined sampling time, and elimination of sample transfer and loss (Chapter 2); (2) to propose a concept that enable the one-step aerosol sampling/electrochemical detection, which might open up a way to online monitoring of atmospheric soluble metals (Chapter 3); (3) to present an alternative way to evaluate the sampling performance of samplers under various pressure drops, which can also be used as the tracer in the investigation of particle processes and behaviors during particle sampling (Chapter 4).

In Chapter 2 and 3, the new strategies and concepts of integrated sampling and detection of atmospheric soluble metals on the same platform to avoid the coupling of sampling and detection units in sequence. In general, a dual-functional interface is created for both sampling and subsequent detection, which could also eliminate sample transfer and loss. The proposed microsystem in Chapter 2 is subject to different sampling duration to ensure the sufficient collection of airborne metals, which are detected by the integrated electrochemical electrode afterwards. In contrast, the system proposed in Chapter 3 uses a gas/liquid interface to realize the capture and detection in a continuous manner. That is, soluble metals are collected on the membrane electrode and diffuse through the nanofiber membrane, which finally reach the electrode surface rapidly. Therefore, it might be developed as an online monitoring system in the future. In Chapter 4, the alternative method for estimating the sampling performance of developed samplers and systems is proposed, as condensation particle counter (CPC) is not able to work properly with a relatively high pressure drop induced by a high flow rate.

Chapter 2 presents an integrated aerodynamic/electrochemical microsystem for collection and detection of nanogram-level airborne bioaccessible metals. Aerosol collection and metal detection were achieved on the same microplatform. Bioaccessible fraction of metals at the

nanogram-level in the atmosphere were the main target. The microsystem was developed for atmospheric routine monitoring and air quality control. This work is published as

Zhao, Y.B., Tang, J., Cen, T., Qiu, G., He, W., Jiang, F., Yu, R., Ludwig, C. and Wang, J. Integrated aerodynamic/electrochemical microsystem for collection and detection of nanogram-level airborne bioaccessible metals. *Sensors and Actuators B: Chemical*. **2022**, *351*. 10.1016/j.snb.2021.130903.

Chapter 3 proposes a concept of aerosol-into-liquid capture and detection that bridges free-flowing gas and static liquid phases to realize one-step capture and detection via the gas/liquid interface, unlike conventional strategies of sampling and detection units in sequence. The system presents effective capture of airborne ultrafine particles and detection of soluble metals at the nanogram level in a direct and cost-effective way, which is demonstrated by real-world samples and might be potentially applied in air quality monitoring, especially for abrupt air pollution events (e.g. wildfires and fireworks). The manuscript of this work has been under review in *Proceedings of the National Academy of Sciences of the United States of America*.

Chapter 4 reports an elution-based method to estimate collection efficiency of samplers not affected by pressure drops and the applicable size range of the method is determined. Size redistribution of downstream monodisperse aerosol is revealed through the proposed method. This work is published as

Zhao, Y.B., Cen, T., Tang, J., He, W., Ludwig, C., Chen, S.C. and Wang, J. An elution-based method for estimating efficiencies of aerosol collection devices not affected by their pressure drops. *Separation and Purification Technology* **2022**, *287*. 10.1016/j.seppur.2022.120590.

In Chapter 5, the results about the integrated aerodynamic/electrochemical systems in Chapter 2 and 3 and the results about the estimation method for collection efficiency in Chapter 4 are summarized, and future perspectives are listed and discussed.

1.8 References

[1] X. Wang, X. Bi, G. Sheng, J. Fu, Chemical Composition and Sources of PM10 and PM2.5 Aerosols in Guangzhou, China, *Environmental Monitoring and Assessment*, **2006**, 119, 425-39, 10.1007/s10661-005-9034-3.

[2] L. Deguillaume, M. Leriche, K. Desboeufs, G. Mailhot, C. George, N. Chaumerliac, Transition Metals in Atmospheric Liquid Phases: Sources, Reactivity, and Sensitive Parameters, *Chemical Reviews*, **2005**, 105, 3388-431, 10.1021/cr040649c.

[3] L.J. Spokes, T.D. Jickells, Speciation of Metals in the Atmosphere, Chemical Speciation in the Environment2002, pp. 159-87.

[4] P. López-García, M.D. Gelado-Caballero, C. Collado-Sánchez, J.J. Hernández-Brito, Solubility of aerosol trace elements: Sources and deposition fluxes in the Canary Region, *Atmospheric Environment*, **2017**, 148, 167-74, https://doi.org/10.1016/j.atmosenv.2016.10.035.

[5] K.W. Fomba, D. van Pinxteren, K. Müller, Y. Iinuma, T. Lee, J.L. Collett Jr, et al., Trace metal characterization of aerosol particles and cloud water during HCCT 2010, *Atmos Chem Phys*, **2015**, 15, 8751-65, 10.5194/acp-15-8751-2015.

[6] A.R. Baker, T.D. Jickells, Mineral particle size as a control on aerosol iron solubility, *Geophysical Research Letters*, **2006**, 33, https://doi.org/10.1029/2006GL026557.

[7] A.S. Wozniak, R.U. Shelley, S.D. McElhenie, W.M. Landing, P.G. Hatcher, Aerosol water soluble organic matter characteristics over the North Atlantic Ocean: Implications for iron-binding ligands and iron solubility, *Marine Chemistry*, **2015**, 173, 162-72, https://doi.org/10.1016/j.marchem.2014.11.002.

[8] F. Yang, C. Liu, H. Qian, Comparison of indoor and outdoor oxidative potential of PM2.5: pollution levels, temporal patterns, and key constituents, *Environment International*, **2021**, 155, 106684, https://doi.org/10.1016/j.envint.2021.106684.

[9] H.-b. Guo, M. Li, Y. Lyu, T.-t. Cheng, J.j. Xv, X. Li, Size-resolved particle oxidative potential in the office, laboratory, and home: Evidence for the importance of water-soluble transition metals, *Environmental Pollution*, **2019**, 246, 704-9, https://doi.org/10.1016/j.envpol.2018.12.094.

[10] T. Fang, H. Guo, L. Zeng, V. Verma, A. Nenes, R.J. Weber, Highly Acidic Ambient Particles, Soluble Metals, and Oxidative Potential: A Link between Sulfate and Aerosol Toxicity, *Environmental Science & Technology*, **2017**, 51, 2611-20, 10.1021/acs.est.6b06151.

[11] A.P. Ault, Aerosol Acidity: Novel Measurements and Implications for Atmospheric Chemistry, *Accounts of Chemical Research*, **2020**, 53, 1703-14, 10.1021/acs.accounts.0c00303.

[12] E. Kogianni, C. Samara, T. Lialiaris, Genotoxicity induced in vitro by water-soluble indoor PM2.5 fractions in relation to heavy metal concentrations, *Environmental Monitoring and Assessment*, **2021**, 193, 82, 10.1007/s10661-021-08884-8.

[13] A.G. Galon-Negru, R.I. Olariu, C. Arsene, Size-resolved measurements of PM2.5 water-soluble elements in Iasi, north-eastern Romania: Seasonality, source apportionment and potential implications for human health, *Science of The Total Environment*, **2019**, 695, 133839, https://doi.org/10.1016/j.scitotenv.2019.133839.

[14] A.V. Filgueiras, I. Lavilla, C. Bendicho, Chemical sequential extraction for metal partitioning in environmental solid samples, *Journal of Environmental Monitoring*, **2002**, 4, 823-57, 10.1039/B207574C.

[15] A.J. Fernández Espinosa, M. Ternero Rodríguez, F.J. Barragán de la Rosa, J.C. Jiménez Sánchez, A chemical speciation of trace metals for fine urban particles, *Atmospheric Environment*, **2002**, 36, 773-80, https://doi.org/10.1016/S1352-2310(01)00534-9.

[16] J.X.C.Y. Anen He, Heavy Metal Speciation Analysis and Distribution Characteristics in Atmospheric Particulate Matters, *Progress in Chemistry*, **2021**, 33, 1627-47,

[17] Z. Zhao, Y. Jing, X.-S. Luo, H. Li, M. Tang, Overview and Research Progresses in Chemical Speciation and In Vitro Bioaccessibility Analyses of Airborne Particulate Trace Metals, *Current Pollution Reports*, **2021**, 7, 540-8, 10.1007/s40726-021-00200-9.

[18] M.M. Nearing, I. Koch, K.J. Reimer, Complementary arsenic speciation methods: A review, *Spectrochimica Acta Part B: Atomic Spectroscopy*, **2014**, 99, 150-62, https://doi.org/10.1016/j.sab.2014.07.001.

[19] J.-J. Xie, C.-G. Yuan, J. Xie, Y.-W. Shen, K.-Q. He, K.-G. Zhang, Speciation and bioaccessibility of heavy metals in PM2.5 in Baoding city, China, *Environmental Pollution*, **2019**, 252, 336-43, https://doi.org/10.1016/j.envpol.2019.04.106.

[20] C.L.S. Wiseman, F. Zereini, Characterizing metal(loid) solubility in airborne PM10, PM2.5 and PM1 in Frankfurt, Germany using simulated lung fluids, *Atmospheric Environment*, **2014**, 89, 282-9, https://doi.org/10.1016/j.atmosenv.2014.02.055.

[21] C. Colombo, A.J. Monhemius, J.A. Plant, Platinum, palladium and rhodium release from vehicle exhaust catalysts and road dust exposed to simulated lung fluids, *Ecotoxicology and Environmental Safety*, **2008**, 71, 722-30, https://doi.org/10.1016/j.ecoenv.2007.11.011.

[22] Y. Zuo, J. Hoigné, Photochemical decomposition of oxalic, glyoxalic and pyruvic acid catalysed by iron in atmospheric waters, *Atmospheric Environment*, **1994**, 28, 1231-9, https://doi.org/10.1016/1352-2310(94)90270-4.

[23] D.J. Jacob, M.R. Hoffmann, A dynamic model for the production of H+ NO3 −, and SO4 2− in urban fog, *Journal of Geophysical Research: Oceans*, **1983**, 88, 6611-21, https://doi.org/10.1029/JC088iC11p06611.

[24] E. Harris, B. Sinha, D. van Pinxteren, A. Tilgner, K.W. Fomba, J. Schneider, et al., Enhanced Role of Transition Metal Ion Catalysis During In-Cloud Oxidation of SO2, *Science*, **2013**, 340, 727-30, 10.1126/science.1230911.

[25] L.J. Spokes, T.D. Jickells, B. Lim, Solubilisation of aerosol trace metals by cloud processing: A laboratory study, *Geochimica et Cosmochimica Acta*, **1994**, 58, 3281-7, https://doi.org/10.1016/0016-7037(94)90056-6.

[26] A.G. Clarke, M. Radojevic, Oxidation of SO2 in rainwater and its role in acid rain chemistry, *Atmospheric Environment (1967)*, **1987**, 21, 1115-23, https://doi.org/10.1016/0004-6981(87)90238-1.

[27] X. Luo, H. Bing, Z. Luo, Y. Wang, L. Jin, Impacts of atmospheric particulate matter pollution on environmental biogeochemistry of trace metals in soil-plant system: A review, *Environmental Pollution*, **2019**, 255, 113138, https://doi.org/10.1016/j.envpol.2019.113138.

[28] N.M. Mahowald, D.S. Hamilton, K.R.M. Mackey, J.K. Moore, A.R. Baker, R.A. Scanza, et al., Aerosol trace metal leaching and impacts on marine microorganisms, *Nature Communications*, **2018**, 9, 2614, 10.1038/s41467-018-04970-7.

[29] V.N. Bashkin, Biogeochemical cycling of trace elements, *Modern biogeochemistry*, **2002**, 161-97,

[30] M.S. Hassanvand, K. Naddafi, S. Faridi, M. Arhami, R. Nabizadeh, M.H. Sowlat, et al., Indoor/outdoor relationships of PM10, PM2.5, and PM1 mass concentrations and their water-soluble ions in a retirement home and a school dormitory, *Atmospheric Environment*, **2014**, 82, 375-82, https://doi.org/10.1016/j.atmosenv.2013.10.048.

[31] M. Viana, I. Rivas, X. Querol, A. Alastuey, M. Álvarez-Pedrerol, L. Bouso, et al., Partitioning of trace elements and metals between quasi-ultrafine, accumulation and coarse aerosols in indoor and outdoor air in schools, *Atmospheric Environment*, **2015**, 106, 392-401, https://doi.org/10.1016/j.atmosenv.2014.07.027.

[32] H. Rohra, A.S. Pipal, R. Tiwari, P. Vats, J. Masih, P. Khare, et al., Particle size dynamics and risk implication of atmospheric aerosols in South-Asian subcontinent, *Chemosphere*, **2020**, 249, 126140, https://doi.org/10.1016/j.chemosphere.2020.126140.

[33] G.J.K. Komarnicki, Lead and cadmium in indoor air and the urban environment, *Environmental Pollution*, **2005**, 136, 47-61, https://doi.org/10.1016/j.envpol.2004.12.006.

[34] A. Anand, S. Yadav, H.C. Phuleria, Chemical characteristics and oxidative potential of indoor and outdoor PM2.5 in densely populated urban slums, *Environmental Research*, **2022**, 212, 113562, https://doi.org/10.1016/j.envres.2022.113562.

[35] X. Feng, L. Shao, C. Xi, T. Jones, D. Zhang, K. BéruBé, Particle-induced oxidative damage by indoor size-segregated particulate matter from coal-burning homes in the Xuanwei lung cancer epidemic area, Yunnan Province, China, *Chemosphere*, **2020**, 256, 127058, https://doi.org/10.1016/j.chemosphere.2020.127058.

[36] L. Shao, Y. Hu, J. Wang, C. Hou, Y. Yang, M. Wu, Particle-induced oxidative damage of indoor PM10 from coal burning homes in the lung cancer area of Xuan Wei, China, *Atmospheric Environment*, **2013**, 77, 959-67, https://doi.org/10.1016/j.atmosenv.2013.05.079.

[37] H. Li, X. Qian, Q.g. Wang, Heavy Metals in Atmospheric Particulate Matter: A Comprehensive Understanding Is Needed for Monitoring and Risk Mitigation, *Environmental Science & Technology*, **2013**, 47, 13210-1, 10.1021/es404751a.

[38] A. Gioda, E. Fuentes-Mattei, B. Jimenez-Velez, Evaluation of cytokine expression in BEAS cells exposed to fine particulate matter (PM2.5) from specialized indoor environments, *International Journal of Environmental Health Research*, **2011**, 21, 106-19, 10.1080/09603123.2010.515668.

[39] P.S. Gilmour, M.C. Schladweiler, A. Nyska, J.K. McGee, R. Thomas, R.H. Jaskot, et al., Systemic Imbalance of Essential Metals and Cardiac Gene Expression in Rats Following Acute Pulmonary Zinc Exposure, *Journal of Toxicology and Environmental Health, Part A*, **2006**, 69, 2011-32, 10.1080/15287390600746173.

[40] R.G. Sangani, J.M. Soukup, A.J. Ghio, Metals in air pollution particles decrease whole-blood coagulation time, *Inhalation Toxicology*, **2010**, 22, 621-6, 10.3109/08958371003599037.

[41] H. Prieditis, I.Y.R. Adamson, Comparative pulmonary toxicity of various soluble metals found in urban particulate dusts, *Experimental Lung Research*, **2002**, 28, 563-76, 10.1080/01902140290096782.

[42] Z. Zhang, P.Y.K. Chau, H.K. Lai, C.M. Wong, A review of effects of particulate matter-associated nickel and vanadium species on cardiovascular and respiratory systems, *International Journal of Environmental Health Research*, **2009**, 19, 175-85, 10.1080/09603120802460392.

[43] F. Kastury, E. Smith, E. Lombi, M.W. Donnelley, P.L. Cmielewski, D.W. Parsons, et al., Dynamics of Lead Bioavailability and Speciation in Indoor Dust and X-ray Spectroscopic Investigation of the Link between Ingestion and Inhalation Pathways, *Environmental Science & Technology*, **2019**, 53, 11486-95, 10.1021/acs.est.9b03249.

[44] J. McNeill, G. Snider, C.L. Weagle, B. Walsh, P. Bissonnette, E. Stone, et al., Large global variations in measured airborne metal concentrations driven by anthropogenic sources, *Scientific Reports*, **2020**, 10, 21817, 10.1038/s41598-020-78789-y.

[45] L.N. Suvarapu, S.-O. Baek, Determination of heavy metals in the ambient atmosphere: A review, *Toxicology and Industrial Health*, **2016**, 33, 79-96, 10.1177/0748233716654827.

[46] A.R. Baker, T.D. Jickells, M. Witt, K.L. Linge, Trends in the solubility of iron, aluminium, manganese and phosphorus in aerosol collected over the Atlantic Ocean, *Marine Chemistry*, **2006**, 98, 43-58, https://doi.org/10.1016/j.marchem.2005.06.004.

[47] C. Baldo, A. Ito, M.D. Krom, W. Li, T. Jones, N. Drake, et al., Iron from coal combustion particles dissolves much faster than mineral dust under simulated atmospheric acidic conditions, *Atmos Chem Phys*, **2022**, 22, 6045-66, 10.5194/acp-22-6045-2022.

[48] A.R. Baker, M. Li, R. Chance, Trace Metal Fractional Solubility in Size-Segregated Aerosols From the Tropical Eastern Atlantic Ocean, *Global Biogeochemical Cycles*, **2020**, 34, e2019GB006510, https://doi.org/10.1029/2019GB006510.

[49] D. Voutsa, C. Samara, Labile and bioaccessible fractions of heavy metals in the airborne particulate matter from urban and industrial areas, *Atmospheric Environment*, **2002**, 36, 3583-90, https://doi.org/10.1016/S1352-2310(02)00282-0.

[50] W. Xing, Q. Zhao, K.G. Scheckel, L. Zheng, L. Li, Inhalation bioaccessibility of Cd, Cu, Pb and Zn and speciation of Pb in particulate matter fractions from areas with different pollution characteristics in Henan Province, China, *Ecotoxicology and Environmental Safety*, **2019**, 175, 192-200, https://doi.org/10.1016/j.ecoenv.2019.03.062.

[51] V. Mugica-Álvarez, J. Figueroa-Lara, M. Romero-Romo, J. Sepúlveda-Sánchez, T. López-Moreno, Concentrations and properties of airborne particles in the Mexico City subway system, *Atmospheric Environment*, **2012**, 49, 284-93, https://doi.org/10.1016/j.atmosenv.2011.11.038.

[52] Y. Yang, D. Gao, R.J. Weber, A method for liquid spectrophotometric measurement of total and water-soluble iron and copper in ambient aerosols, *Atmos Meas Tech*, **2021**, 14, 4707-19, 10.5194/amt-14-4707-2021.

[53] G. Zhang, H. Li, X. Wei, Z. Fu, Preliminary assessment of size distribution of airborne metals and metalloids in the urban aerosols of Guiyang, southwest China, *Atmospheric Pollution Research*, **2015**, 6, 635-43, https://doi.org/10.5094/APR.2015.072.

[54] V. Mohr, M. Miró, A. Limbeck, On-line dynamic extraction system hyphenated to inductively coupled plasma optical emission spectrometry for automatic determination of oral bioaccessible trace metal fractions in airborne particulate matter, *Analytical and Bioanalytical Chemistry*, **2017**, 409, 2747-56, 10.1007/s00216-017-0219-8.

[55] A. Limbeck, C. Wagner, B. Lendl, A. Mukhtar, Determination of water soluble trace metals in airborne particulate matter using a dynamic extraction procedure with on-line inductively coupled plasma optical emission spectrometric detection, *Analytica Chimica Acta*, **2012**, 750, 111-9, https://doi.org/10.1016/j.aca.2012.05.005.

[56] A. Mukhtar, V. Mohr, A. Limbeck, The suitability of extraction solutions to assess bioaccessible trace metal fractions in airborne particulate matter: a comparison of common leaching agents, *Environmental Science and Pollution Research*, **2015**, 22, 16620-30, 10.1007/s11356-015-4789-8.

[57] J.J. Figueroa-Lara, J.M. Murcia-González, R. García-Martínez, M. Romero-Romo, M. Torres Rodríguez, V. Mugica-Álvarez, Effect of platform subway depth on the presence of Airborne PM2.5, metals, and toxic organic species, *Journal of Hazardous Materials*, **2019**, 377, 427-36, https://doi.org/10.1016/j.jhazmat.2019.05.091.

[58] Q. Wang, Y. Ma, J. Tan, N. Zheng, J. Duan, Y. Sun, et al., Characteristics of size-fractionated atmospheric metals and water-soluble metals in two typical episodes in Beijing, *Atmospheric Environment*, **2015**, 119, 294-303, https://doi.org/10.1016/j.atmosenv.2015.08.061.

[59] A. Mukhtar, A. Limbeck, Recent developments in assessment of bio-accessible trace metal fractions in airborne particulate matter: A review, *Analytica Chimica Acta*, **2013**, 774, 11-25, https://doi.org/10.1016/j.aca.2013.02.008.

[60] E. von Schneidemesser, E.A. Stone, T.A. Quraishi, M.M. Shafer, J.J. Schauer, Toxic metals in the atmosphere in Lahore, Pakistan, *Science of The Total Environment*, **2010**, 408, 1640-8, https://doi.org/10.1016/j.scitotenv.2009.12.022.

[61] S.-P. Wu, X. Li, S.-H. Xiao, J. Zhang, J.J. Schwab, Solubility of aerosol minor and trace elements in Xiamen Island, Southeast China: Size distribution, health risk and dry deposition, *Science of The Total Environment*, **2022**, 844, 157100, https://doi.org/10.1016/j.scitotenv.2022.157100.

[62] X. Luo, Z. Zhao, J. Xie, J. Luo, Y. Chen, H. Li, et al., Pulmonary bioaccessibility of trace metals in PM2.5 from different megacities simulated by lung fluid extraction and DGT method, *Chemosphere*, **2019**, 218, 915-21, https://doi.org/10.1016/j.chemosphere.2018.11.079.

[63] B. Leclercq, L.Y. Alleman, E. Perdrix, V. Riffault, M. Happillon, A. Strecker, et al., Particulate metal bioaccessibility in physiological fluids and cell culture media: Toxicological perspectives, *Environmental Research*, **2017**, 156, 148-57, https://doi.org/10.1016/j.envres.2017.03.029.

[64] X. Huang, J. Cheng, D. Bo, R. Betha, R. Balasubramanian, Bioaccessibility of Airborne Particulate-Bound Trace Elements in Shanghai and Health Risk Assessment, *Frontiers in Environmental Science*, **2016**, 4,

[65] B.T. Cartledge, B.J. Majestic, Metal concentrations and soluble iron speciation in fine particulate matter from light rail activity in the Denver-Metropolitan area, *Atmospheric Pollution Research*, **2015**, 6, 495-502, https://doi.org/10.5094/APR.2015.055.

[66] N.K. Gali, S.Y. Jiang, F. Yang, L. Sun, Z. Ning, Redox characteristics of size-segregated PM from different public transport microenvironments in Hong Kong, *Air Quality, Atmosphere & Health*, **2017**, 10, 833-44, 10.1007/s11869-017-0473-0.

[67] S.Y.N. Jiang, F. Yang, K.L. Chan, Z. Ning, Water solubility of metals in coarse PM and PM2.5 in typical urban environment in Hong Kong, *Atmospheric Pollution Research*, **2014**, 5, 236-44, https://doi.org/10.5094/APR.2014.029.

[68] S. Mbengue, L.Y. Alleman, P. Flament, Bioaccessibility of trace elements in fine and ultrafine atmospheric particles in an industrial environment, *Environmental Geochemistry and Health*, **2015**, 37, 875-89, 10.1007/s10653-015-9756-2.

[69] D. Voutsa, A. Anthemidis, G. Giakisikli, K. Mitani, A. Besis, A. Tsolakidou, et al., Size distribution of total and water-soluble fractions of particle-bound elements—assessment of possible risks via inhalation, *Environmental Science and Pollution Research*, **2015**, 22, 13412-26, 10.1007/s11356-015-4559-7.

[70] X. Huang, R. Betha, L.Y. Tan, R. Balasubramanian, Risk assessment of bioaccessible trace elements in smoke haze aerosols versus urban aerosols using simulated lung fluids, *Atmospheric Environment*, **2016**, 125, 505-11, https://doi.org/10.1016/j.atmosenv.2015.06.034.

[71] G. Polezer, A. Oliveira, S. Potgieter-Vermaak, A.F.L. Godoi, R.A.F. de Souza, C.I. Yamamoto, et al., The influence that different urban development models has on PM2.5 elemental and bioaccessible profiles, *Scientific Reports*, **2019**, 9, 14846, 10.1038/s41598-019-51340-4.

[72] Y. Sun, X. Hu, J. Wu, H. Lian, Y. Chen, Fractionation and health risks of atmospheric particle-bound As and heavy metals in summer and winter, *Science of The Total Environment*, **2014**, 493, 487-94, https://doi.org/10.1016/j.scitotenv.2014.06.017.

[73] N.J. Schleicher, S. Norra, F. Chai, Y. Chen, S. Wang, K. Cen, et al., Temporal variability of trace metal mobility of urban particulate matter from Beijing – A contribution to health

impact assessments of aerosols, *Atmospheric Environment*, **2011**, 45, 7248-65, https://doi.org/10.1016/j.atmosenv.2011.08.067.

[74] L.J. Spokes, T.D. Jickells, Factors controlling the solubility of aerosol trace metals in the atmosphere and on mixing into seawater, *Aquatic Geochemistry*, **1995**, 1, 355-74, 10.1007/BF00702739.

[75] T. Kikuchi, H. Ikemoto, K. Takahashi, H. Hasome, H. Ueda, Parameterizing Soil Emission and Atmospheric Oxidation-Reduction in a Model of the Global Biogeochemical Cycle of Mercury, *Environmental Science & Technology*, **2013**, 47, 12266-74, 10.1021/es401105h.

[76] D.S. McLagan, C.P.J. Mitchell, H. Huang, Y.D. Lei, A.S. Cole, A. Steffen, et al., A High-Precision Passive Air Sampler for Gaseous Mercury, *Environmental Science & Technology Letters*, **2016**, 3, 24-9, 10.1021/acs.estlett.5b00319.

[77] B. Fang, H. Zeng, L. Zhang, H. Wang, J. Liu, K. Hao, et al., Toxic metals in outdoor/indoor airborne PM2.5 in port city of Northern, China: Characteristics, sources, and personal exposure risk assessment, *Environmental Pollution*, **2021**, 279, 116937, https://doi.org/10.1016/j.envpol.2021.116937.

[78] M.N. Rashed, Total and Extractable Heavy Metals in Indoor, Outdoor and Street Dust from Aswan City, Egypt, *CLEAN – Soil, Air, Water*, **2008**, 36, 850-7, https://doi.org/10.1002/clen.200800062.

[79] Y. Wu, G. Li, Y. Yang, T. An, Pollution evaluation and health risk assessment of airborne toxic metals in both indoors and outdoors of the Pearl River Delta, China, *Environmental Research*, **2019**, 179, 108793, https://doi.org/10.1016/j.envres.2019.108793.

[80] J.R. Graney, M.S. Landis, G.A. Norris, Concentrations and solubility of metals from indoor and personal exposure PM2.5 samples, *Atmospheric Environment*, **2004**, 38, 237-47, https://doi.org/10.1016/j.atmosenv.2003.09.052.

[81] M. Zhang, S. Zhang, G. Feng, H. Su, F. Zhu, M. Ren, et al., Indoor airborne particle sources and outdoor haze days effect in urban office areas in Guangzhou, *Environmental Research*, **2017**, 154, 60-5, https://doi.org/10.1016/j.envres.2016.12.021.

[82] P.E. Rasmussen, C. Levesque, M. Chénier, H.D. Gardner, Contribution of metals in resuspended dust to indoor and personal inhalation exposures: Relationships between PM10 and settled dust, *Building and Environment*, **2018**, 143, 513-22, https://doi.org/10.1016/j.buildenv.2018.07.044.

[83] E. Resongles, V. Dietze, D.C. Green, R.M. Harrison, R. Ochoa-Gonzalez, A.H. Tremper, et al., Strong evidence for the continued contribution of lead deposited during the 20th century to the atmospheric environment in London of today, *Proceedings of the National Academy of Sciences*, **2021**, 118, e2102791118, 10.1073/pnas.2102791118.

[84] R.M. Harrison, A.M. Jones, J. Gietl, J. Yin, D.C. Green, Estimation of the Contributions of Brake Dust, Tire Wear, and Resuspension to Nonexhaust Traffic Particles Derived from Atmospheric Measurements, *Environmental Science & Technology*, **2012**, 46, 6523-9, 10.1021/es300894r.

[85] J. Qian, J. Peccia, A.R. Ferro, Walking-induced particle resuspension in indoor environments, *Atmospheric Environment*, **2014**, 89, 464-81, https://doi.org/10.1016/j.atmosenv.2014.02.035.

[86] D. O'Connor, D. Hou, Y.S. Ok, J. Mulder, L. Duan, Q. Wu, et al., Mercury speciation, transformation, and transportation in soils, atmospheric flux, and implications for risk management: A critical review, *Environment International*, **2019**, 126, 747-61, https://doi.org/10.1016/j.envint.2019.03.019.

[87] Z.-J. Tang, X. Hu, J.-Q. Qiao, H.-Z. Lian, Size Distribution, Bioaccessibility and Health Risks of Indoor/Outdoor Airborne Toxic Elements Collected from School Office Room, Atmosphere2018.

[88] L. Liu, W. Li, Q. Lin, Y. Wang, J. Zhang, Y. Zhu, et al., Size-dependent aerosol iron solubility in an urban atmosphere, *npj Climate and Atmospheric Science*, **2022**, 5, 53, 10.1038/s41612-022-00277-z.

[89] S.Y. Jiang, D.S. Kaul, F. Yang, L. Sun, Z. Ning, Source apportionment and water solubility of metals in size segregated particles in urban environments, *Science of The Total Environment*, **2015**, 533, 347-55, https://doi.org/10.1016/j.scitotenv.2015.06.146.

[90] K.-H. Kim, E. Kabir, S. Kabir, A review on the human health impact of airborne particulate matter, *Environment International*, **2015**, 74, 136-43, https://doi.org/10.1016/j.envint.2014.10.005.

[91] A. Saffari, N. Daher, M.M. Shafer, J.J. Schauer, C. Sioutas, Global Perspective on the Oxidative Potential of Airborne Particulate Matter: A Synthesis of Research Findings, *Environmental Science & Technology*, **2014**, 48, 7576-83, 10.1021/es500937x.

[92] X. Feng, L. Shao, T. Jones, Y. Li, Y. Cao, M. Zhang, et al., Oxidative potential and water-soluble heavy metals of size-segregated airborne particles in haze and non-haze episodes: Impact of the "Comprehensive Action Plan" in China, *Science of The Total Environment*, **2022**, 814, 152774, https://doi.org/10.1016/j.scitotenv.2021.152774.

[93] A. Sorooshian, J. Csavina, T. Shingler, S. Dey, F.J. Brechtel, A.E. Sáez, et al., Hygroscopic and Chemical Properties of Aerosols Collected near a Copper Smelter: Implications for Public and Environmental Health, *Environmental Science & Technology*, **2012**, 46, 9473-80, 10.1021/es302275k.

[94] S. Canepari, M.L. Astolfi, S. Moretti, R. Curini, Comparison of extracting solutions for elemental fractionation in airborne particulate matter, *Talanta*, **2010**, 82, 834-44, https://doi.org/10.1016/j.talanta.2010.05.068.

[95] P. Smichowski, G. Polla, D. Gómez, Metal fractionation of atmospheric aerosols via sequential chemical extraction: a review, *Analytical and Bioanalytical Chemistry*, **2005**, 381, 302-16, 10.1007/s00216-004-2849-x.

[96] M.M.G. Perron, M. Strzelec, M. Gault-Ringold, B.C. Proemse, P.W. Boyd, A.R. Bowie, Assessment of leaching protocols to determine the solubility of trace metals in aerosols, *Talanta*, **2020**, 208, 120377, https://doi.org/10.1016/j.talanta.2019.120377.

[97] G. Mainelis, Bioaerosol sampling: Classical approaches, advances, and perspectives, *Aerosol Science and Technology*, **2020**, 54, 496-519, 10.1080/02786826.2019.1671950.

[98] B. Ghosh, H. Lal, A. Srivastava, Review of bioaerosols in indoor environment with special reference to sampling, analysis and control mechanisms, *Environment International*, **2015**, 85, 254-72, https://doi.org/10.1016/j.envint.2015.09.018.

[99] C.W. Haig, W.G. Mackay, J.T. Walker, C. Williams, Bioaerosol sampling: sampling mechanisms, bioefficiency and field studies, *Journal of Hospital Infection*, **2016**, 93, 242-55, https://doi.org/10.1016/j.jhin.2016.03.017.

[100] G.J. Parker, C.H. Ong, R.B. Manges, E.M. Stapleton, A.P. Comellas, T.M. Peters, et al., A Novel Method of Collecting and Chemically Characterizing Milligram Quantities of Indoor Airborne Particulate Matter, *Aerosol and Air Quality Research*, **2019**, 19, 2387-95, 10.4209/aaqr.2019.04.0182.

[101] J. Malloy, A. Quintana, C.J. Jensen, K. Liu, Efficient and Robust Metallic Nanowire Foams for Deep Submicrometer Particulate Filtration, *Nano Letters*, **2021**, 21, 2968-74, 10.1021/acs.nanolett.1c00050.

[102] M. Pirhadi, A. Mousavi, S. Taghvaee, M.H. Sowlat, C. Sioutas, An aerosol concentrator/diffusion battery tandem to concentrate and separate ambient accumulation mode particles for evaluating their toxicological properties, *Atmospheric Environment*, **2019**, 213, 81-9, https://doi.org/10.1016/j.atmosenv.2019.05.058.

[103] X. Bian, Y. Lan, B. Wang, Y.S. Zhang, B. Liu, P. Yang, et al., Microfluidic Air Sampler for Highly Efficient Bacterial Aerosol Collection and Identification, *Analytical Chemistry*, **2016**, 88, 11504-12, 10.1021/acs.analchem.6b02708.

[104] Y.-B. Zhao, T. Cen, J. Tang, W. He, C. Ludwig, S.-C. Chen, et al., An elution-based method for estimating efficiencies of aerosol collection devices not affected by their pressure drops, *Separation and Purification Technology*, **2022**, 287, 120590, https://doi.org/10.1016/j.seppur.2022.120590.

[105] S.C. Hong, J.S. Kang, J.E. Lee, S.S. Kim, J.H. Jung, Continuous aerosol size separator using inertial microfluidics and its application to airborne bacteria and viruses, *Lab on a Chip*, **2015**, 15, 1889-97, 10.1039/C5LC00079C.

[106] J. Cox, R. Indugula, S. Vesper, Z. Zhu, R. Jandarov, T. Reponen, Comparison of indoor air sampling and dust collection methods for fungal exposure assessment using quantitative PCR, *Environmental Science: Processes & Impacts*, **2017**, 19, 1312-9, 10.1039/C7EM00257B.

[107] E.O. Gaga, T. Harner, E. Dabek-Zlotorzynska, V. Celo, G. Evans, C.-H. Jeong, et al., Polyurethane Foam (PUF) Disk Samplers for Measuring Trace Metals in Ambient Air, *Environmental Science & Technology Letters*, **2019**, 6, 545-50, 10.1021/acs.estlett.9b00420.

[108] S. Osterwalder, S.M. Dunham-Cheatham, B. Ferreira Araujo, O. Magand, J.L. Thomas, F. Baladima, et al., Fate of Springtime Atmospheric Reactive Mercury: Concentrations and Deposition at Zeppelin, Svalbard, *ACS Earth and Space Chemistry*, **2021**, 5, 3234-46, 10.1021/acsearthspacechem.1c00299.

[109] H.G. Zechmeister, M. Rivera, G. Köllensperger, J. Marrugat, N. Künzli, Indoor monitoring of heavy metals and NO2 using active monitoring by moss and Palmes diffusion tubes, *Environmental Sciences Europe*, **2020**, 32, 156, 10.1186/s12302-020-00439-x.

[110] J. Hofman, B.A. Maher, A.R. Muxworthy, K. Wuyts, A. Castanheiro, R. Samson, Biomagnetic Monitoring of Atmospheric Pollution: A Review of Magnetic Signatures from Biological Sensors, *Environmental Science & Technology*, **2017**, 51, 6648-64, 10.1021/acs.est.7b00832.

[111] M. Pan, A. Eiguren-Fernandez, H. Hsieh, N. Afshar-Mohajer, S.V. Hering, J. Lednicky, et al., Efficient collection of viable virus aerosol through laminar-flow, water-based condensational particle growth, *Journal of Applied Microbiology*, **2016**, 120, 805-15, https://doi.org/10.1111/jam.13051.

[112] K.J. Heo, H.S. Ko, S.B. Jeong, S.B. Kim, J.H. Jung, Enriched Aerosol-to-Hydrosol Transfer for Rapid and Continuous Monitoring of Bioaerosols, *Nano Letters*, **2021**, 21, 1017-24, 10.1021/acs.nanolett.0c04096.

[113] N. Daher, Z. Ning, A.K. Cho, M. Shafer, J.J. Schauer, C. Sioutas, Comparison of the Chemical and Oxidative Characteristics of Particulate Matter (PM) Collected by Different Methods: Filters, Impactors, and BioSamplers, *Aerosol Science and Technology*, **2011**, 45, 1294-304, 10.1080/02786826.2011.590554.

[114] R.J. Weber, D. Orsini, Y. Daun, Y.N. Lee, P.J. Klotz, F. Brechtel, A Particle-into-Liquid Collector for Rapid Measurement of Aerosol Bulk Chemical Composition, *Aerosol Science and Technology*, **2001**, 35, 718-27, 10.1080/02786820152546761.

[115] S.D. Noblitt, G.S. Lewis, Y. Liu, S.V. Hering, J.L. Collett, Jr., C.S. Henry, Interfacing Microchip Electrophoresis to a Growth Tube Particle Collector for Semicontinuous

Monitoring of Aerosol Composition, *Analytical Chemistry*, **2009**, 81, 10029-37, 10.1021/ac901903m.

[116] L. Zheng, P. Kulkarni, M.E. Birch, K. Ashley, S. Wei, Analysis of Crystalline Silica Aerosol Using Portable Raman Spectrometry: Feasibility of Near Real-Time Measurement, *Analytical Chemistry*, **2018**, 90, 6229-39, 10.1021/acs.analchem.8b00830.

[117] D.E. Kerecman, M.J. Apsokardu, S.L. Talledo, M.S. Taylor, Jr., D.N. Haugh, Y. Zhang, et al., Online Characterization of Organic Aerosol by Condensational Growth into Aqueous Droplets Coupled with Droplet-Assisted Ionization, *Analytical Chemistry*, **2021**, 93, 2793-801, 10.1021/acs.analchem.0c03697.

[118] Y. Tian, H. Shen, Q. Wang, A. Liu, W. Gao, X.-W. Chen, et al., Online High Temporal Resolution Measurement of Atmospheric Sulfate and Sulfur Trioxide with a Light Emitting Diode and Liquid Core Waveguide-Based Sensor, *Analytical Chemistry*, **2018**, 90, 7843-7, 10.1021/acs.analchem.8b01055.

[119] Y. Su, W. Wang, W. Wang, L. Zhai, X. Shen, J. Xu, et al., Re-evaluation of BioSampler and its improvement for on-line, time-resolved monitoring of environmental coarse aerosol, *Atmospheric Environment*, **2020**, 225, 117249, https://doi.org/10.1016/j.atmosenv.2019.117249.

[120] P.J. Kauffmann, N.A. Park, R.B. Clark, G.L. Glish, J.E. Dick, Aerosol Electroanalysis by PILSNER: Particle-into-Liquid Sampling for Nanoliter Electrochemical Reactions, *ACS Measurement Science Au*, **2022**, 2, 106-12, 10.1021/acsmeasuresciau.1c00024.

[121] Y.S. Cho, S.C. Hong, J. Choi, J.H. Jung, Development of an automated wet-cyclone system for rapid, continuous and enriched bioaerosol sampling and its application to real-time detection, *Sensors and Actuators B: Chemical*, **2019**, 284, 525-33, https://doi.org/10.1016/j.snb.2018.12.155.

[122] J. Choi, S.C. Hong, W. Kim, J.H. Jung, Highly Enriched, Controllable, Continuous Aerosol Sampling Using Inertial Microfluidics and Its Application to Real-Time Detection of Airborne Bacteria, *ACS Sensors*, **2017**, 2, 513-21, 10.1021/acssensors.6b00753.

[123] I. Mirzaee, M. Song, M. Charmchi, H. Sun, A microfluidics-based on-chip impinger for airborne particle collection, *Lab on a Chip*, **2016**, 16, 2254-64, 10.1039/C6LC00040A.

[124] Z. Ma, Y. Zheng, Y. Cheng, S. Xie, X. Ye, M. Yao, Development of an integrated microfluidic electrostatic sampler for bioaerosol, *Journal of Aerosol Science*, **2016**, 95, 84-94, https://doi.org/10.1016/j.jaerosci.2016.01.003.

[125] Y. Guo, Y. Guo, W. He, Y. Zhao, R. Shen, J. Liu, et al., PET/TPU nanofiber composite filters with high interfacial adhesion strength based on one-step co-electrospinning, *Powder Technology*, **2021**, 387, 136-45, https://doi.org/10.1016/j.powtec.2021.04.020.

[126] J.H. Byeon, J. Hwang, J. Hong Park, K. Young Yoon, B. Ju Ko, S. Hoon Kang, et al., Collection of submicron particles by an electrostatic precipitator using a dielectric barrier discharge, *Journal of Aerosol Science*, **2006**, 37, 1618-28, https://doi.org/10.1016/j.jaerosci.2006.05.003.

[127] D.S. Kim, S.B. Hong, J.-T. Kwon, K. Park, Evaluation of particle growth systems for sampling and analysis of atmospheric fine particles, *Particuology*, **2011**, 9, 606-10, https://doi.org/10.1016/j.partic.2011.04.007.

[128] G. Qiu, M. Spillmann, J. Tang, Y.-B. Zhao, Y. Tao, X. Zhang, et al., On-Site Quantification and Infection Risk Assessment of Airborne SARS-CoV-2 Virus Via a Nanoplasmonic Bioaerosol Sensing System in Healthcare Settings, *Advanced Science*, **2022**, 9, 2204774, https://doi.org/10.1002/advs.202204774.

[129] D. Wang, M.H. Sowlat, M.M. Shafer, J.J. Schauer, C. Sioutas, Development and evaluation of a novel monitor for online measurement of iron, manganese, and chromium in

ambient particulate matter (PM), *Science of The Total Environment*, **2016**, 565, 123-31, https://doi.org/10.1016/j.scitotenv.2016.04.164.

[130] M.H. Sowlat, D. Wang, G. Simonetti, M.M. Shafer, J.J. Schauer, C. Sioutas, Development and field evaluation of an online monitor for near-continuous measurement of iron, manganese, and chromium in coarse airborne particulate matter (PM), *Aerosol Science and Technology*, **2016**, 50, 1306-19, 10.1080/02786826.2016.1221051.

[131] H. Sun, Y. Jia, H. Dong, L. Fan, Graphene oxide nanosheets coupled with paper microfluidics for enhanced on-site airborne trace metal detection, *Microsystems & Nanoengineering*, **2019**, 5, 4, 10.1038/s41378-018-0044-z.

[132] G. Sriram, M.P. Bhat, P. Patil, U.T. Uthappa, H.-Y. Jung, T. Altalhi, et al., Paper-based microfluidic analytical devices for colorimetric detection of toxic ions: A review, *TrAC Trends in Analytical Chemistry*, **2017**, 93, 212-27, https://doi.org/10.1016/j.trac.2017.06.005.

[133] J. Mettakoonpitak, J. Volckens, C.S. Henry, Janus Electrochemical Paper-Based Analytical Devices for Metals Detection in Aerosol Samples, *Analytical Chemistry*, **2020**, 92, 1439-46, 10.1021/acs.analchem.9b04632.

[134] S. Giannoukos, C.P. Lee, M. Tarik, C. Ludwig, S. Biollaz, H. Lamkaddam, et al., Real-Time Detection of Aerosol Metals Using Online Extractive Electrospray Ionization Mass Spectrometry, *Analytical Chemistry*, **2020**, 92, 1316-25, 10.1021/acs.analchem.9b04480.

[135] A. Hess, M. Tarik, C. Ludwig, A hyphenated SMPS–ICPMS coupling setup: Size-resolved element specific analysis of airborne nanoparticles, *Journal of Aerosol Science*, **2015**, 88, 109-18, https://doi.org/10.1016/j.jaerosci.2015.05.016.

[136] X. Tian, H. Jiang, L. Hu, M. Wang, W. Cui, J. Shi, et al., Simultaneous multi-element and multi-isotope detection in single-particle ICP-MS analysis: Principles and applications, *TrAC Trends in Analytical Chemistry*, **2022**, 157, 116746, https://doi.org/10.1016/j.trac.2022.116746.

[137] P. Jitaru, H. Goenaga Infante, F.C. Adams, Simultaneous multi-elemental speciation analysis of organometallic compounds by solid-phase microextraction and multicapillary gas chromatography hyphenated to inductively coupled plasma-time-of-flight-mass spectrometry, *Journal of Analytical Atomic Spectrometry*, **2004**, 19, 867-75, 10.1039/B404106B.

[138] T. Narukawa, A. Takatsu, K. Chiba, K.W. Riley, D.H. French, Investigation on chemical species of arsenic, selenium and antimony in fly ash from coal fuel thermal power stations, *Journal of Environmental Monitoring*, **2005**, 7, 1342-8, 10.1039/B509817C.

[139] J. Zheng, A. Iijima, N. Furuta, Complexation effect of antimony compounds with citric acid and its application to the speciation of antimony(iii) and antimony(v) using HPLC-ICP-MS, *Journal of Analytical Atomic Spectrometry*, **2001**, 16, 812-8, 10.1039/B101943K.

[140] I.A. Leal-Granadillo, J.I.G.a. Alonso, A. Sanz-Medel, Determination of the speciation of organolead compounds in airborne particulate matter by gas chromatography–inductively coupled plasma mass spectrometry, *Analytica Chimica Acta*, **2000**, 423, 21-9, https://doi.org/10.1016/S0003-2670(00)01032-1.

[141] J. Mettakoonpitak, D. Miller-Lionberg, T. Reilly, J. Volckens, C.S. Henry, Low-cost reusable sensor for cobalt and nickel detection in aerosols using adsorptive cathodic square-wave stripping voltammetry, *Journal of Electroanalytical Chemistry*, **2017**, 805, 75-82, https://doi.org/10.1016/j.jelechem.2017.10.026.

[142] J. Mettakoonpitak, J. Mehaffy, J. Volckens, C.S. Henry, AgNP/Bi/Nafion-modified Disposable Electrodes for Sensitive Zn(II), Cd(II), and Pb(II) Detection in Aerosol Samples, *Electroanalysis*, **2017**, 29, 880-9, https://doi.org/10.1002/elan.201600591.

[143] M.R. Palomo-Marín, F. Rueda-Holgado, J. Marín-Expósito, E. Pinilla-Gil, Disposable sputtered-bismuth screen-printed sensors for voltammetric monitoring of cadmium and lead in

atmospheric particulate matter samples, *Talanta*, **2017**, 175, 313-7, https://doi.org/10.1016/j.talanta.2017.07.060.

[144] F. Rueda-Holgado, E. Bernalte, M.R. Palomo-Marín, L. Calvo-Blázquez, F. Cereceda-Balic, E. Pinilla-Gil, Miniaturized voltammetric stripping on screen printed gold electrodes for field determination of copper in atmospheric deposition, *Talanta*, **2012**, 101, 435-9, https://doi.org/10.1016/j.talanta.2012.09.054.

[145] H.d.A. Silva-Neto, T.M.G. Cardoso, W.K.T. Coltro, R.C. Urban, Determination of bioavailable lead in atmospheric aerosols using unmodified screen-printed carbon electrodes, *Analytical Methods*, **2019**, 11, 4875-81, 10.1039/C9AY01301F.

[146] F. Rueda-Holgado, L. Calvo-Blázquez, F. Cereceda-Balic, E. Pinilla-Gil, A semiautomatic system for soluble lead and copper monitoring in atmospheric deposition by coupling of passive elemental fractionation sampling and voltammetric measurement on screen-printed gold electrodes, *Microchemical Journal*, **2016**, 124, 20-5, https://doi.org/10.1016/j.microc.2015.07.012.

[147] D. Wang, M.M. Shafer, J.J. Schauer, C. Sioutas, A new technique for online measurement of total and water-soluble copper (Cu) in coarse particulate matter (PM), *Environmental Pollution*, **2015**, 199, 227-34, https://doi.org/10.1016/j.envpol.2015.02.006.

[148] D. Wang, M.M. Shafer, J.J. Schauer, C. Sioutas, Development of a Technology for Online Measurement of Total and Water-Soluble Copper (Cu) in PM2.5, *Aerosol Science and Technology*, **2014**, 48, 864-74, 10.1080/02786826.2014.937478.

[149] E. Bakker, E. Pretsch, Potentiometry at trace levels, *TrAC Trends in Analytical Chemistry*, **2001**, 20, 11-9, https://doi.org/10.1016/S0167-2940(01)90073-1.

[150] X.-Y. Xiao, Y.-H. Zhao, Y.-Y. Li, Z.-Y. Song, S.-H. Chen, H.-Q. Huang, et al., General Strategies to Construct Highly Efficient Sensing Interfaces for Metal Ions Detection from the Perspective of Catalysis, *Analytical Chemistry*, **2022**, 94, 13631-41, 10.1021/acs.analchem.2c01797.

[151] L. Wang, Y. Cheng, D. Lamb, Z. Chen, P.J. Lesniewski, M. Megharaj, et al., Simultaneously determining multi-metal ions using an ion selective electrode array system, *Environmental Technology & Innovation*, **2016**, 6, 165-76, https://doi.org/10.1016/j.eti.2016.10.001.

[152] L. Sun, C. Sun, X. Sun, Screening highly selective ionophores for heavy metal ion-selective electrodes and potentiometric sensors, *Electrochimica Acta*, **2016**, 220, 690-8, https://doi.org/10.1016/j.electacta.2016.10.156.

[153] Y.-B. Zhao, J. Tang, T. Cen, G. Qiu, W. He, F. Jiang, et al., Integrated aerodynamic/electrochemical microsystem for collection and detection of nanogram-level airborne bioaccessible metals, *Sensors and Actuators B: Chemical*, **2022**, 351, 130903, https://doi.org/10.1016/j.snb.2021.130903.

Chapter 2

Integrated aerodynamic/electrochemical microsystem for collection and detection of nanogram-level airborne bioaccessible metals

Yi-Bo Zhao[1,2], Jiukai Tang[1,2], Tianyu Cen[3,4], Guangyu Qiu[1,2], Weidong He[1,2,5], Fuze Jiang[1,2], Ranxue Yu[1,2,6], Christian Ludwig[3,4], and Jing Wang*[1,2]

[1] Institute of Environmental Engineering, ETH Zurich, 8093 Zurich, Switzerland

[2] Advanced Analytical Technologies, Empa, Ueberlandstrasse 129, 8600 Dübendorf, Switzerland

[3] Environmental Engineering Institute (IIE, GR-LUD), School of Architecture, Civil and Environmental Engineering (ENAC), École Polytechnique Fédérale de Lausanne (EPFL), 1015 Lausanne, Switzerland

[4] Bioenergy and Catalysis Laboratory (LBK-CPM), Energy and Environment Research Division (ENE), Paul Scherrer Institut (PSI), 5232 Villigen PSI, Switzerland

[5] Filter Test Center, School of Resources and Civil Engineering, Northeastern University, NO. 3-11, Wenhua Road, Heping District, Shenyang, Liaoning 110819, China

[6] Key Laboratory of Textile Science & Technology, Ministry of Education, College of Textiles, Donghua University, No. 2999 North Renmin Road, Songjiang, Shanghai 201620, China

***** Correspondence: jing.wang@ifu.baug.ethz.ch

Author contributions

Y.-B. Zhao and J. Wang conceived of the idea and designed the study. Y.-B. Zhao conducted the experiments, data analysis, and manuscript preparation. J. Wang and C. Ludwig contributed to the revision of the manuscript. J. Tang prepared the microfluidic chips. T. Cen and C. Ludwig conducted the ICP-MS measurements. G. Qiu, W. He, F. Jiang and R. Yu helped with the sensing experiments and data analysis. All authors have discussed the results and approved the final version of the manuscript.

This work has been published in *Sensors and Actuators B: Chemical*. **2022**, *351*. DOI: 10.1016/j.snb.2021.130903.

Abstract

The soluble fraction of aerosol particulate matter containing trace metals has the potential to engender toxicity and exacerbate the adverse health effects of particulate matter. In this study, an inertial-impaction-based fluidic chip integrated with electrochemical detection was developed to achieve high collection efficiency and measurements of the bioaccessible metal fraction at the nanogram level. The average collection efficiency for ultrafine and fine particles larger than 50 nm, obtained at a flow rate of 2.5 L/min, was above 70 %. The detection ranges of aerosol soluble copper depended on the collection duration and airflow rate. At a working flow rate of 3.1 L/min and collection efficiency of 70 %, the microsystem was capable of detecting

Cu concentrations above 53 ng/m^3, 32 ng/m^3 and 8 ng/m^3 with 3h, 5 h and 20 h collection periods, respectively, which were in the range of reported atmospheric concentrations. The detection ratio of real-world samples (i.e. PM_{10}-like aerosol) was 100 ± 14 %, indicating excellent aerodynamic collection and reliable electrochemical detection. The collection and sensing performance of the microsystem demonstrates a new step towards an online, mobile, low-cost, and miniaturized routine monitoring system for bioaccessible metals and possibly other soluble components in the aerosols.

Keywords: Aerosol collection; electrochemical detection; fluidic chip; airborne trace metals; bioaccessible

2.1 Introduction

Particulate matter, containing trace metals emitted from anthropogenic and natural sources, is of an environmental concern which moreover affects human health [1] and geochemical cycles [2]. It has been widely recognized that heavy metals engender toxicity and exacerbate the negative health effects of atmospheric particulate matter, and they require comprehensive monitoring and understanding [3]. The chemical speciation of atmospheric heavy metals is crucial to the bioavailability and toxicities of the aerosol particles [4-6]. In particular, the soluble fraction (bioaccessible) of aerosol metals are more easily released into the body fluid of the human physiological system compared to non-soluble metals [5]. Soluble metals in particulate matter such as copper (Cu) are able to produce reactive oxygen species, resulting in oxidative stress and negative health effects [7]. Traditional networks of stationary monitoring are scattered geographically and monitor the air quality at a low spatiotemporal resolution [8]. More comprehensive monitoring and understanding of the aerosol metals at concentrations as low as nanogram level per cubic meter are required. However, this entails some difficult tradeoffs between complicated coupling and miniaturized system, for example between spatiotemporal resolution and cost, that affects air quality control and exposure evaluation greatly [8]. The real-time and spatially resolved routine monitoring of nanogram-level aerosol bioaccessible metals requires the development and combination of advanced aerosol sampling and detection techniques, which offers an opportunity for an interdisciplinary study involving aerodynamics, electrochemistry and engineering design to develop and miniaturize the sensing platform.

Highly efficient aerosol sampling is the crucial step prior to the detection of chemical components of particles, and aerosol samplers such as the impactor [9, 10], aerosol-into-liquid collector [11, 12] and electrostatic air sampler [13, 14] have been developed. In some cases, additional components such as saturation-condensation and particle-to-droplet growth parts are essential to improve the collection efficiencies of fine and ultrafine particulate matter [10]. To achieve a

miniaturized system for particle collection, some lab-on-a-chip designs based on centrifugal and drag force have been used to collect airborne particles [15, 16], and bacterial aerosols [17-20]. A microimpinger has been developed as a compact way to the aerosol-into-liquid collector and liquid-based sampler [21]. Nonetheless, the relatively low sampling volume rate of air (< 100 mL/min) is less likely to provide sufficient samples within several hours for further detection, compared to high volume samplers.

The available detection techniques of trace metals include electrochemical [22, 23] and optical methods [24-27]. Electrochemistry is one of the methods that enables the rapid detection of trace soluble metals with good selectivity and sensitivity [28], and miniaturized sensing system can be realized without significant loss of sensitivity [29]. Electrochemical detection methods such as voltammetry are a viable alternative to ICP-MS measurements [30] as evidenced by their applications to aqueous samples such as drinking water [31], river samples [32] and polluted water [33]. Electrochemical techniques enable the detection of metals such as Cu, Cd, Pb, Fe, Ni [34], and also allow the miniaturization of detection system integrated with microfluidics [35]. The microfluidics techniques allow a significantly reduced amount of samples, faster diffusion of chemicals and so on [36].There are several studies focusing on the development of microfluidics platform integrated with electrochemical electrodes for heavy-metal detection in water samples [37-39]. Nonetheless, the integration of microfluidics and electrochemical detection techniques with aerosol sampling techniques has not been sufficiently developed [40]. For instance, microfluidic techniques are mainly applied as aerosol sampling units to couple with detection instruments such as mass spectrometry. The available studies tend to combine microfluidic electrochemical sensors and aerosol collectors in series to measure aerosol oxidative activity [41], sulfate and nitrate [42].

Because of the relatively low concentration of aerosol metals especially soluble species, proper aerosol collection and detection may impose important limits on the instrument that might result in a bulky benchtop setup. Indeed, conventional instruments such as ICP-MS require complex equipment, laborious operation and professional personnel [34]. Some newly developed and portable techniques such as X-ray fluorescence (XRF), is not able to distinguish soluble fraction from total concentration [27]. There are limited pioneering studies focusing on the offline or online detection of aerosol metal samples using electrochemical detection techniques to achieve more rapid, low-cost and portable aerosol collection and determinations (Table 1) [9, 11, 34, 43-47]. Available studies mainly focus on the passive collection of atmospheric deposits, the coupling to an instrument and the determination of aerosol metals, which may lead to the requirement of a bulky setup or a long time period for collection and measurement. Greater strides should be made towards online, low-cost and mobile sampling and detection systems by better integrating aerosol active sampling and electrochemical detection. To our best knowledge, the

integration of electrochemical detection of metal and aerosol sampling has not been realized on the same miniaturized fluidic platform.

Table 2.1 List of studies of aerosol metal sampling and electrochemical detection.

Target metals	Sampling method	Sampling time	Detection method	Time resolution	Detection limit	Operation mode	References
Cd(II) Pb(II) Cu(II) Fe(II) Ni(II)	Ultrasonic personal aerosol sampler	-	Janus electrochemical paper-based devices	-	0.5 µg/L for Cd, Pb, Fe 1 µg/L for Cu and Ni	Offline	[34]
Co(II) Ni(II)	Filters	-	Nafion/Bi carbon stencil-printed electrodes	-	1 µg/L for Co and 5µg/L for Ni	Offline	[43]
Zn(II) Cd(II) Pb(II)	Ultrasonic personal aerosol samplers and 2.5 µm cut-point cyclones	-	AgNP/Bi/Nafion-modified electrodes	-	5 µg/L for Zn, 0.5 µg/L for Cd and 0.1 µg/L for Pb	Offline	[44]
Cd(II) Pb(II)	Digitel DAH-80 high-volume air sampler	24 h	Sputtered-bismuth screen-printed electrodes	-	11.82 µg/L for Cd and 6.07 µg/L for Pb	Offline	[45]

Cu(II)	Total atmospheric deposition polyethylene collectors	7 days	Screen-printed gold electrodes	-	3.7 µg/L	Offline	[46]
Pb(II)	High-volume sampler	24 h	Unmodified screen-printed carbon electrode	-	0.023 µg/L	Offline	[48]
Pb(II) Cu(II)	Atmospheric sampler	24 h	Screen-printed gold electrodes	> 24 h	7.3 µg/L for Cu and 15.1 µg/L for Pb	Online	[47]
Cu(II)	Two virtual impactors combined with a modified liquid impinger (BioSampler)	2 – 4 h	Copper ion selective electrode	2 – 4 h	10 µg/L	Online	[9]
Cu(II)	An aerosol-into-liquid collector (saturator tank, condensation tubes and high flow	2 – 4 h	Copper ion selective electrode	2 – 4 h	10 µg/L	Online	[11]

	rate im- pactor)

In this study, for the first time, the aerosol collection and electrochemical detection of nanogram-level aerosol soluble metals were achieved in an integrated micro-platform. The collection efficiency and sensing performance were investigated and optimized. Cu is one of the relatively abundant elements in the atmosphere, which can cause adverse health effect by inducing oxidative stress [7], and the concentration of aerosol Cu is at the nanogram level per cubic meter, with a soluble fraction of 20 – 60 % [49]. In the proof-of-concept experiment, lab-generated Cu aerosol and PM_{10}-like aerosol were chosen as the target. The concentration of aerosol Cu and PM_{10}-like samples determined by the integrated microsystem was analyzed and further validated by ICP-MS measurements.

2.2 Material and Methods

2.2.1 Chemicals and apparatus

Sulfuric acid (95 – 98 %), acetic acid (> 98%), Zinc(II) nitrate hexahydrate (98 %), lead(II) nitrate (99.999%), cadmium(II) nitrate tetrahydrate (99.997%), potassium hydroxide (≥ 85 %), Isopropyl alcohol (IPA) and malachite green solution were obtained from Sigma. Copper(II) nitrate hemi(pentahydrate) (98 %) and calcium nitrate tetrahydrate (99 %) were purchased from Alfa Aesar. Iron (III) sulfate pentahydrate (97%) was obtained from Acros organics. Di-Ethyl-Hexyl-Sebacat (DEHS) was obtained from TOPAS. The electrochemical electrode containing three electrodes with a thickness of 150 nm on a glass substrate (ED-SE1-AuPt) were purchased from Micrux Technologies. Electrochemical measurements were conducted using Bio-Logic 300 electrochemical workstation (Bio-Logic, France).

2.2.2 Design and modeling of the microchannel collector

To design a microchannel collector with a proper dimension, simulation of air flow, pressure drop and particle collection was performed using the fluid flow and particle tracing modules in COMSOL Multiphysics 5.4. We assumed that particles stick to the wall once particles contact the wall, and drag force affects particle movement. Particle tracing for fluid flow module was used for simulating the particle movement. The collection efficiency was calculated by releasing 5000 particles with a particle density of 2.2 g/cm^3 at a defined velocity. A channel (~ 220 µL) with a relatively large cross section area (1.6 mm × 1.6 mm) was used to accommodate air flow speed up to 60 m/s and avoid immediate blockage, and the rectangular cross section was

chosen for integrating the electrochemical electrode on one side. The ratio of the radius of curvature to the channel diameter was set to 2 [15]. Based on the critical Reynolds number (Re = 2300), the laminar flow or turbulent flow model was chosen. In this study, the air flow that went through the microchannel inlet (ø 1 mm) was assumed turbulent flow, and the k-omega SST turbulence model was used to calculate the flow near the wall and in the free stream (please see details about mesh independence and boundary conditions in the Supporting Information).

2.2.3 Fabrication of aerosol collection and detection microsystem

The microchannel mold was designed using Auto CAD 2019 and subsequently the microchannel mold was printed using a 3D printer. It was sputtered with 50 nm gold to facilitate efficient peeling-off of Polydimethylsiloxane (PDMS) from the mold. PDMS monomer (Sylgard 184, Dow Corning, Midland, USA) was mixed with the curing agent in the volume ratio of 10:1, and degassed in a vacuum desiccator. Then the PDMS gel was cast onto the mold and the cured PDMS was peeled off after being heated at 70 ^{o}C for four hours. Three PDMS layers and the electrode with the glass substrate were bonded after 1 min plasma treatment (Figure 2.1). The microsystem with a dimension of 35 * 25 * 6 mm consisted of a microchannel (cross section 1.6 *1.6 mm) and electrochemical electrode. In this way, electrochemical measurement could be performed immediately after aerosol collection in the microchannel without sample transferring and loss, which provides a choice to achieve in situ measurements of atmospheric metals.

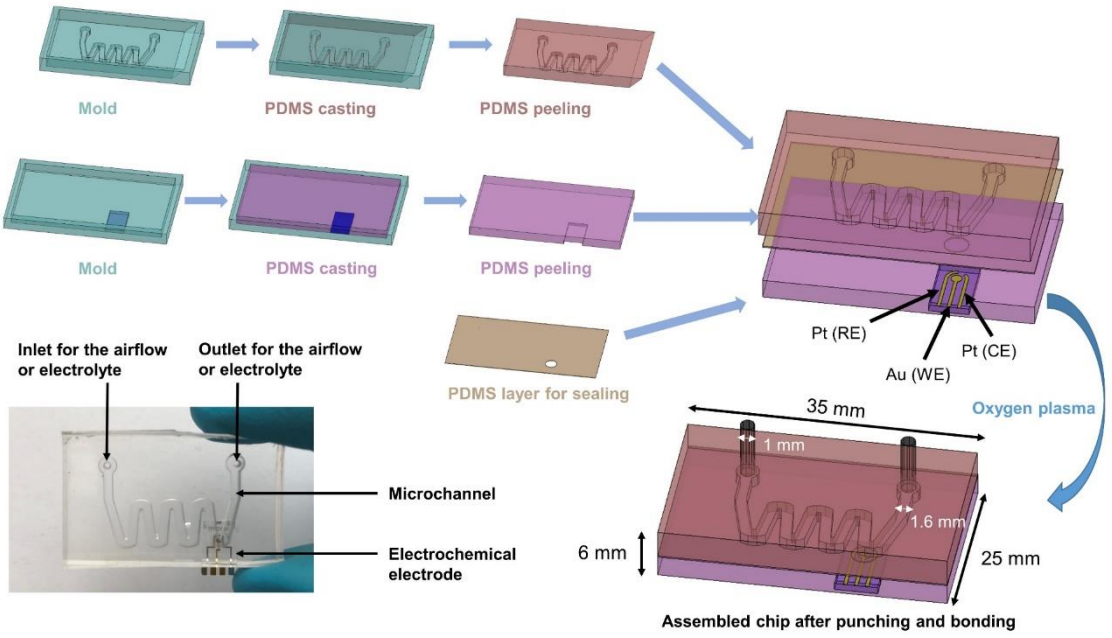

Figure 2.1 The fabrication schematic and photo of the integrated aerodynamic/electrochemical microsystem for aerosol collection and electrochemical detection (RE: reference electrode; WE: working electrode; CE: counter electrode).

Previous studies indicate the residual uncrosslinked oligomers leach from the bulk polymer into the aqueous medium [50, 51], and acids introduced into PDMS microchannel are able to modify the topography of the microchannel wall [52]. Therefore, the microchannel wall surface needs to be treated after peeling-off to alleviate the influence on the sensing performance. The microsystem was heated in oven at 70 ºC for 5 days to ensure the full polymerization of PDMS chains [53, 54]. 0.05 M sulfuric acid and 0.1 M acetate buffer were introduced into microsystem for 6 h in sequence to increases the chemical resistance to sulfuric acid and acetate buffer, and then IPA was added to clean the microchannel for 24 h. 20 µM $Cu(NO_3)_2$ solution was used to generate Cu aerosol (i.e. $Cu(NO_3)_2$ particles) for 12 h to form temporary coating on microchannel wall. Subsequently, 30 min ultrasonication in a bath with 0.1 M acetate buffer was applied, which eliminates the possible chemical reaction between Cu ion and microchannel surface. Prior to each sensing test, it should be heated at 70 ºC for 1 hour to stabilize the microchannel wall. The changes of surface chemical groups due to the cleaning of the microchannel were measured using Fourier transform infrared (FTIR) spectroscopy (Cary 600 series, Agilent, USA).

2.2.4 Aerosol collection and electrochemical measurements

To characterize the particle collection efficiency, NaCl particles (from 1 wt % solution) and DEHS liquid droplet (from 0.5 wt % solution in IPA) were generated using a homemade atomizer at a pressure of 2.8 bar. The particle size distribution of the generated Cu aerosol in terms of electrical mobility diameter was measured by a Scanning mobility particle sizer (SMPS) consisting of a Differential Mobility Analyzer (DMA, model 3080, TSI, USA) and Condensation Particle Counter (CPC, model 3775, TSI, USA). A DMA (DMA, model 3082, TSI, USA) was used to generate monodisperse aerosols, and the particle numbers before (C_{up}) and after (C_{down}) the microsystem were determined by CPC simultaneously (Figure A1). The collection efficiency (η) was calculated based on the following equation:

$$\eta = \frac{C_{up} - C_{down}}{C_{up}} \times 100\% \qquad \text{equation 2.1}$$

Besides Ag/AgCl, platinum and carbon have been widely used as the pseudo reference electrode [55]. In this study, the working electrode (ø 1 mm), counter electrode and reference electrode of the electrochemical electrode were gold, platinum and platinum, respectively. Pt electrode was used as the reference electrode for two reasons. Firstly, ultrasonic treatment was applied prior to electrochemical measurements, so the reference electrode should be stable and robust. Secondly, a smaller electrode was needed to be integrated into the microsystem compared to common screen-printed electrodes. The small electrode with a Pt reference electrode used in the work was commercially available and could be easily obtained. Previous studies suggested

that 0.1 M acetate buffer in the pH range of 4 – 5 was used as the supporting electrolyte [56]. Based on this, 0.1 M acetate buffer (pH 4.45) was chosen as the working electrolyte, and KOH was used to adjust the pH of acetic acid solution. Here 2 µL 0.1 M acetate buffer without or with $Cu(NO_3)_2$ was used as the sample to evaluate the electrochemical performance of the bare electrode without integrating the microchannel. The open circuit potential (OCP) was measured versus conventional Ag/AgCl (SI Analytics, 3 M KCl) in 0.1 M acetic acid (pH 4.45). The temporal stability test indicated that the Pt electrode potential was relatively stable for at least 30 min at a value of 0.589 ± 0.016 V vs. Ag/AgCl (Figure A2). The electrochemical electrode was pre-cleaned in 2 µL 0.05 M H_2SO_4 for 12 cycles between -0.9 and 1.3 V at a scan rate of 100 mV/s prior to each use to avoid the reduction of the active area of the electrode occupied by impurities. It is noted that sulfuric acid should not be introduced into the entire microchannel to avoid the formation of a thin organosulfate particle layer [57]. Instead, the sulfuric acid only covered the electrode area for performing the electrochemical cleaning. Before collecting aerosol particles, the microchannel saturated with 0.1 M acetate buffer was cleaned in an ultrasonic bath for 2 min to remove any reaction product between PDMS and acetic acid. Cyclic voltammetry (CV) was conducted in 0.1 M acetate buffer (pH 4.45) with/without Cu ions at a scan rate of 100 mV/s to determine the potential window of the electrode operation and the position of the Cu oxidation peak. Square Wave Anodic Stripping Voltammetry (SWASV) was performed for quantifying metal content in the liquid phase in the presence of dissolved oxygen [58]. The deposition conditions and stripping parameters including pulse width, step potential and SW amplitude, were optimized prior to the determination of aerosol samples. The conditioning potential was set to 0.2 V for 2 min, to preclean any impurities on the electrode surface before Cu deposition. The calibration was performed using three randomly chosen electrodes to determine the working range with minimal variation of Cu current peak height.

5 µM $Cu(NO_3)_2$ solution was used to generate Cu aerosol and the electrochemical detection was performed after particle collection and ultrasonic treatment. Ultrasonication for 2 min was used to accelerate the dissolution of water-soluble elements [59, 60] and mass transport to possibly reach the distribution equilibrium of Cu ion concentration in the microchannel. The electrolyte samples containing the dissolved airborne Cu after the electrochemical detection were eluted for further ICP-MS validation. To trace and visualize the collection and dissolution of copper ions in the microchannel, Malachite green solution (1 wt % in MiliQ water) was used to generate the aerosol, which was water-soluble and particle-free.

For the evaluation using real-world samples, 0.15 g PM_{10}-like (trace elements) ERM® Certified Reference Material (European Reference Materials, ERM-CZ120) collected in Warsaw, Poland, containing 462 mg Cu in 1 kg sample [61], was suspended in 50 mL Milli-Q water and shaken on a vortex shaker (uniTEXER, LLG Labware) at 1000 rpm for 5 min, followed by

sonication for 30 min [62]. This reaerosolization method is able to generate the representative real-world ambient particulate matter, which agrees well with the original ambient aerosol physically and chemically [62]. After the electrochemical detection, the testing solution in the microsystem was filtered using 0.2 μm PTFE syringe filter (Whatman, Maidstone, UK) to separate the insoluble part from the liquid samples, which was not detectable by the electrode in the microsystem. In this study, only the soluble part was measured and verified with ICP-MS measurement.

2.2.5 Collection and sensing strategies of aerosol trace metals

In general, the procedure for collection and sensing was collecting aerosols with a pump connected to the outlet of the microsystem, and 2 min ultrasonic treatment was applied to homogenize metal ions, prior to electrochemical measurements. The aerosol was drawn into the microchannel, and the particles were captured on the inner wall of the microchannel including the area around the inlet, which was the air/solid interface in the particle collection process. After particle collection on the microchannel wall, the liquid (electrolyte)/solid interface for the particle dissolution process was also formed when the leaching agent was introduced. 0.1 M acetate buffer was the leaching agent and electrochemical electrolyte for extracting and detecting bioaccessible trace metals, to maintain metal ions in a free form instead of complex form, with a higher diffusion coefficient during the deposition step [63]. It should be noted that different leaching agents could result in different bioaccessible fractions, and acetate buffer used in this work was used for the mild extraction [6, 49]. The relatively low volume of the microchannel (~ 220 μL) offered a chance to appropriately concentrate the nanogram-level water soluble trace metals in the liquid phase. No conventional preprocessing such as acid digestion was needed prior to electrochemical sensing. Ultrasonic treatment was applied to increase the dissolution rate and mass transport of Cu(II) ions to reach an stable concentration gradient prior to the electrochemical sensing stage, resulting in a liquid suspension. This should give reproducible concentrations at the electrode, translating into repeatable electrochemical signals, which was the detection ratio (concentration measured by the microsystem/average concentration in the sample). The detection electrode was placed in the last turn of the microchannel (Figure 2.1) to avoid significant fouling by larger particles collected near the inlet.

2.3 Results and Discussion

2.3.1 Aerosol collection performances of the microsystem

According to the verification of the experiments and simulations, the collection efficiency of NaCl particles in the size range of 50 – 550 nm is above 60 % and 70 % at 2 and 2.5 L/min, respectively (Figure 2.2a). The maximal working flow rate in the lab is about 3.1 L/min, so the

expected collection efficiency of the microsystem at 3.1 L/min was above 70 %. The sampling tests and simulations of DEHS particles also show that the collection efficiency of small particles with a lower density (0.9 g/cm^3) was above 60 % (Figure A3). Specifically, the proposed microsystem collects about 80 % of 0.5 µm particles, which is comparable to the typical collection efficiency of the reported lab-on-a-chip designs of above 50 % [15, 21]. According to the simulation shown in Figure 2.2b, the high flow rate of above 40 m/s occurs unevenly in the W-shape microchannel, especially in the area closer to the outlet. The flow velocity near the electrode is about 10 m/s (Figure 2.2b). The working flow rate above 2.5 L/min brings about a higher pressure drop than CPC could withstand to measure the downstream particle number. The simulation results of particle transport at 3.0 L/min indicate particles are collected in the microchannel, including the inlet and the microchannel (Figure 2.2c and d). Small particles such as 50 nm are collected around the inlet and the microchannel wall over the length of the entire channel, whereas 800 nm particles at a high speed are impacted mainly on the inlet (Figure 2.2c and d). In general, the microchannel is used to collect particles with a diameter of less than 1 µm (Figure 2.2d), thereby protecting the electrode from contamination by large particles such as black carbon [64] and mineral dust [65]. Compared to the larger inlet (ø 1.6 mm) applied for the microchannel, the smaller inlet with a diameter of 1 mm leads to turbulent flow and increases collection efficiency, lowering the particle size of 100 % capture (Figure A4). The threshold particle diameter with 100 % collection efficiency at 1.5, 2.25 and 3 L/min are decreased from 1.75 µm, 1.5 µm and 750 nm to 1.25 µm, 1 µm and 500 nm, respectively (Figure A4a and A4b). Therefore, in this work, 1 mm was used as the inlet diameter to increase the collection efficiency. At 3 L/min, the PDMS microchannel is able to withstand a pressure drop up to 13.6 kPa (i.e. 0.13 atm) (Figure A5).

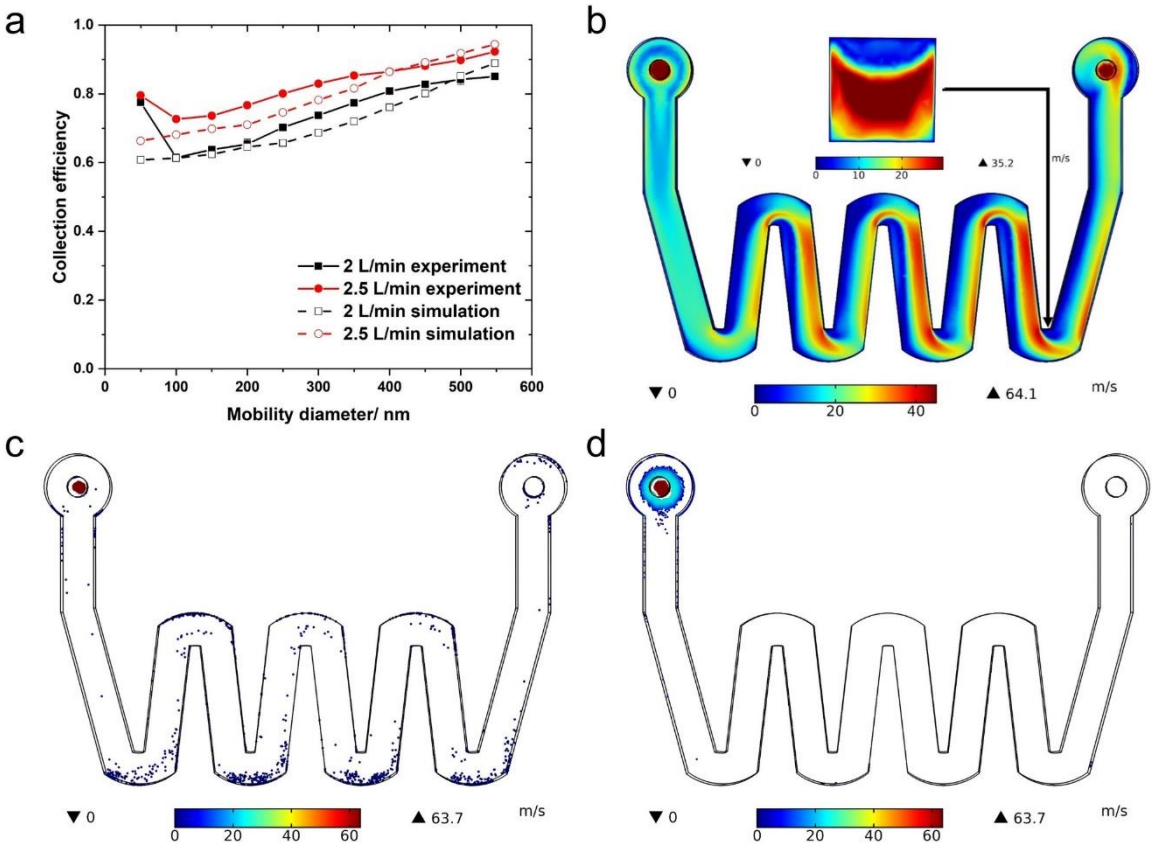

Figure 2.2 (a) Calculated and experimental aerosol collection efficiency of NaCl particles in the size range of 50 – 550 nm (Assuming density: 2.2 g/cm^3) at 2 and 2.5 L/min. (b) Simulated air flow at 3 L/min in the microchannel including the cross section where the electrochemical electrode is. (c) Simulated distribution of collected 50 nm NaCl particles at 3 L/min in the microchannel. (d) Simulated distribution of collected 800 nm NaCl particles at 3 L/min in the microchannel.

2.3.2 Electrochemical characterization of the electrode and optimization of SWASV parameters

As shown in Figure 2.3a, the Au working electrode in 0.1 M acetate buffer is able to provide a wide potential window in the range of -0.8 V to 0.6 V. In the Cu-free acetate buffer, the onset of oxygen reduction and hydrogen evolution are at about -0.3 and -0.8 V, respectively. The oxidation and reduction peaks of Cu in 10 µM solution are at about -0.2 and -0.25 V, respectively (Figure 2.3a), whereas three oxidation peaks of Cu appear at -0.4, -0.3 and -0.2 V in 1 mM Cu solution, which are linked to two overpotential deposition and one underpotential deposition of Cu on the gold electrode surface, respectively. The onset of hydrogen evolution varies as shown in Figure 2.3a, indicating that a slight potential shift may occur in each measurement due to the Pt pseudo-reference used in the work.

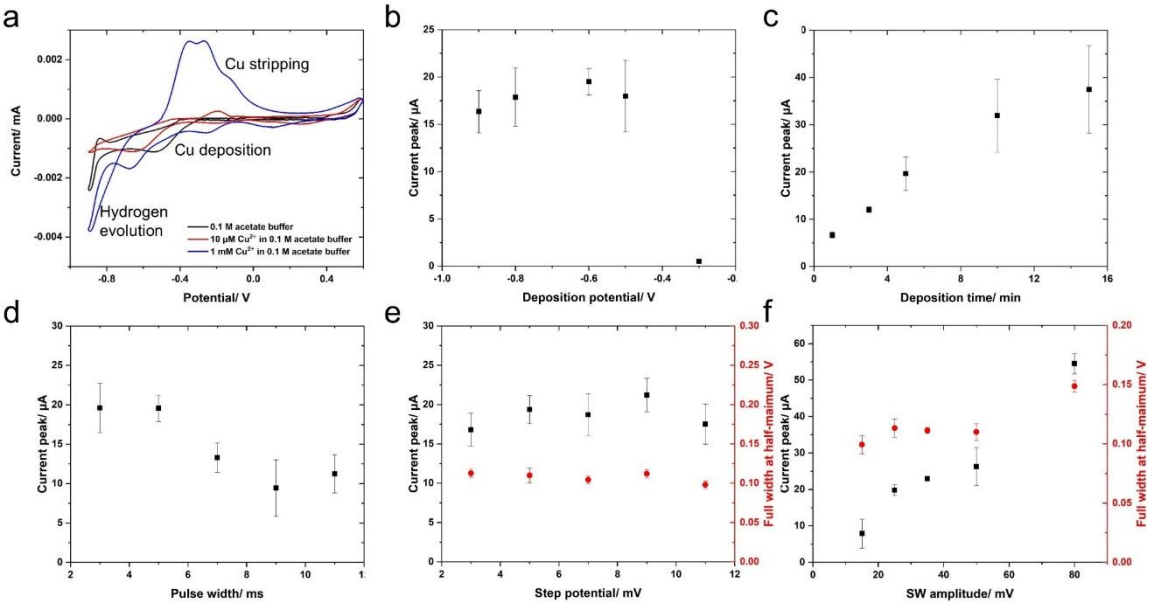

Figure 2.3 Cyclic voltammetry of the bare electrode without microchannel (a) and optimization of SWASV parameters: (b) deposition potential; (c) deposition time; (d) SW amplitude; (e) step potential; (f) pulse width in 0.1 M acetate buffer containing 10 µM Cu. The red and black data points indicated full-width at half-maximum and current peak, respectively.

After determining the potential window and positions of the oxidation and reduction peak of Cu, the SWASV parameters are optimized using a bare electrode without microchannel, including deposition potential, deposition time, pulse width, step potential and square wave (SW) amplitude, to stabilize and maximize the signal current peak and to improve the peak sharpness. Considering the effect of hydrogen evolution and oxygen reduction, we need to carefully select the deposition potential. It is noted that a potential shift of stripping current peak occurs when the deposition potential is more negative than -0.9 V due to the significant hydrogen evolution. The current peak becomes stable with a deposition potential more negative than -0.5 V, exhibiting a coefficient of variation in the range of 7 – 44 % (Figure 2.3b). The relatively stable stripping current peaks also suggest that the potential shift owing to the Pt reference electrode has a limited effect on the Cu deposition with the deposition potential in the range of -0.5 V – 0.9 V. Since the deposition potential of Pb(II) and Cd(II) is close to that of Cu(II) [66], a more negative potential applied in the deposition process may lead to the deposition of Pb and Cd. Therefore, -0.6 V is chosen as the deposition potential to alleviate the interferences from Pb and Cd. The deposition time affects the limit of detection and repeatability of the electrochemical electrode [67]. In this study, the deposition times in the 1 – 15 min range are explored (Figure 2.3c). The overpotential deposition occurs when the deposition time is above 5 min likely due to the continuous deposition of Cu on the Cu layer (overpotential deposition) rather than on the Au layer (underpotential deposition), which causes uncertainty in Cu mass deposited on the gold surface and relatively large variation of current peaks up to 25 %.

The results indicate that the current peak decreases by up to 50 % with different pulse widths (Figure 2.3d). Both sharpness and height of the current peaks are important for the measurement of the target metal in the aerosol samples with complex components, therefore, we use the full width at half-maximum (FWHM) as a second factor to select for optimal values of step potential and SW amplitude [67]. The step potential has a minor influence on FWHM and the current peak is relatively higher with the step potential between 5 and 9 mV (Figure 2.3e). In contrast, the increasing SW amplitude causes a significant 35 % increase in FWHM, which means that the resolution of the current peak deteriorates and the quantitative analysis of specific metals suffers due to possible current peaks overlap [67] (Figure 2.3f). In summary, -0.6 V, 3 min, 5 ms, 5mV, and 35 mV were the optimal values selected for deposition potential, deposition time, pulse width, step potential, and SW amplitude, respectively.

2.3.3 Sensing performance of the trace metal ions in the liquid phase

The calibration curve shown in Figure 2.4a indicates that the limit of detection of the bare electrode is 300 nM in the standard Cu solution, which is 10 times higher than in some previous studies [68]. It suggests that the mass transport of target metals is less efficient, likely owing to not stirring the solution. Here the limit of detection is defined as the threefold background value. The current peak as a function of Cu(II) concentration increases linearly in the range of 300 – 3000 nM and 3 – 10 µM, respectively (Figure 2.4a). However, the variation of the current peak in the range of 3 – 10 µM among different electrodes is much larger than that in the range of 300 – 3000 nM, which indicates an inconsistent performance of different electrodes in the sensing of high concentrations of Cu. According to the SWV current peak of Cu, the Cu current peak is at about -0.1 V, next to the acetate adsorption peak at 0 V [69, 70] (Figure 2.4b).

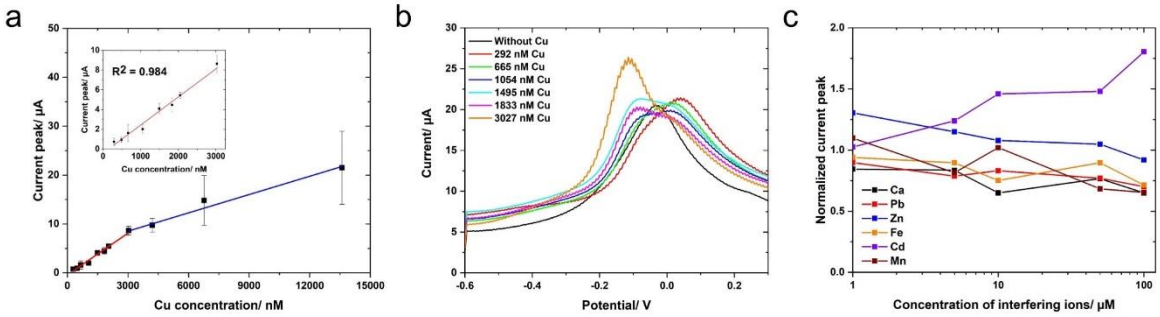

Figure 2.4 Calibration curve of the bare electrode without microchannel for Cu using SWASV(a). (b) Current peak of Cu using SWASV (The left peak and right peak are Cu oxidation peak and acetate adsorption peak, respectively). (c) Interference studies of Cu current peak

in 10 µM Cu containing 1, 5, 10, 50, 100 µM Ca, Fe, Cd, Mn, Pb and Zn, respectively. Deposition time – 0.6 V, deposition time 180 s, SW amplitude 35 mV, step potential 5 mV, pulse width 5 ms.

The verification of sensing selectivity was conducted by testing and calculating the changes of the peak current in the presence of other metal ions [34]. In this interference study, we selected Ca, Pb, Zn, Fe, Cd and Mn as the interfering ions, which were the most abundant metals in the aerosol samples [71-73]. The influence by each of these interfering ions in the concentration range of 1 – 100 µM were separately studied in the presence of 10 µM Cu. In general, Cd and Zn increased the current peak of Cu on average by 40.2 % and 10.0 % respectively, whereas Ca, Pb, Fe and Mn suppressed the Cu current peak by 25.1 %, 20.3 %, 16 % and 14.6 % respectively (Figure 2.4c). The possible reason was that Cd and Zn formed an alloy with Cu [74, 75] and were stripped from the gold surface simultaneously, while some of the other ions might compete with Cu to occupy electroactive sites on gold surface. The observed peak potential deviations were partly attributed to the potential drift of the pseudo Pt reference electrode.

2.3.4 Collection and sensing performance using the laboratory generated metal aerosol

FTIR result indicated that O-H, C-H, C-O, and S=O stretching peaks were enhanced in the 3550 – 3200, 3100 – 3000, 1210 – 1163, and 1070 – 1030 cm^{-1} regions, respectively, due to the cleaning of the inner surface of the microchannel before measurements (Figure A6). A solution of 5 µM $Cu(NO_3)_2$ was used to generate soluble Cu aerosol with an arithmetic mean diameter of 36.9 ± 0.6 nm (Figure 2.5a). For Cu aerosol, $PM_{0.5}$, $PM_{0.5\text{-}1}$, $PM_{1\text{-}2.5}$ and $PM_{2.5\text{-}10}$ accounted for 78.1 %, 18.5 %, 3.2 %, and 0.2 %, respectively (Figure 2.5b). ICP-MS results indicated that the Cu concentration of liquid samples in the microchannel and the concentration on the microchannel wall accounted for 90 % and 10 % of total concentration in collected samples, respectively (Figure A7), indicating no significant adsorption of Cu onto the microchannel wall. To obtain stable and high electrochemical signals, the effect of ultrasonic treatment was investigated to improve the metal dissolution from aerosol particles and its mass transport. The detection ratio varied in the range of 10 – 98 % in the measurements without ultrasonic treatment (Figure A8). Here, the detection ratio was the ratio of Cu concentration derived from electrochemical signals based on the calibration curve of the bare electrode to the ICP-MS verified concentration. In contrast, ultrasonic treatment resulted in a stabilized but lower detection ratio in the range of 10 % to 20 %. Distribution of collected particles, liquid movement, metal dissolution and distribution in the microchannel were involved and possibly resulted in low detection ratio. Therefore, the low detection ratio was investigated using malachite green particles with an arithmetic mean diameter of 79 nm (Figure A9a). Despite the lower number of larger particles, the color was much darker around the inlet where large particles with larger mass are

collected (Figure A9b). The dissolved malachite green particles were not sufficiently distributed in solution after introduction of the liquid (Figure A9c). With a typical diffusion-layer thickness around 40 – 50 µm [76], the concentration of target metal could be highly heterogeneous in local areas around the electrode, which caused various detection ratios in the range of 10 – 98 %. In comparison, the distribution equilibrium with less distinguishable concentration gradient was achieved after ultrasonic treatment (Figure A9d). Therefore, the more uniform distribution of Cu ions in the microchannel was likely to give the low detection ratio by stabilizing the local concentration around the electrode. More studies about the distribution of Cu ions in the microchannel are needed possibly by integrating more electrodes into the microchannel for more data points and simulating the concentration gradients using simulation software.

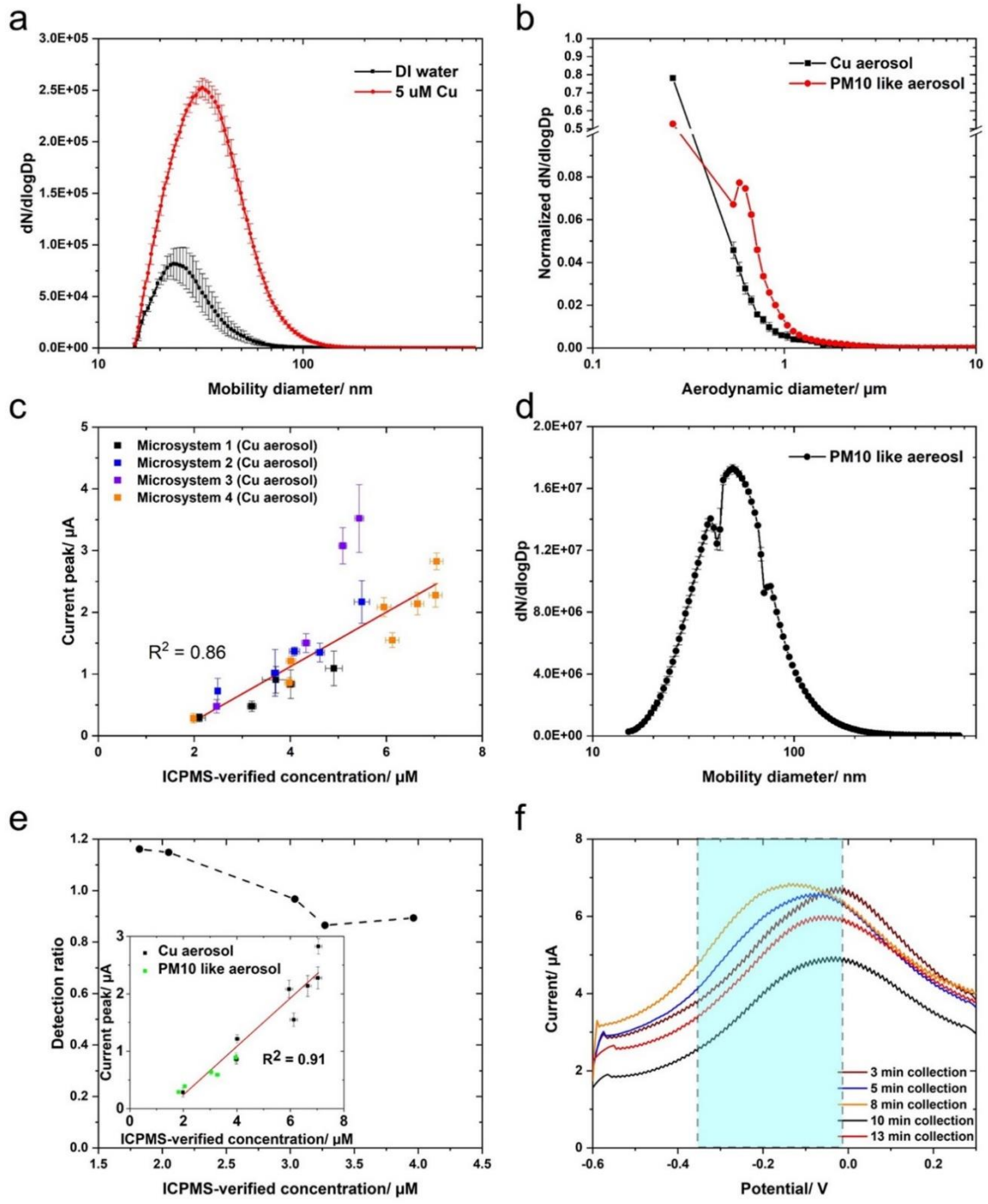

Figure 2.5 Collection and electrochemical detection of aerosol metals using the microsystem: (a) SMPS results of the particle size distribution and particle numbers of the Cu aerosol; (b) Normalized particle size distribution of the Cu aerosol and PM_{10} like aerosol in terms of aerodynamic diameter; (c) Responses of electrochemical signal to lab-generated Cu aerosol using four microsystems in terms of the collection duration; (d) SMPS results of the particle size distribution and particle numbers of the PM_{10} like aerosol; (e) Detection ratio of the electrochemical signals of Cu in the PM_{10} like samples to ICP-MS measurement results; (f) SWV responses to Cu in the PM_{10} like aerosol.

The inter-chip reproducibility of the proposed microsystem was further investigated by testing Cu aerosol in the aqueous concentration range of 2 - 8 µM, which is the ratio of total Cu mass to the volume of the microchannel. For each microsystem, the sensing performance corresponding to the concentration of Cu is linear ($R^2 > 0.83$) (Figure A10a). Cu concentrations derived from electrochemical signals account for 14 ± 4 % of the ICPMS-verified concentrations in the microchannel (Figure A10b), indicating the equilibrium of concentration gradient after 2 min ultrasonic treatment. The linear relationship ($R^2 = 0.86$) between ICPMS-verified concentration and current peak is again confirmed by four microsystems (Figure 2.5c), which supports the reproducibility of the microsystem. According to the global regression, the limit of detection is 1.5 µM, and the total amount of Cu in the microchannel is 21 ng, which means the microsystem is able to detect the accumulated aerosol particles with soluble Cu above 21 ng. Previous study demonstrates that copper in the particulate matter exists in the divalent state, such as hydrated copper sulfate [77], so the sensing performance of the microsystem is less likely to be affected by Cu(I). According to the collection efficiency of NaCl particles, the collection efficiency of 70 % is assumed at the working flow rate of 3.1 L/min, therefore, the microsystem is able to detect aerosol samples with a soluble Cu concentration higher than 32 ng/m3 based on 5 h aerosol collection period, while the limit of detection could be further reduced to 8 ng/m^3 for a collection time of 20 h. This microsystem is applicable in a relatively short collection time at the working flow rate of 3.1 L/min with the reported Cu concentrations, such as 24.4, 117 ± 163.3, and 188 ng/m3 in Switzerland [72], China [73], and São Paulo, Brazil [78], respectively.

2.3.5. Sensing performance of the microsystem using real-world samples

The arithmetic mean diameter of the PM_{10}-like aerosol was 57.1 ± 0.6 nm (Figure 2.5d). In comparison to Cu aerosol, the PM_{10}-like aerosol contained a larger fraction of coarse particles to simulate the real-world environment (Figure 2.5b). In particulate, $PM_{0.5}$, $PM_{0.5\text{-}1}$, $PM_{1\text{-}2.5}$ and $PM_{2.5\text{-}10}$ account for 52.7 %, 42.1 %, 5.0 %, and 0.2 % in terms of particle number, respectively. In fact, the number size distribution of the PM_{10}-like aerosol was quite similar to that of the real-world environment with a mode diameter smaller than 100 nm such as central Los Angeles [62] and London [79]. Based on the calibration curve of a single microsystem (Microsystem 4), the average detection ratio of Cu in the PM_{10}-like aerosol was 100 ± 14 % (Figure 2.5e), which suggests that the simultaneous presence of multiple elements such as Cd, Mn, Zn and organic matters has a minor effect on the sensing performance. It also indicates that metallic copper or the insoluble fraction of particulate copper has a limited effect on the detection of soluble copper ions. In this part, it should be noted that the detection ratio is the ratio of Cu concentration derived from electrochemical signals based on the calibration curve of the microsystem to the

ICPMS-verified concentration. Collection and dissolution of the PM10-liked aerosol also suggest the considerable quantity of black carbon distributes around the inlet and first turn of the microchannel, which prevents significant fouling of the electrode surface (Figure A11). In addition, collected particles are removed by ultrasonic treatment each time after collection and detection, which prevents particle accumulation especially the insoluble fraction, and worse collection and detection performance. Unlike the sharp current peak of Cu solution, the wider and flat current peak of PM_{10}-like aerosol indicated that the oxidation peak of Cu at -0.2 V tends to overlap with the acetate adsorption peak at a more positive potential (i.e. 0 V) (Figure 2.5f). This evidence suggests that deposited Cu on the electrode surface tends to be stripped at a more positive potential when a higher concentration of PM_{10}-like aerosol samples is present in the microchannel. The possible reason is that multiple anions in the PM_{10}-like aerosol, such as sulfate [80], chloride [81] and bromide [82], affect the deposition of Cu on the gold electrode by changing the surface structures and onset potentials of the deposition process, which further influences the corresponding stripping process of Cu. Unlike the interference studies of several metal ions shown in Figure 2.4c, multiple elements present in the real-world aerosol mainly affected the shape of the current peak rather than the current peak intensity (Figure 2.5e and f). Therefore, the results indicated that the microsystem can be applied for practical usage despite interferences from other components such as non-target metal ions. Overall, the collection and sensing performance of the microsystem was validated by real-world aerosol containing metals, carbons, non-metal fractions. Besides that, the performance of this microsystem should be examined in the real-world environment in the next step.

2.4 Conclusions

In this study, a promising integrated aerodynamic/electrochemical microsystem has been successfully developed to collect aerosol with relatively high efficiency to detect soluble copper at the nanogram level. The collection, dissolution and detection of aerosol copper rely on the air/solid and liquid/solid interface of the microchannel and do not require a bulky setup. This microsystem is a promising low-cost alternative to the cumbersome coupling in series for aerosol collection and detection platform. Nonetheless, the collection and sensing performance of this microsystem should be extensively examined in the real-world environment in future studies. The limitation of this microsystem is that the collection time could vary according to different soluble Cu concentration in different regions and cities.

The collection and determination of several metals such as Cu, Cd, Pb, Fe and Ni can be achieved on the current or modified microsystem (by replacing or modifying the electrode). Besides that, bioaccessiblity of aerosol metals could be extensively explored by using different leaching agents such as water, salt solutions, buffer solutions and synthetic body fluids [5], and

detected in situ by the microsystem. In this way, high-resolution monitoring and investigation of bioaccessible aerosol metals could give the rapid response to air quality in terms of human health and facilitate the development of air quality control policies [8]. Furthermore, the application of the microsystem is reasonably extended to the collection and detection of other soluble elements such as nitrate [83] and aerosol oxidative load [84], which offers a new way to develop the online, mobile, low-cost and miniaturized monitoring system for different aerosol components. Therefore, a more comprehensive routine monitoring network of aerosol soluble metals and other components is potentially established to investigate the aerosol processes and protect the human health.

Acknowledgments: Y.-B. Zhao and F. Jiang thank China Scholarship Council for the financial support. We acknowledge Dr. Eric Bakker (University of Geneva, Switzerland) for valuable suggestions. T. Cen and C. Ludwig acknowledge the Swiss National Science Foundation for financial support (project 184817). We thank Dr. Xing Ding for supporting FTIR measurement.

Conflicts of Interest: The authors declare no conflict of interest.

2.5 References

[1] K.R. Daellenbach, G. Uzu, J. Jiang, L.-E. Cassagnes, Z. Leni, A. Vlachou, et al., Sources of particulate-matter air pollution and its oxidative potential in Europe, *Nature*, **2020**, 587, 414-9, 10.1038/s41586-020-2902-8.

[2] N.M. Mahowald, D.S. Hamilton, K.R.M. Mackey, J.K. Moore, A.R. Baker, R.A. Scanza, et al., Aerosol trace metal leaching and impacts on marine microorganisms, *Nature Communications*, **2018**, 9, 2614, 10.1038/s41467-018-04970-7.

[3] H. Li, X. Qian, Q.g. Wang, Heavy Metals in Atmospheric Particulate Matter: A Comprehensive Understanding Is Needed for Monitoring and Risk Mitigation, *Environmental Science & Technology*, **2013**, 47, 13210-1, 10.1021/es404751a.

[4] G. Pérez, M. López-Mesas, M. Valiente, Assessment of Heavy Metals Remobilization by Fractionation: Comparison of Leaching Tests Applied to Roadside Sediments, *Environmental Science & Technology*, **2008**, 42, 2309-15, 10.1021/es0712975.

[5] A. Mukhtar, A. Limbeck, Recent developments in assessment of bio-accessible trace metal fractions in airborne particulate matter: A review, *Analytica Chimica Acta*, **2013**, 774, 11-25, https://doi.org/10.1016/j.aca.2013.02.008.

[6] X. Hu, Y. Zhang, Z. Ding, T. Wang, H. Lian, Y. Sun, et al., Bioaccessibility and health risk of arsenic and heavy metals (Cd, Co, Cr, Cu, Ni, Pb, Zn and Mn) in TSP and PM2.5 in Nanjing, China, *Atmospheric Environment*, **2012**, 57, 146-52, https://doi.org/10.1016/j.atmosenv.2012.04.056.

[7] T. Fang, H. Guo, L. Zeng, V. Verma, A. Nenes, R.J. Weber, Highly Acidic Ambient Particles, Soluble Metals, and Oxidative Potential: A Link between Sulfate and Aerosol Toxicity, *Environmental Science & Technology*, **2017**, 51, 2611-20, 10.1021/acs.est.6b06151.

[8] B. Zhao, L. Yu, C. Wang, C. Shuai, J. Zhu, S. Qu, et al., Urban Air Pollution Mapping Using Fleet Vehicles as Mobile Monitors and Machine Learning, *Environmental Science & Technology*, **2021**, 10.1021/acs.est.0c08034.

[9] D. Wang, M.M. Shafer, J.J. Schauer, C. Sioutas, A new technique for online measurement of total and water-soluble copper (Cu) in coarse particulate matter (PM), *Environmental Pollution*, **2015**, 199, 227-34, https://doi.org/10.1016/j.envpol.2015.02.006.

[10] D. Wang, P. Pakbin, A. Saffari, M.M. Shafer, J.J. Schauer, C. Sioutas, Development and Evaluation of a High-Volume Aerosol-into-Liquid Collector for Fine and Ultrafine Particulate Matter, *Aerosol Science and Technology*, **2013**, 47, 1226-38, 10.1080/02786826.2013.830693.

[11] D. Wang, M.M. Shafer, J.J. Schauer, C. Sioutas, Development of a Technology for Online Measurement of Total and Water-Soluble Copper (Cu) in PM2.5, *Aerosol Science and Technology*, **2014**, 48, 864-74, 10.1080/02786826.2014.937478.

[12] D.A. Orsini, Y. Ma, A. Sullivan, B. Sierau, K. Baumann, R.J. Weber, Refinements to the particle-into-liquid sampler (PILS) for ground and airborne measurements of water soluble aerosol composition, *Atmospheric Environment*, **2003**, 37, 1243-59, https://doi.org/10.1016/S1352-2310(02)01015-4.

[13] H.R. Kim, S. An, J. Hwang, Aerosol-to-Hydrosol Sampling and Simultaneous Enrichment of Airborne Bacteria For Rapid Biosensing, *ACS Sensors*, **2020**, 5, 2763-71, 10.1021/acssensors.0c00555.

[14] J. Bhardwaj, M.-W. Kim, J. Jang, Rapid Airborne Influenza Virus Quantification Using an Antibody-Based Electrochemical Paper Sensor and Electrostatic Particle Concentrator, *Environmental Science & Technology*, **2020**, 54, 10700-12, 10.1021/acs.est.0c00441.

[15] I.V. Novosselov, R.A. Gorder, J.A. Van Amberg, P.C. Ariessohn, Design and Performance of a Low-Cost Micro-Channel Aerosol Collector, *Aerosol Science and Technology*, **2014**, 48, 822-30, 10.1080/02786826.2014.932895.

[16] Y. Xie, J. Rufo, R. Zhong, J. Rich, P. Li, K.W. Leong, et al., Microfluidic Isolation and Enrichment of Nanoparticles, *ACS Nano*, **2020**, 14, 16220-40, 10.1021/acsnano.0c06336.

[17] X. Bian, Y. Lan, B. Wang, Y.S. Zhang, B. Liu, P. Yang, et al., Microfluidic Air Sampler for Highly Efficient Bacterial Aerosol Collection and Identification, *Analytical Chemistry*, **2016**, 88, 11504-12, 10.1021/acs.analchem.6b02708.

[18] J. Choi, S.C. Hong, W. Kim, J.H. Jung, Highly Enriched, Controllable, Continuous Aerosol Sampling Using Inertial Microfluidics and Its Application to Real-Time Detection of Airborne Bacteria, *ACS Sensors*, **2017**, 2, 513-21, 10.1021/acssensors.6b00753.

[19] W. Jing, W. Zhao, S. Liu, L. Li, C.-T. Tsai, X. Fan, et al., Microfluidic Device for Efficient Airborne Bacteria Capture and Enrichment, *Analytical Chemistry*, **2013**, 85, 5255-62, 10.1021/ac400590c.

[20] S.C. Hong, J.S. Kang, J.E. Lee, S.S. Kim, J.H. Jung, Continuous aerosol size separator using inertial microfluidics and its application to airborne bacteria and viruses, *Lab on a Chip*, **2015**, 15, 1889-97, 10.1039/C5LC00079C.

[21] I. Mirzaee, M. Song, M. Charmchi, H. Sun, A microfluidics-based on-chip impinger for airborne particle collection, *Lab on a Chip*, **2016**, 16, 2254-64, 10.1039/C6LC00040A.

[22] W. Zhang, H. Zhang, S.E. Williams, A. Zhou, Microfabricated three-electrode on-chip PDMS device with a vibration motor for stripping voltammetric detection of heavy metal ions, *Talanta*, **2015**, 132, 321-6, https://doi.org/10.1016/j.talanta.2014.08.075.

[23] J. Wang, P. Yu, K. Kan, H. Lv, Z. Liu, B. Sun, et al., Efficient ultra-trace electrochemical detection of Cd2+, Pb2+ and Hg2+ based on hierarchical porous S-doped C3N4 tube

bundles/graphene nanosheets composite, *Chemical Engineering Journal*, **2021**, 420, 130317, https://doi.org/10.1016/j.cej.2021.130317.

[24] N. Ullah, M. Mansha, I. Khan, A. Qurashi, Nanomaterial-based optical chemical sensors for the detection of heavy metals in water: Recent advances and challenges, *TrAC Trends in Analytical Chemistry*, **2018**, 100, 155-66, https://doi.org/10.1016/j.trac.2018.01.002.

[25] C.-Y. Wang, C.-C. Hsu, Online, Continuous, and Interference-Free Monitoring of Trace Heavy Metals in Water Using Plasma Spectroscopy Driven by Actively Modulated Pulsed Power, *Environmental Science & Technology*, **2019**, 53, 10888-96, 10.1021/acs.est.9b02970.

[26] G. Qiu, S.P. Ng, X. Liang, N. Ding, X. Chen, C.-M.L. Wu, Label-Free LSPR Detection of Trace Lead(II) Ions in Drinking Water by Synthetic Poly(mPD-co-ASA) Nanoparticles on Gold Nanoislands, *Analytical Chemistry*, **2017**, 89, 1985-93, 10.1021/acs.analchem.6b04536.

[27] D. Wang, M.H. Sowlat, M.M. Shafer, J.J. Schauer, C. Sioutas, Development and evaluation of a novel monitor for online measurement of iron, manganese, and chromium in ambient particulate matter (PM), *Science of The Total Environment*, **2016**, 565, 123-31, https://doi.org/10.1016/j.scitotenv.2016.04.164.

[28] G. Aragay, J. Pons, A. Merkoçi, Recent Trends in Macro-, Micro-, and Nanomaterial-Based Tools and Strategies for Heavy-Metal Detection, *Chemical Reviews*, **2011**, 111, 3433-58, 10.1021/cr100383r.

[29] J. Kudr, O. Zitka, M. Klimanek, R. Vrba, V. Adam, Microfluidic electrochemical devices for pollution analysis–A review, *Sensors and Actuators B: Chemical*, **2017**, 246, 578-90, https://doi.org/10.1016/j.snb.2017.02.052.

[30] D. Buzica, M. Gerboles, A. Borowiak, P. Trincherini, R. Passarella, V. Pedroni, Comparison of voltammetry and inductively coupled plasma-mass spectrometry for the determination of heavy metals in PM10 airborne particulate matter, *Atmospheric Environment*, **2006**, 40, 4703-10, https://doi.org/10.1016/j.atmosenv.2006.04.015.

[31] S. Li, C. Zhang, S. Wang, Q. Liu, H. Feng, X. Ma, et al., Electrochemical microfluidics techniques for heavy metal ion detection, *Analyst*, **2018**, 143, 4230-46, 10.1039/C8AN01067F.

[32] K. Pi, J. Liu, P. Van Cappellen, Direct Measurement of Aqueous Mercury(II): Combining DNA-Based Sensing with Diffusive Gradients in Thin Films, *Environmental Science & Technology*, **2020**, 54, 13680-9, 10.1021/acs.est.0c03870.

[33] D. Neagu, F. Arduini, J.C. Quintana, P. Di Cori, C. Forni, D. Moscone, Disposable Electrochemical Sensor to Evaluate the Phytoremediation of the Aquatic Plant Lemna minor L. toward Pb2+ and/or Cd2+, *Environmental Science & Technology*, **2014**, 48, 7477-85, 10.1021/es500675x.

[34] J. Mettakoonpitak, J. Volckens, C.S. Henry, Janus Electrochemical Paper-Based Analytical Devices for Metals Detection in Aerosol Samples, *Analytical Chemistry*, **2020**, 92, 1439-46, 10.1021/acs.analchem.9b04632.

[35] A. Fernández-la-Villa, D.F. Pozo-Ayuso, M. Castaño-Álvarez, Microfluidics and electrochemistry: an emerging tandem for next-generation analytical microsystems, *Current Opinion in Electrochemistry*, **2019**, 15, 175-85, https://doi.org/10.1016/j.coelec.2019.05.014.

[36] R. Wang, X. Wang, Sensing of inorganic ions in microfluidic devices, *Sensors and Actuators B: Chemical*, **2021**, 329, 129171, https://doi.org/10.1016/j.snb.2020.129171.

[37] A. Chałupniak, A. Merkoçi, Graphene Oxide–Poly(dimethylsiloxane)-Based Lab-on-a-Chip Platform for Heavy-Metals Preconcentration and Electrochemical Detection, *ACS Applied Materials & Interfaces*, **2017**, 9, 44766-75, 10.1021/acsami.7b12368.

[38] A. Jang, Z. Zou, K.K. Lee, C.H. Ahn, P.L. Bishop, Potentiometric and voltammetric polymer lab chip sensors for determination of nitrate, pH and Cd(II) in water, *Talanta*, **2010**, 83, 1-8, https://doi.org/10.1016/j.talanta.2010.07.061.

[39] P.N. Nge, C.I. Rogers, A.T. Woolley, Advances in Microfluidic Materials, Functions, Integration, and Applications, *Chemical Reviews*, **2013**, 113, 2550-83, 10.1021/cr300337x.

[40] A.R. Metcalf, S. Narayan, C.S. Dutcher, A review of microfluidic concepts and applications for atmospheric aerosol science, *Aerosol Science and Technology*, **2018**, 52, 310-29, 10.1080/02786826.2017.1408952.

[41] Y. Sameenoi, K. Koehler, J. Shapiro, K. Boonsong, Y. Sun, J. Collett, et al., Microfluidic Electrochemical Sensor for On-Line Monitoring of Aerosol Oxidative Activity, *Journal of the American Chemical Society*, **2012**, 134, 10562-8, 10.1021/ja3031104.

[42] S.D. Noblitt, G.S. Lewis, Y. Liu, S.V. Hering, J.L. Collett, C.S. Henry, Interfacing Microchip Electrophoresis to a Growth Tube Particle Collector for Semicontinuous Monitoring of Aerosol Composition, *Analytical Chemistry*, **2009**, 81, 10029-37, 10.1021/ac901903m.

[43] J. Mettakoonpitak, D. Miller-Lionberg, T. Reilly, J. Volckens, C.S. Henry, Low-cost reusable sensor for cobalt and nickel detection in aerosols using adsorptive cathodic square-wave stripping voltammetry, *Journal of Electroanalytical Chemistry*, **2017**, 805, 75-82, https://doi.org/10.1016/j.jelechem.2017.10.026.

[44] J. Mettakoonpitak, J. Mehaffy, J. Volckens, C.S. Henry, AgNP/Bi/Nafion-modified Disposable Electrodes for Sensitive Zn(II), Cd(II), and Pb(II) Detection in Aerosol Samples, *Electroanalysis*, **2017**, 29, 880-9, 10.1002/elan.201600591.

[45] M.R. Palomo-Marín, F. Rueda-Holgado, J. Marín-Expósito, E. Pinilla-Gil, Disposable sputtered-bismuth screen-printed sensors for voltammetric monitoring of cadmium and lead in atmospheric particulate matter samples, *Talanta*, **2017**, 175, 313-7, https://doi.org/10.1016/j.talanta.2017.07.060.

[46] F. Rueda-Holgado, E. Bernalte, M.R. Palomo-Marín, L. Calvo-Blázquez, F. Cereceda-Balic, E. Pinilla-Gil, Miniaturized voltammetric stripping on screen printed gold electrodes for field determination of copper in atmospheric deposition, *Talanta*, **2012**, 101, 435-9, https://doi.org/10.1016/j.talanta.2012.09.054.

[47] F. Rueda-Holgado, L. Calvo-Blázquez, F. Cereceda-Balic, E. Pinilla-Gil, A semiautomatic system for soluble lead and copper monitoring in atmospheric deposition by coupling of passive elemental fractionation sampling and voltammetric measurement on screen-printed gold electrodes, *Microchemical Journal*, **2016**, 124, 20-5, https://doi.org/10.1016/j.microc.2015.07.012.

[48] H.d.A. Silva-Neto, T.M.G. Cardoso, W.K.T. Coltro, R.C. Urban, Determination of bioavailable lead in atmospheric aerosols using unmodified screen-printed carbon electrodes, *Analytical Methods*, **2019**, 11, 4875-81, 10.1039/C9AY01301F.

[49] S. Canepari, M.L. Astolfi, S. Moretti, R. Curini, Comparison of extracting solutions for elemental fractionation in airborne particulate matter, *Talanta*, **2010**, 82, 834-44, https://doi.org/10.1016/j.talanta.2010.05.068.

[50] K.J. Regehr, M. Domenech, J.T. Koepsel, K.C. Carver, S.J. Ellison-Zelski, W.L. Murphy, et al., Biological implications of polydimethylsiloxane-based microfluidic cell culture, *Lab on a Chip*, **2009**, 9, 2132-9, 10.1039/B903043C.

[51] A. Hourlier-Fargette, J. Dervaux, A. Antkowiak, S. Neukirch, Extraction of Silicone Uncrosslinked Chains at Air–Water–Polydimethylsiloxane Triple Lines, *Langmuir*, **2018**, 34, 12244-50, 10.1021/acs.langmuir.8b02128.

[52] C. Provin, T. Fujii, Reaction–diffusion phenomena in a PDMS matrix can modify its topography, *Lab on a Chip*, **2011**, 11, 2948-54, 10.1039/C1LC20218A.

[53] Z. Almutairi, C.L. Ren, L. Simon, Evaluation of polydimethylsiloxane (PDMS) surface modification approaches for microfluidic applications, *Colloids and Surfaces A: Physicochemical and Engineering Aspects*, **2012**, 415, 406-12, https://doi.org/10.1016/j.colsurfa.2012.10.008.

[54] X. Sun, R.T. Kelly, K. Tang, R.D. Smith, Ultrasensitive nanoelectrospray ionization-mass spectrometry using poly(dimethylsiloxane) microchips with monolithically integrated emitters, *Analyst*, **2010**, 135, 2296-302, 10.1039/C0AN00253D.

[55] J. Lee, N. Jäckel, D. Kim, M. Widmaier, S. Sathyamoorthi, P. Srimuk, et al., Porous carbon as a quasi-reference electrode in aqueous electrolytes, *Electrochimica Acta*, **2016**, 222, 1800-5, https://doi.org/10.1016/j.electacta.2016.11.148.

[56] Y. Lu, X. Liang, C. Niyungeko, J. Zhou, J. Xu, G. Tian, A review of the identification and detection of heavy metal ions in the environment by voltammetry, *Talanta*, **2018**, 178, 324-38, https://doi.org/10.1016/j.talanta.2017.08.033.

[57] L. Gitlin, P. Schulze, S. Ohla, H.-J. Bongard, D. Belder, Surface modification of PDMS microfluidic devices by controlled sulfuric acid treatment and the application in chip electrophoresis, *ELECTROPHORESIS*, **2015**, 36, 449-56, https://doi.org/10.1002/elps.201400269.

[58] Z. Zou, A. Jang, E. MacKnight, P.-M. Wu, J. Do, P.L. Bishop, et al., Environmentally friendly disposable sensors with microfabricated on-chip planar bismuth electrode for in situ heavy metal ions measurement, *Sensors and Actuators B: Chemical*, **2008**, 134, 18-24, https://doi.org/10.1016/j.snb.2008.04.005.

[59] G. Emma, J. Snell, J. Charoud-Got, A. Held, H. Emons, Feasibility study of a candidate reference material for ions in PM2.5: does commutability matter also for inorganic matrices?, *Analytical and Bioanalytical Chemistry*, **2018**, 410, 6001-8, 10.1007/s00216-018-1220-6.

[60] K. Ashley, R.N. Andrews, L. Cavazos, M. Demange, Ultrasonic extraction as a sample preparation technique for elemental analysis by atomic spectrometry, *Journal of Analytical Atomic Spectrometry*, **2001**, 16, 1147-53, 10.1039/B102027G.

[61] European Commission's Joint Research Centre, CERTIFICATE OF ANALYSIS ERM®-CZ120, 2010.

[62] S. Taghvaee, A. Mousavi, M.H. Sowlat, C. Sioutas, Development of a novel aerosol generation system for conducting inhalation exposures to ambient particulate matter (PM), *Science of The Total Environment*, **2019**, 665, 1035-45, https://doi.org/10.1016/j.scitotenv.2019.02.214.

[63] L. Baldrianova, P. Agrafiotou, I. Svancara, A.D. Jannakoudakis, S. Sotiropoulos, The effect of acetate concentration, solution pH and conductivity on the anodic stripping voltammetry of lead and cadmium ions at in situ bismuth-plated carbon microelectrodes, *Journal of Electroanalytical Chemistry*, **2011**, 660, 31-6, https://doi.org/10.1016/j.jelechem.2011.05.028.

[64] C.L. Reddington, G. McMeeking, G.W. Mann, H. Coe, M.G. Frontoso, D. Liu, et al., The mass and number size distributions of black carbon aerosol over Europe, *Atmos Chem Phys*, **2013**, 13, 4917-39, 10.5194/acp-13-4917-2013.

[65] H. Maring, D.L. Savoie, M.A. Izaguirre, L. Custals, J.S. Reid, Mineral dust aerosol size distribution change during atmospheric transport, *Journal of Geophysical Research: Atmospheres*, **2003**, 108, https://doi.org/10.1029/2002JD002536.

[66] X. Pei, W. Kang, W. Yue, A. Bange, W.R. Heineman, I. Papautsky, Disposable Copper-Based Electrochemical Sensor for Anodic Stripping Voltammetry, *Analytical Chemistry*, **2014**, 86, 4893-900, 10.1021/ac500277j.

[67] W. Kang, X. Pei, C.A. Rusinek, A. Bange, E.N. Haynes, W.R. Heineman, et al., Determination of Lead with a Copper-Based Electrochemical Sensor, *Analytical Chemistry*, **2017**, 89, 3345-52, 10.1021/acs.analchem.6b03894.

[68] J. Holmes, P. Pathirathna, P. Hashemi, Novel frontiers in voltammetric trace metal analysis: Towards real time, on-site, in situ measurements, *TrAC Trends in Analytical Chemistry*, **2019**, 111, 206-19, https://doi.org/10.1016/j.trac.2018.11.003.

[69] C.P. Byers, B.S. Hoener, W.-S. Chang, S. Link, C.F. Landes, Single-Particle Plasmon Voltammetry (spPV) for Detecting Anion Adsorption, *Nano Letters*, **2016**, 16, 2314-21, 10.1021/acs.nanolett.5b04990.

[70] A. Berná, J.M. Delgado, J.M. Orts, A. Rodes, J.M. Feliu, Spectroelectrochemical study of the adsorption of acetate anions at gold single crystal and thin-film electrodes, *Electrochimica Acta*, **2008**, 53, 2309-21, https://doi.org/10.1016/j.electacta.2007.09.055.

[71] Y. Yue, H. Chen, A. Setyan, M. Elser, M. Dietrich, J. Li, et al., Size-Resolved Endotoxin and Oxidative Potential of Ambient Particles in Beijing and Zürich, *Environmental Science & Technology*, **2018**, 52, 6816-24, 10.1021/acs.est.8b01167.

[72] M. Furger, M.C. Minguillón, V. Yadav, J.G. Slowik, C. Hüglin, R. Fröhlich, et al., Elemental composition of ambient aerosols measured with high temporal resolution using an online XRF spectrometer, *Atmos Meas Tech*, **2017**, 10, 2061-76, 10.5194/amt-10-2061-2017.

[73] J. Duan, J. Tan, Atmospheric heavy metals and Arsenic in China: Situation, sources and control policies, *Atmospheric Environment*, **2013**, 74, 93-101, https://doi.org/10.1016/j.atmosenv.2013.03.031.

[74] N.T. Tuan, J. Park, J. Lee, J. Gwak, D. Lee, Synthesis of nanoporous Cu films by dealloying of electrochemically deposited Cu–Zn alloy films, *Corrosion Science*, **2014**, 80, 7-11, https://doi.org/10.1016/j.corsci.2013.11.043.

[75] B. Bozzini, P.L. Cavallotti, Electrodeposition and characterization of Au–Cu–Cd alloys, *Journal of Applied Electrochemistry*, **2001**, 31, 897-903, 10.1023/A:1017592018364.

[76] J.Y. Gao, Studying Dissolution with a Model Integrating Solid–Liquid Interface Kinetics and Diffusion Kinetics, *Analytical Chemistry*, **2012**, 84, 10671-8, 10.1021/ac302297a.

[77] F.E. Huggins, G.P. Huffman, J.D. Robertson, Speciation of elements in NIST particulate matter SRMs 1648 and 1650, *Journal of Hazardous Materials*, **2000**, 74, 1-23, https://doi.org/10.1016/S0304-3894(99)00195-8.

[78] G.M. Pereira, K. Teinilä, D. Custódio, A. Gomes Santos, H. Xian, R. Hillamo, et al., Particulate pollutants in the Brazilian city of São Paulo: 1-year investigation for the chemical composition and source apportionment, *Atmos Chem Phys*, **2017**, 17, 11943-69, 10.5194/acp-17-11943-2017.

[79] R.M. Harrison, D.C.S. Beddows, M.S. Alam, A. Singh, J. Brean, R. Xu, et al., Interpretation of particle number size distributions measured across an urban area during the FASTER campaign, *Atmos Chem Phys*, **2019**, 19, 39-55, 10.5194/acp-19-39-2019.

[80] B. Madry, K. Wandelt, M. Nowicki, Sulfate structures on copper deposits on Au(111): In situ STM investigations, *Electrochimica Acta*, **2016**, 217, 249-61, https://doi.org/10.1016/j.electacta.2016.09.061.

[81] F. Möller, O.M. Magnussen, R.J. Behm, CuCl adlayer formation and Cl induced surface alloying: An in situ STM study on Cu underpotential deposition on Au(110) electrode surfaces, *Electrochimica Acta*, **1995**, 40, 1259-65, https://doi.org/10.1016/0013-4686(95)00056-K.

[82] E. Herrero, S. Glazier, L.J. Buller, H.D. Abruña, X-ray and electrochemical studies of Cu upd on single crystal electrodes in the presence of bromide: comparison between Au(111) and Pt(111) electrodes, *Journal of Electroanalytical Chemistry*, **1999**, 461, 121-30, https://doi.org/10.1016/S0022-0728(98)00066-7.

[83] L. Yu, Q. Zhang, Q. Xu, D. Jin, G. Jin, K. Li, et al., Electrochemical detection of nitrate in PM2.5 with a copper-modified carbon fiber micro-disk electrode, *Talanta*, **2015**, 143, 245-53, https://doi.org/10.1016/j.talanta.2015.04.049.

[84] K.A. Koehler, J. Shapiro, Y. Sameenoi, C. Henry, J. Volckens, Laboratory Evaluation of a Microfluidic Electrochemical Sensor for Aerosol Oxidative Load, *Aerosol Science and Technology*, **2014**, 48, 489-97, 10.1080/02786826.2014.891722.

Appendix A

Graphical Abstract

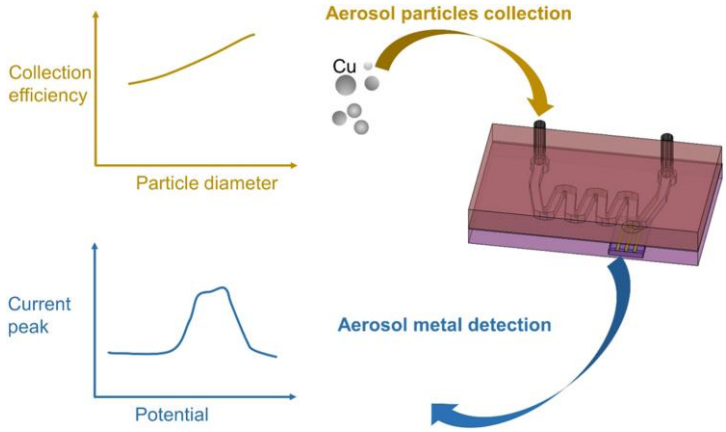

Numerical simulation

Stokes number [15] was calculated for the bends and the inlet at 2.5 L/min (Table A1) based on the following equation:

$$St = \frac{\rho_p {D_p}^2 U_0 C_C}{9 \rho_g v_g D_H}$$

where ρ_p is the particle density, D_p is the particle diameter, U_0 is the air velocity, C_C is the Cunningham slip correction, ρ_g is the air density, v_g is the air viscosity, and D_H is the hydraulic diameter of the channel. The Stokes numbers for the bends and the inlet suggestes that the inelt tends to collect more particles compared to the bends.

Table A1 Stokes numbers for the bends and the inlet.

	50 nm	**100 nm**	**200 nm**	**400 nm**	**500 nm**

Inlet 2 L/min	7.43E-03	1.69E-02	4.32E-02	1.28E-01	1.88E-01
Inlet 2.5 L/min	9.41E-03	2.15E-02	5.47E-02	1.62E-01	2.38E-01
Bends 2 L/min	1.42E-03	3.25E-03	8.28E-03	2.46E-02	3.59E-02
Bends 2.5 L/min	1.80E-03	4.11E-03	1.05E-02	3.11E-02	4.56E-02

Reynolds number was calculated based on the following equation:

$$\mathrm{Re} = \frac{W D_H}{\mu A}$$

where W is the mass flowrate of the air (kg/s), D_H is the hydraulic diameter (m), μ is the dynamic viscosity of the fluid (kg/(m·s)), A is the cross-sectional area (m^2). Dean number was calculated based on the following equation:

$$\mathrm{De} = \mathrm{Re}\sqrt{\frac{D_H}{2R_c}}$$

where R_c is the radius of curvature of the path of the channel. The Reynolds number and Dean number for the inlet and bends were calculated in Table A2. The Reynolds number was decreasing from above 2300 to below 2000 when entering the inlet, which indicated the transition from turbulent to laminar flow. The Dean number was higher than 400, indicating turbulent flow going through the bends (curvatures). Therefore, turbulent flow model was employed to simulate the flow in the microchannel.

Table A2 Reynolds number and Dean number for the inlet and bends.

	2 L/min	2.5 L/min
Reynolds number for the inlet	2.87E+03	3.59E+03
Reynolds number for the bends	1.41E+03	1.76E+03
Dean number for the bends	705	881

For the boundary condition, wall condition was defined as no slip. The number of boundary layers was two, and the boundary layer stretching factor was 1.2. The thickness adjustment factor was 5. The mesh independence was also performed, and the mesh size was changed from coaser, coarse, normal to fine. In particular, the coarser mesh consists of 34565 domain elements, 5192 boundary elements, and 804 edge elements, whereas the coarse mesh includes 57830 domain elements, 8434 boundary elements, and 1030 edge elements. The normal mesh consists of 185520 domain elements, 17092 boundary elements, and 1486 edge elements, while the fine mesh includes 281255 domain elements, 25266 boundary elements, and 1838 edge elements. 100, 300 and 500 nm particles were selected for the investigation of the mess indepedence. The collection efficiencies were stabilized with normal and fine mesh size (Table A3). In contrast, coarser and coarse mesh tend to overestimate the collection efficiency. It indicated that boundary layer was well resolved with the fine mesh. In the numerical simulation, the fine mesh size was used to obtain more accurate results.

Table A3 Simulated collection efficiency of the microchannel with different mesh size in the size range of 50 – 548 nm (NaCl particles).

	Coarser	**Coarse**	**Normal**	**Fine**
100 nm	0.948	0.779	0.681	0.681
300 nm	0.959	0.833	0.767	0.782
500 nm	0.977	0.931	0.910	0.918

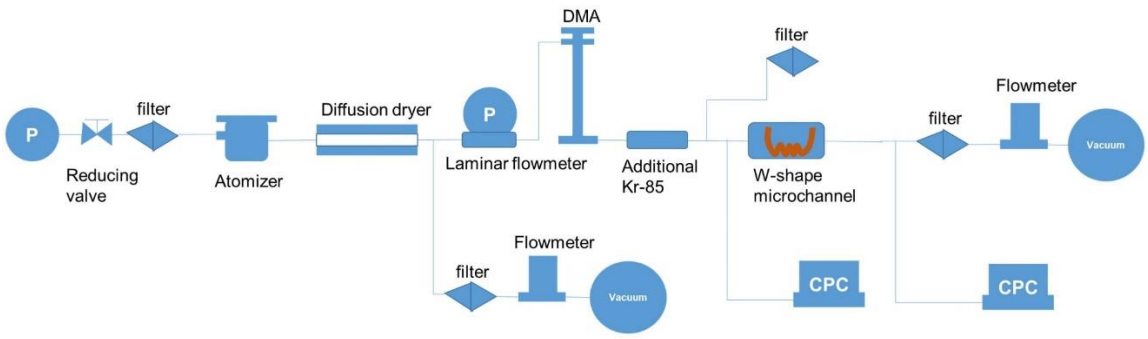

Figure A1 Schematic of experimental setup for the collection efficiency.

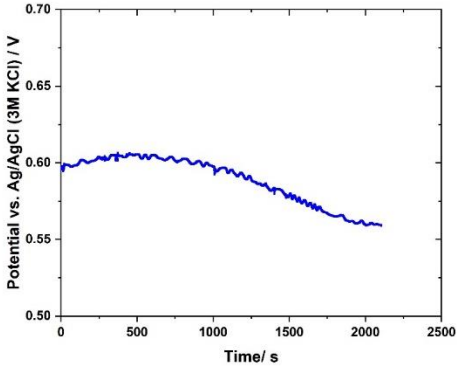

Figure A2 Open circuit potential of the Pt pseudo-reference electrode (p-RE) against the commercial Ag/AgCl (3 M KCl) reference electrodes in 0.1 M acetic acid (pH 4.45).

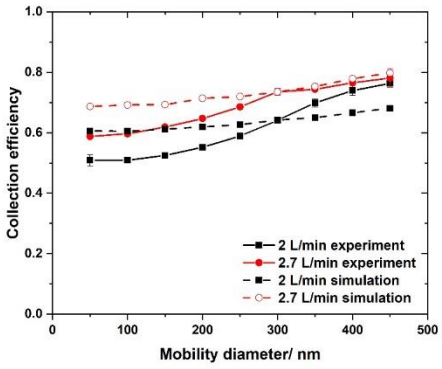

Figure A3 Experimental and simulated collection efficiency of DEHS particles at 2 and 2.7 L/min (assuming DEHS particle density of 900 kg/m^3).

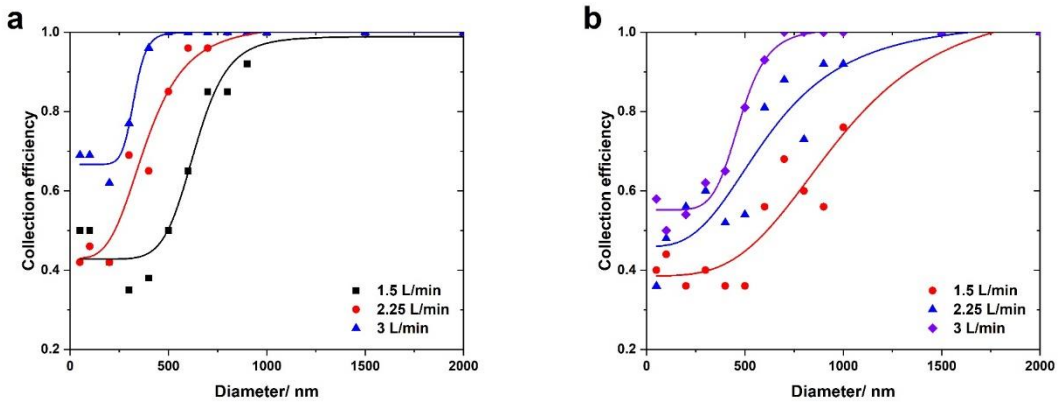

Figure A4 Comparison of simulated NaCl collection efficiency using different inlet diameters: (a) 1 mm, and (b) 1.6 mm at a flow rate of 1.5, 2.25 and 3 L/min, respectively.

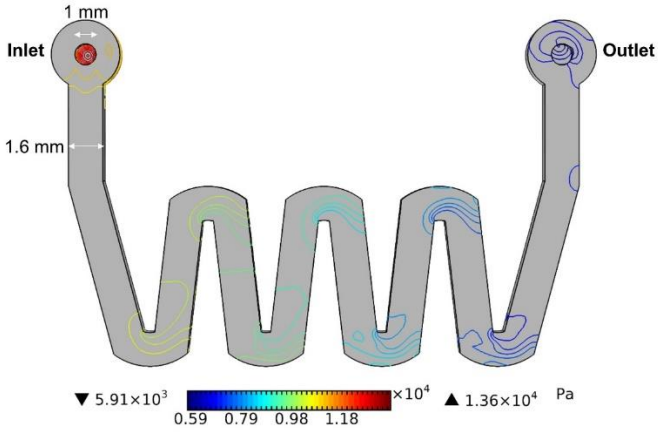

Figure A5 Simulation of pressure drop of the microchannel at 3 L/min.

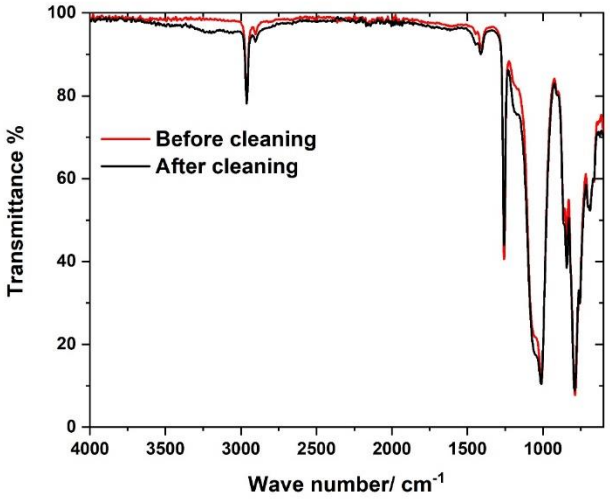

Figure A6 FTIR spectrum of the inner surface of the microchannel before and after cleaning.

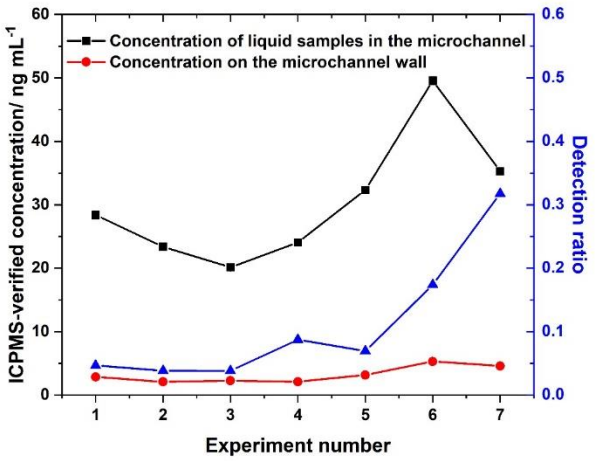

Figure A7 The detection ratio, ICPMS-verified concentration of liquid sample in the microchannel and on the microchannel wall after introducing 0.1 M acetate buffer with 1 min ultrasonic treatment.

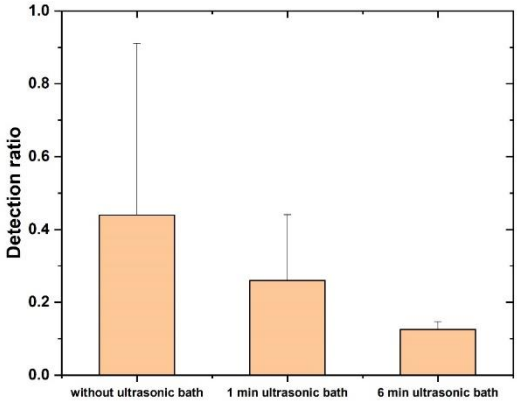

Figure A8 The detection ratio as a function of the duration of ultrasonic bath in the sealed microchannel.

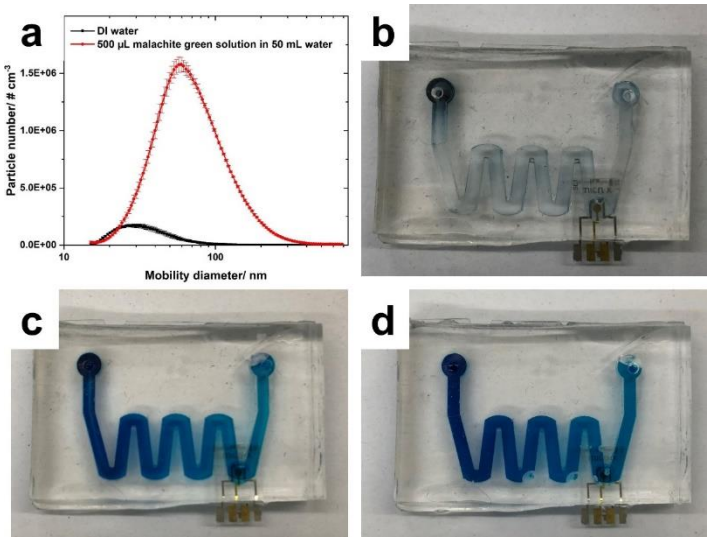

Figure A9 Collection and dissolution of malachite green particles for 1 h: (a) SMPS results of the particle size distribution and particle number of the malachite green particles; (b) before and (c) after introducing DI water without ultrasonic treatment; (d) with 6 min ultrasonic treatment.

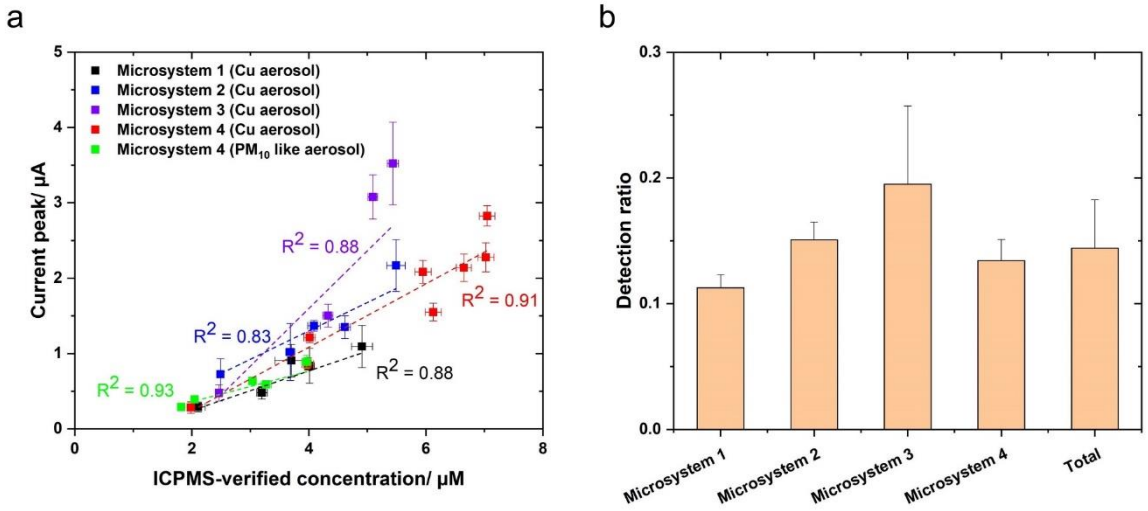

Figure A10 (a) Relationship between ICPMS-verified concentration and current peak, and (b) detection ratio of four microsystems.

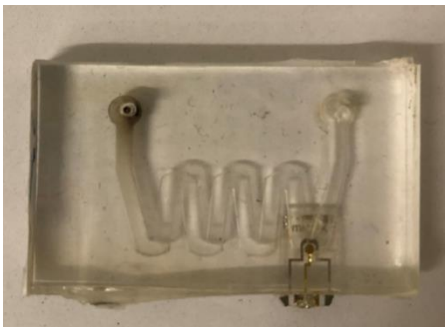

Figure A11 The distribution of PM10 like samples in the microchannel with introducing 0.1 M acetate buffer after 2 min ultrasonic treatment.

Chapter 3

Aerosol-into-liquid capture and detection of atmospheric soluble metals across the gas-liquid interface using Janus-membrane electrodes

Yi-Bo Zhao[1,2], Tianyu Cen[3,4], Fuze Jiang[1,2], Weidong He[1,2,5], Xiaole Zhang[1,2], Xiaoxiao Feng[1,2], Min Gao[1,2], Christian Ludwig[3,4], Eric Bakker[6], and Jing Wang[1,2*]

[1] Institute of Environmental Engineering, ETH Zürich, Zürich 8093, Switzerland
[2] Laboratory for Advanced Analytical Technologies, Empa, Swiss Federal Laboratories for Materials Science and Technology, Dübendorf 8600, Switzerland
[3] Environmental Engineering Institute (IIE, GR-LUD), School of Architecture, Civil and Environmental Engineering (ENAC), École Polytechnique Fédérale de Lausanne (EPFL), Lausanne 1015, Switzerland
[4] Bioenergy and Catalysis Laboratory (LBK-CPM), Energy and Environment Research Division (ENE), Paul Scherrer Institut (PSI), Villigen PSI 5232, Switzerland
[5] Filter Test Center, College of Resources and Civil Engineering, Northeastern University, NO. 3-11, Wenhua Road, Heping District, Shenyang, Liaoning 110819, China
[6] Department of Inorganic and Analytical Chemistry, University of Geneva, Quai Ernest-Ansermet 30, Geneva 1211, Switzerland

Author contributions

Y.-B. Zhao and J. Wang conceived the idea and designed the experiment. Y.-B. Zhao conducted the experiments, data analysis, and manuscript preparation. J. Wang, C. Ludwig and E. Bakker contributed to the revision of the manuscript. T. Cen and C. Ludwig conducted the ICP-MS measurements. F. Jiang, W. He, and E. Bakker helped with the fabrication of the membrane electrode, instrumental setup, and data analysis. X. Zhang, X. Feng, and M. Gao performed numerical simulations and data analysis. All authors have discussed the results and approved the final version of the manuscript.

This work has been published in *Proceedings of the National Academy of Sciences*. **2023**, *120*. DOI: 10.1073/pnas.2219388120.

Abstract

The soluble fraction of atmospheric transition metals is particularly associated with health effects such as reactive oxygen species compared to total metals. However, direct measurements of the soluble fraction are restricted to sampling and detection units in sequence burdened with a compromise between time resolution and system bulkiness. Here, we propose the concept of aerosol-into-liquid capture and detection, which allowed one-step particle capture and detection via the Janus-membrane electrode at the gas-liquid interface, enabling active enrichment and enhanced mass transport of metal ions. The integrated aerodynamic/electrochemical (IAE) system was capable of capturing airborne particles with a cutoff size down to 50 nm and detecting Pb(II) with a limit of detection of 95.7 ng. The proposed concept can

pave the way for cost-effective and miniaturized systems, for the capture and detection of airborne soluble metals in air quality monitoring, especially for abrupt air pollution events with high airborne metal concentrations (e.g. wildfires and fireworks).

Keywords: Atmospheric soluble metals, Aerosol-into-liquid, Aerodynamic/electrochemical system, Gas-liquid interface, Air quality

3.1 Introduction

Toxic and non-biodegradable transition metals in the atmosphere released from extensive anthropogenic activities and natural emissions [1-3], are raising a significant threat to human health and the environment [4-6], in particular during acute air pollution accidents and emergencies (e.g. building fires and wildfires), which are now considered a poorly-understood global problem requiring time-consuming efforts of sampling and analysis [7]. For instance, the 2019 Notre-Dame Cathedral fire released a great amount of lead into the atmosphere, which was confirmed by the elevated Pb concentrations in honey samples collected after three months [8]. Children were subjected to the threat of lead poisoning in this acute pollution event [9]. Wildfires also result in a significantly elevated level of transition metals (e.g. Pb and Cd) due to fire burning and metal remobilization [10, 11]. These abrupt air pollution events might have long-term health effects by contaminating air, water, soil, and indoor environments [12]. More importantly, the soluble fraction of particle-bound transition metals enhances the persistent toxicity and health effects [13-16], which is particularly harmful to humans due to its toxicity and bioaccessibility [17, 18], accounting for 0 – 80 % of total metals in airborne particulate matter (PM) [19, 20]. For instance, water-soluble transition metals in the accumulation mode have positive correlations with reactive oxygen species and oxidative stress [21, 22]. Therefore, the detection of the soluble fraction in particle-bound transition metals is of great significance for public health, especially in order to give rapid responses to acute pollution events.

Monitoring by on-site, mobile, decentralized detection methods is a promising way to achieve rapid responses by eliminating sample transport, storage, and benchtop operation. In general, the common strategy is coupling different functional units (e.g. particle collection and measurement units) using benchtop or homemade instruments to determine the total airborne metals. Inductively coupled plasma mass spectrometry (ICP-MS) has been coupled with Scanning Mobility Particle Sizer (SMPS) to obtain size-resolved chemical information and particle characteristics simultaneously [23]. Real-time detection of aerosol metals has been carried out using Extractive Electrospray Ionization Mass Spectrometry [24]. The combination of filter sampling and X-ray fluorescence analysis achieved the multi-metals monitoring with a high time resolution, such as Cooper Xact 625i [25] and Horiba PX-375 [26]. Nonetheless, these

detection techniques such as XRF require professional experiences and safety measures of radiative sources, and are not able to distinguish the soluble fraction of metals in an oxidation state, though the health effects of metals are speciation-driven [27]. A limited number of homemade on-site techniques have been developed based on electrochemical methods [28] or well-established spectrophotometric techniques [27, 29], coupled with aerosol collection techniques. The state-of-the-art techniques are summarized in Table B1. Previous studies mainly focused on total metal detection using the combination of the available aerosol collection with detection techniques, resulting in possible bulky coupling and extra uncertainty due to additional connections and sample preparation. However, studies in monitoring the soluble fraction of airborne soluble metals remain challenging and are scarce. Developing a more compact system for on-site detection of the soluble fraction of particle-bound transition metals, through integrating aerosol collection with detection techniques, still requires more novel coupling strategies and efforts.

Due to low power, high sensitivity, and selectivity for in-situ measurements [30, 31], electrochemical detection is of great interest for sensing transition metal ions, such as electrolytic deposition with subsequent electrochemical detection, non-electrolytic pre-concentration, and zero-current measurements [32]. Among them, voltammetric methods are the most sensitive for transition metal ions detection [33]. The voltammetric determination of transition metals in PM_{10} was proved with a normalized deviation of less than 15 %, compared to ICP-MS [34]. For example, a Nafion/Bi modified carbon electrode was used to determine Co(II) and Ni(II) in the aerosol collected on filters with limits of detection of 1 µg/L and 5 µg/L, respectively [35]. Electrochemical detection combined with aerosol collection techniques is a conventional and promising method to achieve the miniaturized platform of particle collection and detection. The aerosol collection techniques include passive collection [36] and capturing particles into liquid (wet collection surfaces [29, 37-40] and condensation growth method [41]). Nonetheless, to avoid independent functional units in sequence, there is an emerging trend that integrates collection and electrochemical detection in the same platform [42]. The new coupling strategy is to create a dual-functional interface between particle collection and electrochemical sensing, by eliminating additional connections for sample transport, preprocessing, and storage.

In this study, we propose a new collection and sensing concept that allows for immediate sensing after particle collection via a gas/liquid interface. In this way, the mass transport of metal ions was enhanced by dissolving metals as close to the electrode surface as possible. Accordingly, a gold-coated Polyacrylonitrile (PAN) nanofiber served as the aerosol-into-liquid electrode (AILE) with collection and sensing functions. It is a Janus membrane electrode with a virgin PAN surface on one side and a gold surface on the other side. A system integrating electrochemical methods with aerosol dynamics was developed to fulfill the aerosol-into-

liquid concept via this membrane. In the proof-of-concept experiments, the integrated aerodynamic/electrochemical (IAE) system was examined using lab-generated lead aerosols and PM_{10}-like aerosols. The new concept achieved in the designed IAE system could afford a unique route toward the on-site monitoring of atmospheric metals and other additional components with a miniaturized size for rapid responses to abrupt pollution events.

3.2 Material and Methods

3.2.1 Chemicals and reagents

Deionized water (> 18.2 MΩ cm) was derived from the Milli-Q system (Merck Millipore). Polyacrylonitrile (PAN, Mw 534000, powder), N, N-dimethylformamide (DMF, ≥ 99.8%), lead (II) nitrate (99.999 %), glacial acetic acid (99.7 %), sulfuric acid (95 – 98 %), potassium hydroxide (> 85 %) and cadmium nitrate tetrahydrate (99.997 %) were purchased from Sigma-Aldrich. Copper (II) nitrate hemi(pentahydrate) (98 %) was obtained from Alfa Aesar. 0.1 mM metal ions solutions were prepared for further dilution in 0.1 M acetate buffer (pH 4.45).

3.2.2 Preparation of the AILE electrodes

The commonly used materials for sensing transition metal ions in terms of electrochemical sensors are glassy carbon, gold, and boron-doped diamond, besides mercury and bismuth [43]. Here we employed a PAN nanofiber membrane and gold as aerodynamic functional material and electrochemical sensing surface, respectively. The PAN nanofiber membrane with a thickness of ~ 30 μm was obtained by electrospinning [44]. In brief, 8 wt.% PAN/DMF solution was prepared and employed for 2 h with an extrusion rate of 1 mL/h, and the distance between the tip and collector was 15 cm. Prior to gold deposition, the PAN nanofiber membrane was laminated at 75 ^{o}C (GBC Fusion 1100 L), to improve lamination and mechanical strength [44]. Gold (~ 50 nm) was sputtered on one side of the PAN nanofiber membrane by magnetron sputtering (Leica EM ACE 600).

Due to the adsorption of metal ions onto PAN nanofiber [45, 46], 40 mg prepared PAN nanofiber membrane (~ 135 cm^2) was put into 30 mL of a 10 μM Pb solution for 24 h and then into the Pb-free 0.1 M acetate buffer and then MilliQ water for 24 h after rinsing with MilliQ water respectively, to examine the adsorption and desorption behaviors. The sample solution was shaken on a rotary shaker (KS 260 basic, IKA), operating at room temperature and 100 rpm. 1 mL of the sample solution was withdrawn at 10 min, 30 min, 1 h, 2 h, 5 h, 10 h, and 24 h, which was acidified to 1 % (w/w) HNO_3 and refrigerated until the ICP-MS measurement.

The PAN nanofiber was then transferred into 30 mL 10 µM Pb solution for 24 h again to investigate the repeated adsorption behavior. The electrolyte uptake ratio of the PAN nanofiber-based gold electrode was approximately 50 g/g. The fiber diameter and porosity of the PAN nanofiber membrane and PAN nanofiber-based gold electrode were determined with ImageJ 1.50e on SEM images. The gold wire (99.9 %, MaTecK) was used to connect the potentiostat with PAN nanofiber-based gold electrode. The Teflon tape was used to fix the working area of PAN nanofiber-based gold electrodes (Ø = 1.6 cm) for the detection of metal ions in the liquid phase (Figure B1). Cyclic voltammetry in the potential range of -0.2 – 1.2 V vs. Reversible Hydrogen Electrode (RHE) for about 20 cycles and chronoamperometry at 1.0 V was performed to activate the PAN nanofiber-based gold electrode in 0.1 M acetate buffer (pH 4.45) and electrochemically remove any impurities before the metal ions detection each time, to obtain the active and reproducible electrode surface [47].

3.2.3 Electrochemical detection methods in the liquid phase

The electrochemical studies were carried out using either SP-240 potentiostat or SP-300 potentiostat (Bio-Logic Science Instruments, France). Specifically, the detection of metal ions in the liquid phase was conducted in a standard three-electrode electrochemical cell (saturated with Argon during experiments) with an Ag/AgCl (SI Analytics or Microelectrodes, 3 M KCl) reference electrode (Figure B15) and Pt wire counter electrode. 100 mL 0.1 M acetate buffer (pH 4.45), prepared by mixing glacial acetic acid and potassium hydroxide, was the electrolyte to eliminate sample matrix effects. A gold rotating disk electrode (RDE) (Ageo = 0.20 cm^2) was sonicated in 0.15 M nitrate acid and 0.2 M hydrochloric acid for 10 min respectively, and then polished with 0.05 µm alumina polishing slurry (Pace Technologies, USA). The rotation rate (1600 rpm) of gold RDE was controlled by Pine instruments set up for RDE.

The working principle is accumulating soluble metals on the electrode surface (metal reduction) and then obtaining the signal (metal oxidation). Anodic Stripping Voltammetry (ASV) is the technique that allows metal reduction and then metal oxidation. The following parameters were used: conditioning potential (E_{cond}) 1 V vs. RHE for 4 min, deposition potential (E_{dep}) -0.2 V for 5 min, and equilibration time (t_{eq}) for 30 s (only in the case of RDE). The stripping charge using ASV was calculated by integrating current over time, and then background charging should be subtracted from it. Square Wave Anodic Stripping Voltammetry (SWASV) is widely used in the detection without oxygen removal [48]. The following parameters were used: conditioning potential (E_{cond}) 1 V vs. RHE for 4 min, deposition potential (E_{dep}) -0.2 V for 5 min, SW amplitude (E_{amp}) 25 mV, step potential (Estep) 5 mV, pulse width 5 ms. Experiments with each concentration were repeated three times, to obtain the deviation and ensure accuracy.

3.2.4 The IAE system for detecting aerosol Pb(II)

Materials (e.g. metal, glass, and polytetrafluoroethylene (PTFE)) for the electrochemical sensing system should be carefully selected. For example, stainless steel was used for the tubing and nozzle plate to avoid particle deposition and losses during the particle collection, whereas PTFE was employed in the electrochemical cell due to its hydrophobicity, conductive resistance, and contamination resistance. From the perspective of electrochemistry, a small volume of the cell (Ø = 1.6 cm) was employed to reduce mass transport and improve the detection limit. PAN nanofiber-based gold electrode (3 × 3 cm) with a gold wire was mounted on PTFE plates, to achieve a precise distance between the jet and the electrode via a nozzle-to-plate distance adjuster. The actual collection and sensing area (Ø = 1.6 cm) was isolated by a circle of glue (Araldite, Switzerland) to achieve waterproof beyond the real sensing area (Figure B1). The PAN side without gold was used to face flows and capture particles. It should be noted that the PAN side with a gold surface immerses into the electrolyte, to alleviate the intense reaction of oxygen reduction on active sites during the metal deposition. The counter and flexible reference electrode was long enough to reach the PTFE plate part so that the distance between the working and reference or counter electrode was minimized to reduce the ohmic drop induced by the electrolyte.

For the aerodynamic part, a micro-orifice cascade impactor was designed and fabricated using stainless steel for particle collection based on inertial impaction. The flow rate should be increased gradually to avoid the sudden spilling of the electrolyte from the PTFE cell. The Stokes number (Stk) was calculated based on the following equation.

$$\mathrm{Stk} = \frac{\rho_p d_p^2 C_c U}{9\mu W}$$

where ρ_p is the particle density, d_p is the 50% cutoff diameter of particles, C_c is the slip correction factor, U is the average jet velocity, μ is the dynamic viscosity of the air ($1.8*10^{-5}$ kg ms-1) and W is the diameter of the nozzle. The Stokes number (Stk_{50}) should be 0.49 using a round-nozzle impactor [49]. The cutoff size diameter is calculated with the following equation:

$$D_{p50} = \sqrt{\frac{9\pi\mu D_j^3 Stk_{50}}{4\rho_p Q C_c}}$$

where D_j is the diameter of the nozzle, and Q is the flow rate. Meanwhile, Reynolds number (Re) should be in the range of 500 – 3000 to achieve maximum collection efficiency, which is defined as follows.

$$\mathrm{Re} = \frac{\rho W V_0}{\mu}$$

where ρ is the gas density, W is the nozzle diameter, V_0 is the velocity, and μ is the viscosity. To achieve a relatively low Reynolds number and pressure drop, we chose 151 and 201 nozzles. Considering the low porosity (1 %) of the nozzle plate to avoid the cross-flow effect, the diameter of the tube is set to 16 mm. Impactor operating parameters such as S/W should be in the range from 0.5 to 10 [29, 50]. Considering S/W for the 8th stage in Microorifice Uniform Deposit Impactor (MOUDI) [51], the jet-to-plate distance was set to 1 mm. The aerodynamic and electrochemical function modules were connected through two PTFE tubing, to balance air pressure and electrolyte height.

3.2.5 Evaluation of collection efficiency and sensing performance of the IAE system

A homemade atomizer and a diffusion dryer were used to generate and dry the aerosol with a flow rate of 3.8 L/min. Size resolved information including size distribution and particle number was measured using the Scanning Mobility Particle Sizer (SMPS), which consists of a differential mobility analyzer (DMA, TSI model 3081) and a condensation particle counter (CPC, TSI model 3775). The concentration of metal ions in the aerosol was determined by ICP-MS. The particle number and concentration of aerosol were determined by measuring upstream (C_{up}) and downstream (C_{down}). The collection efficiency (η) of the inertial impactor was calculated as follows:

$$\eta = \frac{C_{up} - C_{down}}{C_{up}} \times 100\%$$

The particle loss and aerosol-into-liquid transfer efficiency of the system were evaluated using NaCl monodisperse particles selected by DMA and collected for 2 hours. More specifically, the nozzle plate, PAN membrane, and PTFE plate were eluted by 10 mL milli-Q water after particle collection, and 10 mL electrolyte (here we used Millli-Q water to avoid Na contamination) in the system was also preserved for NaCl determination by ICP-MS. NaCl concentrations from the PAN membrane and electrolyte were used to estimate the aerosol-into-liquid transfer efficiency. To simulate and visualize the collection of trace airborne soluble elements in the integrated system, 0.2 wt% malachite green solution was used in the particle generation system to produce colored particles for 1 h.

To correlate the concentration of metal ions in the aerosol with the electrochemical signal, two filter holders with 1 μm 47 mm polycarbonate membrane filters (effective diameter 35 mm) (Sterlitech, USA) or 0.45 μm cellulose nitrate filters (Sartorius Stedim biotech, Germany) were placed in the effluent flow of the electrochemical sensing system and in parallel

at the same flowrate (i.e. 7.1 L/min), respectively (Figure B16 and B17). The filters were ultrasonically extracted for 30 min in centrifuge tubes using 1 mL acetate buffer. Subsequently, 9 mL water was added and combined ultrasonically for another 30 min. The combined extracts were filtered using syringe filters (0.2 µm) to remove the insoluble fractions.

$Pb(NO_3)_2$ and PM_{10}-like (trace elements) ERM® Certified Reference Material (European Reference Materials, ERM-CZ120) in acetate buffer (pH 4.45) were generated from a homemade atomizer as particles and used for establishing the calibration curve. 50 mg PM_{10}-like (trace elements) ERM® Certified Reference Material, was suspended in 50 mL acetate buffer (pH 4.45) and shaken on a vortex shaker (uniTEXER, LLG Labware) at 1000 rpm for 5 min, followed by sonication for 30 min [52]. PM10 suspension solution was diluted using acetate buffer to obtain different aerosol concentrations. It is noted that the Pb solution and PM suspension were prepared with acetate buffer to reduce metal hydration. The collection time of the integrated system was 1 h. Ambient aerosol around the laboratory (n = 2) was measured for the performance evaluation in the real-world environment. The following parameters for the electrochemical technique were used: conditioning potential (E_{cond}) 1 V vs. RHE for 4 min, deposition potential (E_{dep}) 0 V for 1 h, SW amplitude (E_{amp}) 25 mV, step potential (E_{step}) 5 mV, pulse width 5 ms, and quiet time (no airflow) 0 min.

3.2.6 Numerical simulation of the aerosol dynamics and metal ion diffusion

The aerosol dynamics and particle capture were simulated using COMSOL Multiphysics 6.0. Laminar flow, and particle tracing for fluid flow modules were involved. The geometric dimensions were set the same as the real setup, and further simplified. In the aerodynamic simulation, the Reynolds number was smaller than 1000, and therefore the laminar regime could be assumed [53]. Matlab was used to simulate the Pb(II) diffusion processes in the case of conventional aqueous detection and the aerosol-into-liquid concept. The AILE electrode was simplified into a film with a thickness of 15 µm due to the complex structure of nanofibers on a millimeter scale. A detailed description of the simulations can be found in the Supporting Information.

3.3 Results

3.3.1 Capture and sensing strategy of the IAE system

The schematics and photo of the IAE system are shown in Figure 3.1. The aerodynamic and electrochemical function modules were connected through the AILE electrode between the inertial impaction plate and the electrochemical cell (Figure 3.1a). The AILE electrode supported by the electrolyte was facing the micrometer-sized nozzles delivering airflow at a jet-

to-electrode distance of about 1 mm (Figure 3.1b). By joining the gas phase (air-jets containing particles) and the liquid phase (electrolyte), the AILE electrode worked as the impaction substrate for particles and the pores of the membrane served as liquid reservoirs to dissolve metals (Figure 3.1c). The sensing strategy is to collect particles and dissolve metal ions on one side of the AILE electrode and perform electrochemical sensing reactions on the other side of the membrane electrode (gold-coated surface). In detail, particles are collected based on the inertial impaction and soluble metal ions from the particles are dissolved on electrolyte-soaked hydrophilic PAN nanofiber. Metal ions then diffuse vertically to the gold surface by mass transport for redox reaction (i.e. metal reduction and subsequent oxidation, see Figure 3.1c). The metal reduction is used to accumulate metal ions on the electrode surface, while the oxidation is employed to obtain metal signals by producing an oxidation current. The IAE system was realized with a dimension of 100 mm × 70 mm × 100 mm in x-, y-, and z-axes, respectively (Figure 3.1d).

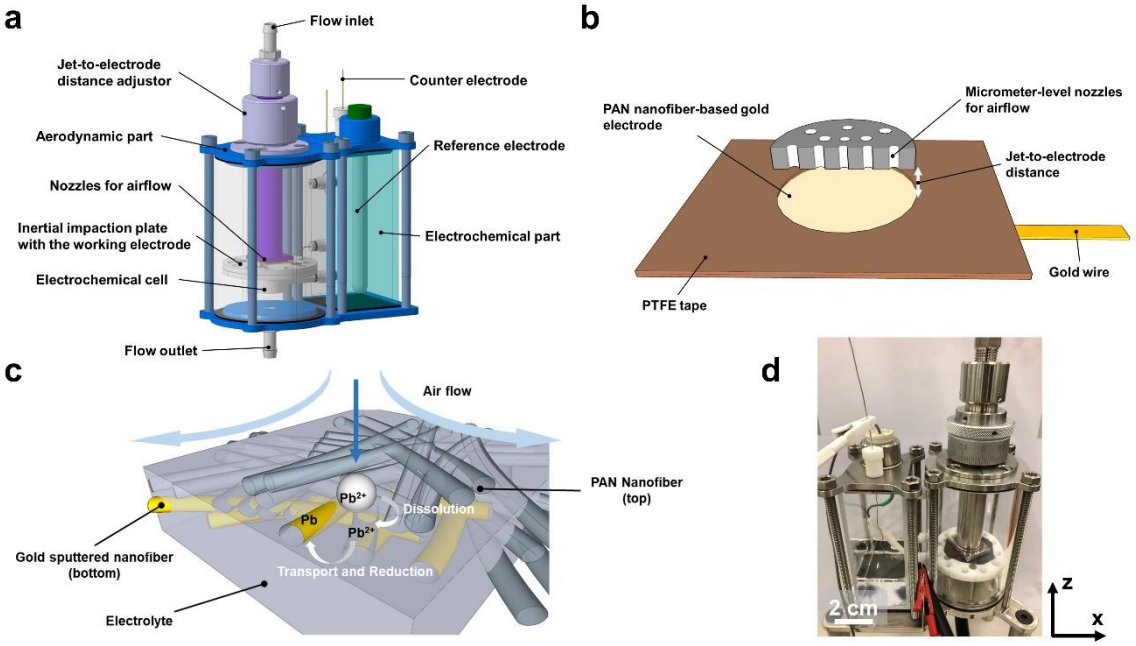

Figure 3.1 Integrated aerodynamic/electrochemical (IAE) system for capturing and detecting airborne bioaccessible metals. a Schematic of the designed IAE system to achieve aerosol-into-liquid capture and detection, b detailed schematic of the gas/liquid interface separated by AILE electrode with a jet-to-electrode distance of around 1 mm, c schematic illustration of the aerosol-into-liquid collection and detection of particle-bound metal ions on the AILE electrode, d photo of the IAE system with a dimension of 100 mm × 70 mm × 100 mm in x-, y-, and z-axes.

3.3.2 Characterization of the AILE electrode

The fabrication of the AILE electrode required several steps including electrospinning, hot lamination, and gold sputtering (Figure 3.2a). Additional electrode assembly was also applied to support the soft electrode and the electrode area (Figure B1). The morphologies of the PAN nanofiber and the AILE electrode are shown in Figure 3.2b and 3.2c. The PAN nanofibers without hot lamination were loose while the membrane became compact with a clear layer-by-layer structure after hot lamination. The diameter and porosity were quantified and the average diameters of pure PAN and gold-coated PAN were 225.5 ± 51.7 and 235.7 ± 54.1 nm, respectively (Figure 3.1d). It indicates that hot lamination and gold sputtering have a minor effect on the diameter size distribution. The porosity values of pure PAN and gold-coated PAN were 61.5 % and 46.8 %, respectively. The adsorption behavior of Pb(II) onto the AILE electrode was also examined using ICP-MS. 2.8 % of the total Pb(II) at a relatively low concentration (10 µM) was adsorbed on PAN nanofibers (Figure 3.1e), and the average adsorption capacity was 3.45 µg/g, which indicates insignificant adsorption of Pb(II) on PAN nanofibers and its minor effect on sensing performance. Adsorption and desorption were fast since the concentration of lead in the solution was not changed much in each phase (Figure 3.2e). A relatively stable concentration of lead in the repeated adsorption revealed that the AILE electrode was reusable without much effect of Pb(II) adsorption.

The water wettability of the PAN nanofiber was analyzed via water contact angle, which was about 37^{o} [44]. The PAN membrane was hydrophilic and had an affinity for water to form a non-porous liquid-saturated membrane, which was desirable for separating the liquid phase from the gas phase without disturbance from a fast-moving gas flow. Gold rotating disk electrode (RDE) was used to investigate the Pb redox reaction in steady states. The roughness factor (~ 1.71) of the gold RDE was obtained by stripping a gold oxide layer in 0.5 M H_2SO_4 and the conversion factor of 390 µC cm^{-2} was used [54], whereas the roughness factor of the PAN nanofiber-based gold electrode was 3.92 (Figure B2). Considering the porosity of the PAN nanofiber-based gold electrode of 46.8 %, which resulted in a smaller geometric area, the roughness factor of the gold surface could increase up to 7.37. It indicated a rougher gold surface of the PAN nanofiber-based gold electrode compared to gold RDE [55].

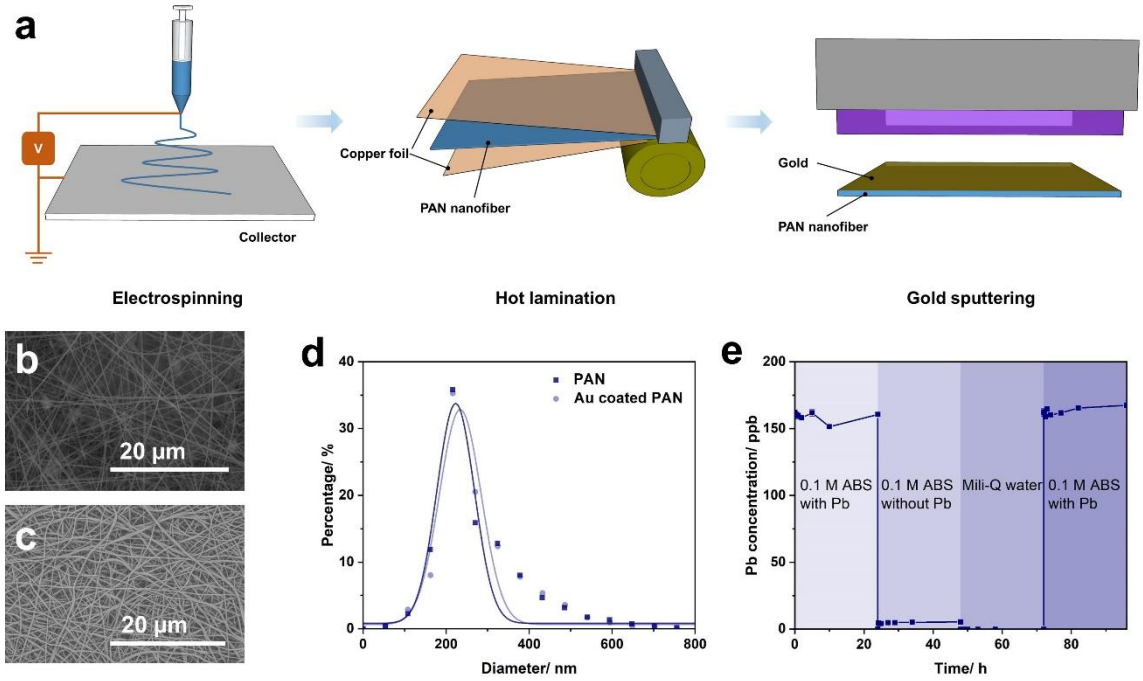

Figure 3.2 Fabrication and characterization of the AILE electrode. a Schematic illustration of fabricating the AILE electrode, b scanning electron microscopy (SEM) image of the PAN nanofiber after hot lamination, c SEM image of the gold surface of the AILE electrode, d diameter size distributions and the Gaussian fitting of the PAN nanofiber, and the AILE electrode, e adsorption of Pb(II) onto the PAN nanofiber, desorption of Pb(II) from the PAN nanofiber and adsorption of Pb(II) onto the PAN nanofiber as a function of submersion time (adsorption experiment: 40 mg PAN nanofiber in 30 mL 0.1 M acetate buffer solution (ABS) (pH 4.45) containing 10 µM Pb(II) for 24 h; desorption experiment: the PAN nanofiber was transferred into 30 mL ABS for 24 h and then into 30 mL Milli-Q water for 24 h).

3.3.3 Electrochemical characterization and detection of Pb(II) in the liquid phase

The detection of atmospheric soluble metals is a liquid-based method, so the gold RDE and PAN nanofiber-based gold electrodes were employed to examine the feasibility of sensing Pb(II) in the liquid phase. As shown in Figure 3.3a, the oxidation and reduction potentials of Pb(II) were 0.4 – 0.6 V and 0.3 – 0.5 V respectively. The onsets of the oxygen reduction and hydrogen evolution were at 0.4 V and -0.1 V, respectively (Figure 3.3a and Figure B3). Therefore, the deposition potential was set at -0.2 V, to avoid competitive hydrogen evolution reactions in view of the limited number of active sites on the gold surface, despite the fact that hydrogen evolution reaction has limited effects on Pb deposition [56]. Gold rotating disk electrode (RDE) was considered a flat bare gold surface to detect metal ions under tunable conditions. In particular, a high rotation rate (i.e. 1600 rpm) allowed the continuous deposition of metal ions on the electrode with constant mass transport, to simulate the presence of metal

ions with high concentrations. Figure 3.3b indicated that there were one underpotential deposition (UPD) and two overpotential depositions (OPD) of lead on the gold surface. In general, the relationships between concentrations and integrated charge were quite linear (Figure B4-B6), which indicated that gold as a sensing material was capable of detecting Pb(II) in the liquid phase.

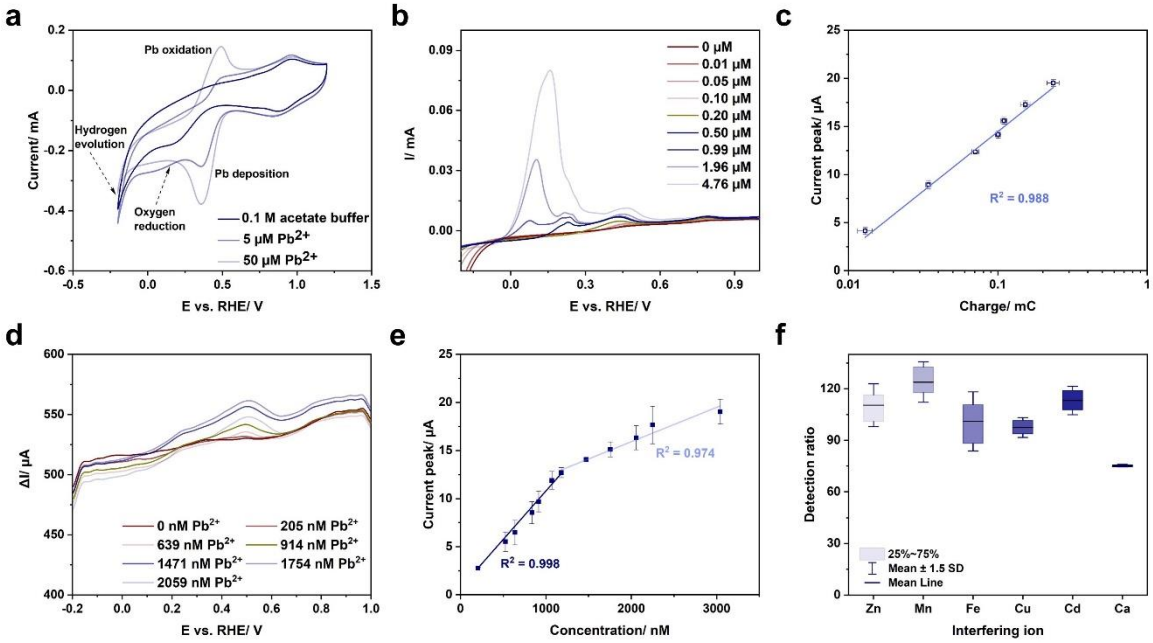

Figure 3.3 Characterization and sensing performance of the AILE electrode. a Cyclic voltammetry in 0.1 M acetate buffer (pH 4.45) without and with Pb(II) at 100 mV/s in a three-electrode system under air, b RDE experiments using anodic stripping voltammetry (ASV) on the stripping current as a function of concentration gradients of Pb(II) at 1600 rpm in 0.1 M acetate buffer in an Argon-saturated environment, c relationship between the stripping charge using anodic stripping voltammetry and the current peak using square wave stripping voltammetry with an AILE electrode (Ø = 16 mm), d responses upon concentration gradients of Pb(II) for the AILE electrode, e relationship between the current peak (in the range of 0.3 – 0.6 V) and the Pb(II) concentration gradients, f selectivity of the AILE electrode towards 1 µM Pb(II) in the presence of 50 times higher concentration of other metal ions (Zn(II), Mn(II), Fe(III), Cu(II), Cd(II) and Ca(II)), respectively.

For the AILE electrode, the oxidation potential range of Pb(II) was 0.25 – 0.60 V (Figure B5). It should be noted that the limit of detection in the liquid phase depends on the deposition (reduction) time in certain ranges [57], which means a longer deposition time results in more deposited metals and a lower limit of detection. The conversion of stripping charges to Pb concentration revealed that 0.204 ± 0.024 % Pb(II) was reduced on the gold surface without stirring in the solution after 5 min deposition (Figure 3.3c). According to the square wave

voltammetry (SWV) signals, the peaks fell into the range of 0.3 – 0.6 V (Figure 3.3d). The relationship between electrode area and current peak suggested that a smaller electrode area on the mm^2 scale was more preferable due to slower changes in the current peak value in comparison of the electrode area (0.11 $\mu A/mm^2$) (Figure B7), suggesting the signal obtained from a smaller area of the electrode could be comparable to that obtained from a large electrode. Figure 3.3e illustrated the detection performance with a relatively low concentration of metal ions (< 1.2 µM) in the presence of oxygen ($R^2 > 0.99$). The limit of detection was 79.2 nM, according to the equation for limit of detection (LOD) = 3 δ/S, where δ is the standard deviation of the background signal, and S is the ratio of the Pb concentration to the current signal. The interference study was conducted with different ions, and the range of detection ratio was 80 – 130 % (Figure 3.3f). Particularly, Cu(II) might interfere with the Pb signal by the replacement of Pb deposition [58], resulting in a detection ratio of around 90 % (Figure 3.3f). Overall, the AILE electrode was sensitive and selective for detecting Pb in the liquid phase.

3.3.4 Collection efficiency and particle loss of the IAE system

The cutoff diameter at 3.0, 5.0, 7.1, and 7.9 L/min was about 300, 150, 80, and 50 nm, respectively (Figure 3.4a). The collection efficiency increased with a higher flow rate, and it mainly affected the collection of particles smaller than 300 nm. The setup for determining the collection efficiency of the system was shown in Figure B8. The collection efficiency was not strongly influenced by the nozzle-to-plate distance especially when it was smaller than 1.5 mm (Figure 3.4b). The vertical deformation of the AILE electrode with different nozzle-to-plate distances could play a role in the effect of the nozzle-to-plate distance on the collection efficiency. Pore number and size also affected the collection efficiency, and a higher velocity caused by the lower porosity of the nozzle plate resulted in higher collection efficiencies (Figure 3.4c). Specifically, given the same volumetric flow rate, 0.59 % and 0.64 % porosity led to a smaller cutoff size of around 70 nm and maximum collection efficiency up to 100 %, while 1.05 % and 0.93 % porosity caused the larger cutoff size of 200 nm and maximum collection efficiency of about 80 %. It should be noted that the number of reaerosolized water droplets from the electrode could affect the measured collection efficiency of particles larger than 300 nm because the number of challenge particles decreased with larger particle sizes. The collected particles on different parts of the system were investigated to estimate the effective particle collection rate and aerosol-into-liquid transfer rate (Figure 3.4d and 3.4e). Particles larger than 100 nm were well collected in the electrolyte by diffusing through the AILE electrode, and particle loss of smaller particles became significant likely due to particle diffusion in the airflow hitting the nozzle plate and PTFE plate (Figure 3.4d). The effective particle collection rate was above 80 % and the aerosol-into-liquid transfer was above 90 %, which demonstrated a minimum particle loss and proved the feasibility of the aerosol-into-liquid concept (Figure 3.4e). Here, the effective particle collection rate was defined as the fraction of

collected particles on the AILE electrode and subsequently diffusing to the electrolyte, while the aerosol-into-liquid transfer was the fraction of the collected particles diffusing into the electrolyte. Figure 3.4f showed that the collection efficiencies curve for particles larger than 200 nm reached a stabilized plateau, suggesting that the soft membrane surface used in this system reduced the solid particle bouncing significantly, which occurs with particles larger than 200 nm in many studies of designed impactors [59, 60].

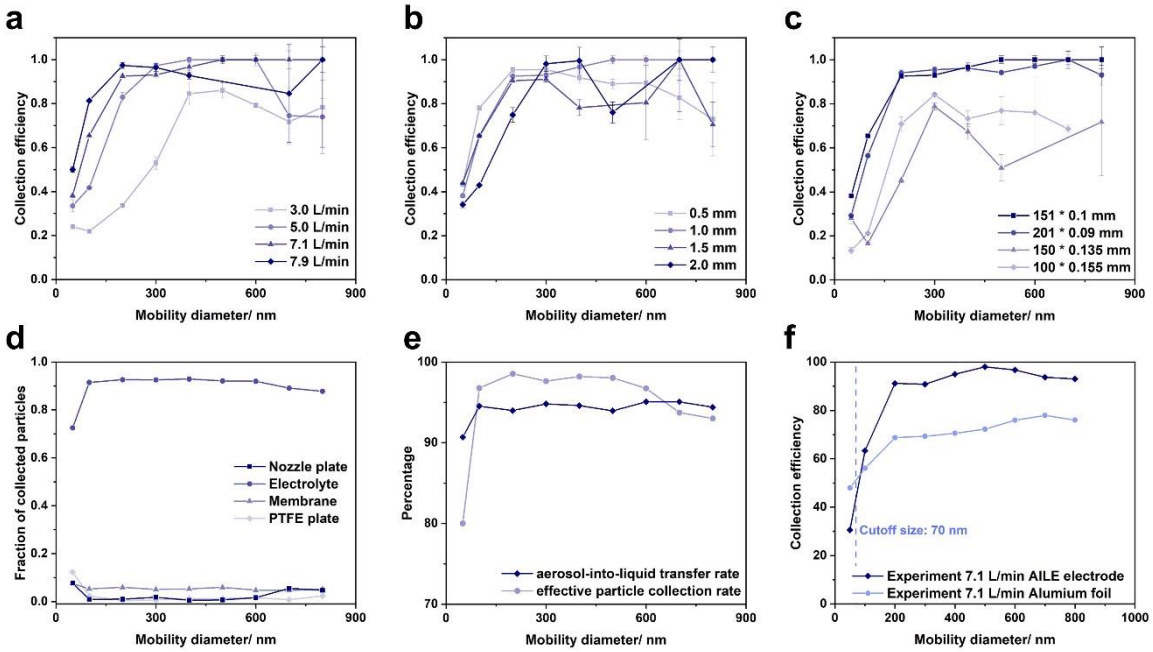

Figure 3.4 The integrated aerodynamic/electrochemical (IAE) system and its collection performance. a Collection efficiency of the IAE system as a function of different flow rates (1 wt% NaCl), b collection efficiency of the IAE system as a function of different nozzle-to-plate distance (1 wt% NaCl), c collection efficiency of the IAE system as a function of different nozzle number and pore size (1 wt% NaCl), d percentage of the size-resolved particle collection on PTFE plate, membrane (AILE electrode), electrolyte, and nozzle plate, e particle losses and aerosol-into-liquid transfer rate of the IAE system using monodisperse NaCl particles selected by DMA after 2 h collection at 7.1 L/min, f comparison of the collection efficiency using an AILE electrode as the impaction plate with that using an aluminum foil.

The whole system was operated at relatively low pressures (e.g. 0.85 atm), and particles with a cutoff diameter of 50 – 300 nm can be captured (Figure 3.4a-c). The measured cutoff size was in good agreement with the theoretical calculation of the inertial impactor (~ 70 nm) (Figure 3.4f). The minimal collection efficiency at 3 L/min is above 20 % rather than zero likely due to some airflow penetration, which is consistent with the collection performance of porous materials reported previously [61, 62]. The curvatures on the impaction surface induced by round jets also increased the jet-to-plate distance/nozzle size (S/W) ratio, to affect the cutoff diameter [63]. Nonetheless, the roughness of the surface increases the slip length for flows

up to the micron level [64], which is the Navier slip condition, to increase the capture probability of particles.

3.3.5 Aerosol-into-liquid collection and detection of particle-bound Pb(II)

The mean mobility diameter of the lab-generated aerosol (including Pb(II) and PM_{10}-like aerosol) was 37.41 ± 6.12 nm (Figure 3.5a), whereas that of the ambient aerosol in Dübendorf, Switzerland during the experiment was 117.98 ± 3.51 nm (Figure B9). The particle number of $PM_{0.5}$, $PM_{0.5\text{-}1}$, $PM_{1\text{-}2.5}$, and $PM_{2.5\text{-}10}$ of the Pb(II) aerosols accounted for 97.4 %, 2.1 %, 0.5 %, and 0.1 % in terms of particle number, respectively (Figure 3.5b). The ambient aerosol in Dübendorf during the experiment has a larger mean mobility diameter, with $PM_{0.5}$, $PM_{0.5\text{-}1}$, $PM_{1\text{-}2.5}$, and $PM_{2.5\text{-}10}$ number fraction of 90.8 %, 7.6 %, 1.4 %, and 0.2 %, respectively. In contrast, PM_{10}-like aerosol can be representative of real-world aerosol with an increased number of particles larger than 1 μm (e.g. dust-enriched aerosol and fire-induced aerosol [65]), which consists of 71.8 %, 22.6 %, 5.5 %, 0.1 % of $PM_{0.5}$, $PM_{0.5\text{-}1}$, $PM_{1\text{-}2.5}$, and $PM_{2.5\text{-}10}$ (Figure 3.5b). PM_{10}-like particles were collected from the road tunnel "Wisłostrada" in Warsaw, Poland, with total carbon (11.1 %) and Silicon (22.9 %) as the major components (Table B3), which were used to be reaerosolized in the lab. In addition, the particle number of the lab-generated PM_{10}-like aerosol was up to 6.58 folds and 547.22 folds higher than that in the ambient environment according to the APS and SMPS measurements, respectively (Figure B9), which is also a typical characteristic of abrupt air pollution accidents. We also exploited the performance of the IAE system in the ambient environment. The result showed no Pb signal, which means the airborne Pb(II) concentration was below the limit of detection of the system (Figure B10). The parallel upstream and downstream filters determined by ICP-MS confirmed that no detectable Pb(II) was found during the same time duration of particle collection with a sampling flow rate of 4 L/min (Figure B16 and Table B2), which suggested that the common filter method followed by ICP-MS was also not able to detect the low level of atmospheric soluble metals with 1-hour collection time. A previous study also found a very low airborne Pb concentration of PM_{10} in Dübendorf, Switzerland (0.344 ng/m^3) [66]. The metal compositions of the ambient environment mainly included Mg, Al, K, Ca, Fe, and Zn [66], which highlighted the absence of false positives using the IAE system in the ambient environment with the presence of low Pb(II) concentrations.

It was found that the particle-free airflow and pressure drop had a limited effect on hydrogen evolution (-1.04 ± 0.02 mA) and oxygen reduction (-0.10 ± 0.02 mA) at -0.2 V and 0.2 V, respectively (Figure B11b), indicating a relatively steady state of electrochemical environment under impingement of various flow rates up to 7.1 L/min. Compared to the CV in the liquid phase, a higher current of oxygen reduction reaction at < 0.25 V in the integrated system indicated the strong exposure of the membrane electrode to oxygen in the air (Figure B11d). In

particular, the deposition current at 0 V was -1.34 ± 0.26 mA at equilibrium with the AILE electrode in the IAE system, which was 5.25 folds higher than that completely in the liquid phase. The oxygen reduction reaction might affect the Pb(II) deposition by occupying the limited electrochemical active sites. Nonetheless, the deposition current remained stable at -0.2 V and 0.2 V, where hydrogen evolution and oxygen reduction reaction dominated respectively (Figure 3.5c). It demonstrated that the airflow rate had a negligible effect on the AILE electrode in the IAE system, resulting in a steady electrochemical environment for Pb(II) sensing.

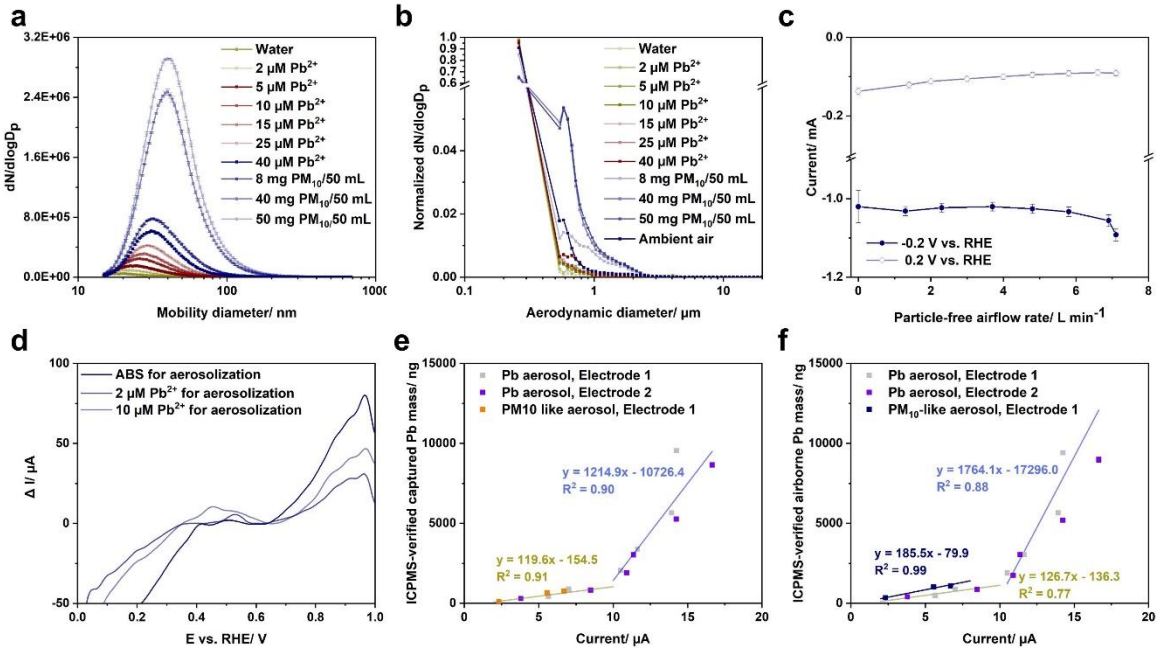

Figure 3.5 Sensing performance using the lab-generated metal aerosol and PM_{10}-like aerosol. a SMPS scanning of the particle size distribution of the lab-generated Pb(II) particles and PM_{10}-like aerosol, b normalized particle size distribution of the lab-generated lead particles and PM_{10}-like aerosol in terms of aerodynamic diameter, c chronoamperometry current at 0.2 V and -0.2 V vs. RHE for about 1 min at different airflow rate, d example of square wave stripping (SWV) voltammetry of lab-generated Pb(II) aerosol, e concentration-dependent responses of the SWASV technique corresponding to captured Pb(II) into the aqueous phase from Pb(II) and PM_{10}-like aerosols, f concentration-dependent responses to airborne Pb(II) and PM_{10}-like aerosol using the SWASV technique. The relationships between current peaks and ICP-MS verified concentrations using Pb aerosols were considered as the calibration curves. ICP-MS verified concentrations were obtained from parallel filters and electrolytes followed by ICP-MS analysis.

The current peaks were mainly in the range of 0.3 – 0.6 V and increased with higher airborne Pb(II) concentration (Figure 3.5d). It showed linear relationships between peak currents and Pb(II) concentrations (Figure 3.5e and 3.5f). The limit of detection of the membrane electrode was 90.3 ng with a 1-hour collection duration, according to the equation LOD = 3δ/S, where δ

is the standard deviation of the background current signal, and S is the ratio of the current signal to the captured Pb mass [ng]. The electrolyte volume contained in the integrated system was around 43 mL after a 1-hour operation, so the limit of detection was 10.1 nM, which was 7.8 folds lower than that of the detection in the liquid phase. The sensing conditions of the conventional aqueous detection and aerosol-into-liquid concept were listed in Table A4. It demonstrated the sensing concept of air-into-liquid increased the mass transport of Pb(II) by constantly introducing Pb(II) through a shorter distance (i.e. the thickness of the AILE electrode) than the diffusion layer in the conventional aqueous detection. The detection ratio of PM_{10}-like aerosols was 90.2 ± 17.1 %, indicating a minimum effect from insoluble particles based on the aerosol-into-liquid transfer and selectivity of the AILE electrode. The detection ratio was the calculated Pb mass obtained from electrochemical signals according to the calibration curves (Pb aerosols in Figure 3.5e) compared to ICP-MS verified concentrations. Again, the high detection ratio of PM_{10}-like aerosols highlighted the system selectivity in the presence of real-world samples. For example, the concentrations of total carbon, calcium, chlorine, and iron in PM_{10}-like aerosols were over 985.2, 557.9, 88.8, and 337.6 folds higher than that of Pb, respectively (Table A3). The penetration ratio of the Pb(II) aerosol and PM_{10}-like aerosol through the membrane electrode was 99.4 ± 2.2% and 62.1 ± 22.5 %, respectively. The lower penetration of PM_{10}-like aerosol is likely due to the particle loss around nozzles and penetration loss through insoluble particle loads. The penetration of soluble metals could be a preprocessing-free process (e.g. without sonication), and a previous study indicated that it could cause relatively lower recoveries of Pb (87.0 %) and Cu (78.2 %), in comparison with recoveries of Pb (91.6 %) and Cu (87.3 %) after sonication [67]. The limit of detection for airborne Pb aerosol and PM_{10}-like aerosol in the environment was 95.7 ng and 140.0 ng with 1-hour collection at 7.1 L/min, respectively. This limit of detection might be applied in heavily polluted regions (e.g. Hanoi [68], Beijing [69], and Xi'an [70] with a soluble Pb concentration of around 100 ng/m^3) and abrupt air pollution events (e.g. wildfire [71] and festival firework [72] with an elevated Pb concentration of above 100 ng/m^3). It was noted that a huge potential to improve the limit of detection was discussed in the discussion section below. The collection efficiency of lab-generated Pb and PM_{10}-like aerosols in the integrated system was 84.7 ± 3.3 %. Overall, the integrated system exhibited the applicability, selectivity and stability of our IAE system for the Pb(II) collection and detection in the aerosol with high particle numbers and large particle sizes, which usually appears in abrupt air pollution accidents.

3.3.6 Mechanism of aerosol-into-liquid collection and sensing

The flow velocity field within the system showed that the flow rate was generally lower than 3 m/s, whereas it increased up to 160 m/s around the nozzle plate (Figure 3.6a). Both experimental and simulation results showed that the jet-to-electrode distances affected the collection efficiency (Figure 3.6b). Simulation analysis indicated that the aerosol-into-liquid concept

could achieve a faster mass transport with a longer collection time, compared to the conventional aqueous detection (Figure 3.6c). For example, the mass transport using the aerosol-into-liquid concept would increase up to 15-fold of that using the conventional aqueous detection with a collection time of 5 min. For the aerosol-into-liquid concept, the mass transport of metal ions reaching the electrode surface was mainly driven by the concentration gradient, while the electrolyte evaporation in the opposite direction of metal diffusion, and metal adsorption had a minor effect on the mass transport (Figure B20c). Nonetheless, the sufficient mass transport in the aerosol-into-liquid concept was not fully utilized in the Pb(II) sensing, and the utilization ratio was 4.65 ± 1.02 % compared to the conventional aqueous detection (Figure B12), which was likely due to the stronger oxygen reduction reaction on the electrode surface in the aerosol-into-liquid concept (Figure B11d). Since the detection of Pb(II) was an accumulation of reduced Pb on the electrode surface, the utilization ratio was defined as the fraction of reduced Pb(II) reaching the electrode surface. Figure 3.6d indicated that the air jet with a velocity of 100 m/s impinging on the electrolyte-supported membrane led to vertical deformation, which had a minor effect on the collection performance according to the good agreement between experimental and simulation results shown in Figure 3.6b.

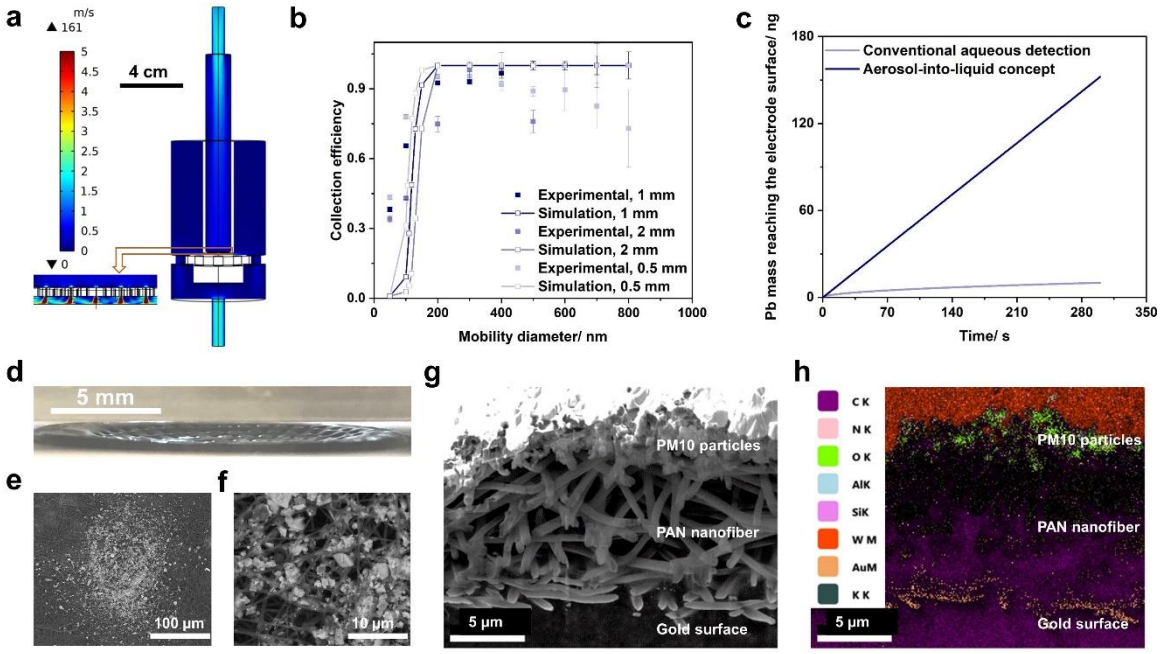

Figure 3.6 Collection and sensing mechanism using the IAE system. a Airflow field inside the IAE system at an inflow rate of 7.1 L/min, b comparison of experimental and simulated collection efficiency with 151 × 0.1 mm (diameter) nozzles at 7.1 L/min in terms of jet-to-plate distance, c Diffusion simulation of Pb(II) based on the concept of aerosol-into-liquid collection and detection, and the conventional detection method, given a Pb(II) concentration of 205 nM, d photo of electrolyte-supported electrode membrane deformation with the flow jet at 100 m/s through 151 × 0.1 mm nozzles, e and f SEM image of the particle collection on

the AILE electrode, g cross-sectional plasma FIB/SEM image of the AILE electrode with collected particles, h cross-sectional elemental mapping of the AILE electrode with collected particles.

SEM images showed that PM_{10} particles were well distributed homogenously among nanofibers of the membrane surface (Figure 3.6e and 3.6f), rather than forming deposition build-ups. The diameter of the particle distribution area facing each nozzle was around 200 μm (Figure 3.6e). PM_{10} particles were mostly collected on the nanofiber surface (Figure 3.6g and 3.6h), which provides a unique way to avoid fouling from solid particles on the downward electrode surface resulting in the disabled electrode. In contrast, the soluble fraction penetrates and reaches the electrode surface for electrochemical sensing, as shown in SEM mapping that Na and K were also determined in the middle of the AILE electrode cross-section (Figure B13). Therefore, the electrolyte-supported PAN membrane electrode demonstrated a stable and efficient structure for particle collection and immediate metal detection by separating gas and liquid phase via a solid nanofiber membrane. Metals could be rapidly released for particles immediately after contacting the aqueous solution [73]. Capillary forces are dominant in attaching particles at the air-water interface [74], and the presence of acetic acid in some cases, enhances the hydrophilic properties of particles [75]. These factors could facilitate the metal dissolution and mass transport through the electrode. The aerosol-into-liquid collection of hydrophilic malachite green particles indicated sufficient aerosol-into-liquid dissolution and transfer of soluble particles through the membrane electrode, resulting in a relatively homogeneous distribution of malachite green on the membrane and the electrolyte, respectively (Figure B14). It also indicated that based on the concept of aerosol-into-liquid collection and detection achieved via the AILE electrode, sample preprocessing was not necessarily applied using the IAE system for collection and detection. It was noted that the aerosol-into-liquid dissolution of soluble particles could be distinct from that of insoluble particles in aerosol (e.g. longer penetration distance due to particle loads, less dissolution efficiency from insoluble-containing particles).

3.4 Discussion

A concept of aerosol-into-liquid capture and detection was introduced to design the on-site, near-continuous, low-cost, and miniaturized system for capturing and determining airborne soluble metals. This concept opens up a new way for sampling and measurement, which can rapidly respond to atmospheric processes and pollution events. The IAE system designed based on this concept was validated using lab-generated and ambient aerosols. The electrochemical detection was achieved under a high airflow rate (e.g. 100 m/s) and low pressure (e.g. 0.85 atm). Interestingly, the collection and detection performances were superior compared to conventional collection techniques (e.g. metal-based impactors) and electrochemical

detection methods (e.g. electrochemical detection in solutions with a homogenous concentration), such as lower cutoff sizes, minimum particle bouncing, minimum sample preprocessing, a lower limit of detection, and minimum insoluble particle fouling. It was suggested that future designs based on this concept should benefit not only from reduced system sizes, but also from improved collection and detection performance. The electrochemical voltammetry methods can achieve the detection of multiple metals such as Cd, Pb, Cu, Fe, and Ni ions [76], which are expected to be realized in our system via modifying either sensing materials or sensing techniques. As shown in Table B1, the electrochemical method has been successfully developed to detect multiple metals such as Fe, Cu, Ni, Zn, and Pb ions in aerosol samples on the same electrode without significant interference from unintended metals. These studies show the limit of detection of different metals was comparable to that of Pb(II) obtained in this work, which indicates that a similar limit of detection could be achieved for other airborne metals. Membranes should be carefully selected and developed depending on the types of metals to be sampled and detected, to avoid significant adsorption or changes in the chemical form of soluble metals. In the future, we also anticipate that the system offers a platform for collecting and detecting other soluble components in the aerosol. Moreover, the availability and development of the AILE electrode by designing pore size, thickness, and structure of nanofibers could also enable the collection and detection of aerosol insoluble components.

For the collection scheme, it is noted that the aerosol-into-liquid concept is different from the particle-into-liquid sampler (PILS), which employs particle condensation growth to capture particles into liquid [77]. In contrast, the collection method of this work is similar to a wet-surface impactor, where the liquid impaction film tends to collapse with a cutoff collection size of smaller than 200 nm due to the increased force of air jets [29]. In comparison, the electrolyte-supported AILE electrode is capable of withstanding the air jets resulting in a cutoff size down to 50 nm. To avoid the sampling (e.g. PILS) and detection (e.g. UV/VIS spectrometer) units in sequence, the AILE electrode achieves the direct detection of soluble metals on one side after collecting particles on the other side. The separation of soluble fractions from total metals is a necessary step before determining metal solubility or bioaccessibility, and exploring their relationship with adverse health effects such as reactive oxygen species [21]. The conventional separation step involves sonication and submicrometer-graded filter filtration [78]. In contrast, our concept and system are able to skip this step via the aerosol-into-liquid process.

To our knowledge, there are several commercial continuous metal monitors such as Xact 625i and PX-375, to achieve a low limit of detection with a high time resolution (Table A5). However, our concept and IAE system could fit in the field where the shortages of these commercial instruments are. For instance, the IAE system based on the aerosol-into-liquid concept can be adapted into decentralized and rapid monitoring at a high spatial resolution because of

up to 40X smaller size and 400X lower cost as shown in Table A5. Screen-printed electrodes enable low-cost, miniaturized systems for decentralized and on-site determination of airborne metals [79]. Our system functions similarly to the combination of a screen-printed electrode system and a sampling method of airborne metals, which also suggests that our proposed system can be further miniaturized and simplified if a screen-printed porous and hydrophilic working electrode is available to replace the three electrodes used in the present system. More importantly, the IAE system is sensitive to metal solubility, which is strongly associated with adverse health issues, whereas the available commercial instruments offer information on total elements. Overall, the aerosol-into-liquid concept will contribute to extensive measurements, understanding, and risk assessments of atmospheric soluble metals.

The range of soluble fractions of metals in PM varies greatly depending on many factors such as sampling locations and emission sources. For example, a review summarized the soluble metals in PM using water as the leaching agent, and the soluble fraction of Pb was in a wide range of 3.8 % to 88 % [20]. There are many leaching agents used for the extraction of bioaccessible metals, such as water, acetate buffer, artificial lysosomal fluid (ALF), and Gamble's solution, which exhibit various levels of metal solubility and might bring about different definitions of bioaccessible metals [20]. The electrolyte (0.1 M acetate buffer) we used in the experiment could be relevant in assessments of bioaccessibility and investigations of metal toxicity, however, the results might differ from the metal dissolution in vivo. Further, the electrolyte in the proposed system can be changed for the dissolution of airborne metals according to the needs of target applications (e.g. simulation of airborne metal dissolution in body fluids). The extraction of soluble metals in this work was performed in 45 mL 0.1 M acetate buffer (pH 4.45) for 1 hour at room temperature. Further investigations based on the proposed concept and system could also be devoted to the variability of soluble metals by separating insoluble and soluble metals using the Janus-membrane electrode, which might effectively contribute to the understanding of soluble metals.

Despite the excellent performance validated using reaerosolized PM_{10}-like particles (real-world samples), the monitoring of soluble metals using the system in ambient air is still challenging due to the higher limit of detection compared to ambient Pb concentrations in most cases. Nonetheless, based on this concept, the limit of detection is expected to achieve potential improvements by advancing the used electrochemical voltammetry method. For example, as the collection time of 1 hour is carried out using the system, the limit of detection in a unit of ng/m^3 is possibly reduced by prolonging the collection time to collect more air volume (e.g. by 2X with a 2-hour collection time). Only 4.65 % Pb mass is utilized in the Pb(II) sensing compared to the conventional aqueous detection likely due to the strong oxygen reduction reaction, the limit of detection therefore could be potentially improved (by 20X if Pb mass is fully utilized) using oxygen scavenger agents in the electrolyte. Another explanation for a low

utilized Pb mass could be that the mass transport of Pb(II) is much faster than the Pb deposition on the sensing surface. Moreover, a bare gold electrode is used to prove the aerosol-into-liquid concept in this work, which can be modified by adding nanostructures or changing material compositions to further improve the limit of detection ideally by order of magnitudes.

Conflicts of interest

There are no conflicts of interest to declare.

Acknowledgement

Y.-B. Zhao and F. Jiang acknowledge financial support from the China Scholarship Council (CSC). T. Cen and C. Ludwig acknowledge the Swiss National Science Foundation for financial support (project 184817). Y.-B. Zhao thanks Daniel Rechenmacher for the drawing and manufacture of the aerodynamic/electrochemical sensing system. The authors gratefully acknowledge ScopeM at ETH Zürich, especially Karsten Kunze, for their support and assistance in this work.

3.6 References

[1] Y. Chang, K. Huang, M. Xie, C. Deng, Z. Zou, S. Liu, et al., First long-term and near real-time measurement of trace elements in China's urban atmosphere: temporal variability, source apportionment and precipitation effect, *Atmos Chem Phys*, **2018**, 18, 11793-812, 10.5194/acp-18-11793-2018.

[2] H. Li, X. Qian, Q.g. Wang, Heavy Metals in Atmospheric Particulate Matter: A Comprehensive Understanding Is Needed for Monitoring and Risk Mitigation, *Environ Sci Technol*, **2013**, 47, 13210-1, 10.1021/es404751a.

[3] J. Duan, J. Tan, Atmospheric heavy metals and Arsenic in China: Situation, sources and control policies, *Atmospheric Environment*, **2013**, 74, 93-101, https://doi.org/10.1016/j.atmosenv.2013.03.031.

[4] N.M. Mahowald, D.S. Hamilton, K.R.M. Mackey, J.K. Moore, A.R. Baker, R.A. Scanza, et al., Aerosol trace metal leaching and impacts on marine microorganisms, *Nat Commun*, **2018**, 9, 2614, 10.1038/s41467-018-04970-7.

[5] G. Aragay, A. Merkoçi, Nanomaterials application in electrochemical detection of heavy metals, *Electrochimica Acta*, **2012**, 84, 49-61, https://doi.org/10.1016/j.electacta.2012.04.044.

[6] H.Z. Tian, C.Y. Zhu, J.J. Gao, K. Cheng, J.M. Hao, K. Wang, et al., Quantitative assessment of atmospheric emissions of toxic heavy metals from anthropogenic sources in China: historical trend, spatial distribution, uncertainties, and control policies, *Atmos Chem Phys*, **2015**, 15, 10127-47, 10.5194/acp-15-10127-2015.

[7] G. Le Roux, F. De Vleeschouwer, D. Weiss, O. Masson, E. Pinelli, W. Shotyk, Learning from the Past: Fires, Architecture, and Environmental Lead Emissions, *Environmental Science & Technology*, **2019**, 53, 8482-4, 10.1021/acs.est.9b03869.

[8] K.E. Smith, D. Weis, C. Chauvel, S. Moulin, Honey Maps the Pb Fallout from the 2019 Fire at Notre-Dame Cathedral, Paris: A Geochemical Perspective, *Environmental Science & Technology Letters*, **2020**, 7, 753-9, 10.1021/acs.estlett.0c00485.

[9] R. Levin, C.L. Zilli Vieira, M.H. Rosenbaum, K. Bischoff, D.C. Mordarski, M.J. Brown, The urban lead (Pb) burden in humans, animals and the natural environment, *Environmental Research*, **2021**, 193, 110377, https://doi.org/10.1016/j.envres.2020.110377.

[10] C.F. Isley, M.P. Taylor, Atmospheric remobilization of natural and anthropogenic contaminants during wildfires, *Environmental Pollution*, **2020**, 267, 115400, https://doi.org/10.1016/j.envpol.2020.115400.

[11] I. Campos, N. Abrantes, J.J. Keizer, C. Vale, P. Pereira, Major and trace elements in soils and ashes of eucalypt and pine forest plantations in Portugal following a wildfire, *Science of The Total Environment*, **2016**, 572, 1363-76, https://doi.org/10.1016/j.scitotenv.2016.01.190.

[12] J. Korsiak, L. Pinault, T. Christidis, R.T. Burnett, M. Abrahamowicz, S. Weichenthal, Long-term exposure to wildfires and cancer incidence in Canada: a population-based observational cohort study, *The Lancet Planetary Health*, **2022**, 6, e400-e9, 10.1016/S2542-5196(22)00067-5.

[13] V. Bollati, B. Marinelli, P. Apostoli, M. Bonzini, F. Nordio, M. Hoxha, et al., Exposure to metal-rich particulate matter modifies the expression of candidate microRNAs in peripheral blood leukocytes, *Environmental health perspectives*, **2010**, 118, 763-8, 10.1289/ehp.0901300.

[14] Y. Zhang, X. Ji, T. Ku, G. Li, N. Sang, Heavy metals bound to fine particulate matter from northern China induce season-dependent health risks: A study based on myocardial toxicity, *Environmental Pollution*, **2016**, 216, 380-90, https://doi.org/10.1016/j.envpol.2016.05.072.

[15] E. Resongles, V. Dietze, D.C. Green, R.M. Harrison, R. Ochoa-Gonzalez, A.H. Tremper, et al., Strong evidence for the continued contribution of lead deposited during the 20th century to the atmospheric environment in London of today, *Proc Natl Acad Sci*, **2021**, 118, e2102791118, 10.1073/pnas.2102791118.

[16] T. Schwaba, W. Bleidorn, C.J. Hopwood, J.E. Gebauer, P.J. Rentfrow, J. Potter, et al., The impact of childhood lead exposure on adult personality: Evidence from the United States, Europe, and a large-scale natural experiment, *Proceedings of the National Academy of Sciences*, **2021**, 118, e2020104118, 10.1073/pnas.2020104118.

[17] W. Birmili, A.G. Allen, F. Bary, R.M. Harrison, Trace Metal Concentrations and Water Solubility in Size-Fractionated Atmospheric Particles and Influence of Road Traffic, *Environmental Science & Technology*, **2006**, 40, 1144-53, 10.1021/es0486925.

[18] W. Li, T. Wang, S. Zhou, S. Lee, Y. Huang, Y. Gao, et al., Microscopic Observation of Metal-Containing Particles from Chinese Continental Outflow Observed from a Non-Industrial Site, *Environmental Science & Technology*, **2013**, 47, 9124-31, 10.1021/es400109q.

[19] S. Canepari, M.L. Astolfi, S. Moretti, R. Curini, Comparison of extracting solutions for elemental fractionation in airborne particulate matter, *Talanta*, **2010**, 82, 834-44, https://doi.org/10.1016/j.talanta.2010.05.068.

[20] A. Mukhtar, A. Limbeck, Recent developments in assessment of bio-accessible trace metal fractions in airborne particulate matter: A review, *Anal Chim Acta*, **2013**, 774, 11-25, https://doi.org/10.1016/j.aca.2013.02.008.

[21] Y. Lyu, H. Guo, T. Cheng, X. Li, Particle Size Distributions of Oxidative Potential of Lung-Deposited Particles: Assessing Contributions from Quinones and Water-Soluble Metals, *Environmental Science & Technology*, **2018**, 52, 6592-600, 10.1021/acs.est.7b06686.

[22] M. Shiraiwa, K. Ueda, A. Pozzer, G. Lammel, C.J. Kampf, A. Fushimi, et al., Aerosol Health Effects from Molecular to Global Scales, *Environmental Science & Technology*, **2017**, 51, 13545-67, 10.1021/acs.est.7b04417.

[23] D. Foppiano, M. Tarik, E. Müller Gubler, C. Ludwig, Emissions of Secondary Formed ZnO Nano-Objects from the Combustion of Impregnated Wood. An Online Size-Resolved Elemental Investigation, *Environmental Science & Technology*, **2018**, 52, 895-903, 10.1021/acs.est.7b03584.

[24] S. Giannoukos, C.P. Lee, M. Tarik, C. Ludwig, S. Biollaz, H. Lamkaddam, et al., Real-Time Detection of Aerosol Metals Using Online Extractive Electrospray Ionization Mass Spectrometry, *Anal Chem*, **2020**, 92, 1316-25, 10.1021/acs.analchem.9b04480.

[25] P. Rai, M. Furger, J.G. Slowik, H. Zhong, Y. Tong, L. Wang, et al., Characteristics and sources of hourly elements in PM10 and PM2.5 during wintertime in Beijing, *Environmental Pollution*, **2021**, 278, 116865, https://doi.org/10.1016/j.envpol.2021.116865.

[26] J.M. Creamean, P.J. Neiman, T. Coleman, C.J. Senff, G. Kirgis, R.J. Alvarez, et al., Colorado air quality impacted by long-range-transported aerosol: a set of case studies during the 2015 Pacific Northwest fires, *Atmos Chem Phys*, **2016**, 16, 12329-45, 10.5194/acp-16-12329-2016.

[27] D. Wang, M.H. Sowlat, M.M. Shafer, J.J. Schauer, C. Sioutas, Development and evaluation of a novel monitor for online measurement of iron, manganese, and chromium in ambient particulate matter (PM), *Sci Total Environ*, **2016**, 565, 123-31, https://doi.org/10.1016/j.scitotenv.2016.04.164.

[28] D. Wang, M.M. Shafer, J.J. Schauer, C. Sioutas, A new technique for online measurement of total and water-soluble copper (Cu) in coarse particulate matter (PM), *Environ Pollut*, **2015**, 199, 227-34, https://doi.org/10.1016/j.envpol.2015.02.006.

[29] A. Karlsson, K. Irgum, H.-C. Hansson, Single-stage flowing liquid film impactor for continuous on-line particle analysis, *Journal of Aerosol Science*, **1997**, 28, 1539-51, https://doi.org/10.1016/S0021-8502(97)00013-X.

[30] L. Cui, J. Wu, H. Ju, Electrochemical sensing of heavy metal ions with inorganic, organic and bio-materials, *Biosensors and Bioelectronics*, **2015**, 63, 276-86, https://doi.org/10.1016/j.bios.2014.07.052.

[31] G. Aragay, J. Pons, A. Merkoçi, Recent Trends in Macro-, Micro-, and Nanomaterial-Based Tools and Strategies for Heavy-Metal Detection, *Chemical Reviews*, **2011**, 111, 3433-58, 10.1021/cr100383r.

[32] K. Kalcher, L.M. Moretto, Environmental analysis by electrochemical sensors and biosensors: Applications Volume 2: Springer; 2015.

[33] Y. Lu, X. Liang, C. Niyungeko, J. Zhou, J. Xu, G. Tian, A review of the identification and detection of heavy metal ions in the environment by voltammetry, *Talanta*, **2018**, 178, 324-38, https://doi.org/10.1016/j.talanta.2017.08.033.

[34] D. Buzica, M. Gerboles, A. Borowiak, P. Trincherini, R. Passarella, V. Pedroni, Comparison of voltammetry and inductively coupled plasma-mass spectrometry for the determination of heavy metals in PM10 airborne particulate matter, *Atmospheric Environment*, **2006**, 40, 4703-10, https://doi.org/10.1016/j.atmosenv.2006.04.015.

[35] J. Mettakoonpitak, D. Miller-Lionberg, T. Reilly, J. Volckens, C.S. Henry, Low-cost reusable sensor for cobalt and nickel detection in aerosols using adsorptive cathodic square-wave stripping voltammetry, *J Electroanal Chem*, **2017**, 805, 75-82, https://doi.org/10.1016/j.jelechem.2017.10.026.

[36] F. Rueda-Holgado, L. Calvo-Blázquez, F. Cereceda-Balic, E. Pinilla-Gil, A semiautomatic system for soluble lead and copper monitoring in atmospheric deposition by coupling of passive elemental fractionation sampling and voltammetric measurement on screen-printed gold electrodes, *Microchem J*, **2016**, 124, 20-5, https://doi.org/10.1016/j.microc.2015.07.012.

[37] M. Takeuchi, S.M.R. Ullah, P.K. Dasgupta, D.R. Collins, A. Williams, Continuous Collection of Soluble Atmospheric Particles with a Wetted Hydrophilic Filter, *Analytical Chemistry*, **2005**, 77, 8031-40, 10.1021/ac051539o.

[38] S.J. Fuller, F.P.H. Wragg, J. Nutter, M. Kalberer, Comparison of on-line and off-line methods to quantify reactive oxygen species (ROS) in atmospheric aerosols, *Atmospheric Environment*, **2014**, 92, 97-103, https://doi.org/10.1016/j.atmosenv.2014.04.006.

[39] J. Zhou, E.A. Bruns, P. Zotter, G. Stefenelli, A.S.H. Prévôt, U. Baltensperger, et al., Development, characterization and first deployment of an improved online reactive oxygen species analyzer, *Atmos Meas Tech*, **2018**, 11, 65-80, 10.5194/amt-11-65-2018.

[40] E. Ito, T. Tamadate, Y. Inomata, T. Seto, Water-based particle size magnifier for wet sampling of aerosol particles, *Aerosol Science and Technology*, **2021**, 1-15, 10.1080/02786826.2021.1940828.

[41] D. Wang, J. Jiang, J. Deng, Y. Li, J. Hao, A Sampler for Collecting Fine Particles into Liquid Suspensions, *Aerosol and Air Quality Research*, **2020**, 10.4209/aaqr.2019.12.0616.

[42] Y.-B. Zhao, J. Tang, T. Cen, G. Qiu, W. He, F. Jiang, et al., Integrated aerodynamic/electrochemical microsystem for collection and detection of nanogram-level airborne bioaccessible metals, *Sensors and Actuators B: Chemical*, **2022**, 351, 130903, https://doi.org/10.1016/j.snb.2021.130903.

[43] M. Li, H. Gou, I. Al-Ogaidi, N. Wu, Nanostructured Sensors for Detection of Heavy Metals: A Review, *ACS Sustainable Chemistry & Engineering*, **2013**, 1, 713-23, 10.1021/sc400019a.

[44] F. Jiang, W. Ju, Z. Pan, L. Lin, Y. Yue, Y.-B. Zhao, et al., Conformal Cu Coating on Electrospun Nanofibers for 3D Electro-Conductive Networks, *Advanced Electronic Materials*, **2020**, 6, 1900767, 10.1002/aelm.201900767.

[45] P. Kampalanonwat, P. Supaphol, Preparation and Adsorption Behavior of Aminated Electrospun Polyacrylonitrile Nanofiber Mats for Heavy Metal Ion Removal, *ACS Applied Materials & Interfaces*, **2010**, 2, 3619-27, 10.1021/am1008024.

[46] R. Zhao, X. Li, B. Sun, M. Shen, X. Tan, Y. Ding, et al., Preparation of phosphorylated polyacrylonitrile-based nanofiber mat and its application for heavy metal ion removal, *Chemical Engineering Journal*, **2015**, 268, 290-9, https://doi.org/10.1016/j.cej.2015.01.061.

[47] M.P. Romano, M.G. Lionetto, A. Mangone, A.R. De Bartolomeo, M.E. Giordano, D. Contini, et al., Development and characterization of a gold nanoparticles glassy carbon modified electrode for dithiotreitol (DTT) detection suitable to be applied for determination of atmospheric particulate oxidative potential, *Analytica Chimica Acta*, **2022**, 339556, https://doi.org/10.1016/j.aca.2022.339556.

[48] Z. Zou, A. Jang, E. MacKnight, P.-M. Wu, J. Do, P.L. Bishop, et al., Environmentally friendly disposable sensors with microfabricated on-chip planar bismuth electrode for in situ heavy metal ions measurement, *Sensors and Actuators B: Chemical*, **2008**, 134, 18-24, https://doi.org/10.1016/j.snb.2008.04.005.

[49] W.C. Hinds, Aerosol technology: properties, behavior, and measurement of airborne particles: John Wiley & Sons; 1999.

[50] V.A. Marple, D.L. Roberts, F.J. Romay, N.C. Miller, K.G. Truman, M. Van Oort, et al., Next Generation Pharmaceutical Impactor (A New Impactor for Pharmaceutical Inhaler Testing). Part I: Design, *Journal of Aerosol Medicine*, **2003**, 16, 283-99, 10.1089/089426803769017659.

[51] C.-N. Liu, A. Awasthi, Y.-H. Hung, C.-J. Tsai, Collection efficiency and interstage loss of nanoparticles in micro-orifice-based cascade impactors, *Atmospheric Environment*, **2013**, 69, 325-33, https://doi.org/10.1016/j.atmosenv.2012.12.003.

[52] S. Taghvaee, A. Mousavi, M.H. Sowlat, C. Sioutas, Development of a novel aerosol generation system for conducting inhalation exposures to ambient particulate matter (PM), *Science of The Total Environment*, **2019**, 665, 1035-45, https://doi.org/10.1016/j.scitotenv.2019.02.214.

[53] C.W.J. Berendsen, J.C.H. Zeegers, G.C.F.L. Kruis, M. Riepen, A.A. Darhuber, Rupture of Thin Liquid Films Induced by Impinging Air-Jets, *Langmuir*, **2012**, 28, 9977-85, 10.1021/la301353f.

[54] M.D. Scanlon, U. Salaj-Kosla, S. Belochapkine, D. MacAodha, D. Leech, Y. Ding, et al., Characterization of Nanoporous Gold Electrodes for Bioelectrochemical Applications, *Langmuir*, **2012**, 28, 2251-61, 10.1021/la202945s.

[55] M. Libansky, J. Zima, J. Barek, A. Reznickova, V. Svorcik, H. Dejmkova, Basic electrochemical properties of sputtered gold film electrodes, *Electrochimica Acta*, **2017**, 251, 452-60, https://doi.org/10.1016/j.electacta.2017.08.048.

[56] M. Finšgar, K. Xhanari, B. Petovar, Copper-film electrodes for Pb(II) trace analysis and a detailed electrochemical impedance spectroscopy study, *Microchemical Journal*, **2019**, 147, 863-71, https://doi.org/10.1016/j.microc.2019.04.007.

[57] C.M. Quiroa-Montalván, L.E. Gómez-Pineda, L. Álvarez-Contreras, R. Valdez, N. Arjona, M.T. Oropeza-Guzmán, Ordered Mesoporous Carbon Decorated with Magnetite for the Detection of Heavy Metals by Square Wave Anodic Stripping Voltammetry, *Journal of The Electrochemical Society*, **2017**, 164, B304-B13, 10.1149/2.0231707jes.

[58] C.-H. Lin, P.-H. Li, M. Yang, J.-J. Ye, X.-J. Huang, Metal Replacement Causing Interference in Stripping Analysis of Multiple Heavy Metal Analytes: Kinetic Study on Cd(II) and Cu(II) Electroanalysis via Experiment and Simulation, *Analytical Chemistry*, **2019**, 91, 9978-85, 10.1021/acs.analchem.9b01724.

[59] C.-J. Tsai, C.-N. Liu, S.-M. Hung, S.-C. Chen, S.-N. Uang, Y.-S. Cheng, et al., Novel Active Personal Nanoparticle Sampler for the Exposure Assessment of Nanoparticles in Workplaces, *Environmental Science & Technology*, **2012**, 46, 4546-52, 10.1021/es204580f.

[60] C. Misra, S. Kim, S. Shen, C. Sioutas, A high flow rate, very low pressure drop impactor for inertial separation of ultrafine from accumulation mode particles, *Journal of Aerosol Science*, **2002**, 33, 735-52, https://doi.org/10.1016/S0021-8502(01)00210-5.

[61] C.-H. Huang, C.-J. Tsai, T.-S. Shih, Particle collection efficiency of an inertial impactor with porous metal substrates, *Journal of Aerosol Science*, **2001**, 32, 1035-44, https://doi.org/10.1016/S0021-8502(01)00038-6.

[62] M. Marjamäki, J. Keskinen, Effect of impaction plate roughness and porosity on collection efficiency, *Journal of Aerosol Science*, **2004**, 35, 301-8, https://doi.org/10.1016/j.jaerosci.2003.09.001.

[63] S. Park, W. Choe, H. Lee, J.Y. Park, J. Kim, S.Y. Moon, et al., Stabilization of liquid instabilities with ionized gas jets, *Nature*, **2021**, 592, 49-53, 10.1038/s41586-021-03359-9.

[64] S. Jiménez Bolaños, B. Vernescu, Derivation of the Navier slip and slip length for viscous flows over a rough boundary, *Physics of Fluids*, **2017**, 29, 057103, 10.1063/1.4982899.

[65] X. Yang, C. Zhao, Y. Yang, X. Yan, H. Fan, Statistical aerosol properties associated with fire events from 2002 to 2019 and a case analysis in 2019 over Australia, *Atmos Chem Phys*, **2021**, 21, 3833-53, 10.5194/acp-21-3833-2021.

[66] Y. Yue, H. Chen, A. Setyan, M. Elser, M. Dietrich, J. Li, et al., Size-Resolved Endotoxin and Oxidative Potential of Ambient Particles in Beijing and Zürich, *Environmental Science & Technology*, **2018**, 52, 6816-24, 10.1021/acs.est.8b01167.

[67] K. Ashley, R.N. Andrews, L. Cavazos, M. Demange, Ultrasonic extraction as a sample preparation technique for elemental analysis by atomic spectrometry, *Journal of Analytical Atomic Spectrometry*, **2001**, 16, 1147-53, 10.1039/B102027G.

[68] T.T. Hien, N.D.T. Chi, D.H. Huy, H.A. Le, D.E. Oram, G.L. Forster, et al., Soluble trace metals associated with atmospheric fine particulate matter in the two most populous cities in Vietnam, *Atmospheric Environment: X*, **2022**, 15, 100178, https://doi.org/10.1016/j.aeaoa.2022.100178.

[69] Q. Wang, Y. Ma, J. Tan, N. Zheng, J. Duan, Y. Sun, et al., Characteristics of size-fractionated atmospheric metals and water-soluble metals in two typical episodes in Beijing, *Atmospheric Environment*, **2015**, 119, 294-303, https://doi.org/10.1016/j.atmosenv.2015.08.061.

[70] X. He, P. Liu, W. Zhao, H. Xu, R. Zhang, Z. Shen, Size distribution of water-soluble metals in atmospheric particles in Xi'an, China: Seasonal variations, bioavailability, and health risk assessment, *Atmospheric Pollution Research*, **2021**, 12, 101090, https://doi.org/10.1016/j.apr.2021.101090.

[71] California Air Resources Board, Camp Fire Air Quality Data Analysis, 2021.

[72] A. Singh, P. Pant, F.D. Pope, Air quality during and after festivals: Aerosol concentrations, composition and health effects, *Atmospheric Research*, **2019**, 227, 220-32, https://doi.org/10.1016/j.atmosres.2019.05.012.

[73] V. Di Marco, A. Tapparo, D. Badocco, S. D'Aronco, P. Pastore, C. Giorio, Metal Ion Release from Fine Particulate Matter Sampled in the Po Valley to an Aqueous Solution Mimicking Fog Water: Kinetics and Solubility, *Aerosol and Air Quality Research*, **2020**, 20, 720-9, 10.4209/aaqr.2019.10.0498.

[74] N. Chatterjee, M. Flury, Effect of Particle Shape on Capillary Forces Acting on Particles at the Air–Water Interface, *Langmuir*, **2013**, 29, 7903-11, 10.1021/la4017504.

[75] Q. Ma, Y. Liu, C. Liu, H. He, Heterogeneous reaction of acetic acid on MgO, α-Al2O3, and CaCO3 and the effect on the hygroscopic behaviour of these particles, *Physical Chemistry Chemical Physics*, **2012**, 14, 8403-9, 10.1039/C2CP40510E.

[76] J. Mettakoonpitak, J. Volckens, C.S. Henry, Janus Electrochemical Paper-Based Analytical Devices for Metals Detection in Aerosol Samples, *Anal Chem*, **2020**, 92, 1439-46, 10.1021/acs.analchem.9b04632.

[77] R.J. Weber, D. Orsini, Y. Daun, Y.N. Lee, P.J. Klotz, F. Brechtel, A Particle-into-Liquid Collector for Rapid Measurement of Aerosol Bulk Chemical Composition, *Aerosol Sci Technol*, **2001**, 35, 718-27, 10.1080/02786820152546761.

[78] B.T. Cartledge, A.R. Marcotte, P. Herckes, A.D. Anbar, B.J. Majestic, The Impact of Particle Size, Relative Humidity, and Sulfur Dioxide on Iron Solubility in Simulated Atmospheric Marine Aerosols, *Environmental Science & Technology*, **2015**, 49, 7179-87, 10.1021/acs.est.5b02452.

[79] F. Rueda-Holgado, E. Bernalte, M.R. Palomo-Marín, L. Calvo-Blázquez, F. Cereceda-Balic, E. Pinilla-Gil, Miniaturized voltammetric stripping on screen printed gold electrodes for field determination of copper in atmospheric deposition, *Talanta*, **2012**, 101, 435-9, https://doi.org/10.1016/j.talanta.2012.09.054.

[80] J. Mettakoonpitak, J. Mehaffy, J. Volckens, C.S. Henry, AgNP/Bi/Nafion-modified Disposable Electrodes for Sensitive Zn(II), Cd(II), and Pb(II) Detection in Aerosol Samples, *Electroanalysis*, **2017**, 29, 880-9, https://doi.org/10.1002/elan.201600591.

[81] M.R. Palomo-Marín, F. Rueda-Holgado, J. Marín-Expósito, E. Pinilla-Gil, Disposable sputtered-bismuth screen-printed sensors for voltammetric monitoring of cadmium and lead in

atmospheric particulate matter samples, *Talanta*, **2017**, 175, 313-7, https://doi.org/10.1016/j.talanta.2017.07.060.

[82] H.d.A. Silva-Neto, T.M.G. Cardoso, W.K.T. Coltro, R.C. Urban, Determination of bioavailable lead in atmospheric aerosols using unmodified screen-printed carbon electrodes, *Analytical Methods*, **2019**, 11, 4875-81, 10.1039/C9AY01301F.

[83] H. Sun, Y. Jia, H. Dong, L. Fan, Graphene oxide nanosheets coupled with paper microfluidics for enhanced on-site airborne trace metal detection, *Microsystems & Nanoengineering*, **2019**, 5, 4, 10.1038/s41378-018-0044-z.

[84] D. Wang, M.M. Shafer, J.J. Schauer, C. Sioutas, Development of a Technology for Online Measurement of Total and Water-Soluble Copper (Cu) in PM2.5, *Aerosol Science and Technology*, **2014**, 48, 864-74, 10.1080/02786826.2014.937478.

[85] M.H. Sowlat, D. Wang, G. Simonetti, M.M. Shafer, J.J. Schauer, C. Sioutas, Development and field evaluation of an online monitor for near-continuous measurement of iron, manganese, and chromium in coarse airborne particulate matter (PM), *Aerosol Science and Technology*, **2016**, 50, 1306-19, 10.1080/02786826.2016.1221051.

[86] H. Sato, M. Yui, H. Yoshikawa, Ionic Diffusion Coefficients of Cs+, Pb2+, Sm3+, Ni2+, SeO2- 4 and TcO− 4 in Free Water Determined from Conductivity Measurements, *J Nucl Sci Technol*, **1996**, 33, 950-5, 10.1080/18811248.1996.9732037.

Appendix B

Table B1 State-of-the-art techniques for collecting and sensing atmospheric metals.

Met-als	Sampling method	Sam-pling dura-tion	Detection tech-nique	Time reso-lution	Detection limit	Oper-ation mode	Refs.
Cd, Pb, Cu, Fe, Ni	Personal aerosol sampler	-	Electrochemical paper-based de-vices	-	0.5 µg/L for Cd, Pb, Fe, and 1µg/L for Cu, Ni	offline	[76]
Co, Ni	Filters	-	Nafion/Bi carbon stencil printed electrodes	-	1 µg/L for Co and 5 µg/L for Ni	offline	[35]
Zn, Cd, Pb	Personal aerosol samplers	-	AgNP/Bi/Nafion-modified electrodes	-	5 µg/L for Zn, 0.5 µg/L for Cd and 0.1 µg/L for Pb	offline	[80]

Cd, Pb	Digital DAH-80 high-volume air sampler	24 h	Sputtered-bismuth screen printed electrodes	-	11.82 µg/L for Cd and 6.07 µg/L for Pb	offline	[81]
Cu	Total atmospheric deposition polyethylene collectors	7 days	Screen-printed gold electrodes	-	3.7 µg/L	offline	[79]
Pb	High-volume sampler	24 h	Unmodified screen-printed carbon electrode	-	0.023 µg/L	offline	[82]
Fe, Cu, Ni	Unmanned aerial vehicle multiaxial sampling	4 h	Cellphone colorimetric detection using graphene oxide coated microfluidic paper-based analytical devices	> 4.5 h	41.5 µg/L for Fe, 12.75 µg/L for Cu, and 24.75 µg/L for Ni	Online	[83]
Pb, Cu	Atmospheric sampler	24 h	Screen-printed gold Electrodes	> 24 h	7.3 µg/L for Cu and 15.1 µg/L for Pb	Online	[36]
Cu	Two virtual impactors combined with a modified liquid impinger	2 – 4 h	Copper ion selective electrode	2 – 4 h	10 µg/L	Online	[28]
Cu	An aerosol-into-liquid collector (saturator	2 – 4 h	Copper ion selective electrode	2 – 4 h	10 µg/L	Online	[84]

	tank, condensation tubes and high flow rate impactor)						
Fe, Mn, Cr	Coarse particulate matter collection module	2 h	UV/VIS spectrophotometry	> 2 h	0.3 µg/L for Fe, 0.2 µg/L for Mn, and 0.2 µg/L for Cr	Online	[85]
Fe, Mn, Cr	Aerosol-into-liquid collector	2 h	Micro volume flow cell spectrophotometry	> 2 h	0.3 µg/L for Fe, 0.2 µg/L for Mn, and 0.2 µg/L for Cr	Online	[27]
Pb	Collection on a Janus membrane electrode	1 h	The gold surface of the Janus membrane electrode	1 h	2.09 µg/L for Pb	-	This work

Table B2 The main composition of the PM10-like particles.

Element	Mass fraction (mg/kg)	Element	Mass fraction (mg/kg)
Arsenic	7.1	Magnesium	13200
Cadmium	0.9	Manganese	611
Lead	113	Molybdenum	33.2
Nickel	58	Neodymium	22.2
Aluminium	34100	Potassium	10998
Antimony	64.7	Rubidium	52.3
Barium	562.2	Samarium	4.1
Bromine	10.2	Scandium	7.4
Caesium	3.1	Silicon	229000
Calcium	63043	Sodium	14211

Cerium	56.8	Strontium	251
Chloride	10033	Tantalum	1.0
Chromium	201	Terbium	0.6
Cobalt	14.3	Thorium	7.0
Copper	462	Titanium	4372
Dysprosium	3.3	Total carbon	111333
Elemental carbon	45433	Total organic carbon	76633
Europium	0.8	Tungsten	4.1
Gallium	8.7	Uranium	2.6
Gold	0.02	Vanadium	72.6
Hanium	8.4	Ytterbium	1.7
Iron	38144	Zinc	1240
Lanthanum	25	Zirconium	341

The detailed information about the PM10-like particles can be found at https://crm.jrc.ec.europa.eu/p/40454/40470/By-application-field/Environment/ERM-CZ120-FINE-DUST-PM10-LIKE-elements/ERM-CZ120.

Table B3 ICP-MS analysis of upstream and downstream filters for 1-hour particle collection at 7.1 L/min in the ambient environment (n = 4).

	concentration ppb	RSD	SD	Note
Upstream filter ambient air 1 h_1	-0.57	9.37	-0.05341	< LOD
Downstream filter ambient air 1 h_1	-0.44	7.27	-0.03199	< LOD
Upstream filter ambient air 1 h_2	-0.55	3.51	-0.01931	< LOD
Downstream filter ambient air 1 h_2	-0.59	5.77	-0.03404	< LOD

< LOD : no soluble lead was detected using ICP-MS analysis.

Table B4 Sensing conditions of the conventional aqueous detection and the aerosol-into-liquid concept.

Conventional aqueous detection	Aerosol-into-liquid concept

The AILE electrode was put in an electrochemical glass cell containing a uniform Pb(II) concentration with a three-electrode system.	Particle-bound Pb carried by airflow with a constant flow rate were captured by the AILE electrode in the IAE system. A concentration gradient of Pb(II) formed across the AILE electrode.

Table B5 Comparison of the IAE system in this study to commercial instruments.

Instrument	Working principle	Price	Weight	Metal speciation	Limit of detection (Pb)
Cooper Xact 625i	Reel-to-reel filter tape sampling and nondestructive energy dispersive X-ray fluorescence analysis	$ 4095131	83.01 kg2	Total metal	< 2.43 ng/m3 2
Horiba PX-375	X-ray fluorescence and Beta-ray attenuation on filter tapes	> $ 1244983	> 40 kg4	Total metal	< 5.3 ng/m3 4
This work	One step collection and electrochemical detection of metals on a dual-functional membrane electrode	<< $ 1000	~ 2 kg	Soluble metal	95.7 ng

1 https://m.antpedia.com/instrument/21262/

2 https://www.ecotech.com/wp-content/uploads/2017/03/Cooper-Environmental-Monitoring-625i-Spec-Sheet.pdf

3 https://ektimo.com.au/products-equipment/px-375-continuous-particulate-monitor-and-xrf-analyser/

4 https://www.horiba.com/int/process-and-environmental/products/detail/action/show/Product/px-375-181/

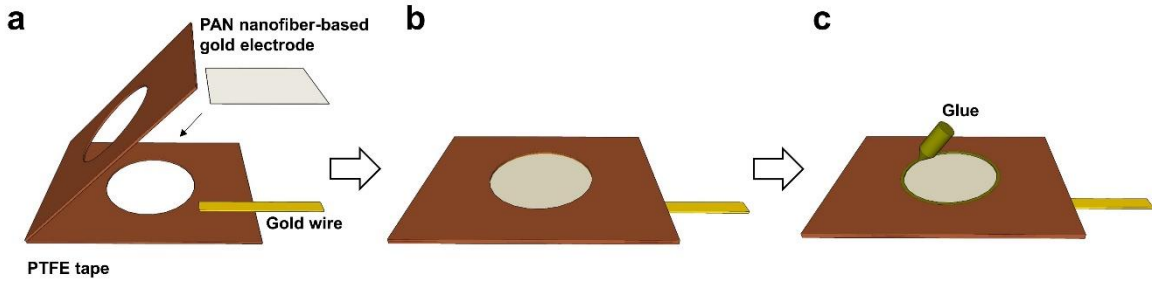

Figure B1 Schematic of the electrode assembly. (a) Teflon tape (3 * 3.5 cm) punching (Ø 2 cm) → (b) Teflon tape, electrode, gold wire → (c) glue sealing.

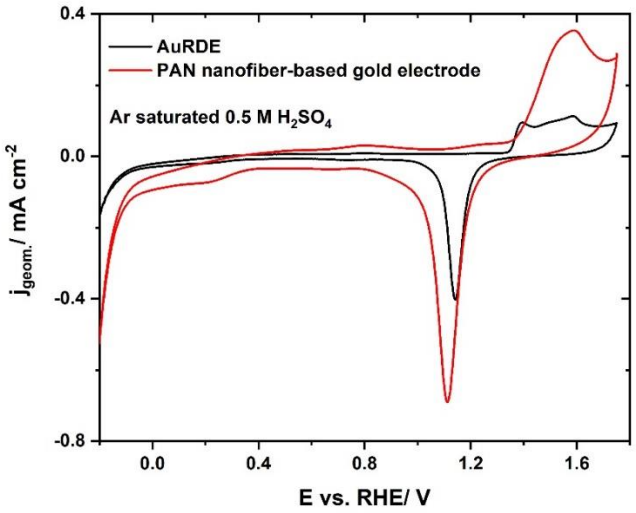

Figure B2 Cyclic voltammograms of the Au rotating disk electrode (RDE) and polyacrylonitrile (PAN) nanofiber-based gold electrode at a scan rate of 50 mV s^{-1} in the Ar saturated 0.5 M H_2SO_4.

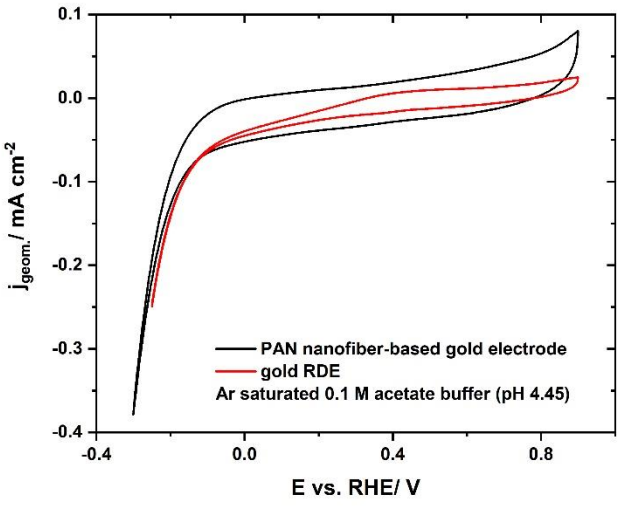

Figure B3 Cyclic voltammograms of gold RDE and PAN nanofiber-based gold electrode in Ar-saturated 0.1 M acetate buffer (pH 4.45).

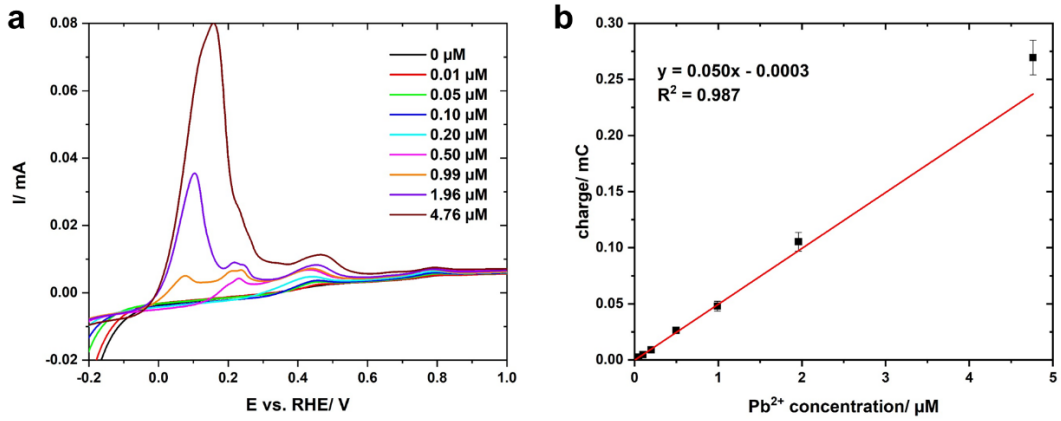

Figure B4 (a) Anodic stripping voltammetry of $Pb(NO_3)_2$ using gold RDE in 0.1 M acetate buffer (pH = 4.45) saturated with Argon at a scan rate of 50 mV/s, (b) relationship between the concentration and stripping charge. The stripping charges indicated that 0.304 ± 0.114 % Pb (II) participated in the reduction reaction on the electrode surface at 1600 rpm.

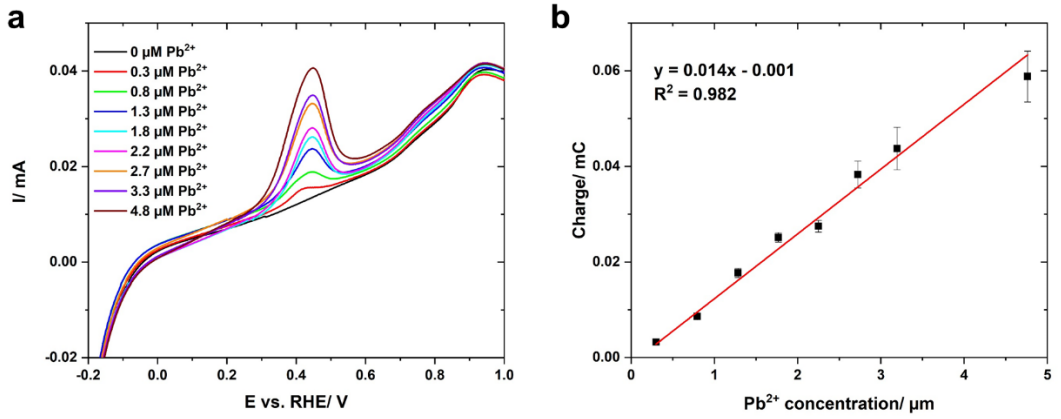

Figure B5 (a) Anodic stripping voltammetry of $Pb(NO_3)_2$ using PAN nanofiber-based gold electrode in 0.1 M acetate buffer (pH = 4.45) saturated with Argon at a scan rate of 50 mV/s, (b) relationship between the concentration and stripping charge. The charge was used as the indication of signal in anodic stripping voltammetry.

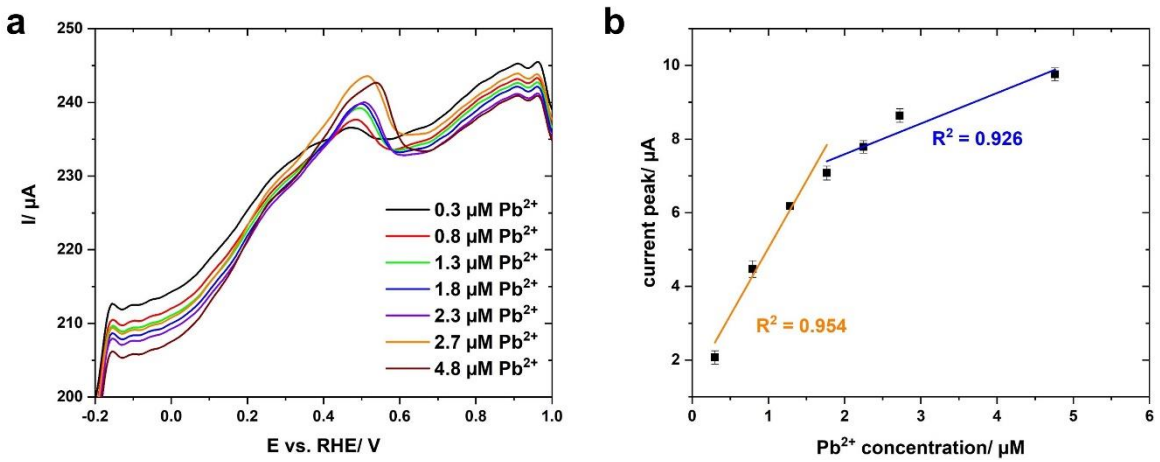

Figure B6 (a) Square wave stripping voltammetry of $Pb(NO_3)_2$ using PAN nanofiber-based gold electrode in 0.1 M acetate buffer (pH = 4.45) saturated with Argon, (b) relationship between the concentration and current peak. Current peak was used as the indication of signal in square wave stripping voltammetry.

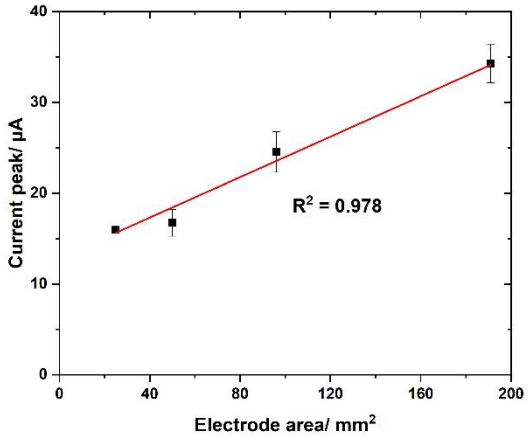

Figure B7 Relationship between the electrode area of the PAN nanofiber-based gold electrode and current peak.

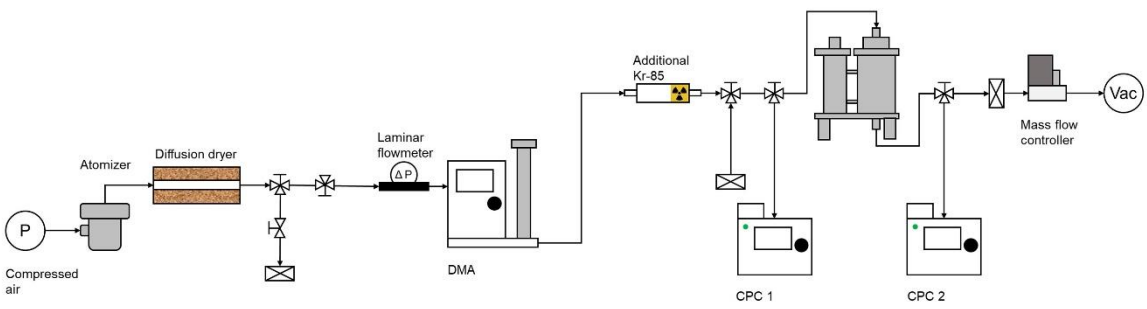

Figure B8 Setup for evaluating the collection efficiency of the IAE system. Condensation Particle Counter (CPC)1 and CPC2 were used for counting the upstream and downstream particle number, respectively.

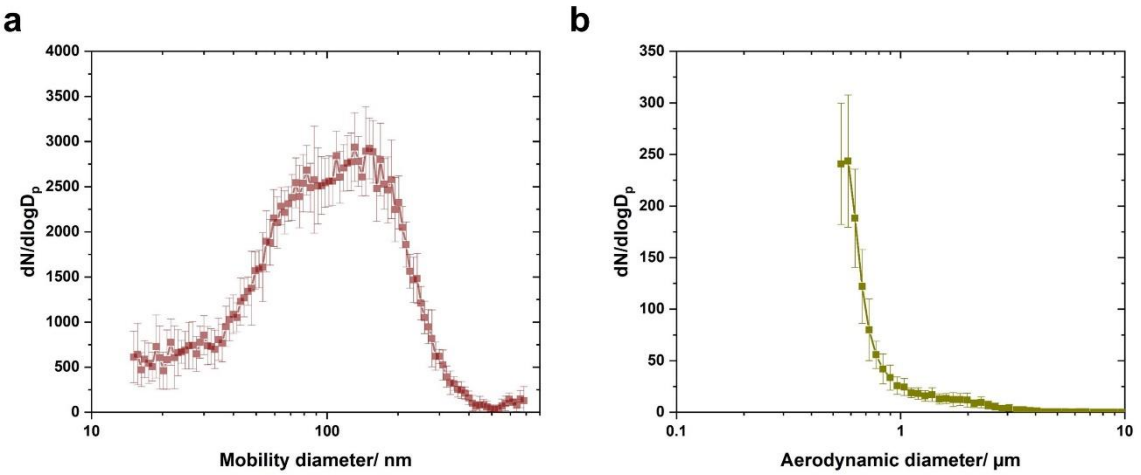

Figure B9 Size distribution of the ambient aerosol in Dubendorf, Switzerland, in terms of (a) mobility diameter and (b) aerodyanmic diameter obtained from scanning mobility particle sizer (SMPS) and aerodynamic particle sizer (APS), respectively.

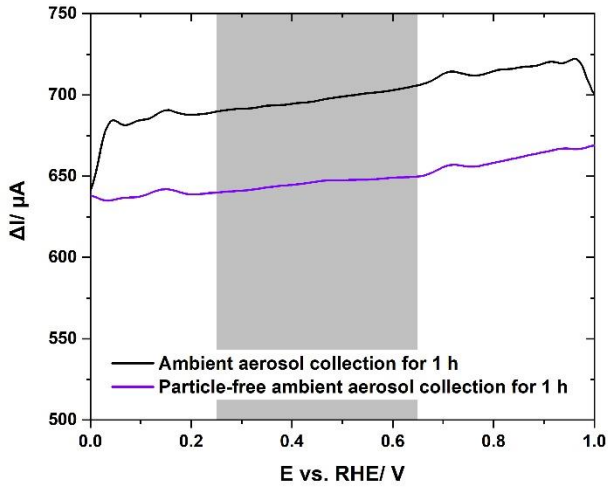

Figure B10 SWV response to the ambient aerosol for 1-hour collection at a flow rate of 7.1 L/min. Particle-free means the ambient aerosol was filtered using a high efficiency particulate air (HEPA) filter.

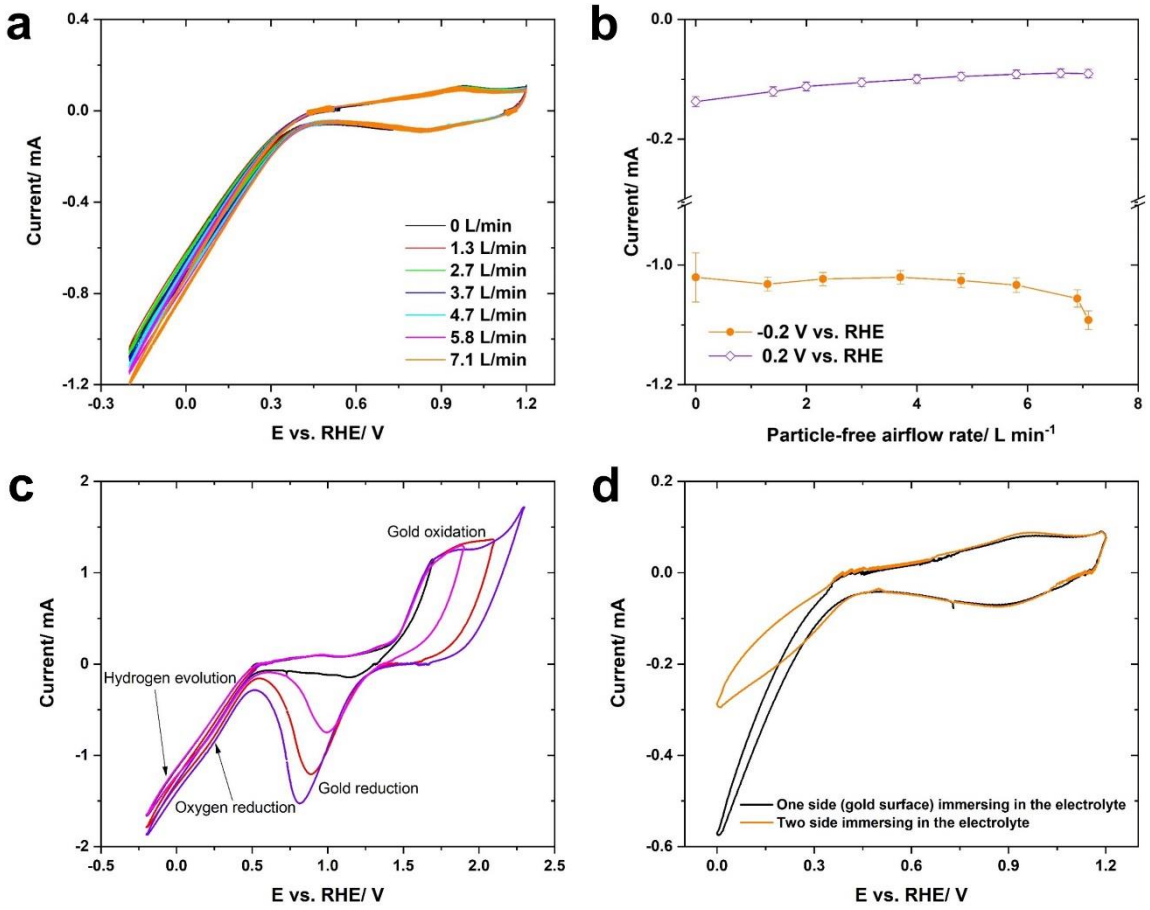

Figure B11 Characterization of the PAN nanofiber-based gold electrode in the integrated system: (a) Cyclic voltammetry (CV) of PAN nanofiber-based gold electrode at 100 mV/s, mounted in the system at a particle-free airflow rate, (b) chronoamperometry current at 0.2 V and -0.2 V vs. RHE for about 1 min at different airflows, (c) cyclic voltammetry of PAN nanofiber-based gold electrode with different potential ranges, (d) CV of the one side and two sides of the electrode immersing in the electrolyte.

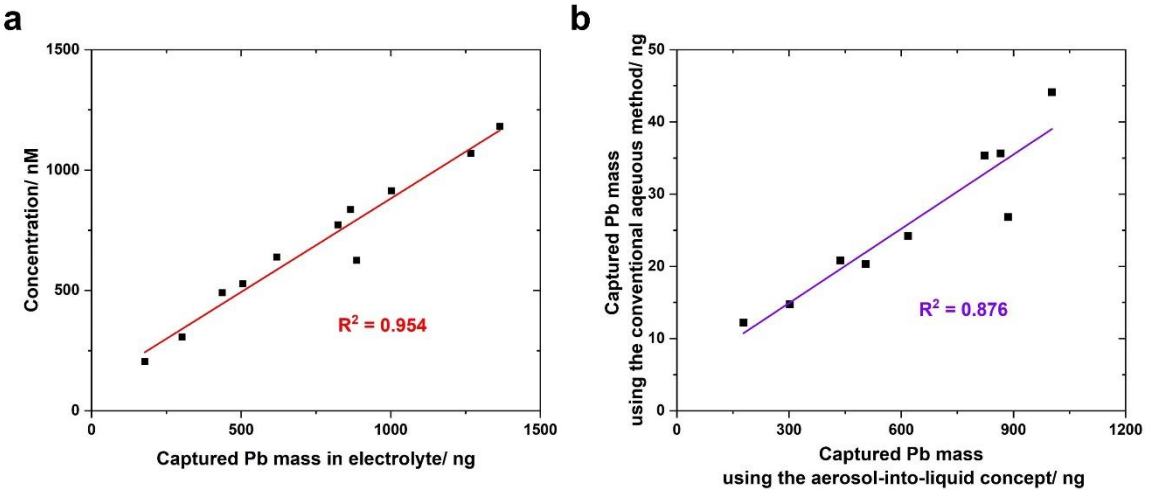

Figure B12 (a) Relationship between the captured Pb masses using the aerosol-into-liquid concept and Pb(II) concentrations using the conventional aqueous detection, given the same

peak current, (b) relationship between the captured Pb masses using the aerosol-into-liquid concept and the needed Pb(II) masses using the conventional aqueous detection to obtain the same peak current.

a

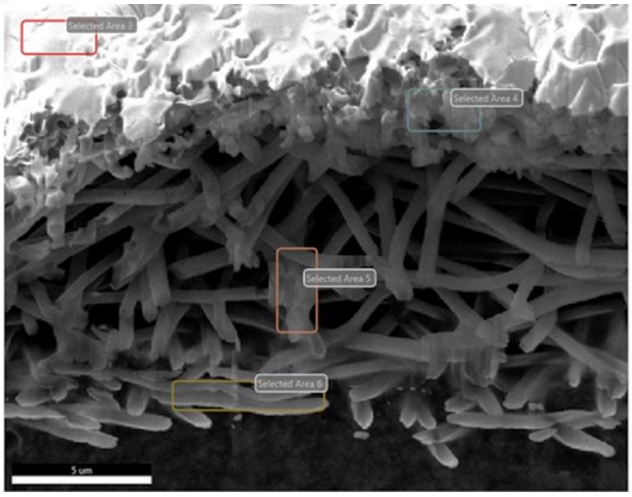

b

	Area 3	Area 4	Area 5	Area 6
C	19.90	54.26	78.18	62.57
O	2.30	21.73	2.12	1.33
Xe	8.31	-	-	-
W	69.49	-	0.71	0.83
N	-	4.10	11.65	6.22
Na	-	0.49	0.33	-
Mg	-	0.42	-	-
Al	-	2.15	-	-
Si	-	8.13	0.19	-
K	-	4.15	1.31	-
Fe	-	3.28	-	
Au	-	1.28	5.51	29.04

Figure B13 (a) The selected area for the SEM mapping, (b) the weight percentage of elements in the selected area. Area 3, 4, 5, and 6 indicated the sample preparation for plasma FIB, PM_{10} particle collection area, cross section area of the membrane electrode, and the gold surface of the membrane electrode. Pb concentration was not detectable due to its ultratrace level.

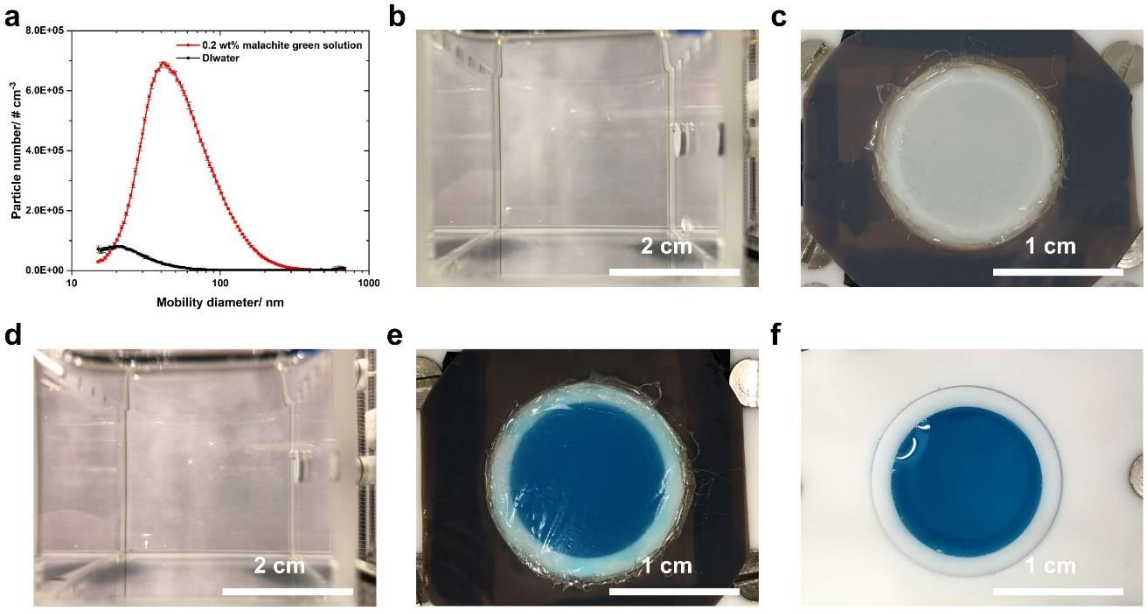

Figure B14 Collection and dissolution of malachite green particles for 1 h: (a) SMPS scanning of the size distribution and particle number generated from 0.2 wt% malachite green particles, (b) glass container and (c) PAN membrane assembly without gold surface before the particle collection, (d) glass container, (e) PAN membrane assembly without gold surface and (f) PTFE part without the PAN membrane assembly after the particle collection.

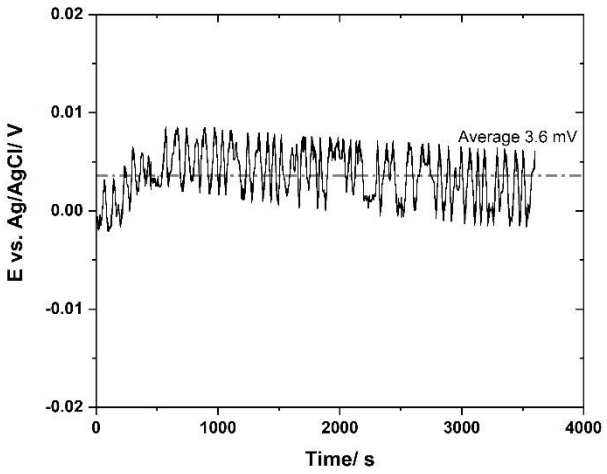

Figure B15 Open circuit potential of the flexible Ag/AgCl (3M KCl) vs. bulky Ag/AgCl (3M KCl).

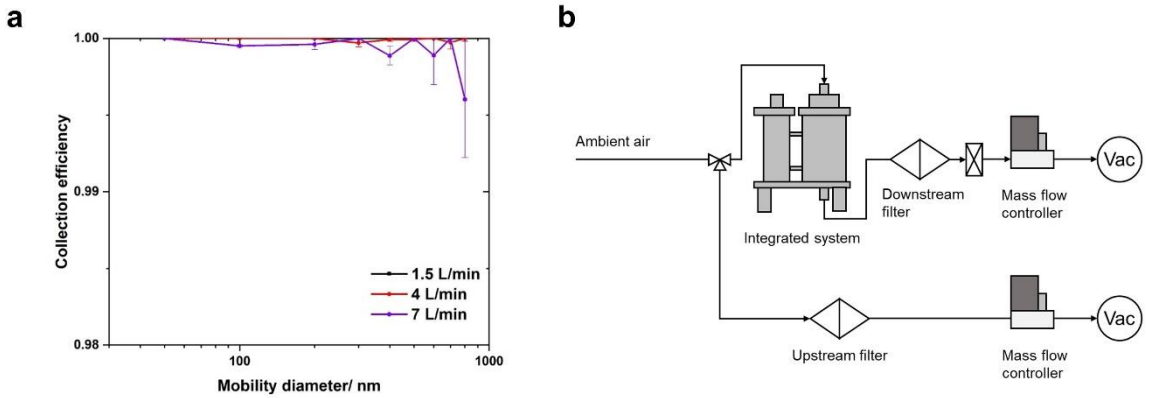

Figure B16 (a) Collection efficiency of the polycarbonate (PC) filter with a pore size of 1 µm at different flow rates, (b) schematic of the setup for evaluating the collection and detection performance of the integrated system with an inflow rate of 7.1 L/min in the ambient environment. The flow rate for the upstream filter was 7.1 L/min.

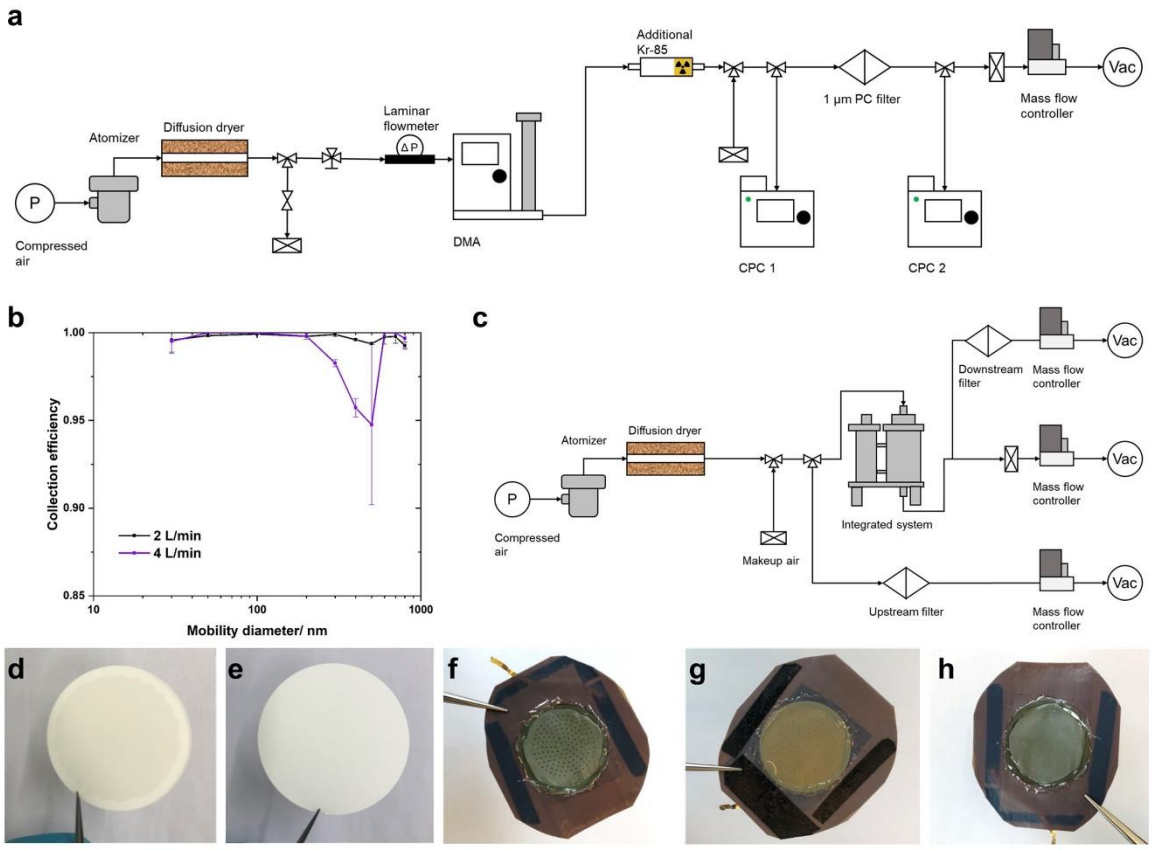

Figure B17 (a) Setup for the evaluation of collection efficiency of the cellulose nitrate filter used as the upstream and downstream filter, (b) collection efficiency of the cellulose nitrate filter with a pore size of 0.45 µm at different flow rates, (c) schematic of the setup for evaluating the collection and detection performance of the integrated system with an inflow rate of 7.1 L/min using lab-generated aerosols, and the flow rates for the upstream and downstream filters were 4 L/min and 4 L/min, respectively (d) and (e) were the upstream and downstream filters after collecting PM_{10}-like aerosol, respectively, (f), (g), and (h) were the PAN nanofiber and gold side of the assembled electrode after PM_{10}-like aerosol collection before cleaning and the PAN nanofiber side of the electrode after cleaning, respectively. The upstream and the downstream filter were 0.45 µm cellulose nitrate filters.

Boundary conditions

To simplify the simulation, a symmetric or axisymmetric geometry was used. The wall condition was defined as no slip, and fully developed flow was applied in the inlet. The pressure of the outlet was defined as 0, and backflow was suppressed. The number of layers was 8, and the stretching factor was 1.2. In the particle tracing module, the Schiller-Naumann drag law and Cunningham-Millikan-Davies effect were applied. 5000 particles were released from the airflow inlet to obtain the particle collection efficiency on the impaction plate.

Mesh used for simulation

For the simulation of the IAE system, the mesh of fine size was used to generate 1205931 domain elements, 90404 boundary elements, and 4506 degree elements (Figure B18b). The simplified nozzle structure was used in the simulation of particle capture. The mesh of extra fine was used to ensure the simulation accuracy. In the simulation with a jet-to-plate distance of 0.5 cm, 1 cm, and 2 cm, 21008 domain elements and 394 boundary elements, 24805 domain elements and 439 boundary elements (Figure B19b), and 47267 domain elements and 675 boundary elements were generated, respectively.

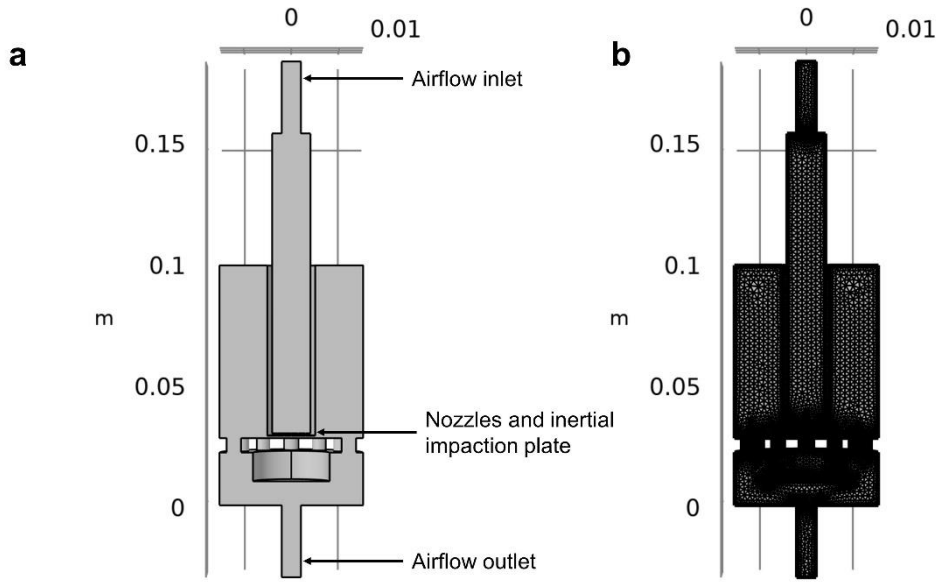

Figure B18 (a) The symmetric geometry and (b) the computational mesh of the integrated system used in the simulation.

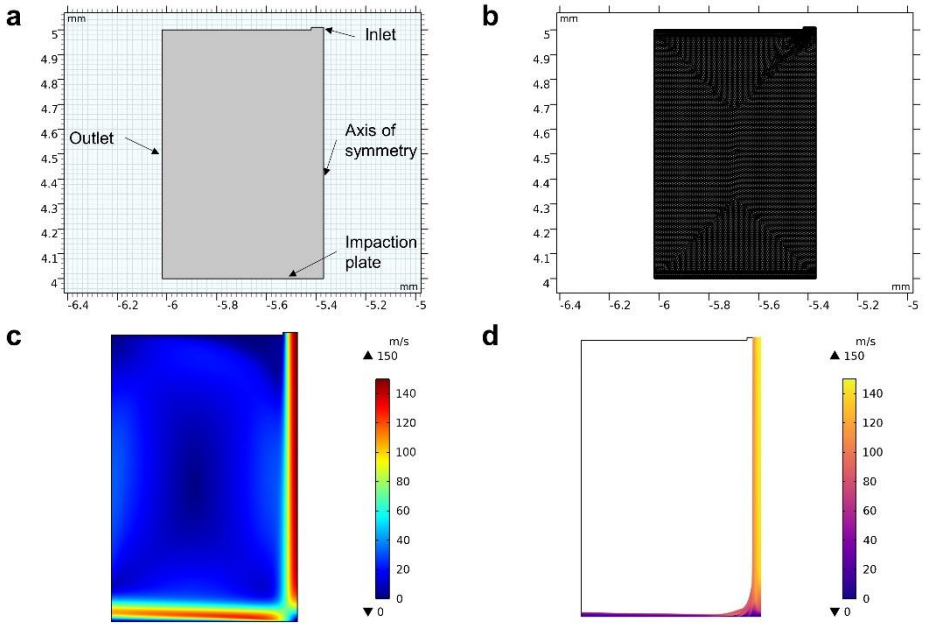

Figure B19 (a) The axisymmetric geometry and (b) the computational mesh of the nozzle and impaction plate used in the simulation, (c) numerical simulation of flow jet of 100 m/s via a 100 µm nozzle impinging on the fixed surface with a jet-to-distance of 1mm, (d) simulated particle trajectories of 150 nm solid particle with a density of 2200 kg/m^3.

Numerical simulation of the Pb(II) mass transport

The Pb(II) mass transport was simulated in the case of the conventional aqueous detection (Figure B18a) and the aerosol-into-liquid capture and detection (Figure B18b). The conventional aqueous detection was to put the AILE electrode in the electrolyte containing certain Pb(II) concentrations, while the aerosol-into-liquid concept was to capture the Pb(II) particles on the AILE electrode for sensing. To compare the Pb(II) mass transport using these two methods, the same amount of Pb(II) was given, which was considered as the aerosol sample detected by traditional detection-after-preparation (conventional aqueous detection) and direct detection without sample preprocessing (aerosol-into-liquid concept). The amount of Pb(II) was calculated using a liquid volume of 45 mL, and the Pb(II) concentration was based on the experimental conditions. The mass transport in the conventional aqueous detection was validated by the experimental results (Figure B18c).

In the simulation of the conventional aqueous detection, the initial Pb(II) concentration was homogenous in the electrolyte, and L was 22.5 cm. The concentration of Pb(II) concentration on the electrode surface was assumed as zero as the deposition of Pb(II) on the electrode surface was fast enough to consume the Pb(II) on the surface. The initial condition was $C|_{t=0} = C_0$, and the boundary conditions were $\frac{\partial C}{\partial x}\Big|_{x=0} = 0$, and $C|_{x=L} = 0$. The governing equation was $\frac{\partial C}{\partial t} = D_v \cdot \frac{\partial^2 C}{\partial x^2}$. It was noted that the simulation was axisymmetric as the diffusion of Pb(II) occurred on both sides of the AILE electrode.

For the simulation of the aerosol-into-liquid concept, a constant flux was assumed due to a constant air flow containing Pb(II) particles, and the L was defined as the thickness of the AILE electrode (15 µm). The initial condition was $C|_{t=0} = 0$, and the boundary conditions were flux $= D_v \frac{\partial C}{\partial x}\Big|_{x=0}$ and $C|_{x=L} = 0$. The governing equation was $\frac{\partial C}{\partial t} = D_v \cdot \frac{\partial^2 C}{\partial x^2} + q_{ab} + v \cdot \frac{\partial C}{\partial x}$, which refers to diffusion + adsorption + advection caused by evaporation. The diffusion coefficient of Pb ions in the simulation was $9.45*10^{-10}$ [86].

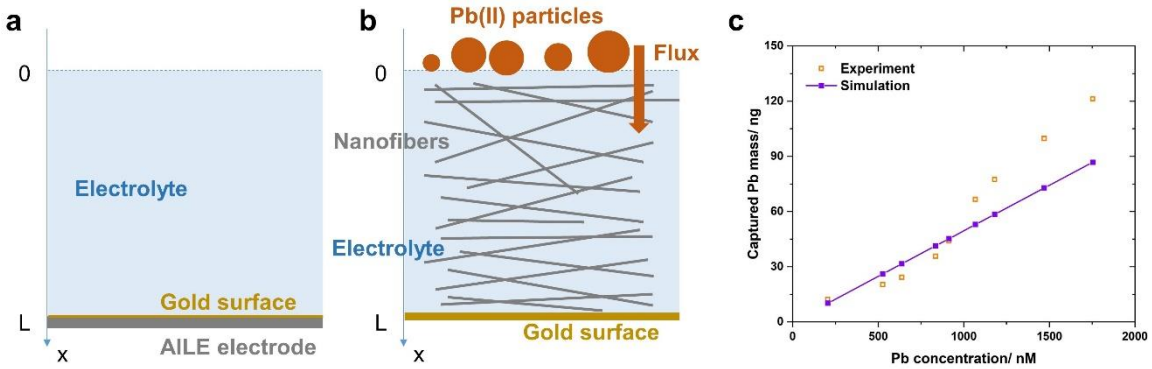

Figure B20 Schematic illustration of the (a) conventional aqueous (b) detection and the aerosol-into-liquid concept, and the (c) comparison of simulation and experimental results for the conventional aqueous detection.

Chapter 4

An elution-based method for estimating efficiencies of aerosol collection devices not affected by their pressure drops

Yi-Bo Zhao[1,2], Tianyu Cen[3,4], Jiukai Tang[1,2], Weidong He[1,2,5], Christian Ludwig[3,4], Sheng-Chieh Chen[6], and Jing Wang[1,2*]

[1] Institute of Environmental Engineering, ETH Zürich, 8093 Zürich, Switzerland
[2] Advanced Analytical Technologies, Empa, Ueberlandstrasse 129, 8600 Dübendorf, Switzerland
[3] Environmental Engineering Institute (IIE, GR-LUD), School of Architecture, Civil and Environmental Engineering (ENAC), École Polytechnique Fédérale de Lausanne (EPFL), 1015 Lausanne, Switzerland
[4] Bioenergy and Catalysis Laboratory (LBK-CPM), Energy and Environment Research Division (ENE), Paul Scherrer Institut (PSI), 5232 Villigen PSI, Switzerland
[5] Filter Test Center, School of Resources and Civil Engineering, Northeastern University, NO. 3-11, Wenhua Road, Heping District, Shenyang, Liaoning 110819, China
[6] Department of Mechanical and Nuclear Engineering, Virginia Commonwealth University, 401 West Main St., Richmond, VA, 23284, USA

* corresponding authors

Author contributions

Yi-Bo Zhao: Conceptualization, Methodology, Investigation, Writing – original draft. Tianyu Cen: Investigation, Resources, Formal analysis. Jiukai Tang: Investigation, Resources. Weidong He: Formal analysis, Data curation. Christian Ludwig: Validation, Formal analysis, Writing – review & editing. Sheng-Chieh Chen: Validation, Writing – review & editing. Jing Wang: Conceptualization, Resources, Writing – review & editing, Supervision.

This work has been published in *Separation and Purification Technology*. **2022**, 287. DOI: 10.1016/j.seppur.2022.120590.

Abstract

The evaluation of collection efficiencies of aerosol samplers becomes challenging with high pressure drops. The evaluation approaches applied at various conditions deserve further development, especially when a high pressure drop is induced by the sampler. In this work, an elution-based method using NaCl aerosol was proposed to estimate the size-resolved collection efficiency which was not affected by the pressure drop. More specifically, a Condensation Particle Counter (CPC) was used to count the upstream particle number, and the collected NaCl particles were eluted and determined by Inductively Coupled Plasma Mass Spectrometry (ICP-MS) for estimating the collected particle number. The relationship between number-based concentration and mass-based concentration of NaCl particles was established. A stainless steel impactor for Differential Mobility Analyzer (DMA), polydimethylsiloxane (PDMS)-based microchannel, and a homemade impactor containing 151 nozzles with a diameter of 0.1 mm were employed to investigate the feasibility of the elution method. DMA-selected particles with a nominal size are considered to be the monodisperse aerosol, which was commonly used for

estimating the collection efficiencies of samplers, but size redistribution of downstream monodisperse aerosol with the particle size smaller than 100 nm and larger than the cutoff size (D_{50}) was revealed through the elution method, which affected the collection efficiency measured by either conventional CPC- or elution-based method. It was found that the elution method was dependent on the D_{50} value of the sampler, and the applicable size range was from 100 nm to D_{50} (D_{50} < 500 nm) or from 100 nm to 500 nm (D_{50} > 500 nm). This study provided insights into the size-dependent particle transport through aerosol samplers, and the development of an elution-based method to estimate pressure drop-independent collection efficiencies.

Keywords: Elution; NaCl; Collection efficiency; Aerosol sampler; Pressure drop; Size redistribution

4.1 Introduction

Aerosol samplers such as impactors, impingers, and cyclones are widely used to collect or classify airborne particles [1]. To evaluate the aerosol samplers, its size-resolved collection efficiency is normally investigated. The online aerosol instruments such as the scanning mobility particle sizer (SMPS) or aerodynamic particle sizer (APS) are often employed to measure the upstream (N_{up}) and downstream (N_{down}) particle number concentrations of the samplers to determine the collection efficiency (η_P) [2]:

$$\eta_P = \frac{N_{up} - N_{down}}{N_{up}} \quad (1)$$

However, obtaining an accurate particle size and number concentration becomes challenging when the inlet pressure of the online instruments is outside the operating range due to the high pressure drop induced by samplers [3]. For example, Condensation Particle Counter (CPC) 3775 could operate normally only at an inlet pressure of 0.75 to 1.05 atm [4]. Under a low pressure condition (e.g. 0.5 atm), the counting efficiency of a CPC can be largely reduced due to the particle diffusion loss for small particles and lower particle growth rates by the butanol condensation [5-7].

To alleviate the problem of the collection efficiency measurement affected by a high pressure drop, some instrumental modifications with additional devices for online particle counting have been made. For example, a pressure reducer was built to balance the pressure drop between upstream and downstream, so that the aerodynamic particle size spectrometer was able to work at a pressure drop as high as 0.5 atm [5]. A modification in the sampling line with a foil bag was made to allow the operation of SMPS at a low pressure [8]. A sample extractor with the piston arrangement is applied to reach the pressure equilibration required by APS and SMPS

[9]. A Differential Mobility Particle Sizer (DMPS) system for low-pressure and low-temperature application was developed, which was able to work in the pressure range of 100 – 1000 hPa [10]. A modified CPC 7610 with a pressure equalizing tube was employed to measure particle concentration at pressures as low as 160 hPa [11]. More recently, a commercial low-pressure ejector has been investigated in a pressure range of 20 – 180 mbar and size range of 15 – 80 nm [12, 13]. TSI model 3068 electrometer or Keithley model 6514 electrometer are alternative ways to estimate the downstream particle number by measuring electric currents under low pressure conditions [14, 15], however, the charging status of the particles needs to be well controlled.

Besides the online instrumental counting, elution-based methods such as fluorometric techniques were used to estimate the collection efficiency [16]. Fluorescein labelled aerosol were collected and eluted into a solution, and then the fluorescein intensity was analyzed by a fluorometer. For example, oleic acid particles containing the uranine dye tracer were used to determine the collection efficiency of the Electrical Low-Pressure Impactor [17]. Fluorescence polystyrene microspheres were also employed to estimate the collection efficiency by elution and counting [18, 19], but the elution efficiency could vary from 50 % to 100 % [20], which might result in an inaccurate estimation of the collection efficiency. Highly hydrophilic ammonium fluorescein particles were also used for estimating the collection efficiency and particle loss of a designed particle-into-liquid sampler [21]. The main disadvantage of the fluorometric method is that fluorescence is not specific and fades quickly [22]. The application of the fluorometric method is mainly limited by the fixed sizes of fluorescein insoluble particles, while estimation of collection efficiency in terms of particle number remains uncertain using mass concentrations of soluble fluorescein particles generated from a liquid solution.

Besides fluorometric techniques and modifications of online instrumental counting, it is beneficial to develop an alternative method that estimates the collection efficiency of samplers in a simple and reliable manner in a tunable size range, and is not affected by the pressure drop. Many common aerosol samplers are made out of metal, and polydimethylsiloxane (PDMS) is becoming more widely used in the fabrication of miniaturized aerosol sampling units [23]. In this study, an elution-based method using NaCl particles was developed and examined using metal- and PDMS-based aerosol samplers, and a homemade impactor. Upstream CPC particle number and ICPMS-measured Na concentration of collected particles were analyzed to address the downstream CPC operation issue at high pressure drops and to calculate the collection efficiency. On one hand, with this method, ICP-MS was introduced for estimating the collection efficiency of samplers under high pressure drop to avoid the incompetence or modification of the online instruments such as CPC, SMPS and APS. On the other hand, this study also extended the application of the elution-based methods to investigate the size-resolved particle transport through samplers.

4.2 Materials and Method

4.2.1 Generation of the NaCl aerosol

Particle candidates such as NaCl [24], KCl, dust [25, 26], SiO_2 [27], Polystyrene Latex Beads (PSL) [28], Di-Ethyl-Hexyl-Sebacat (DEHS) and silver nanoparticles [29] are widely used as the challenge particles in evaluating the collection efficiencies of samplers. Herein, NaCl solution was used to generate NaCl particles from a homemade atomizer at 2.8 bar with a flow rate of 3.8 L/min. Two Differential Mobility Analyzers (DMA 3080 and 3082, TSI) were used in parallel (Figure 4.1) to generate a sufficient number of monodisperse NaCl particles smaller than 100 nm (aerosol flow: sheath flow = 1: 10), while one DMA (3082) was used for generating the particles larger than 100 nm. The aerosol flow was kept the same for the two DMAs used for particles smaller than 100 nm. The size selection of the DMA was confirmed using 310 nm polystyrene latex (PSL) particles (Figure C1). An additional neutralizer after the DMA was installed to neutralize the monodisperse particles and to minimize the filtration efficiency induced by electrostatic forces (i.e. particle losses) [29]. In this work, monodisperse particles were defined as the DMA-selected particles with a nominal size. The aerosol inflow to the DMA was 0.6 and 0.3 L/min for classifying particles smaller and larger than 400 nm, respectively (Figure 4.1). The aerosol flow was kept same (0.6 L/min) for the two DMA used for particles smaller than 100 nm. The collection time was adjusted to ensure sufficiently high particle concentration, which was prepared as ppb-level elution sample and measured by ICP-MS. In this study, 30, 50, 80, 100, 200, 300, 400, 500, 600, 700, 800 nm particles were collected for 16 h, 8 h, 2 h, 80 min, 40 min, 20 min, 20 min, 20 min, 20 min, 20 min, 20 min, respectively. A conventional impactor with a nozzle diameter of 0.0710 cm for DMA 3080 [30] and a designed PDMS microchannel [31] were used in this study to develop and validate the estimation method. To reduce the particle bouncing, Tween 20 viscous liquid (Sigma-Aldrich) was used to coat the surface of the impactor [32, 33], which is miscible in water. All tubing was rinsed with Milli-Q water in an ultrasonic bath to avoid any contamination from tubing. Particle numbers of specific sizes counted by the upstream and downstream CPCs were corrected by dummy measurements, i.e., the particle sampler was replaced by a short empty tube and all the other parts of the setup stayed the same. Then the ratio of particle number concentration counted by upstream and downstream CPCs was obtained to correct the CPC-counted upstream particle number concentration. The result showed that the typical ratio of particle numbers was lower than 1 for the particles in the size range of 50 – 300 nm (Figure C2). In detail, the lowest ratio was around 0.8 for about 100 nm particles.

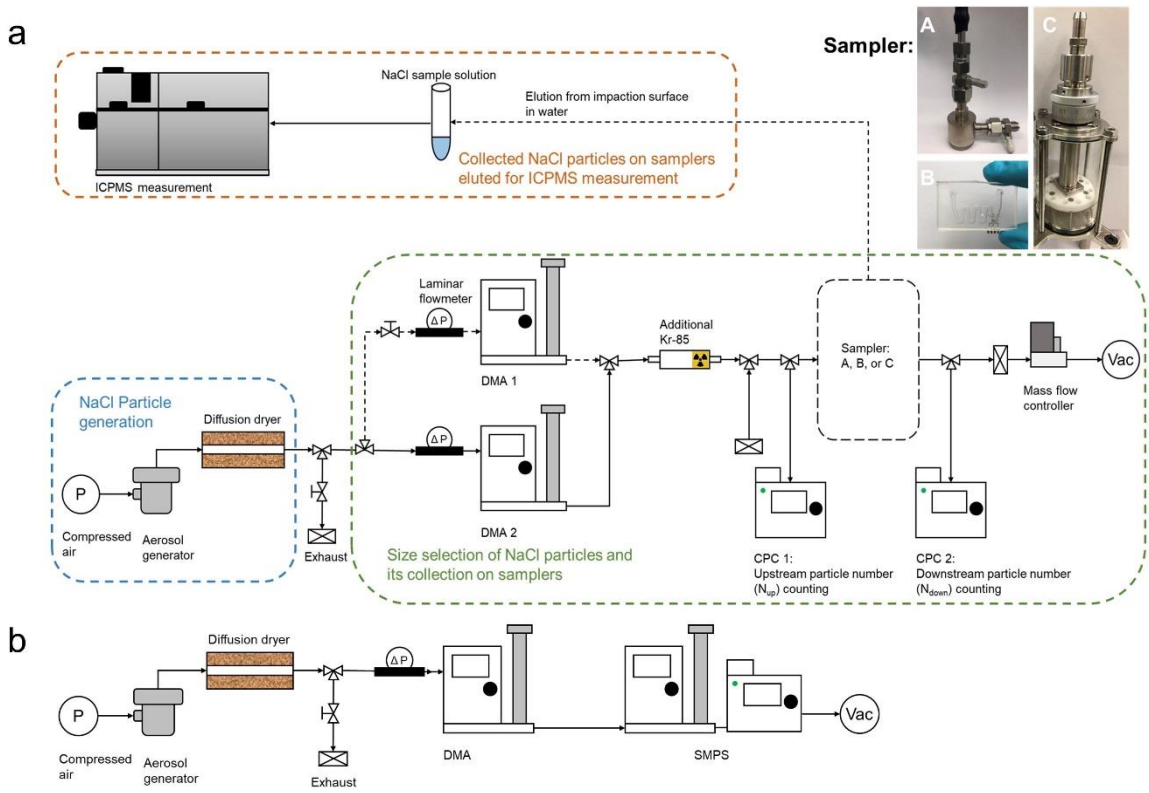

Figure 4.1 Setup schematic of (a) collection efficiency evaluation and (b) size distribution determination using SMPS for monodisperse particles. Dash lines for DMA mean the optional connections. Sampler A, B and C represent the metal-based impactor for DMA, PDMS-based microchannel and homemade impactor, respectively.

According to the relationship between NaCl solution concentrations and generated particle numbers shown in Figure 4.2, 0.05 wt% was used to generate particles smaller than 50 nm, while 1 wt% was used to generate particles larger than 50 nm, to maximize the generated particle number. The results indicated that the water residuals in the aerosol accounted for less than 0.5 % of the total particle volume using 0.05 and 1 wt% NaCl solutions. Therefore, it was reasonable to assume that the fraction of impurities in NaCl particles was negligible. The collected NaCl particles smaller than 100 nm and larger than 100 nm were eluted by MiliQ water as 5 and 10 mL samples in centrifuge tubes, respectively, and 1 % HNO_3 (Supelco, Suprapur) was added prior to ICP-MS measurements. The dissolution of the NaCl particles collected from samplers was affected by particle sizes and mass concentrations. For example, small particles and low mass concentrations could lead to relatively insufficient elution process. The effects of these factors were further discussed in section 4.3.4. The conversion of particle number to the corresponding mass concentration in water is based on the following equation:

$$C_P = \frac{N_P \cdot 0.4 \cdot V_P \cdot \rho_P}{V_{sample}} \quad (2)$$

where N_P is the total NaCl particle number, C_P is the NaCl mass concentration in water (μg/L), V_{sample} is the volume of the liquid sample (mL), 0.4 is the mass fraction of sodium in

NaCl, V_P is the volume of a single NaCl particle (assuming a spherical particle with a nominal mobility diameter), ρ_P is the density of NaCl particle (assuming 2.16 g/cm^3 [34]). It is noted that the results derived from equation (2) are also affected by various factors, such as particle shape and particle diameters used in the equation. For example, the relationship between aerodynamic and geometric diameters is based on the ratio of the square root of slip correction of these two diameters [35], and dynamic shape factor and particle density are involved to convert mobility diameter into aerodynamic diameter [36]. In this work, CPC-counted collection efficiency (η_{CPC}) refers to equation (1). And the calculated collection efficiency (η_{cal}) is based on the following equation:

$$\eta_{cal} = \frac{C_{ICP}}{C_{up}} \tag{3}$$

where C_{ICP} is the Na concentration derived from ICP-MS measurements, and C_{up} is the mass concentration of Na in upstream particles calculated by equation (2).

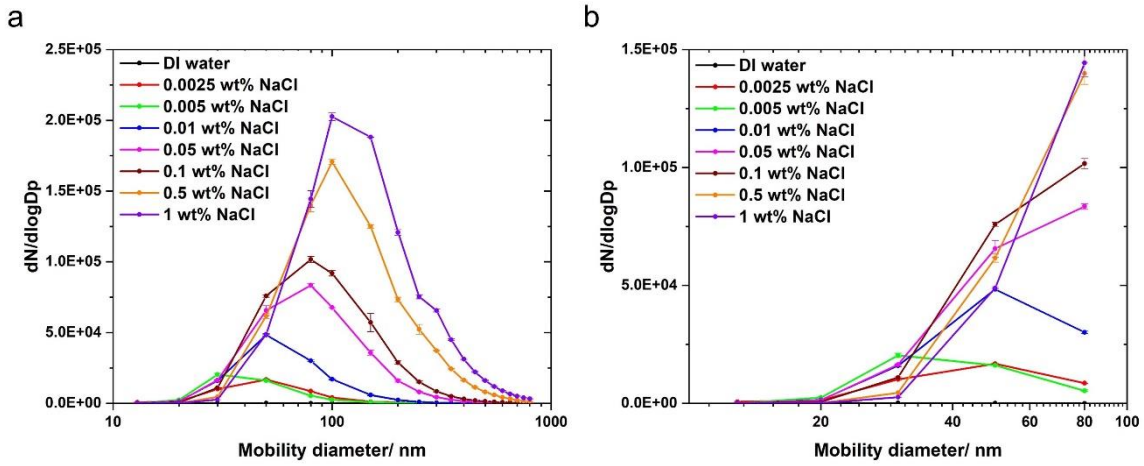

Figure 4.2 Relationship between NaCl solution concentration (0.0025, 0.005, 0.01, 0.05, 0.1, 0.5 and 1 wt %) and generated particle number concentration in the size range of (a) 13 – 800 nm and (b) 13 – 80 nm in terms of electrical mobility diameter at 2.8 bar.

4.2.2 Design and fabrication of the microchannel collector and the homemade impactor

A microchannel with a cross section area (1.6 mm × 1.6 mm) was used to investigate the feasibility of the elution-based method (Figure C3). The detailed description of the microchannel was reported in the previous study [31]. The ratio of the radius of curvature to the microchannel diameter was 2 [20]. The microchannel mold was designed using Auto CAD and printed using a 3D printer. PDMS monomer (Sylgard 184, Dow Corning, Midland, USA) was mixed with curing agent in the volume ratio of 10:1, and then degassed in a vacuum desiccator. The PDMS gels were subsequently cast onto the mold and peeled off after being heated at 70 ºC for four

hours, and these PDMS peelings were bound after plasma treatment. The schematic of the microchannel is shown in Figure C3.

The homemade impactor consisted of stainless steel tubing and cover, Polytetrafluoroethylene (PTFE) mounting plate with an aluminum foil as the impaction plate, and glass wall (Figure C4). It was noted that some parts such as the inner wall were not metal-based materials, which could cause particle loss. The homemade impactor containing 151 nozzles with a diameter of 0.1 mm at 6.4 L/min resulted in a cutoff size of 74 nm in terms of NaCl particles.

4.2.3 Theory

The cutoff diameter of the impactor is defined as the following [30]:

$$D_{50} = \sqrt{\frac{9\pi Stk\mu W^3}{4\rho_P C_c Q}} \tag{4}$$

where D_{50} is the cutoff diameter, Stk is the cut-off Stokes number, which is 0.23, μ is the gas viscosity (g/(cm·s)), W is the nozzle diameter (cm), ρ_P is the particle density (g/cm^3) , Q is the volumetric flow rate (cm^3/s), C_c is the Cunningham Slip Correction according to the following equation [37]:

$$C_c = 1 + \frac{p_0\lambda_0}{pD_P}\left[2.34 + 1.05\exp\left(-0.39\frac{pD_P}{p_0\lambda_0}\right)\right] \tag{5}$$

where p_0 is the pressure at the reference state (pa), λ_0 is mean free path at the reference state (nm), p is the pressure (pa), and D_P is the particle diameter (nm).

4.2.4 Mass size distribution of monodisperse NaCl aerosol

The NanoMOUDI 122NR is a well-designed sampler, which has the stage cut-sizes of 10000, 5600, 3200, 1800, 1000, 560, 320, 180, 100, 56, 32, 18, and 10 nm at a sampling flow rate of 30 L/min [38]. It was used to determine the mass size distribution of monodisperse NaCl particles and examine if the elution-based method is applicable for multiple-stage impactors. In the experiment, particles were collected on aluminum foils at a flow rate of 26.0 – 26.5 L/min. DMA configuration and flow concept were the same as described above to generate monodisperse NaCl particles. Monodisperse particles with the mobility diameter of 50, 100, 300, 500, 600, and 700 nm were generated for 11 h, 3 h, 1 h, 1 h, 1 h, and 1 h, respectively. Particle samples were eluted using Mili-Q water from aluminum foils on impaction stages.

4.3 Results and Discussion

4.3.1 Collection efficiency of the impactor and the microchannel collector

The theoretical cutoff diameters were 315 and 375 nm at 2 and 1.5 L/min of the impactor calculated by equation (4), respectively (Figure 4.3a). Considering the shape factor of 1.08 [39-41], the corrected electrical mobility diameters were 327 and 390 nm for the theoretical cutoff diameter, respectively. However, the experimental cutoff diameters at 2 and 1.5 L/min were larger than 600 nm (Figure 4.3a), which indicated the significant solid particle bouncing on metal surface [42]. The collection efficiency for 1000 nm NaCl at 1.5 L/min and 2 L/min was 50.9 ± 5.7 % and 33.5 ± 15.2 %, respectively. The collection efficiency was lower with a higher velocity due to the increasing fraction of bounce [43]. Previous studies showed that particle bouncing was likely to occur on designed impactors when the particle was larger than 200 nm [44, 45]. In contrast, the collection efficiency of Tween 20 coated impactor at 2 L/min was improved and the experimental cutoff diameter was about 400 nm (Figure 4.3b). It demonstrated that Tween 20 was capable of reducing the particle bouncing and facilitating the estimation of actual collection efficiency with the elution-based method (Figure 4.3b). The calculated collection efficiency based on the elution-based method indicated the underestimation of the performance of particle collection (Figure 4.3a). In comparison with the impactor without the Tween 20 coating layer, the calculated collection efficiency with the Tween 20 coating layer agreed better with the CPC-counted collection efficiency (Figure 4.3b).

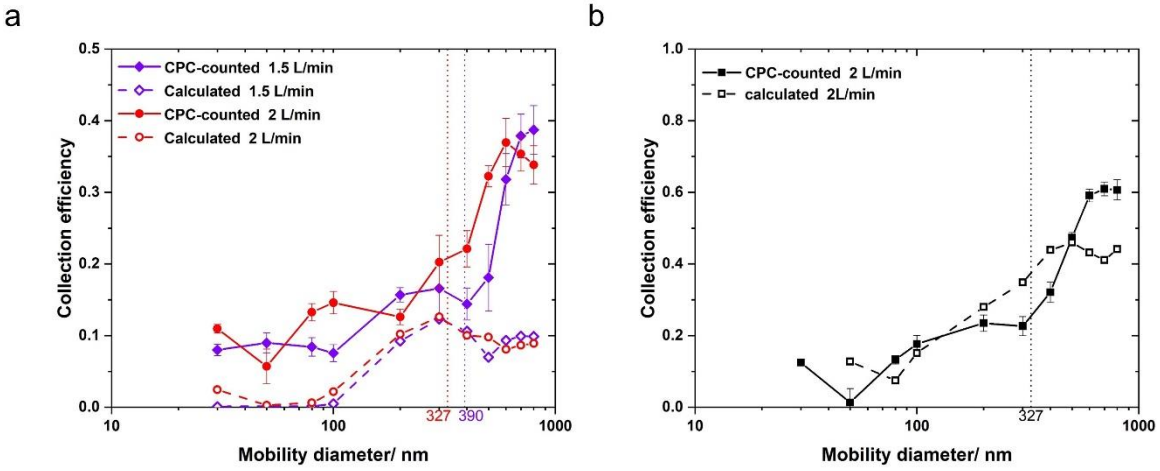

Figure 4.3 Experimental and calculated collection efficiency of NaCl particles in the impactor for DMA (a) without and (b) with Tween 20 coating at 1.5 and 2 L/min. Vertical dash lines indicate the cutoff diameter at the applied flow rates.

The microchannel was a W-shape particle collector, and employed to collect particles under inertial force. The cutoff diameters of the microchannel at 1 and 1.5 L/min were about 800 and 500 nm, respectively (Figure 4.4). Similarly, without Tween 20 coating layer, the calculated collection efficiency of the microchannel diverged from the CPC-counted collection efficiency, especially in the size range of 500 – 800 nm. As shown in Figure C5, particle loss and particle

bouncing due to lower particle number and larger particles size were the main factors to affect the collection efficiency in the size range of 500 – 800 nm.

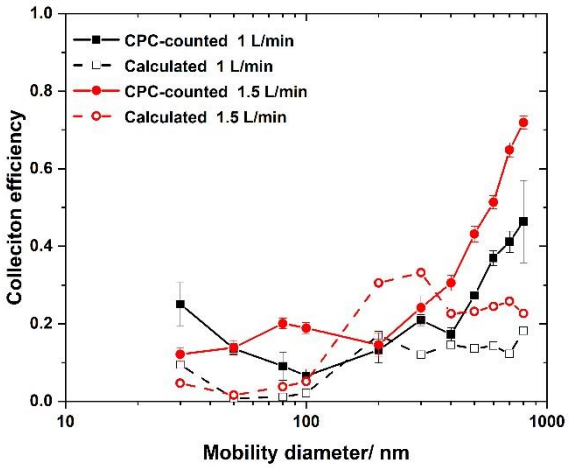

Figure 4.4 Experimental and calculated collection efficiency of NaCl particles in the micro-channel at 1 and 1.5 L/min.

4.3.2 Comparison of CPC-counted and calculated collection efficiencies and downstream particle concentrations

Figure 4.5 showed the ratio of collected and downstream particle concentration. Here, the ratio of the collected concentration was defined $(C_{up} - C_{down})/ C_{ICP}$, and the ratio of the downstream particle concentration was $(C_{up} - C_{ICP})/ C_{down}$. The ratio of the collected particle concentration without Tween 20 coating indicated possible particle mass loss in the size range of 30 – 100 and 500 – 800 nm (Figure 4.5a), because the collected particle mass concentration obtained by ICP-MS measurements was lower. Compared to the ratio on the PDMS-based microchannel, the ratio of the collected particle concentration on the metal-based impactor was higher by 3.27 times in the size range of 50 – 100 nm, and it was 22.2 times higher in terms of 30 nm particles (Figure 4.5a). It demonstrated that smaller particles diffused with a high diffusivity [46] and stuck to interior wall or impaction surface of the impactor during particle transport, which caused particle loss and changes of size distribution of monodisperse particles. In particular, the lower ratios of the collected particle concentration for the microchannel than those for the impactor suggested the particle loss on the interior wall especially for the particles smaller than 100 nm (Figure C5a). Therefore, the actual collection efficiency of small particles in the size range of 30 – 100 nm was likely to be lower than the CPC-counted collection efficiency shown in Figure 4.5a and 4.5b. A previous study also elaborated that spontaneous particle loss occurs during the particle collection [19].

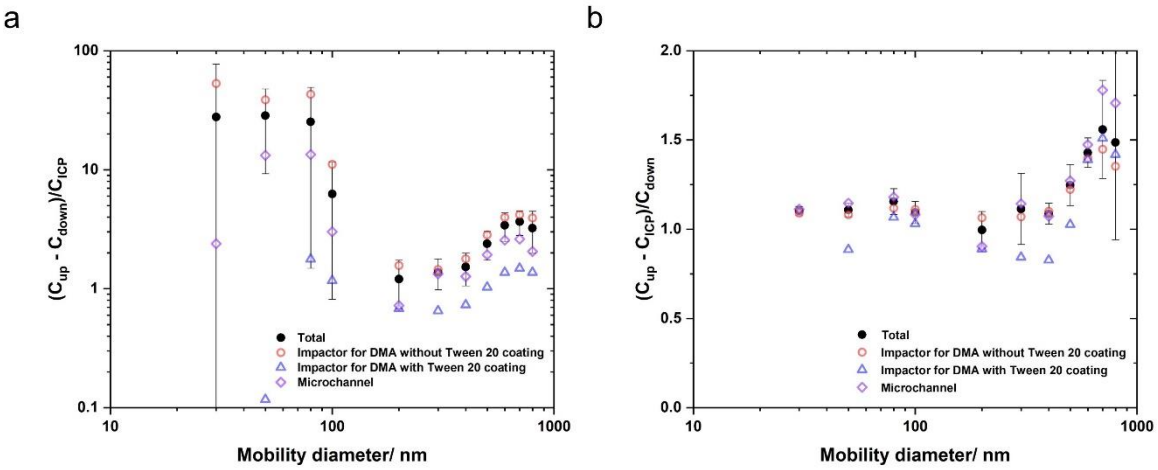

Figure 4.5 (a) Ratio of size-resolved CPC-counted to the calculated collected particle concentration, and (b) ratio of calculated to CPC-counted downstream particle concentration. Total is the average of the microchannel and the impactor without Tween 20 coating.

Besides that, elution efficiency played an important role for the ratio being over 1, which was discussed in more details in section 4.3.4. The actual geometric diameter is larger than the nominal geometric diameter we used in the conversion equation according to the size distribution determined by SMPS (Figure 4.6a and b), which could lead to a ratio of lower than 1. Nonetheless, the downstream particle concentration ratio in the size range of 30 – 500 nm was close to 1. More specifically, the downstream particle concentration ratio without Tween 20 coating was 0.94 ± 0.10 with the particle smaller than 500 nm. It implied that particle loss and changes of size distribution of monodisperse particles had a minor effect on the estimation of collection efficiency using the elution-based method, provided the theoretical collection efficiency was lower than 50 %. The theoretical collection efficiency of 50 % was determined based on the equation of cutoff size.

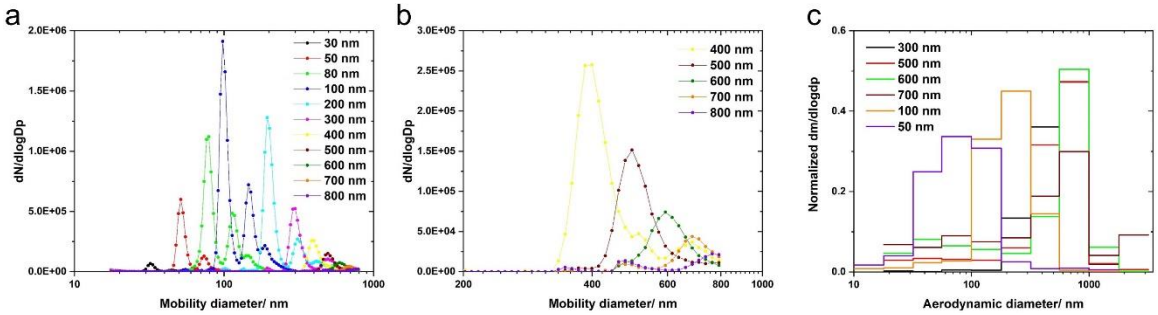

Figure 4.6 Size distribution of the monodisperse (a) 30 – 800 nm and (b) 400 – 800 nm NaCl particles, (c) mass size distribution of monodisperse NaCl in terms of aerodynamic diameter.

The discrepancy between CPC-counted concentration and calculated concentration was becoming evident with particles larger than 500 nm (Figure 4.5a and b). It was likely due to the change

of size distributions of upstream and downstream monodisperse large particle, which affected the actual average geometric diameter. According to the size distribution of monodisperse particles shown in Figure 4.6a and b, the defined particle diameter was not the only size in monodisperse particles. In detail, the lower limit of the particle diameter of the monodisperse NaCl particles (when the particle concentration approached 0) was 82.9 ± 7.2 % and 30.2 ± 1.4 % of the defined monodisperse diameter in the range of 30 – 300 nm and 500 – 800 nm respectively, indicating a broader size range of monodisperse particles of 500 – 800 nm. It was more convenient to change the average geometric diameter by altering the size distribution of downstream monodisperse particles in the size range of 500 – 800 nm through particle bouncing. The mass distribution determined by Nano MOUDI also confirmed the wide range of monodisperse NaCl particles selected by DMA (Figure 4.6c). For example, 50 nm and 500 nm monodisperse NaCl particles distribute in the aerodynamic diameter range of 32 – 180 nm and 320 – 1000 nm, respectively. It also indicated that the elution-based method was applicable for single-stage samplers rather than multiple-stage samplers, since it would be unpredictable to convert mass concentration into particle number, considering possible size redistribution of monodisperse NaCl particles.

Despite the variation of concentration ratios as a function of particle size, the limited difference between the average downstream concentration ratio on the impactor and microchannel implied that different materials had a limited effect on the estimation of downstream concentration (Figure 4.5b). However, the elution efficiency from the PDMS surface was not consistent in the size range of 700 – 800 nm (Figure C5b). According to the size distribution of monodisperse NaCl aerosol upstream and downstream impactor and microchannel (Figure 4.7), particle bouncing on the impactor was clearly observed with the particle size larger than 500 nm as the fraction of large particles was larger compared to the upstream size distribution. It implies that other elution methods such as fluorometric method with highly hydrophilic fluorescein particles, are also not applicable for aerosol samplers with particle bouncing in large particle size ranges. It was also confirmed by a previous study that the collection efficiency of Berner impactor was much lower especially with the particle size larger than cutoff size, evaluated by using ammonium fluorescein particles due to the particle bounce from the substrate [47]. In contrast, no significant change of size distribution in the downstream microchannel was observed.

It was noted that larger and multiple-charged particles were not included in the equation about the conversion of CPC-counted particle number into particle mass, as a nominal mobility diameter was used in the equation. The minor peaks of larger and multiple-charged particles shown in Figure 4.7 would increase the mean mobility diameter, which increases the CPC-calculated mass concentrations and decreases the ICP-based collection efficiencies.

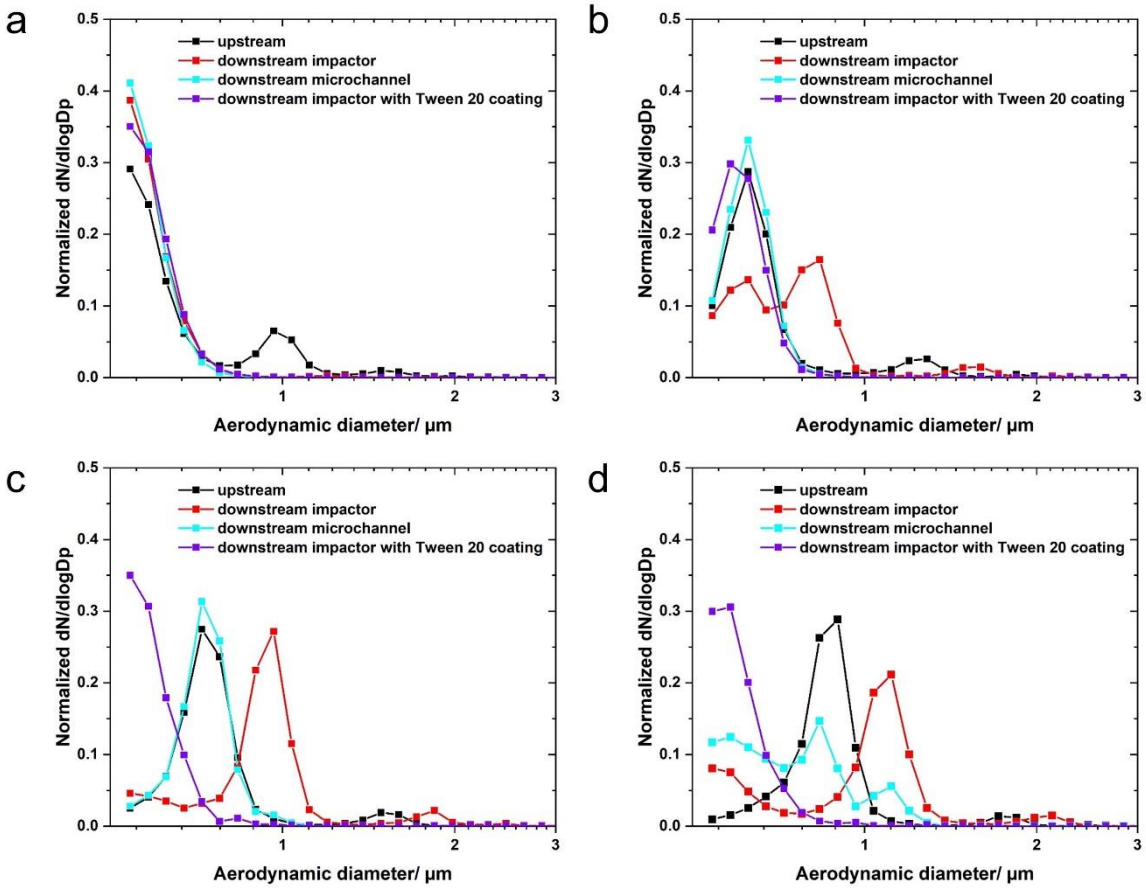

Figure 4.7 Size distribution of upstream and downstream impactor for DMA and microchannel in terms of aerodynamic diameter at 1.5 L/min with monodisperse (a) 500, (b) 600, (c) 700, and (d) 800 nm NaCl selected by DMA.

Air flow leaves an oil-free area on the impaction plate facing the orifice, and the pores of the metal plate act as oil reservoirs [44]. The Tween 20 coating layer could stabilize the ratio of collected particle concentration and downstream concentration to 0.97 ± 0.34 and 1.00 ± 0.22 in the size range of 80 – 800 nm. Moreover, it prevented the particle bouncing and might also change the geometric structure of the impaction plate to form a curved rather than flat metal surface used and therefore can collect more particles, which is similar to an additional punched impaction plate used to increase the collection efficiency [48]. Nonetheless, the ratio of concentration of collected particles on impaction plate and downstream concentration was lower than 1 in the size range of 30 – 50 nm and 200 – 400 nm, as a result of higher ICP-MS result (C_{ICP}). The main reason was that Na concentration in the pure Tween 20 solution measured by ICP-MS was 366 ± 11 ppm, which was high enough to increase the Na concentration in the elution samples. The volume of Tween 20 used for a coating layer was on a microliter level (e.g. 5 µL), so a slight variation of the added volume could lead to a different concentration of Na, making it difficult to subtract concentrations of Na in the Tween 20 from ICP-MS validated concentrations. Tween 20 coating layer also led to a slight reaerosolization and higher downstream particle counting by generating 28.8 ± 4.3 particles per cm^3 (Figure C6). Therefore,

coating solutions such as Tween 20 containing Na were not recommended to be applied for the elution-based method.

4.3.3 Size redistribution of the downstream monodisperse aerosol

In average, the ratios of the CPC-counted collected particle number to the calculated particle number derived from ICPMS verified concentration were above 10 and 2 in the size range of 30 – 100 and 500 – 800 nm, respectively (Figure 4.5a). Particle diffusion of small particles and particle bouncing of large particles led to the size redistribution, which increased the actual average geometric diameter of monodisperse NaCl aerosols by depositing smaller particles on the impaction plate. APS-measured aerodynamic diameters of upstream and downstream impactor indicated an increasing geometric diameter of monodisperse 600, 700 and 800 nm particles by 12.8 % at 1.5 L/min (Table S1). It was noted that the sizing accuracy of APS was affected by unit-to-unit variability (up to 10 % deviation) and the number of resolved bins [49], which could cause the difference between the measured aerodynamic diameter and that derived from the mobility diameter theoretically. APS results suggested that smaller particles in the monodisperse aerosol were captured by sampler, whereas larger particles left away likely due to particle bouncing, which confirmed the size redistribution of downstream aerosol in the range of 600 – 800 nm (Figure 4.7). Here, the size redistribution was defined as the change in the normalized particle number as a function of particle sizes. In contrast, the ratio was close to 1 in the size range of 100 – 500 nm (Figure 4.8a), which indicated a relatively consistent upstream and downstream size distribution when the theoretical collection efficiency was lower than 50 %. Good correlation between calculated and CPC-counted collection efficiency in the size range of 100 – 500 nm indicated the applicable range of the elution-based method (Figure 4.8b). The non-zero intercept implied a minor effect of particle loss on the inner wall of samplers or sample loss during elution process, resulting in a higher CPC-counted collection efficiency compared to calculated collection efficiency.

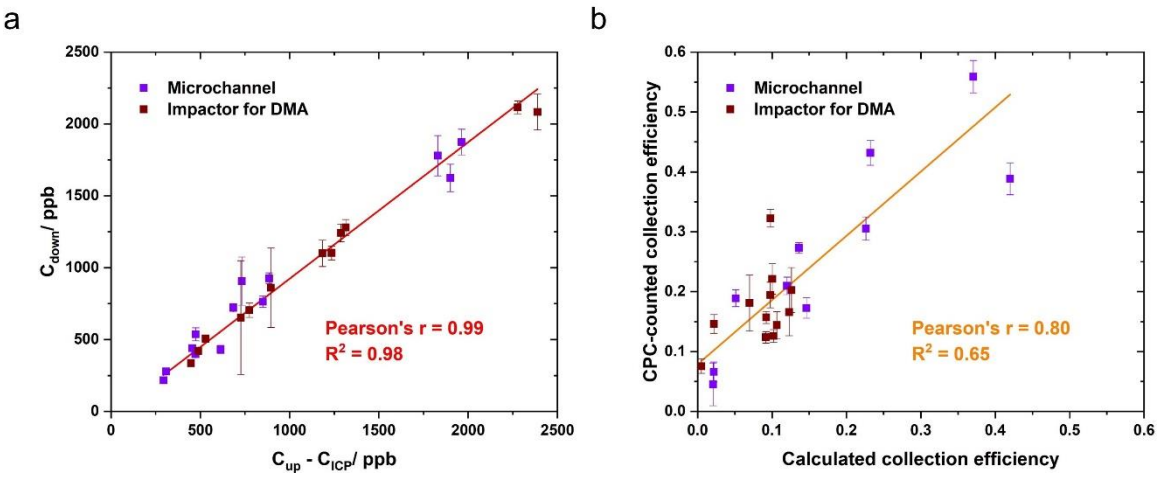

Figure 4.8 Global relationship between the calculated and CPC-counted (a) downstream particle concentration, and (b) collection efficiency of the impactor and the microchannel in the size range of 100 – 500 nm.

4.3.4 The effect of cutoff size and elution efficiency on the elution-based method

As the result showed, the applicable size range possibly depended on the cutoff size of the single-stage sampler. More specifically, the cutoff size of the impactor and the microchannel were about 400 and 800 nm, respectively (Figure 4.3 and 4.4), while the applicable size range was smaller than 500 nm. Therefore, a homemade impactor with a cutoff size of 74 nm was employed to investigate the effect of cutoff size on the method. Figure 4.9 suggested that the collection efficiency of 100 nm NaCl particles was successfully estimated according to CPC-counted collection efficiencies, whereas collection efficiencies of other particle sizes were underestimated compared to CPC-counted collection efficiencies. It was observed that the ratio of CPC-counted collected particle concentration to ICP-MS concentration was 2 – 20 in the size range smaller than 100 nm (Figure 4.10a), which indicated size redistribution remains similar with low or high collection efficiency. In contrast, the ratio of collected particle concentration was constant and close to 1 with 100 nm particles, which was close to the theoretical cutoff size of 74 nm. Similarly, the ratio of calculated to CPC-counted downstream particle concentration was close to 1 with 100 nm NaCl particles (Figure 4.10b). The ratio of collected particle concentration and downstream particle concentration varied greatly in the size range of 600 – 800 nm (Figure C7). It indicated that the elution method was associated with the cutoff size of samplers, which was found to be the upper limit of the size range of 100 – 500 nm.

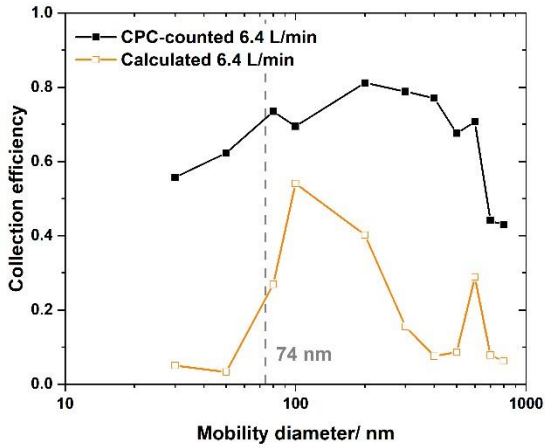

Figure 4.9 Experimental and calculated collection efficiency of NaCl particles in the homemade impactor at 6.4 L/min.

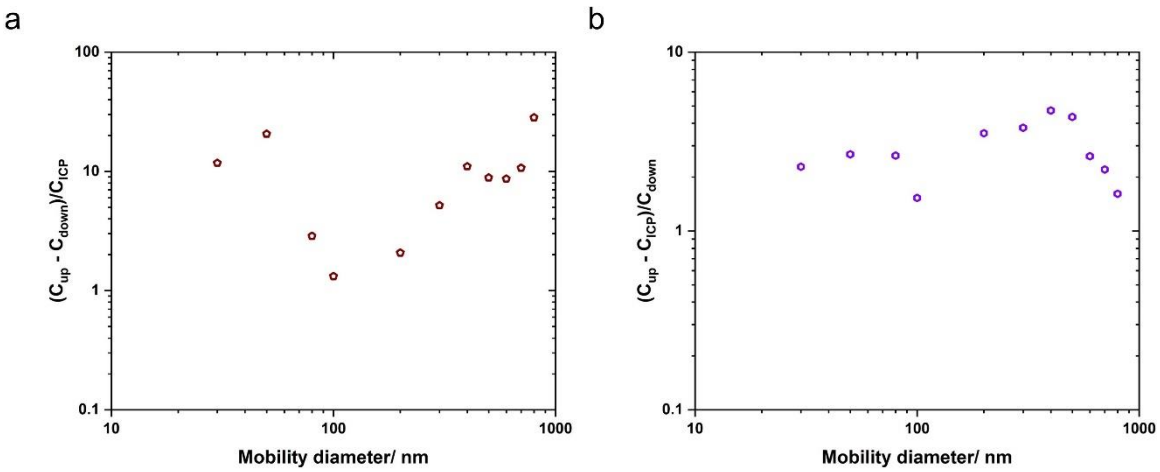

Figure 4.10 (a) Average ratio of size-resolved CPC-counted to the calculated collected particle concentration, and (b) average ratio of calculated to CPC-counted downstream particle concentration using the homemade impactor at 6.4 L/min.

To understand the role of elution efficiency in the elution-based method, the ratio of the collected particle concentration for the impactor, microchannel and homemade impactor were compared (Figure 4.5a and 4.10a). The elution efficiency was mainly affected by the surface of the impaction plate, so we assumed a fixed elution efficiency as a function of particle size regardless of collection efficiencies. A similar ratio (~ 10) for the particle smaller 100 nm was observed, indicating a more significant role of elution efficiency over the size redistribution of downstream monodisperse particles, whereas the ratio was increasing from 2 to 10 with increasing collection efficiencies for the particles larger than 100 nm, which implied the size redistribution of downstream monodisperse particles dominated the changes of the ratio.

4.4 Conclusions

In this study, an elution-based method was proposed to estimate particle collection efficiency of samples regardless of pressure drops. Based on the correlation between CPC-counted and calculated collection efficiencies, CPC was used to measure the upstream particle number, and eluted samples from samplers were employed to estimate the collected particle concentration in the size range of 100 nm – D_{50} (D_{50} < 500 nm) or 100 – 500 nm (D_{50} > 500 nm). Nonetheless, the elution-based method might be applicable in a wider size range if a more monodisperse NaCl particles could be generated in future studies, especially for particles larger than 500 nm.

Size redistribution of monodisperse NaCl particles due to the diffusion of particles smaller than 100 nm and bouncing of particles larger than D_{50} or 500 nm were found to affect the estimation of collection efficiency. Specifically, elution efficiency played a more important role than size redistribution in the range of 30 – 100 nm and affected the estimated collection efficiencies,

while size redistribution was more significant with a higher collection efficiency in the size range of 500 – 800 nm. In addition, size redistribution occurred with a collection efficiency of higher than 50 % in the size range of 100 – 500 nm. Thus, this method was also capable of investigating the transport and size redistribution of monodisperse particles through aerosol samplers. A more accurate conversion from particle number into mass concentration as a function of particle size can also be investigated to avoid the effects of the conversion and facilitate the particle transport studies using the elution-based method.

Conflicts of interest

There are no conflicts of interest to declare.

Acknowledgement

Y.-B. Zhao thanks the financial support from China Scholarship Council (CSC). T. Cen and C. Ludwig acknowledge the Swiss National Science Foundation for financial support (project 184817). We thank Daniel Rechenmacher for the drawing and manufacture of the homemade impactor.

4.4 References

[1] C.W. Haig, W.G. Mackay, J.T. Walker, C. Williams, Bioaerosol sampling: sampling mechanisms, bioefficiency and field studies, *Journal of Hospital Infection*, **2016**, 93, 242-55, https://doi.org/10.1016/j.jhin.2016.03.017.

[2] J. Wang, P. Tronville, Toward standardized test methods to determine the effectiveness of filtration media against airborne nanoparticles, *Journal of Nanoparticle Research*, **2014**, 16, 2417, 10.1007/s11051-014-2417-z.

[3] J. Kangasluoma, A. Franchin, J. Duplissy, L. Ahonen, F. Korhonen, M. Attoui, et al., Operation of the Airmodus A11 nano Condensation Nucleus Counter at various inlet pressures and various operation temperatures, and design of a new inlet system, *Atmos Meas Tech*, **2016**, 9, 2977-88, 10.5194/amt-9-2977-2016.

[4] TSI corporation, Model 3775 Condensation Particle Counter Operation and Service Manual 2007.

[5] S.A. Grinshpun, K. Willeke, V. Ulevicius, A. Juozaitis, S. Terzieva, J. Donnelly, et al., Effect of Impaction, Bounce and Reaerosolization on the Collection Efficiency of Impingers, *Aerosol Science and Technology*, **1997**, 26, 326-42, 10.1080/02786829708965434.

[6] Z. Zhang, B.Y.H. Liu, Performance of TSI 3760 Condensation Nuclei Counter at Reduced Pressures and Flow Rates, *Aerosol Science and Technology*, **1991**, 15, 228-38, 10.1080/02786829108959530.

[7] M. He, S. Dhaniyala, M. Wagner, Characterization of filter performance under low-pressure operation, *Aerosol Science and Technology*, **2016**, 50, 417-28, 10.1080/02786826.2016.1162902.

[8] F. Ober, M. Mayer, H. Büttner, F. Ebert, Aerosol Measurement in Low-Pressure Systems with Standard Scanning Mobility Particle Sizers, *Particle & Particle Systems Characterization*, **2002**, 19, 229-39, https://doi.org/10.1002/1521-4117(200208)19:4<229::AID-PPSC229>3.0.CO;2-8.

[9] J.A. Hubbard, J.E. Brockmann, J. Dellinger, D.A. Lucero, A.L. Sanchez, B.L. Servantes, Fibrous Filter Efficiency and Pressure Drop in the Viscous-Inertial Transition Flow Regime, *Aerosol Science and Technology*, **2012**, 46, 138-47, 10.1080/02786826.2011.616555.

[10] M. Seifert, R. Tiede, M. Schnaiter, C. Linke, O. Möhler, U. Schurath, et al., Operation and performance of a differential mobility particle sizer and a TSI 3010 condensation particle counter at stratospheric temperatures and pressures, *Journal of Aerosol Science*, **2004**, 35, 981-93, https://doi.org/10.1016/j.jaerosci.2004.03.002.

[11] M. Hermann, A. Wiedensohler, Counting efficiency of condensation particle counters at low-pressures with illustrative data from the upper troposphere, *Journal of Aerosol Science*, **2001**, 32, 975-91, https://doi.org/10.1016/S0021-8502(01)00037-4.

[12] T. Rosenberger, A. Münzer, D. Kiesler, H. Wiggers, F.E. Kruis, Ejector-based sampling from low-pressure aerosol reactors, *Journal of Aerosol Science*, **2018**, 123, 105-15, https://doi.org/10.1016/j.jaerosci.2018.06.003.

[13] T. Rosenberger, J. Neises, D. Kiesler, F.E. Kruis, Ejector-based nanoparticle sampling from pressures down to 20 mbar, *Journal of Aerosol Science*, **2020**, 144, 105531, https://doi.org/10.1016/j.jaerosci.2020.105531.

[14] C.-J. Tsai, D.-R. Chen, H. Chein, S.-C. Chen, J.-L. Roth, Y.-D. Hsu, et al., Theoretical and experimental study of an axial flow cyclone for fine particle removal in vacuum conditions, *Journal of Aerosol Science*, **2004**, 35, 1105-18, https://doi.org/10.1016/j.jaerosci.2004.03.007.

[15] S.-C. Chen, C.-J. Tsai, An axial flow cyclone to remove nanoparticles at low pressure conditions, *Journal of Nanoparticle Research*, **2007**, 9, 71-83, 10.1007/s11051-006-9152-z.

[16] J. Kesavan, R.W. Doherty, Use of Fluorescein in Aerosol Studies, Edgewood chemical biological center aberdeen proving ground md2000.

[17] M. Marjamäki, J. Keskinen, D.-R. Chen, D.Y.H. Pui, Performance evaluation of the electrical low-pressure impactor (ELPI), *Journal of Aerosol Science*, **2000**, 31, 249-61, https://doi.org/10.1016/S0021-8502(99)00052-X.

[18] D. Wang, M.M. Shafer, J.J. Schauer, C. Sioutas, A new technique for online measurement of total and water-soluble copper (Cu) in coarse particulate matter (PM), *Environ Pollut*, **2015**, 199, 227-34, https://doi.org/10.1016/j.envpol.2015.02.006.

[19] K.S. Lim, K.W. Lee, Collection efficiency and particle loss of virtual impactors with different methods of increasing pressure drop, *Journal of Aerosol Science*, **2006**, 37, 1188-97, https://doi.org/10.1016/j.jaerosci.2005.11.011.

[20] I.V. Novosselov, R.A. Gorder, J.A. Van Amberg, P.C. Ariessohn, Design and Performance of a Low-Cost Micro-Channel Aerosol Collector, *Aerosol Science and Technology*, **2014**, 48, 822-30, 10.1080/02786826.2014.932895.

[21] D. Wang, J. Jiang, J. Deng, Y. Li, J. Hao, A Sampler for Collecting Fine Particles into Liquid Suspensions, *Aerosol Air Qual Res*, **2020**, 10.4209/aaqr.2019.12.0616.

[22] J.P. Lodge Jr, Methods of air sampling and analysis: CRC Press; 1988.

[23] A.R. Metcalf, S. Narayan, C.S. Dutcher, A review of microfluidic concepts and applications for atmospheric aerosol science, *Aerosol Science and Technology*, **2018**, 52, 310-29, 10.1080/02786826.2017.1408952.

[24] D.A. Japuntich, L.M. Franklin, D.Y. Pui, T.H. Kuehn, S.C. Kim, A.S. Viner, A comparison of two nano-sized particle air filtration tests in the diameter range of 10 to 400 nanometers, *Journal of Nanoparticle Research*, **2007**, 9, 93-107, 10.1007/s11051-006-9179-1.

[25] J.E. Yit, B.T. Chew, Y.H. Yau, A review of air filter test standards for particulate matter of general ventilation, *Building Services Engineering Research and Technology*, **2020**, 41, 758-71, 10.1177/0143624420915626.

[26] J.-H. Lim, S.-H. Oh, S. Kang, K.-J. Lee, S.-J. Yook, Development of cutoff size adjustable omnidirectional inlet cyclone separator, *Separation and Purification Technology*, **2021**, 276, 119397, https://doi.org/10.1016/j.seppur.2021.119397.

[27] G.-Y. Lin, L.-T. Cuc, W. Lu, C.-J. Tsai, H.-M. Chein, F.-T. Chang, High-efficiency wet electrocyclone for removing fine and nanosized particles, *Separation and Purification Technology*, **2013**, 114, 99-107, https://doi.org/10.1016/j.seppur.2013.04.039.

[28] J.-H. Lim, D. Park, S.-J. Yook, Development of a multi-slit virtual impactor as a high-volume bio-aerosol sampler, *Separation and Purification Technology*, **2020**, 250, 117275, https://doi.org/10.1016/j.seppur.2020.117275.

[29] P. Sachinidou, Y.K. Bahk, M. Tang, N. Zhang, S.S.C. Chen, D.Y.H. Pui, et al., Inter-Laboratory Validation of the Method to Determine the Filtration Efficiency for Airborne Particles in the 3–500 nm Range and Results Sensitivity Analysis, *Aerosol and Air Quality Research*, **2017**, 17, 2669-80, 10.4209/aaqr.2017.03.0104.

[30] TSI corporation, Series 3080 Electrostatic Classifiers Operation and Service Manual, 2009.

[31] Y.-B. Zhao, J. Tang, T. Cen, G. Qiu, W. He, F. Jiang, et al., Integrated aerodynamic/electrochemical microsystem for collection and detection of nanogram-level airborne bioaccessible metals, *Sensor Actuator B: Chem*, **2022**, 351, 130903, https://doi.org/10.1016/j.snb.2021.130903.

[32] H.N. Phan, A.R. McFarland, Aerosol-to-Hydrosol Transfer Stages for Use in Bioaerosol Sampling, *Aerosol Science and Technology*, **2004**, 38, 300-10, 10.1080/02786820490426183.

[33] S. Rodrigues, A.M.R. da Costa, N. Flórez-Fernández, M.D. Torres, M.L. Faleiro, F. Buttini, et al., Inhalable Spray-Dried Chondroitin Sulphate Microparticles: Effect of Different Solvents on Particle Properties and Drug Activity, *Polymers*, **2020**, 12, 10.3390/polym12020425.

[34] L. Morawska, G. Johnson, Z.D. Ristovski, V. Agranovski, Relation between particle mass and number for submicrometer airborne particles, *Atmospheric Environment*, **1999**, 33, 1983-90, https://doi.org/10.1016/S1352-2310(98)00433-6.

[35] O.R. Moss, Shape Factors for Airborne Particles, *American Industrial Hygiene Association Journal*, **1971**, 32, 221-9, 10.1080/0002889718506442.

[36] W. Stöber, A note on the aerodynamic diameter and the mobility of non-spherical aerosol particles, *Journal of Aerosol Science*, **1971**, 2, 453-6, https://doi.org/10.1016/0021-8502(71)90048-6.

[37] W.C. Hinds, Aerosol technology: properties, behavior, and measurement of airborne particles: John Wiley & Sons; 1999.

[38] Y. Yue, H. Chen, A. Setyan, M. Elser, M. Dietrich, J. Li, et al., Size-Resolved Endotoxin and Oxidative Potential of Ambient Particles in Beijing and Zürich, *Environ Sci Technol*, **2018**, 52, 6816-24, 10.1021/acs.est.8b01167.

[39] P.F. DeCarlo, J.G. Slowik, D.R. Worsnop, P. Davidovits, J.L. Jimenez, Particle Morphology and Density Characterization by Combined Mobility and Aerodynamic Diameter Measurements. Part 1: Theory, *Aerosol Science and Technology*, **2004**, 38, 1185-205, 10.1080/027868290903907.

[40] A. Khlystov, C. Stanier, S.N. Pandis, An Algorithm for Combining Electrical Mobility and Aerodynamic Size Distributions Data when Measuring Ambient Aerosol Special Issue of

Aerosol Science and Technology on Findings from the Fine Particulate Matter Supersites Program, *Aerosol Science and Technology*, **2004**, 38, 229-38, 10.1080/02786820390229543.

[41] Z. Wang, S.M. King, E. Freney, T. Rosenoern, M.L. Smith, Q. Chen, et al., The Dynamic Shape Factor of Sodium Chloride Nanoparticles as Regulated by Drying Rate, *Aerosol Science and Technology*, **2010**, 44, 939-53, 10.1080/02786826.2010.503204.

[42] J. Dirgo, D. Leith, Cyclone Collection Efficiency: Comparison of Experimental Results with Theoretical Predictions, *Aerosol Science and Technology*, **1985**, 4, 401-15, 10.1080/02786828508959066.

[43] H.-C. Wang, W. John, Comparative Bounce Properties of Particle Materials, *Aerosol Science and Technology*, **1987**, 7, 285-99, 10.1080/02786828708959165.

[44] C.-J. Tsai, C.-N. Liu, S.-M. Hung, S.-C. Chen, S.-N. Uang, Y.-S. Cheng, et al., Novel Active Personal Nanoparticle Sampler for the Exposure Assessment of Nanoparticles in Workplaces, *Environ Sci Technol*, **2012**, 46, 4546-52, 10.1021/es204580f.

[45] C. Misra, S. Kim, S. Shen, C. Sioutas, A high flow rate, very low pressure drop impactor for inertial separation of ultrafine from accumulation mode particles, *J Aerosol Sci*, **2002**, 33, 735-52, https://doi.org/10.1016/S0021-8502(01)00210-5.

[46] M. Fierz, L. Scherrer, H. Burtscher, Real-time measurement of aerosol size distributions with an electrical diffusion battery, *Journal of Aerosol Science*, **2002**, 33, 1049-60, https://doi.org/10.1016/S0021-8502(02)00057-5.

[47] R.E. Hillamo, E.I. Kauppinen, On the Performance of the Berner Low Pressure Impactor, *Aerosol Science and Technology*, **1991**, 14, 33-47, 10.1080/02786829108959469.

[48] T.-W. Cheon, J.-Y. Lee, J.-Y. Bae, S.-J. Yook, Enhancement of Collection Efficiency of an Inertial Impactor Using an Additional Punched Impaction Plate, *Aerosol and Air Quality Research*, **2017**, 17, 2349-57, 10.4209/aaqr.2017.01.0018.

[49] S. Pfeifer, T. Müller, K. Weinhold, N. Zikova, S. Martins dos Santos, A. Marinoni, et al., Intercomparison of 15 aerodynamic particle size spectrometers (APS 3321): uncertainties in particle sizing and number size distribution, *Atmos Meas Tech*, **2016**, 9, 1545-51, 10.5194/amt-9-1545-2016.

Appendix C

Graphical Abstract

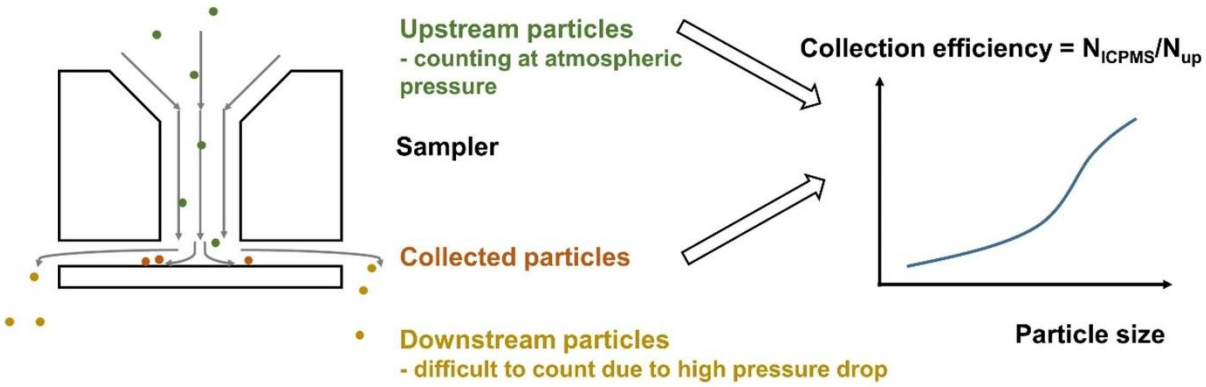

Table C1 Mean aerodynamic diameter of upstream and downstream impactor for DMA determined by APS at 1.5 L/min.

Mobility diameter/ nm	Upstream/ µm	Downstream impactor/ µm	Down/up Ratio
600	0.675	0.737	1.09
700	0.760	0.905	1.19
800	0.862	0.950	1.10

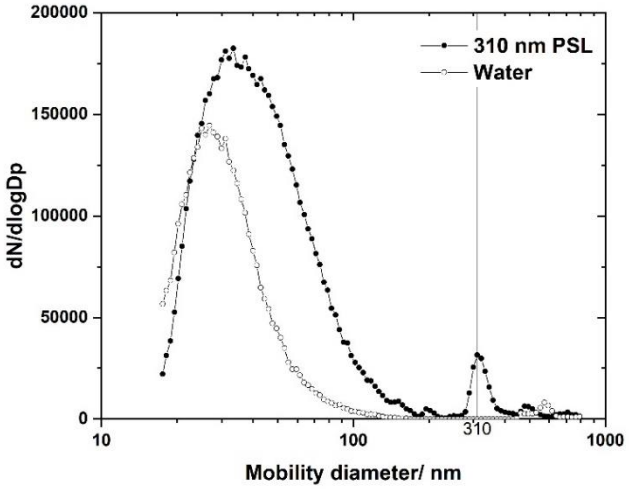

Figure C1 SMPS scanning of 310 nm PSL particles at an inlet flow of 0.3 L/min using 5 µL PSL solution in 100 mL water.

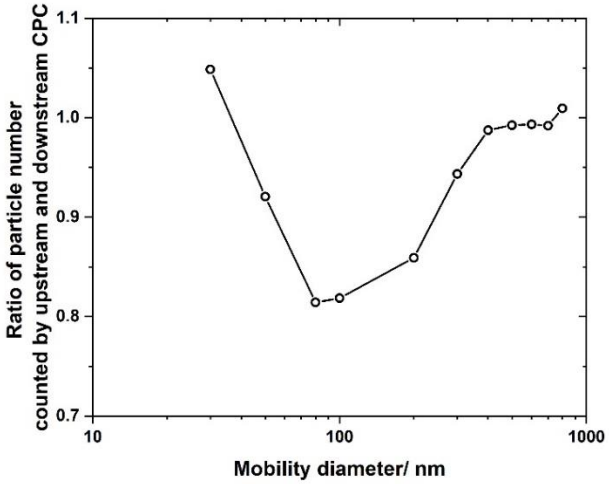

Figure C2 Typical ratio of particle number counted by upstream and downstream CPC with the setup used in the study in the dummy experiment.

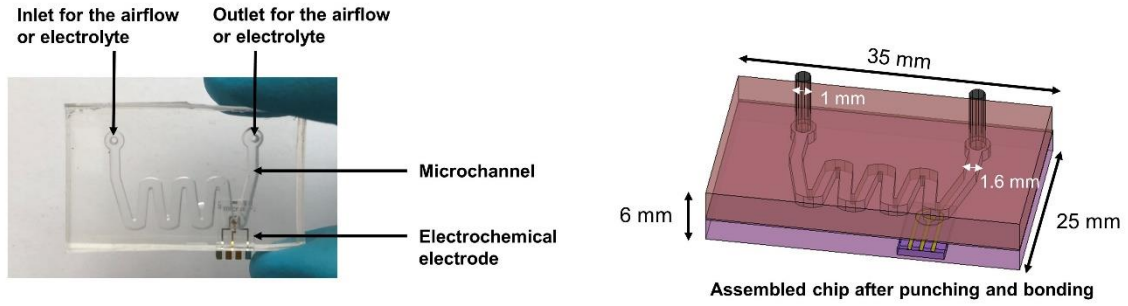

Figure C3 Photo and schematic of the microchannel.

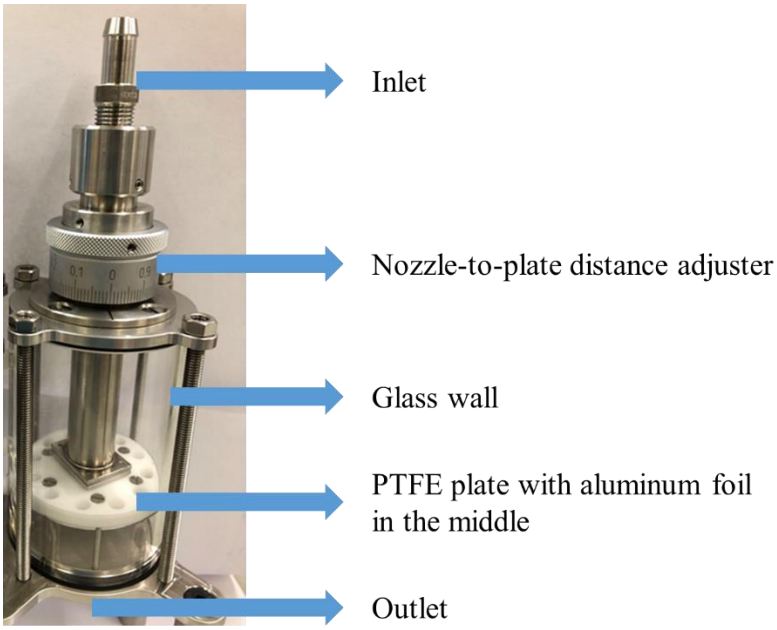

Figure C4 Photo of the homemade impactor.

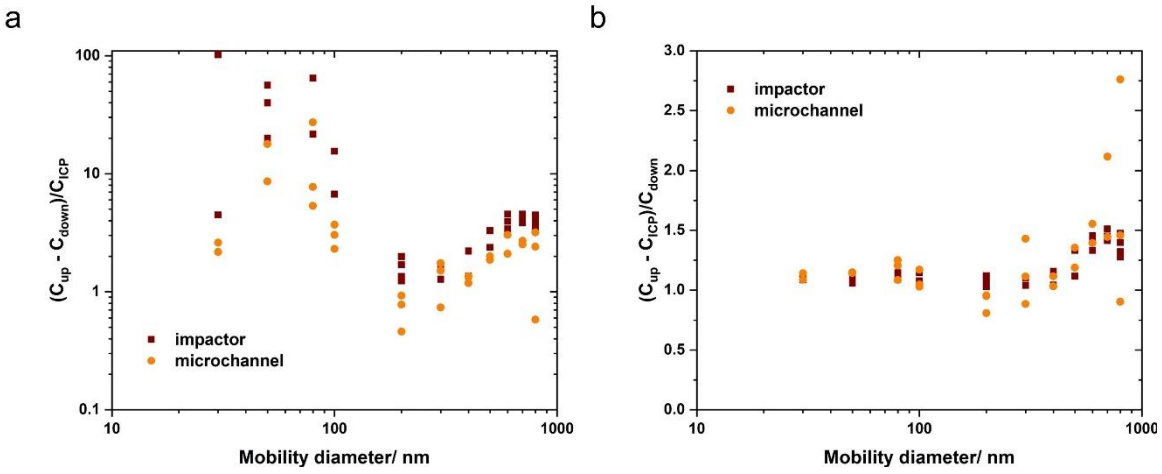

Figure C5 (a) collected particle concentration and (b) downstream particle concentration of the impactor and microchannel.

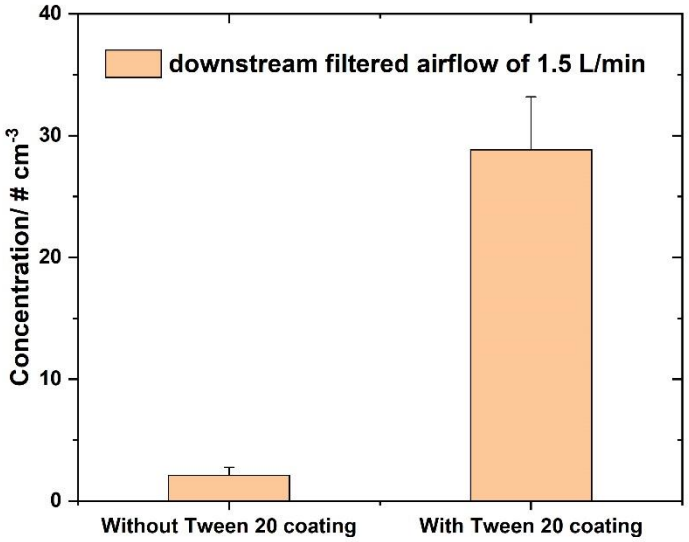

Figure C6 Reaerosolization of Tween 20 coating layer counted by the downstream CPC.

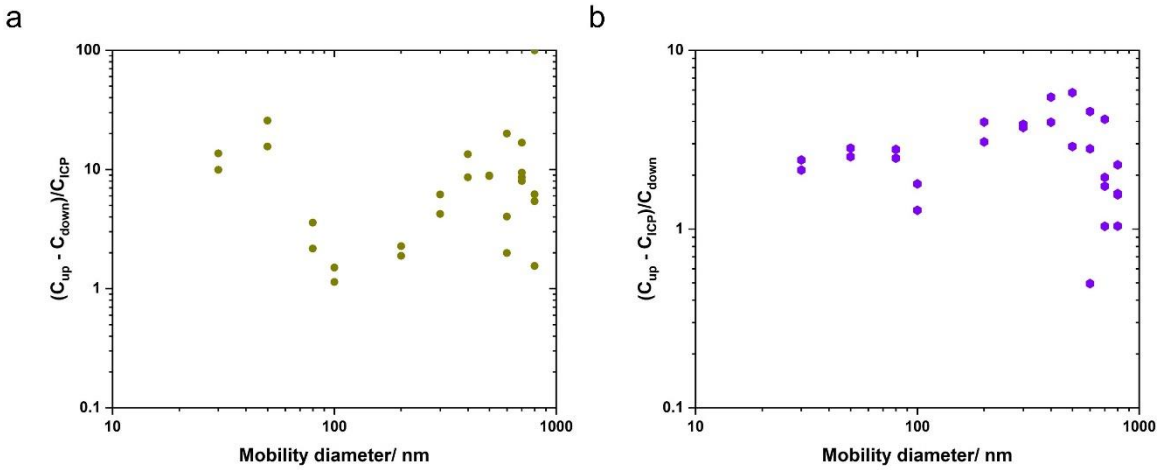

Figure C7 (a) collected particle concentration and (b) downstream particle concentration of the homemade impactor at 6.4 L/min.

Chapter 5

Summary and Outlook

5.1 Summary

Transition metals in the atmosphere are raising a significant threat to human health and the environment, and soluble fraction of particle-bound transition metals are strongly associated with adverse health effects, which require time-consuming efforts and great expense to complete sampling and detection steps due to their low concentrations and technology limitations. Therefore, the detection of the soluble fraction in particle-bound transition metals is significant for public health, ideally in a cost-effective and mobile way. Nonetheless, the monitoring techniques of atmospheric soluble metals is constrained due to their low concentrations and technique limitations. For example, the extraction of airborne soluble metals usually requires time-consuming efforts, such as submicron filter filtration after sonication. After the development of sampling and detection platforms for airborne soluble metals, it becomes hard to estimate the sampling performance using the conventional upstream and downstream particle counting under high pressure drops out of working ranges. Higher pressures drops indicate higher flow rates and larger amount of collected particle mass in environmental applications, which requires alternative ways to evaluate the sampling performance under various pressure drops. In this thesis, new strategies and concepts of capture and detection of airborne soluble metals (e.g. Pb and Cu) are developed using microfluidic, aerosol, electrochemical techniques to create dual-functional interfaces for collection and detection in mobile and cost-effective ways in comparison to conventional coupling of sampling and detection units in sequence, contributing to extensive monitoring of air quality, and explore the evaluation of collection efficiencies of samplers under high pressure drop, which can cause the malfunction of aerosol measure instruments.

In Chapter 2, a promising integrated aerodynamic/electrochemical microsystem has been successfully developed to collect aerosol with relatively high efficiency to detect soluble copper at the nanogram level. The collection, dissolution and detection of aerosol copper rely on the air/solid and liquid/solid interface of the microchannel and do not require a bulky setup. This microsystem is a promising and cost-effective alternative to the cumbersome coupling in series for aerosol collection and detection platform. Nonetheless, the collection and sensing performance of this microsystem should be extensively examined in the real-world environment in

future studies. The limitation of this microsystem is that the collection time could vary according to different soluble Cu concentration in different regions and cities. The collection and determination of several metals such as Cu, Cd, Pb, Fe and Ni can be achieved on the current or modified microsystem (by replacing or modifying the electrode). Besides that, bioaccessiblity of aerosol metals could be extensively explored by using different leaching agents such as water, salt solutions, buffer solutions and synthetic body fluids, and detected *in situ* by the microsystem. In this way, high-resolution monitoring and investigation of bioaccessible aerosol metals could give the rapid response to air quality in terms of human health and facilitate the development of air quality control policies. Furthermore, the application of the microsystem is reasonably extended to the collection and detection of other soluble elements such as nitrate and aerosol oxidative load, which offers a new way to develop the online, mobile, low-cost and miniaturized monitoring system for different aerosol components. Therefore, a more comprehensive routine monitoring network of aerosol soluble metals and other components is potentially established to investigate the aerosol processes and protect the human health.

In Chapter 3, we propose a new collection and sensing concept that allows for immediate sensing after particle collection via a gas/liquid interface. In this way, the mass transport of metal ions is enhanced by dissolving metals as close to the electrode surface as possible. Accordingly, a gold-coated Polyacrylonitrile (PAN) nanofiber serves as the aerosol-into-liquid electrode (AILE) with collection and sensing functions. It is a Janus membrane electrode with a virgin PAN surface on one side and a gold surface on the other side. A system integrating electrochemical methods with aerosol dynamics is developed to fulfill the aerosol-into-liquid concept via this membrane. In the proof-of-concept experiments, the integrated aerodynamic/electrochemical (IAE) system was examined using lab-generated lead aerosols and PM10-like aerosols. The integrated aerodynamic/electrochemical (IAE) system was capable of capturing airborne particles with a cutoff size down to 50 nm and detecting Pb(II) with a limit of detection of 95.7 ng. The new concept achieved in the designed IAE system could afford a unique route toward the on-site monitoring of atmospheric metals and other additional components with a miniaturized size for rapid responses to abrupt pollution events.

In Chapter 4, an elution-based method is proposed to estimate particle collection efficiency of samples regardless of pressure drops. Based on the correlation between CPC-counted and calculated collection efficiencies, CPC is used to measure the upstream particle number, and eluted samples from samplers are employed to estimate the collected particle concentration in the size

range of 100 nm – D_{50} (D_{50} < 500 nm) or 100 – 500 nm (D_{50} > 500 nm). Nonetheless, the elution-based method might be applicable in a wider size range if a more monodisperse NaCl particles could be generated in future studies, especially for particles larger than 500 nm. Size redistribution of monodisperse NaCl particles due to the diffusion of particles smaller than 100 nm and bouncing of particles larger than D_{50} or 500 nm were found to affect the estimation of collection efficiency. Specifically, elution efficiency played a more important role than size redistribution in the range of 30 – 100 nm and affected the estimated collection efficiencies, while size redistribution was more significant with a higher collection efficiency in the size range of 500 – 800 nm. In addition, size redistribution occurred with a collection efficiency of higher than 50 % in the size range of 100 – 500 nm. Thus, this method was also capable of investigating the transport and size redistribution of monodisperse particles through aerosol samplers. A more accurate conversion from particle number into mass con-centration as a function of particle size can also be investigated to avoid the effects of the conversion and facilitate the particle transport studies using the elution-based method.

5.2 Outlook

5.2.1 Extraction Procedure-Dependent Solubility of Metals

The detection of airborne soluble metals through electrochemical techniques requires the dissolution of samples in the liquid phase, the extraction using specific leaching agents is therefore essential, which might represent different levels of metal solubility. Different extraction procedures have been proposed to extract and determine the soluble and bioaccessible metals. Many leaching agents are used for this purpose, such as Chelex [1]. For example, the inhalation bioaccessibility using the artificial lysosomal fluid and the simulated lung fluid showed differences [2]. The solubility is sensitive to different extraction procedures, which makes it challenging to define the determined soluble fractions of metals [3]. In particular, a recent review called for a urgent development of standardized methods to simulate biological fluids for assessments of metal bioaccessibility [4]. The relationship between bioavailability extracted by simulated fluids and particle sizes remain uncertainties. The definition of soluble metals based on standardized extraction procedures could facilitate the comparison among different studies and promote the understanding of effects of soluble metals on environment and human health. In this regard, electrochemical techniques could be promising in the determination of the soluble metals via different electrolytes, which also act as the leaching agents. In addition, the bioavailability and toxicity of metals could be directly obtained from electrochemical platforms.

5.2.2 Lab-generated Aerosol Metals to Simulate the Ambient Environment

The common test strategies of newly developed sensing platform are to directly examine it in field studies. Not all developed sensors and platforms at their early stages are capable of detecting aerosol metals at a lower level than the average concentrations in the ambient environment likely due to the limit of detection or the limitation of aerosol sampling volume. In this case, it is more reasonable to combine the available sampling and detection platform (e.g. X-ray fluorescence) with a low limit of detection (e.g. < 10 ng/m^3) in sequence, which might hinder the participation of sensor groups in the development of novel sensors and platform for airborne metals. It is of importance to develop the generation protocols of aerosol metals with different concentrations and controllable particle sizes, which perform similar to spiked liquid samples for validating aqueous sensors.

Dry particle dispersers are the available to generate suspended solid particles with a high airborne concentration (mg/m^3 – g/m^3) and mass flow from powder materials, such as Palas RGB-1000 [5], which are poorly used to simulate the particle concentration in ambient environment. A previous study proposed the reaerosolization of aqueous filter extracts to produce stable PM physically and chemically, but this method was not able to fully recover insoluble components such as elemental carbon [6]. Wet generation of particles could also lead to a particle number peak of a smaller size with possible composition redistribution on particles in the liquid phase, compared to dry generation methods [7], which might affect the evaluation of collection efficiency and subsequent sensing performance. There are also some discussions about the comparison of standardized particles with ambient particles [8]. The pH plays a crucial role in wet generation techniques to prepare lab-generated aerosols, changing the solubility of metals in aerosol significantly [9], which might change the chemical states in collected aerosol samples and affect performance of sampling/detection platforms, especially for electrochemical detection platforms. The changes in solubility can lead to uncertainties in recovery rate and limit of detection of electrochemical sensing platforms.

5.2.3 Integrated Sampling/Detection Systems

Unlike the metal sensing in aqueous mediums, it is hard to realize continuous measurements of aerosol metals due to the ultratrace concentration (nanogram per cubic meter or less). The transfer of collected aerosol into detection platforms might cause sample loss and underestimation

of targets in aerosols [10]. In some cases, airborne concentration of metals could also near or below the detection limits of benchtop instruments [11]. The practical way is collecting and accumulating particles for a certain time with a high sampling volume rate to reach above the limit of detection of detection instruments. Therefore, the conventional collection and detection strategy is to couple benchtop or homemade sampling with sensing platform in sequence by additional connections or operations (e.g., sample preparation prior to detections) especially for soluble metal detection. Xact is an instrument that achieve measurements of metals with a high time resolution using energy dispersive XRF after collecting aerosols on filter tapes [12]. More novel strategies and efforts are needed to develop the integrated sampling/detection system for soluble metals in a mobile and low-cost way. In comparison, the integrated sampling/detection platforms for monitoring bioaerosol have been developed based on microfluidic techniques to realize collection, processing, and detection [13, 14]. From the perspective of electrochemistry, there is a promising trend that the two-phase interface serves as both aerosol collection and detection surface, which is the sampling surface integrated with electrochemical electrode surfaces [15], or only electrochemical electrode surface itself [16].

5.3 References

[1] E. Kogianni, A. Kouras, C. Samara, Indoor concentrations of PM2.5 and associated water-soluble and labile heavy metal fractions in workplaces: implications for inhalation health risk assessment, *Environmental Science and Pollution Research*, **2021**, 28, 58983-93, 10.1007/s11356-019-07584-8.

[2] Z.-J. Tang, X. Hu, J.-Q. Qiao, H.-Z. Lian, Size Distribution, Bioaccessibility and Health Risks of Indoor/Outdoor Airborne Toxic Elements Collected from School Office Room, Atmosphere2018.

[3] W. Birmili, A.G. Allen, F. Bary, R.M. Harrison, Trace Metal Concentrations and Water Solubility in Size-Fractionated Atmospheric Particles and Influence of Road Traffic, *Environmental Science & Technology*, **2006**, 40, 1144-53, 10.1021/es0486925.

[4] C.L.S. Wiseman, Analytical methods for assessing metal bioaccessibility in airborne particulate matter: A scoping review, *Analytica Chimica Acta*, **2015**, 877, 9-18, https://doi.org/10.1016/j.aca.2015.01.024.

[5] T. Myojo, T. Oyabu, K. Nishi, C. Kadoya, I. Tanaka, M. Ono-Ogasawara, et al., Aerosol generation and measurement of multi-wall carbon nanotubes, *Journal of Nanoparticle Research*, **2009**, 11, 91-9, 10.1007/s11051-008-9450-8.

[6] S. Taghvaee, A. Mousavi, M.H. Sowlat, C. Sioutas, Development of a novel aerosol generation system for conducting inhalation exposures to ambient particulate matter (PM), *Science of The Total Environment*, **2019**, 665, 1035-45, https://doi.org/10.1016/j.scitotenv.2019.02.214.

[7] H. Herich, T. Tritscher, A. Wiacek, M. Gysel, E. Weingartner, U. Lohmann, et al., Water uptake of clay and desert dust aerosol particles at sub- and supersaturated water vapor conditions, *Physical Chemistry Chemical Physics*, **2009**, 11, 7804-9, 10.1039/B901585J.

[8] V.J. Farahani, M. Pirhadi, C. Sioutas, Are standardized diesel exhaust particles (DEP) representative of ambient particles in air pollution toxicological studies?, *Science of The Total Environment*, **2021**, 788, 147854, https://doi.org/10.1016/j.scitotenv.2021.147854.

[9] L.J. Spokes, T.D. Jickells, Factors controlling the solubility of aerosol trace metals in the atmosphere and on mixing into seawater, *Aquatic Geochemistry*, **1995**, 1, 355-74, 10.1007/BF00702739.

[10] L. Wang, W. Qi, Y. Liu, D. Essien, Q. Zhang, J. Lin, Recent Advances on Bioaerosol Collection and Detection in Microfluidic Chips, *Analytical Chemistry*, **2021**, 93, 9013-22, 10.1021/acs.analchem.1c00908.

[11] J. Niu, P.E. Rasmussen, A. Wheeler, R. Williams, M. Chénier, Evaluation of airborne particulate matter and metals data in personal, indoor and outdoor environments using ED-XRF and ICP-MS and co-located duplicate samples, *Atmospheric Environment*, **2010**, 44, 235-45, https://doi.org/10.1016/j.atmosenv.2009.10.009.

[12] A.H. Tremper, A. Font, M. Priestman, S.H. Hamad, T.C. Chung, A. Pribadi, et al., Field and laboratory evaluation of a high time resolution x-ray fluorescence instrument for determining the elemental composition of ambient aerosols, *Atmos Meas Tech*, **2018**, 11, 3541-57, 10.5194/amt-11-3541-2018.

[13] I. Lee, E. Jeon, J. Lee, On-site bioaerosol sampling and detection in microfluidic platforms, *TrAC Trends in Analytical Chemistry*, **2023**, 158, 116880, https://doi.org/10.1016/j.trac.2022.116880.

[14] J. Choi, J. Lee, J.H. Jung, Fully integrated optofluidic SERS platform for real-time and continuous characterization of airborne microorganisms, *Biosensors and Bioelectronics*, **2020**, 169, 112611, https://doi.org/10.1016/j.bios.2020.112611.

[15] Y.-B. Zhao, J. Tang, T. Cen, G. Qiu, W. He, F. Jiang, et al., Integrated aerodynamic/electrochemical microsystem for collection and detection of nanogram-level airborne bioaccessible metals, *Sensors and Actuators B: Chemical*, **2022**, 351, 130903, https://doi.org/10.1016/j.snb.2021.130903.

[16] S. Frutos-Puerto, C. Miró, E. Pinilla-Gil, Screen-Printed Gold Electrodes as Passive Samplers and Voltammetric Platforms for the Determination of Gaseous Elemental Mercury, *Analytical Chemistry*, **2021**, 93, 3122-9, 10.1021/acs.analchem.0c04347.